Key controls, age, source of metals, and role of organic matter on the origin of Laisvall-type Pb-Zn deposits and their relationship to calcite-fluorite-Zn ± Pb sulfide vein-type mineralization in Baltica Basement (Sweden)

Saintilan, Nicolas

UNIVERSITE DE GENEVE FACULTE DES SCIENCES
Section des Sciences de la Terre et de l'Environnement
Département des Sciences de la Terre Superviseur: Professeur Lluís Fontboté

GEOLOGICAL SURVEY OF SWEDEN Co-superviseur: Dr. Michael B. Stephens

Key Controls, Age, Source of Metals, and Role of Organic Matter on the Origin of Laisvall-Type Pb-Zn Deposits and their Relationship to Calcite-Fluorite-Zn ± Pb Sulfide Vein-Type Mineralization in Baltica Basement (Sweden)

THESE

présentée à la Faculté des Sciences de l'Université de Genève pour obtenir le grade de
Docteur ès sciences, mention Sciences de la Terre

par

Nicolas J. Saintilan

de

Saint-James (Normandie, France)

Thèse N°4793

GENEVE

Atelier de reproduction ReproMail

Juin 2015

UNIVERSITÉ
DE GENÈVE

FACULTÉ DES SCIENCES

Doctorat ès sciences
Mention sciences de la Terre

Thèse de ***Monsieur Nicolas Joël Dominique SAINTILAN***

intitulée :

"Key Controls, Age, Source of Metals, and Role of Organic Matter on the Origin of Laisvall-Type Pb-Zn Deposits and their Relationship to Calcite-Fluorite-Zn±Pb Sulfide Vein-Type Mineralization in Baltica Basement (Sweden)"

La Faculté des sciences, sur le préavis de Monsieur L. FONTBOTE, professeur ordinaire et directeur de thèse (Département des sciences de la Terre), Monsieur M. B. STEPHENS, professeur et codirecteur de thèse (Geological Survey of Sweden et Luleå University of Technology, Luleå, Sweden), Monsieur S. E. KESLER, professeur (Department of Earth and Environmental Sciences , University of Michigan, Ann Arbor, United States of America), R. L. ALLEN, docteur (Geology Research and Development, Boliden Group, Garpenberg et Economic Geology, Luleå University of Technology, Luleå, Sweden) et J. E. SPANGENBERG, docteur (Institut des dynamiques de la surface terrestre, Université de Lausanne, Lausanne), autorise l'impression de la présente thèse, sans exprimer d'opinion sur les propositions qui y sont énoncées.

Genève, le 15 juin 2015

Thèse - 4793 -

Le Doyen

N.B. - La thèse doit porter la déclaration précédente et remplir les conditions énumérées dans les "Informations relatives aux thèses de doctorat à l'Université de Genève".

This PhD thesis is dedicated to "the Man from the Isle of Man", the late John M. Moore (2011) who was my Professor in Exploration Geology at Rhodes University, Grahamstown, South Africa, and contributed to make the geologist and, to some extent, the man I am today.

TABLE OF CONTENTS

English abstract

A multi-disciplinary approach was used to study the Pb-Zn sulfide ore deposits hosted by Ediacaran to Cambrian sandstone at Laisvall (64 Mt at 4.0% Pb, 0.6% Zn, and 9.0 g/t Ag) and Vassbo (3.2 Mt, 5.7% Pb, 0.3% Zn, 18 g/t Ag) along the erosional front of the Caledonian orogen, Sweden. The aim was to refine the genetic model of the Laisvall deposit and, by extension, propose a model for mineralization at Vassbo. New data presented in five chapters show that these epigenetic strata-bound sandstone-hosted Pb-Zn deposits have the key characteristics to classify them as a sub-type of Mississippi Valley-type (MVT) Pb-Zn deposits.

Chapter 1 presents the controls of reactivated basement structures in Proterozoic basement of the Fennoscandian Shield on the Laisvall and Vassbo sandstone-hosted Pb-Zn deposits. Evidence from high-resolution airborne magnetic data shows that linear anomalies correspond to geologic features in the Proterozoic basement and the strata-bound Pb-Zn deposits are spatially associated with areas of change in the trend of the magnetic lineaments; N–S to NE–SW and WNW–ESE to NW–SE in the Laisvall area, and, NNE–SSW to NNW–SSE and NW–SE to W–E in the Vassbo area. In the Laisvall area, some magnetic minima and edges along magnetic gradients can be correlated with faults in the Proterozoic basement. The reactivation of these basement structures is expressed in the Ediacaran–Cambrian sedimentary cover rocks as newly formed faults with Phanerozoic displacement. Ore grade modeling shows that the highest Pb and Zn grades in Laisvall delineate orebodies and orebody trends that follow these faults. Areas where the faults change strike contain some of the largest and richest orebodies. In the Vassbo area, the orebody footprint reflects a folded dolerite dike in the underlying Proterozoic basement which is recognized by a magnetic maximum and an edge along magnetic gradient. It is considered that intrusion of this dike in the basement either produced a local fracture network or was driven by preexisting basement structures. The main orebodies display funnel-shape geometry, fault-rooted at Laisvall and located close to the hinges of the folded dolerite dike in basement at Vassbo. Metal distribution patterns are characterized by Pb-rich cores proximal to basement-steered structures and Zn-rich shells more distal from these structures. The highest Pb and Zn grades occur at the top of sandstone paleoaquifers and are suggested to reflect conditions of higher porosity and supply of reduced sulfur for the metal-bearing fluids.

Chapter 2 provides the first absolute age determination of the Laisvall deposit based on Rb-Sr geochronology on sphalerite using the crush-leach technique. Three sphalerite residues from disseminated sphalerite mineralization interstitial to detrital quartz crystals in sandstone show Rb-Sr isotope systematics indicative of undisturbed primary precipitates. The ID-TIMS data points of these residues yield an isochron model age of 467 ± 5 Ma (MSWD = 1.4). ID-TIMS data were complemented by LA-ICPMS analyses on the same sphalerite samples. The data support the hypothesis that the measured ID-TIMS Rb and Sr contents in these sphalerite residues are held in the sphalerite structure itself and are not related to micro-inclusions. It is proposed that sphalerite can incorporate Rb and Sr in its structure during rapid growth. Since the isochron is based on three points, the obtained age is to be considered as preliminary. Yet, the obtained age is fully consistent with

geologic evidence reported by previous authors and pointing to Middle Ordovician timing of ore formation.The obtained Middle Ordovician (467 ± 5 Ma) mineralization age at Laisvall is interpreted as a far-field foreland response to an early Caledonian arc-continent collision and the subsequent development of a foreland basin. It is proposed that basinal brines formed in the foredeep of the orogen could be conveyed cratonward toward the forebulge, interact with permeable crystalline basement rocks, and resurge as metal-bearing brines in sandstone along reactivated Paleoproterozoic crystalline basement faults. The attempt to date disseminated sphalerite mineralization close to the basal Caledonian décollement at Laisvall or, included in tectonically disrupted allochthonous units inside the Caledonian orogen at Dorotea failed because of disturbance of the Rb-Sr system, probably owing to post-mineralization admixture of fluids rich in Sr.

Calculation of lead source model ages for the Middle Ordovician Laisvall deposit suggests that the line defined by the lead isotopic composition of Pb-Zn sulfides, in a conventional $^{207}Pb/^{204}Pb$ vs. $^{206}Pb/^{204}Pb$ diagram, corresponds to a mixing line for which a lead source is needed in addition to a predominant source from basement rocks. In **Chapter 3**, by using the Pb isotopic composition of separate HCl-HNO_3 leachate and HF-HNO_3 residue whole rock fraction from shale hydrocarbon source rock (Alum Shale Formation), granite basement samples and K-feldspar in the granite in the stratigraphy at Laisvall, two lead sources were constrained: (1) Mainly radiogenic Pb leached from basement rocks; (2) subordinate but significant input of low-radiogenic Pb derived from the Alum Shale Formation. Available evidences suggest that the radiogenic Pb leached from crystalline basement rocks is transported as chloride complexes as foreseen by the standard MVT model. By contrast, the low radiogenic Pb end-member results from the leaching of the following components in shale hydrocarbon source rocks: (i) HCl-HNO_3 leachable organic molecules providing organo-metallic Pb; (ii) microscopic fragments of K-feldspars; and (iii) pyrite ± other sulfides. A working hypothesis suggests that the low-radiogenic Pb end-member is mainly contributed by Pb-bearing organic molecules in a petroleum-aqueous phase system accumulated in sandstone paleoaquifers (cf. **Chapter 4**) and derived from anomalously metal-rich carbonaceous shales of the Alum Shale Formation.

In **Chapter 4**, we refine the previously proposed two-fluid mixing model for the Laisvall (Rb-Sr mineralization age of 467 ± 5 Ma) and Vassbo deposits. The extensive sulfur isotope study carried out on sphalerite, galena, and pyrite combined with previous data shows that the sandstone paleoaquifers supplied most of the reduced sulfur for Pb-Zn sulfide mineralization (with high $\delta^{34}S$ values, average 24 to 29‰ VCDT) via thermochemical sulfate reduction (TSR) by hydrocarbons. New organic geochemistry data show that the Alum Shale Formation was the source of hydrocarbons and other organic compounds (e.g., organic acids and other oxidized compounds) involved in the mineralizing processes. Hydrocarbons were produced in shale source rock buried in the early Caledonian foreland basin, and hydrocarbon migration occurred cratonward toward the forebulge for mineralization in sandstone at Laisvall. Metal-bearing brines migrated along the lower units of the basin, along the unconformity between Ediacaran to Cambrian sediments and the crystalline basement,

and along fractures, including gently dipping sheet joints, in the upper part of the basement. These brines were contained in pre-Ediacaran, rift-related feldspathic sandstones and arkoses (Risbäck Group) containing detritus from the Baltica continent, which were preserved in the deeper part of the early Caledonian foreland basin. Diagenetic calcite and barite cements protected sandstone from quartz cementation and the available porosity for epigenetic mineralization was almost four times higher in calcite- and barite-cemented sandstone paleoaquifers (29 %) than in those mainly cemented by quartz (8 %). Barite precipitated and cemented sandstone through the mixing of (i) basement-interacted (high radiogenic Sr ratios of 0.718–0.722), Ba-bearing, neutral, and relatively reduced fluids; with (ii) a sulfate pool (δ^{34}S values = 14–33‰) in sandstone comprising Cambrian to Ordovician seawater diluted by subsurface formation waters. The change from calcite-barite cementation to Pb-Zn sulfide precipitation in sandstone illustrates a major change in the plumbing system at Laisvall. It is proposed that the reactivated basement structures at Laisvall were first used by the Ba-bearing, reduced and neutral fluids described above. These fluids were in equilibrium with basement rocks and had a long pre-mineralization residence time in the basement. As a result of the early Caledonian orogenic activity, fluids migrated cratonward and Ba-bearing fluids were firstly expelled from their host structures into overlying sandstone by using basement structures. Subsequently, slightly acidic metal-bearing brines migrated through the same plumbing system. The early Caledonian arc-continent collision can account for the necessary flow to prevent these brines from equilibrating with the basement rocks. A key feature of Laisvall-type Pb-Zn mineralization supported by new evidences from ore grade distribution presented in **Chapter 1**, organic geochemistry and textural evidence for the presence of solid organic matter intergrown with sphalerite suggest that much of the richest parts of the orebodies corresponds to the upper parts of the sandstone paleoaquifers, along an upward migrating and fluctuating interface between hydrocarbon-wet and water-wet porosity, where significant quantities of reduced sulfur via TSR was produced and accumulated.

The Åkerlandet and Järvsand basement-hosted vein occurrences are located along the current erosional front of the Caledonian orogen. Similar mineralization in form of veinlets are found at Laisvall in the granitic basement beneath unconformable Ediacaran to Cambrian siliciclastic cover rocks that are in turn overlain by Caledonian thrust nappes (**Chapter 5**). Fractures filled in by calcite, fluorite ± pyrite ± galena have strike orientations at NNW–SSE and NNE–SSW to NE–SW at all deposits. At Laisvall, these orientations match those of the interpreted feeder faults to the Laisvall Pb-Zn deposit in sandstone which are inferred to be rooted downwards into the crystalline basement.

At Åkerlandet, at least two mineral generations preceded fluorite and calcite precipitation. Fractures composing a sinistral N–S shear zone in transtension with NW–SE R-Riedel shears formed or re-opened in late Sveconorwegian time as a result of bulk horizontal ENE–WSW extension as suggested by the preliminary dating of adularia at 950 to 980 Ma by ^{40}Ar-^{39}Ar thermochronology. Adularia-quartz precipitated in open space from slightly acidic, low-temperature fluids prior to

sphalerite ± galena mineralization with proposed ages at 544 ± 4 Ma (late Ediacaran) or at 468 ± 5 Ma (Middle Ordovician; sphalerite Rb-Sr isotope geochemistry, **cf. Chapter 2**). Zn ± Pb sulfides were formed by saline, relatively oxidizing, low-temperature (110° to 160°C) and slightly acidic hydrothermal fluids transporting metals and deriving H_2S ($\delta^{34}S$ values of –3.1 to 0.1‰) from the leaching of minor sulfides in basement rocks that were sericitized in places.

At Laisvall, basement structures were used as plumbing system by oxidizing, slightly acidic, metal-bearing brines involved in Pb-Zn mineralization in overlying sandstone in Middle Ordovician time. These basement channelways were subsequently re-occupied post Pb-Zn mineralization in sandstone by fluids that were in equilibrium with basement rocks. Fluorite and calcite precipitation in basement fractures resulted from the mixing of (i) evolved, basement-interacted (calcite and fluorite with $^{87}Sr/^{86}Sr$ ratios of 0.717–0.732), near neutral (pH around 5 to 6), metal-poor and relatively reduced (negative Eu anomaly recorded in calcite, log f_{O2} = around –55) fluids with (ii) organic matter-interacted, H_2S-bearing fluids likely derived from sedimentary cover rocks including the middle Cambrian to Lower Ordovician Alum Shale Formation.

Résumé en français

Une approche pluridisciplinaire a été effectuée pour l'étude des gisements à sulfures de Pb et Zn contenus dans des grès d'âge Ediacaran à Cambrien à Laisvall (64 Mt, 4.0% Pb, 0.6% Zn, 9.0 g/t Ag) et Vassbo (3.2 Mt, 5.7% Pb, 0.3% Zn, 18 g/t Ag) le long du front d'érosion des Calédonides Scandinaves en Suède. Le but était d'affiner le modèle de formation du gisement de Laisvall, et par extension, proposer un modèle de minéralisation à Vassbo. Les nouvelles données présentées en cinq chapitres montrent que ces gisements peuvent être considérés comme une sous-classe de gisement Pb-Zn Mississippi Valley-type (MVT).

Le **Chapitre 1** définit les contrôles exercés sur les gisements de Laisvall et Vassbo par la réactivation de structures tectoniques du socle Protérozoïque (bouclier Fennoscandien). Les données aériennes à haute-résolution du signal magnétique montrent des anomalies linéaires correspondant à des structures géologiques du socle. Les gisements à sulfures de Pb et Zn sont associés à des zones de changement de l'azimut des linéations magnétiques; N–S à NE–SO et ONO–ESE à NO–SE à Laisvall, et, NNE–SSO à NNO–SSE et NO–SE à O–E à Vassbo. Des minima magnétiques et des crêtes le long de gradients magnétiques sont corrélés à des failles dans le socle à Laisvall. La réactivation des structures du socle prend la forme de faille de mouvement Phanérozoïque dans les roches sédimentaires édiacarennes et cambriennes. A Laisvall, la modélisation du gisement montre que les teneurs les plus élevées de Pb et Zn dessinent des corps minéralisés qui suivent les failles. A Vassbo, les contours des corps minéralisés reflètent la présence d'un dike plissé de dolérite du socle. Ce dike est identifié par un maximum et une crête magnétiques. Son intrusion a soit produit son réseau de fractures ou s'est insinué dans un réseau préexistant. Les corps minéralisés des deux gisements dessinent des géométriques en entonnoir, à proximité de failles ou de crêtes de pli de dolérite. La distribution des teneurs en métaux montrent des cœurs riches en Pb proche des structures contrôlées par les structures du socle, et des horizons riches en Zn dans les zones plus distales. Les teneurs les plus élevées en Pb et Zn se retrouvent au toit des paléo-aquifères de grès et ceci suggère la présence de zones plus perméables et poreuses et/ou de concentrations plus importantes en agent réducteur pour les fluides métallifères.

Le **Chapitre 2** présente le premier âge absolu pour la minéralisation à Laisvall sur la base de géochronologie Rb-Sr sur sphalérite utilisant la technique du crush-leach. Trois résidus de sphalérite, échantillonnés dans la minéralisation disséminée dans les interstices entre les grains de quartz détritique, montrent que leur système isotopique Rb-Sr est resté non perturbé. Les données ID-TIMS des ces résidus définissent un âge modèle d'isochrone à 467 ± 5 Ma (MSWD = 1.4), âge en accord avec des observations géologiques. Ces données ont été complétées par des analyses laser sur les mêmes échantillons de sphalérite. La comparaison de ces données suggère que les teneurs en Rb et Sr déterminées par ID-TIMS dans les résidus sont incorporés dans la structure de la sphalérite et non pas dans des inclusions contenues dans la sphalérite. Une possible explication est que la sphalérite croissant rapidement peut incorporer Rb et Sr. L'âge isochrone de minéralisation de 467 ± 5 Ma peut être interprétée comme une réponse à la collision précoce Calédonienne entre un arc et un continent,

causant le développement d'un bassin d'avant-pays. Des fluides de bassin se sont formés dans l'avant-fosseet ont migré vers le craton, dans la zone du bourrelet frontal. Durant la migration, les fluides ont interagi avec le socle où ils se sont chargés en métaux, principalement le long de failles réactivées du socle à Laisvall. La tentative de datation de minéralisation à sphalérite à Laisvall située à proximité du décollement calédonien ou incluse à Dorotea dans les nappes allochtones de l'orogène calédonien a échoué car le système isotopique Rb-Sr des sphalérites analysées a été perturbé après minéralisation par des fluides riches en Sr.

Le calcul de l'âge modèle pour une source de Pb présenté dans le **Chapitre 3** montre que la composition isotopique de Pb des sulfures de Pb et Zn à Laisvall correspond à un mélange entre deux sources. L'étude de la composition isotopique de Pb des fractions "lessivables" et "résiduelles" des roches granitiques du socle et des roches mères de pétrole de la stratigraphie suggère que le plomb a été essentiellement dérivé des roches du socle. Toutefois, une source secondaire de Pb, dérivée des roches mères de pétrole et transportée par un système pétrolier s'accumulant dans les grès au site de minéralisation, est quantifiable.

Le **Chapitre 4** présente une refonte du modèle proposé lors d'études précédentes pour la formation des gisements de Laisvall et de Vassbo, et, basé sur le mélange de deux fluides. Les valeurs positives d'isotopes de soufre de la sphalérite, galène et pyrite du **Chapitre 4** (moyenne de 24–29‰ VCDT) montrent que le grès contenait une source abondante de sulfure d'hydrogène (H_2S) produite par réduction thermochimique du sulfate aqueux par des hydrocarbures (TSR). Les données de géochimie organique suggèrent que ces hydrocarbures ne sont pas endémiques au grès mais qu'ils ont été produits par les roches mères de la Formation Alum Shale enfouies dans l'avant-fosse. La migration des hydrocarbures s'est déroulée vers le craton et le bourrelet du bassin d'avant-pays. Des fluides de bassin métallifères ont migré dans les unités inférieures du bassin, le long de la discontinuité entre les sédiments Ediacaren et Cambrien et le socle, et le long de fractures incluant des joints à pendage modéré dans la partie supérieure du socle. Ces fluides étaient contenus à l'origine dans des sédiments pré-Ediacaren, composés d'arkoses et de grès feldspathiques déposés lors de la formation du rift et contenant des débris du continent Baltica. Ces roches sédimentaires étaient préservées dans la partie profonde du bassin d'avant-pays. La calcite et la barytine ont été des ciments diagénétiques cruciaux qui ont protégé les grès de la cémentation par le quartz. La porosité disponible pour la minéralisation était presque quatre fois supérieure dans les grès cimentés par la calcite et la barytine (29 %) par rapport à ceux cimentés principalement par du quartz (8 %). La barytine a précipité par mélange de (i) des fluides à barium, neutres, relativement réduits et qui avaient interagi avec le socle, et (ii) une source de sulfate contenue dans les grès et comprenant de l'eau de mer cambrienne et ordovicienne diluée par des eaux de formation de sub-surface. La transition des ciments à barytine et calcite à la minéralisation à Pb-Zn illustre un changement majeur dans le système hydrologique à Laisvall. Les structures réactivées du socle furent utilisées d'abord par les fluides réduits à barium qui avaient longtemps résidé dans le socle. En conséquence de l'activité calédonienne précoce, ces fluides

ont été éjectés de leurs structures vers le haut dans les grès. Par la suite, des fluides de bassin chargés en métaux ont migré par les mêmes structures et n'ont pas pu s'équilibrer avec les roches du socle. Un aspect clé des minéralisations de type Laisvall, étayé par la distribution des teneurs en métaux dans le gisement, les résultats de géochimie organique et la présence de matière organique solide intimement liée à la sphalérite, suggère que les parties les plus riches de la minéralisation correspondent à la partie supérieure de chaque paléoaquifère le long d'une interface fluctuant et migrant vers le haut entre hydrocarbures et eau où des quantités significatives de sulfure s'étaient accumulées durant TSR.

Les gîtes sous forme de veines dans le bouclier Fennoscandien à Åkerlandet et Järvsand sont situés le long du front d'érosion de l'orogène calédonien. Des minéralisations similaires sous forme de veinules se trouvent à Laisvall dans le socle granitique sous les roches sédimentaires siliciclastiques discordantes d'âge Ediacaren à Cambrien qui sont elles-mêmes recouvertes par les nappes calédoniennes (**Chapitre 5**). Des fractures emplies de calcite, fluorite ± pyrite ou galène sont orientées à NNO–SSE et NNE–SSO à NE–SO dans tous ces gîtes, et non moins, à Laisvall où ces orientations, dans les grès contenant la minéralisation à sulfures de Pb-Zn, correspondent aux mêmes orientations des failles interprétées comme ayant leurs racines dans le socle cristallin.

En réponse à l'activité orogénique calédonienne précoce, des structures du socle ont été utilisées comme système de tuyaux pour des fluides salins, oxydants, légèrement acides et métallifères impliqués dans la minéralisation à sulfures de Pb et Zn à l'Ordovicien Moyen dans les grès déposés sur le socle. Ces structures ont été occupées par la suite et après la minéralisation à Pb-Zn dans les grès à l'Ordovicien Moyen par des fluides réduits (anomalie Eu négative dans la calcite, log = environ –55) et neutre (pH aux alentours de 5 à 6) en équilibre avec les roches du socle. Fluorite et calcite précipitèrent à partir de fluides évolués, neutre, déficients en métaux et ayant interagi avec le socle (ratios $^{87}Sr/^{86}Sr$ de 0.717–0.732 dans calcite et fluorite). Ces fluides relativement réduits ont interagi avec du pétrole liquide dans les fractures à Åkerlandet, ou, ont été dilués dans les fractures du socle à Laisvall par d'autres fluides à H_2S et ayant interagi avec de la matière organique. Ces fluides ont pour origine les roches sédimentaires de couverture, incluant la Formation Alum Shale d'âge Cambrian moyen à Ordovicien précoce.

A Åkerlandet, au moins deux générations de minéraux ont précédé la fluorite et la calcite. Des fractures d'une zone de cisaillement sénestre N–S en transtension avec des fractures Riedel NO–SE se sont formées ou ré-ouvertes durant une phase tardive de l'orogénèse Sveconorvégienne. Ces fractures résultèrent d'une extension globale ENE–OSO comme l'a montré la datation d'adulaire par thermochronologie ^{40}Ar-^{39}Ar à 950–980 Ma. L'adulaire et le quartz ont précipité à partir fluides légèrement acides (pH ~4–5), de basse température (100°–200° C) avant la sphalérite ± galène datée à 544 ± 4 Ma (Ediacaren tardif) ou à 468 ± 5 Ma (Ordovician Moyen) par géochimie isotopique Rb-Sr (**cf. Chapitre 2**). Les sulfures de Zn ± Pb se sont formés à partir de fluides hydrothermaux salins, relativement oxydants, de basse température (110° à 160°C) et légèrement acides transportant des

métaux et dérivant H_2S (valeurs $\delta^{34}S$ de –3.1 à 0.1‰)) de la lixiviation de rares sulfures dans les roches du socles qui ont elles été séricitisées par endroit.

INTRODUCTION

The Laisvall (64 Mt at 4.0% Pb, 0.6% Zn, and 9.0 g/t Ag) and Vassbo (3.2 Mt, 5.7% Pb, 0.3% Zn, 18 g/t Ag) deposits hosted by Ediacaran to Cambrian siliciclastic rock along the erosional front of the Caledonian orogen, following the classic work by Grip (1954, 1960, 1967), were extensively studied in the late 1970's and 1980's (Christofferson et al., 1979; Rickard et al., 1975, 1979, 1981; Rickard, 1983; Bjørlykke and Sangster, 1981; Lindblom, 1986). Summary articles were published in the early 1990's (Bjørlykke et al., 1991; Romer, 1992). The main scientific issue was the genetic controversy between an epigenetic model based on the two fluid mixing hypotheses involving compressive tectonics (cf. Rickard et al., 1979), and, an early diagenetic model based on groundwater transport of metals from the underlying basement under stable tectonic conditions (Bjørlykke and Sangster, 1981), although, subsequently, Bjørlykke et al. (1991) placed the formation at a later stage with the involvement of sedimentary brines. The overview work by Romer (1992) and modern investigations of the composition of inclusion fluids in halogen and noble gases (Kendrick et al., 2005) invoked evolved metal-bearing basement-interacted seawater brines migrating through basement structures in the mineralizing process. In addition, Kendrick et al. (2005) showed that the mineralizing fluids interacted with organic matter as suggested by Rickard et al. (1975, 1979) and Lindblom (1986).

Boliden AB (Sweden) recognized the need to improve the exploration model for Laisvall-type deposits in the Scandinavian Caledonides. The Exploration Managers (Hans Årebäck, PhD and Erik Lundstam with the help of the Senior Geologist Rolf Jonsson) and the Manager Geology Research and Development (Rodney L. Allen, PhD) proposed to Boliden exploration board and managers a PhD project to be carried out under the supervision of Prof. Lluís Fontboté at the University of Geneva, Switzerland and the co-supervision of Michael B. Stephens (PhD), Geological Survey of Sweden (SGU), who had worked with the geology of the Caledonian orogen and the Fennoscandian Shield in Scandinavia for more than 35 years. The project was subsequently supported financially and logistically by Boliden AB, the Swiss National Science Foundation (SNF), and the Geological Survey of Sweden. Yearly update meetings were held in Sweden and at the University of Geneva, with participation of all parts.

The project aimed to refine the genetic model for Laisvall and, by extension, that of Vassbo. Four main scientific issues were raised when planning the research project: (1) identifying the tectonic and structural controls exerted by basement structures on the location and genesis of these deposits if any, (2) determine the first absolute age for Pb-Zn mineralization and constrain the geodynamic settings that governed the flow of mineralizing fluids, (3) constrain the sources of metals, (4) describe the source and role of organic matter for mineralization in sandstone. In addition, a possible genetic link between calcite-fluorite-Zn ± Pb sulfide vein deposits in Proterozoic basement along the erosional front of the Caledonian orogen and the Laisvall and Vassbo deposits should be re-evaluated.

The project crucially benefited from the access to (1) the core archives of Boliden AB in Boliden and the Geological Survey of Sweden in Malå, (2) the extensive database of exploration boreholes for the discovery of the Laisvall and Vassbo deposits that allowed 3D modeling of geology

and ore grade distribution, and (3) internal exploration reports of Boliden AB from the early 1930's to present. Regional-scale and mine-scale investigations were carried out using combined interpretation of high-resolution airborne magnetic data, structural analysis, ore-grade and geologic modeling in 3D space at both deposits. Sample- to mineral-scale studies made use of various microscopy techniques (e.g., reflected and transmitted light, optical cathodoluminescence, SEM, and QEMSCAN) to study the relationships between ore and gangue minerals cementing sandstone paleoaquifers. Sphalerite and calcite-fluorite mineral chemistry combining microprobe and laser ablation inductively coupled mass spectrometry analyses (LA-ICPMS, collaboration with Dr. K. Kouzmanov, University of Geneva and Dr. A. Ulianov, University of Lausanne, Switzerland) with isotope dilution thermal ionization mass spectrometry (ID-TIMS) were used for absolute geochronology studies (Rb-Sr and Sm-Nd, respectively; collaboration with Dr. J. Schneider, University of Freiberg, Germany). ^{40}Ar-^{39}Ar thermochronology (collaboration with Dr. R. Spikings, University of Geneva) was used on newly discovered adularia. Radiogenic and stable isotope geochemistry (e.g., Pb, Sr, S, C, O, and N, collaboration with Dr. M. Chiaradia, University of Geneva, and PD Dr. J. E. Spangenberg, University of Lausanne) were carried out to study the source of metals, source of reduced sulfur, and origin and composition of the mineralizing fluids. Organic geochemistry studies of hydrocarbons in barren and mineralized sandstone samples, and shale hydrocarbon source rock constrained the source of organic compounds involved in the mineralizing processes (collaboration with J. E. Spangenberg). The Ph.D. Thesis results are presented in the following five chapters:

1. Control of reactivated Proterozoic basement structures on sandstone-hosted Pb-Zn deposits along the Caledonian front, Sweden: Evidence from airborne magnetic data, structural analysis, and ore-grade modeling.
2. A Middle Ordovician age for the Laisvall sandstone-hosted Pb-Zn deposit, Sweden: A response to early Caledonian orogenic activity.
3. Unconventional lead source in the Mississippi Valley-type (MVT) Laisvall Pb-Zn deposit: the contribution from shale hydrocarbon source rocks.
4. A refined genetic model for the Laisvall and Vassbo Mississippi Valley-type sandstone-hosted deposits, Sweden: constraints from paragenetic studies, organic geochemistry, and S, C, N and Sr isotope data.
5. Polyphase vein-type mineralization in the Fennoscandian Shield at Åkerlandet, Järvsand and Laisvall along the erosional front of the Caledonian orogen, Sweden.

Improving the genetic model for MVT mineralization of the Laisvall-type is important because the potential of finding additional resources along the erosional front of the Caledonian orogen, but also, beneath and within this mountain range, exists. At a wider scale of thinking, it can be reminded that sediment-hosted Pb-Zn deposits contain the largest Pb and Zn resources in the world and represent by far the main supplier for the production of these metals (Leach et al., 2005). Half the world's reserves for Zn and Pb are found in "sedimentary exhalative deposits" (SEDEX). MVT

deposits represent a subordinate source of Pb and Zn. The largest 30 MVT deposits contain each between 2.5 and 10 Mt of total Pb + Zn metal content. However, MVT deposits have the advantage to form clusters or districts including several individual deposits. While each MVT ore district has a distinctive combination of ore assemblages, ore controls, host rocks, alteration, isotope and geochemistry features, deposits within a single district usually have similar attributes and ore controls (Leach et al., 2005). Robust genetic and exploration models for a given mining district favor mineral exploration for MVT deposits and facilitate mining operations. In addition, the paucity of pyrite and penalty elements in MVT ores and the frequent presence of gangue minerals able to neutralize Acidic Mining Drainage are major pro's for mineral processing.

MVT deposits are mostly found in carbonate rocks of Phanerozoic age and deposits in older rocks remain scarce (e.g., MVT deposits in the Paleoproterozoic Earaheedy Basin, Western Australia; Muhling et al., 2012) despite the abundance of Proterozoic carbonate rocks (Leach et al., 2005). The sub-type of MVT deposits in sandstone (Leach et al., 2005; this study) has been considered as a minor source of metals by world standards but these deposits also have been less explored for. It is anticipated that the findings in the current work on the Laisvall and Vassbo deposits in Ediacaran to Cambrian sandstone may help exploration activities for similar deposits in Proterozoic (e.g., Wollaston domain, northern Saskatchewan, Canada), Carboniferous (Appalachian orogen, Nova Scotia, Canada), Triassic (e.g., Maubach-Mechernich, Germany; Largentière, France; Zeida, Morocco), Cretaceous (e.g., Bou-Sellam, Morocco; Kroussou area; Gabon), and Mesozoic to Cenozoic rocks. These youngest sedimentary sequences host the largest and youngest sandstone-hosted Zn-Pb deposit in the world at Jinding, China (200 Mt at 6.1 % Zn and 1.3 % Pb; Li and Kyle, 1997; Chi et al., 2005; Xue et al., 2007).

REFERENCES

Bjørlykke, A., and Sangster, D.F., 1981, An overview of sandstone lead deposits and their relation to red-bed copper and carbonate-hosted lead-zinc deposits: ECONOMIC GEOLOGY 75th Anniversary Volume, p.179-213.

Bjørlykke, A., Sangster, D.F., and Fehn, U, 1991, Relation between high heat-producing (HHP) granites and strata-bound lead-zinc deposits, in Pagel, M., and Leroy, J.-L., eds., Source, transport and deposition of metals: Balkema, Rotterdam, p. 257-260.

Chi, G., Qing, H., Xue, C., Zeng, R., 2005, An overpressured fluid system associated with the giant sandstone-hosted Jinding Zn-Pb deposit, western Yunnan, China, *in* Jingwen, M., Bierlein, F.P., eds., Mineral Deposit Research: Meeting the Global Challenge, Springer, Berlin-Heidelberg, pp 93-96.

Christofferson, H.C., Wallin, B., Selkman, S., Rickard, D.T., 1979, Mineralization controls in the sandstone lead-zinc deposit at Vassbo, Sweden: ECONOMIC GEOLOGY, v. 74, p. 1239-1249.

Grip, E., 1954, Blymalmen vid Laisvall, dess geologi och jämförelse med några utländska förekomster: Geologiska Föreningens i Stockholm Förhandlingar (GFF), v. 76, p. 357-380 (in Swedish).

Grip, E., 1960, The lead deposits of the eastern borders of the Caledonides in Sweden. 21st International Geological Congress, Copenhagen, Norden 16, p. 149-159.

Grip, E., 1967, On the genesis of the lead ores of the eastern border of the Caledonides in Scandinavia: Society of Economic Geologists Monograp 3, p. 208-218

Kendrick, M.A., Burgess, R., Harrison, D., and Bjørlykke, A., 2005, Noble gas and halogen evidence for the origin of Scandinavian sandstone-hosted Pb-Zn deposits: Geochimica et Cosmochimica Acta, v. 69, p. 109-129.

Li, N., Kyle, J.R., 1997, Geologic controls of Sandstone-hosted Zn-Pb-(Sr) mineralization, Jinding Deposit, Yunnan Province, China – A new environment for sediment-hosted Zn-Pb deposits, *in* Rongflu, P., ed., Energy and mineral resources for the 21st Century, Geology of mineral deposits, Mineral economics, Proceedings 30th international geological congress 9, Beijing, China, pp 67-82.

Lindblom, S., 1986, Textural and fluid inclusion evidence for ore deposition in the Pb-Zn deposit at Laisvall, Sweden: ECONOMIC GEOLOGY, v. 81, p. 46-64.

Leach, D.L., Sangster, D.F., Kelley, K.D., Large, R.R., Garven, G., Allen, C.R., Gutzmer, J., Walters, S., 2005, Sediment-hosted Pb-Zn deposits: A global perspective: ECONOMIC GEOLOGY 100th Anniversary Volume, p. 561–607.

Muhling, J.R., Fletcher, I.R., Rasmussen, B., 2012, Dating fluid flow and Mississippi Valley-type base-metal mineralisation in the Paleoproterozoic Earaheedy Basin, Western Australia: Precambrian Research v. 212-213, p. 75-90.

Rickard, D.T., 1983, Precipitation and mixing mechanisms in Laisvall-type sandstone Pb-Zn deposits, *in* Kirsvarsanyi, G., Hagni, R., Pratt, W., and Koening, J.W., eds., Proceedings of the International Conference on Mississippi Valley Type Lead-Zinc Deposits: Rolla, Missouri, 1983

Rickard, D.T., Willdén, M., Mårde, Y., and Ryhage, R., 1975, Hydrocarbons associated with lead-zinc oresat Laisvall, Sweden: Nature, v. 255, p. 131-133.

Rickard, D.T., Willdén, M.Y., Marinder, N.E., and Donnelly, T.H., 1979, Studies on the genesis of the Laisvall sandstone lead-zinc deposit, Sweden: ECONOMIC GEOLOGY, v. 74, p.1255-1285.

Rickard, D.T., Coleman, M., and Swainbank, I., 1981, Lead and sulfur isotopic compositions of galena from the Laisvall sandstone lead-zinc deposit, Sweden: ECONOMIC GEOLOGY, v. 76, p. 2042-2046.

Romer, R.L., 1992, Sandstone-hosted Pb-Zn mineral deposits and their relation to the tectonic mobilization of the Baltic Shield during the Caledonian orogeny–a reinterpretation: Mineralogy and Petrology, v. 47, p. 67-85.

Xue, C., Zeng, R., Liu, S., Chi, G., Qing, H., Chen, Y., Yang, J., Wang, D., 2007, Geologic, fluid inclusion and isotopic characteristics of the Jinding Zn–Pb deposit, western Yunnan, South China: A review: Ore Geology Reviews, v. 31, p. 337-359.

CHAPTER 1

Control of Reactivated Proterozoic Basement Structures on Sandstone-Hosted Pb-Zn Deposits along the Caledonian Front, Sweden: Evidence from Airborne Magnetic Data, Structural Analysis, and Ore-Grade Modeling

Published manuscript as: Saintilan, N.J., Stephens, M.B., Lundstam, E., and Fontboté, L., 2015, Control of Reactivated Proterozoic Basement Structures on Sandstone-Hosted Pb-Zn Deposits along the Caledonian Front, Sweden: Evidence from Airborne Magnetic Data, Structural Analysis, and Ore-Grade Modeling: ECONOMIC GEOLOGY, v. 110, p. 91-117.

Economic Geology, v. 110, pp. 91–117

Control of Reactivated Proterozoic Basement Structures on Sandstone-Hosted Pb-Zn Deposits along the Caledonian Front, Sweden: Evidence from Airborne Magnetic Data, Structural Analysis, and Ore-Grade Modeling

Nicolas J. Saintilan,[1,†] Michael B. Stephens,[2, 3] Erik Lundstam,[4] and Lluís Fontboté[1]

[1]*University of Geneva, Department of Earth and Environmental Sciences, Rue des Maraîchers 13, 1205 Genève, Switzerland*

[2]*Geological Survey of Sweden (SGU), Box 670, SE-751 28 Uppsala, Sweden*

[3]*Department of Civil, Environmental and Natural Resources Engineering, Division of Geosciences, Luleå University of Technology, SE-971 87 Luleå, Sweden*

[4]*Boliden AB, SE-776 98 Garpenberg, Sweden*

Abstract

Strata-bound, nonstratiform, epigenetic galena-sphalerite-cement mineralization in Ediacaran-Cambrian sandstone, including the previously mined deposits at Laisvall and Vassbo, occurs along the eastern erosional front of the Caledonian orogen in Sweden. The sandstone is part of an autochthonous siliciclastic sedimentary sequence that rests unconformably on top of Proterozoic crystalline basement beneath the Caledonian thrust nappes.

Linear anomalies have been identified in high-resolution airborne magnetic data that correspond to geologic features in the Proterozoic basement. Furthermore, the Laisvall and Vassbo strata-bound Pb-Zn deposits are both spatially associated with areas of change in the trend of the magnetic lineaments. Magnetic anomalies, trending either N-S to NE-SW and WNW-ESE to NW-SE in the Laisvall area, and NNE-SSW to NNW-SSE and NW-SE to W-E in the Vassbo area, were identified.

In the Laisvall area, some magnetic minima and edges along magnetic gradients can be correlated with faults in the Proterozoic basement. The reactivation of these basement structures is expressed in the Ediacaran-Cambrian sedimentary cover rocks as newly formed faults with Phanerozoic displacement. Along individual faults belonging to two sets (NE-SW to N-S and WNW-ESE to NW-SE), synsedimentary block movement has been recognized. The highest Pb and Zn grades in Laisvall delineate orebodies and orebody trends that follow these faults. Areas where the faults change strike contain some of the largest and richest orebodies.

In the Vassbo area, the orebody footprint reflects a folded dolerite dike in the underlying Proterozoic basement. The dike, modeled on the basis of borehole data, is recognized by a magnetic maximum and an edge along a magnetic gradient. No faults have been mapped at the ground surface as being related to the location of dolerite dikes in the basement. However, it is considered that the basement dikes illustrate a structural control, emplacement either producing a local fracture network or being driven by preexisting basement structures.

The main orebodies in both deposits display funnel-shape geometry, fault-rooted in Laisvall and located close to the hinges of the folded dolerite dike in the basement at Vassbo. Metal distribution patterns are similar in both deposits and are characterized by Pb-rich cores proximal to the basement-steered structures while Zn-rich shells are distal from these structures. The funnel-shaped ore geometry is interpreted to reflect a fault-rooted migration path and the metal precipitation mechanism.

In both deposits, the highest Pb and Zn grades occur at the top of sandstone paleoaquifers. Similar mineralization footprints, variation in grades, and paleoaquifer settings were recognized in several carbonate-hosted Mississippi Valley-type (MVT) Zn-Pb deposits (e.g., San Vicente deposit, Peru; Topla-Mežica deposits, Slovenia). This geometry is suggestive of a sour gas trap that accumulated by density at the top of paleoaquifers. This gas could have provided H_2S by thermogenic sulfate reduction to the metal-bearing fluids and triggered precipitation of Pb-Zn sulfides.

The combined evidence from the airborne magnetic data, the structural analysis and the geometry of the orebodies, and metal distribution suggests that the basement faults reactivated during the Ediacaran-Cambrian sedimentation, acted at a later time as feeders for the metal-bearing fluids to fertile horizons for mineralization, and localized deformation during postsedimentary and postmineralization tectonics.

Introduction

Strata-bound and nonstratiform Pb-Zn sulfide mineralizations, including the previously mined deposits at Laisvall and Vassbo, occur along the eastern front of the Caledonian orogen in Sweden and Norway over a distance of more than 1,000 km (Zachrisson, 1980; Stephens, 1986). Mineralization is hosted by Ediacaran-Cambrian sandstone. The sandstone forms part of a siliciclastic sedimentary sequence, which either rests unconformably on top of Proterozoic crystalline basement (Fennoscandian Shield) beneath the Caledonian thrust nappes or is part of the lowermost allochthonous units of the Caledonian orogen (Christofferson et al., 1979; Willdén, 1980; Gee et al., 1985).

The Laisvall Pb-Zn deposit, situated in the northern part of Sweden (Figs. 1A), was operated by Boliden AB as an underground mine until 2001. Mineralization was discovered in 1939 and mining operations started in 1941 (Grip, 1954). During 60 years of mining operations, 64.3 million metric tons (Mt) of ore

† Corresponding author: e-mail, nicolas.saintilan@unige.ch

Submitted: November 21, 2013
Accepted: April 8, 2014

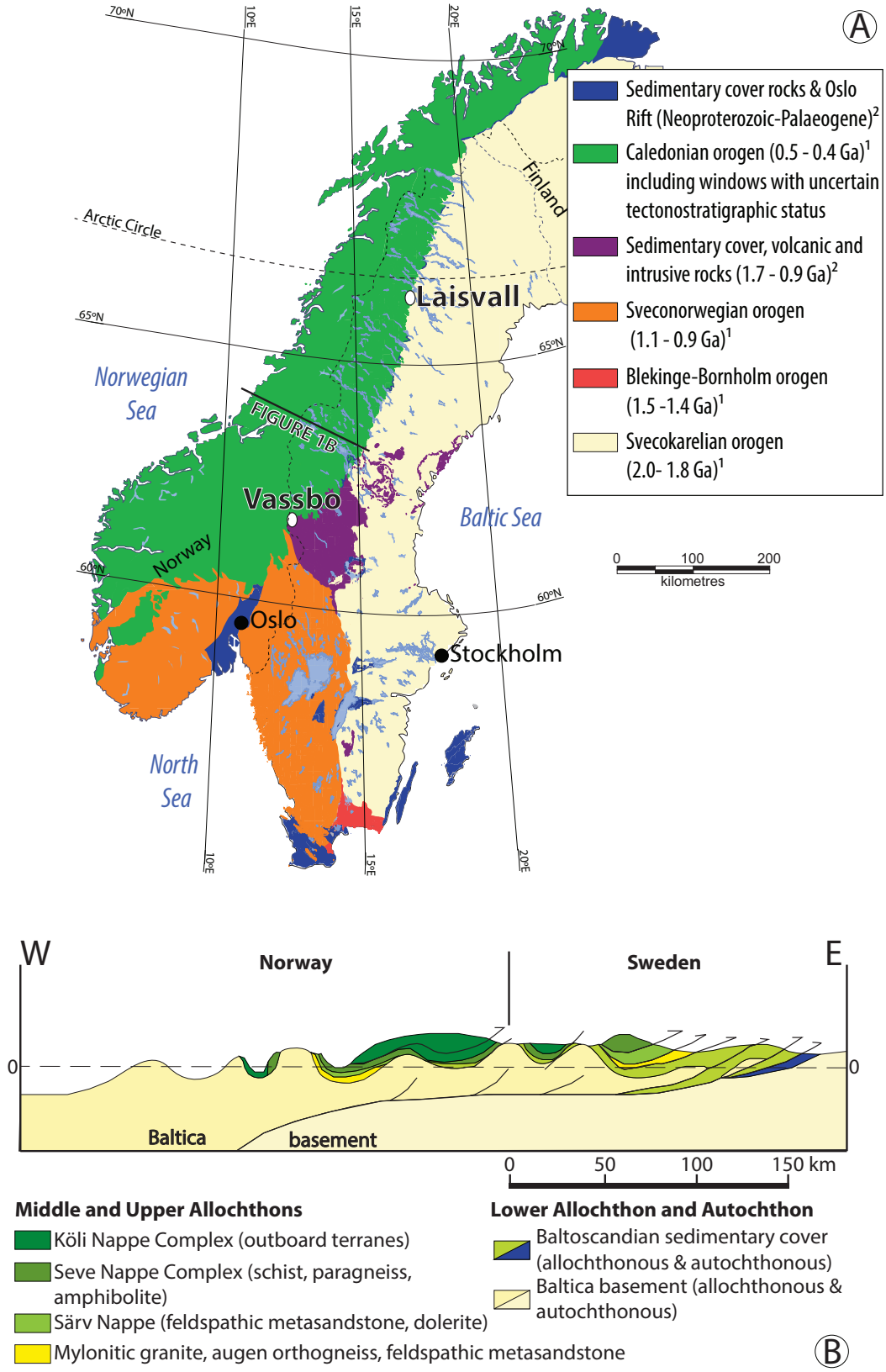

FIG. 1. A. Major tectonic units in Norway and Sweden: [1] = age of orogenic activity, [2] = age of rock formation (modified after Gee et al., 2008, and after the acquisition of data from the Geological Survey of Sweden´s bedrock map database of Sweden at the scale 1:1,000,000). B. Cross section through the central part of the Caledonian orogen in Scandinavia, showing the tectonostratigraphic framework of this orogen (modified after Gee et al., 2010).

at 0.6% Zn, 4.0% Pb, and 9.0 g/t Ag were extracted (Willdén, 2004). The Vassbo Pb-Zn deposit, located in the central part of the country (Figs. 1A), was discovered in 1948. The mine opened in 1960 and produced 5 Mt of ore at 5.5% Pb until it closed down in 1982 (Årebäck, pers. commun., 2010).

The current study focuses on the structural and broader tectonic controls on the spatial occurrence of the Laisvall and Vassbo strata-bound Pb-Zn deposits, which are hosted in the autochthonous sandstone. The aims of the work are to evaluate a possible correlation between magnetic lineaments and structures in the Ediacaran-Cambrian silicilastic cover rocks and to assess whether preexisting structures in the Proterozoic basement could not only have governed sedimentation in the Ediacaran-Cambrian but also could have been utilized later as conduits for the mineralizing fluids.

Different opinions currently exist concerning the role of basement structures beneath these deposits in the context of their genesis (Christofferson et al., 1979; Rickard et al., 1979; Bjørlykke and Sangster, 1981; Romer 1992). Christofferson et al. (1979), Rickard et al. (1979), and Willdén (1980) suggested that the localization of the ore was controlled by permeability variations in the sandstone, and the location and deposition of the sandstone in turn by the paleotopography of the Proterozoic basement. These authors considered the basement beneath the deposits to be essentially impermeable. In contrast, Romer (1992) suggested that the distribution of sandstone-hosted Pb-Zn deposits was controlled by basement structures reactivated during some stage of the Caledonian orogeny. This reactivation made the basement permeable and susceptible to large-scale fluid migration.

To achieve the aims of this study, airborne magnetic data as well as borehole data, mine map information, and other legacy data from both Laisvall and Vassbo have been used in order to generate integrated geometric models for lithologic units and ore grades in three-dimensional space for both deposits.

Interpretation of the airborne magnetic data and structural analysis, in combination with the lithologic and ore-grade modeling in three-dimensional space at the Laisvall and Vassbo deposits, strongly suggest that preexisting basement structures controlled the location of these deposits and also the location of single orebodies within the deposits. Furthermore, the Pb and Zn grade distribution outline funnel-shape, fault-rooted orebodies in sandstone paleoaquifers. Grade distribution maps highlight the existence in the autochthonous sandstone of several main feeder faults, caused by the reactivation of preexisting basement structures. Similarly to the findings at the Navan Irish-type Zn-Pb deposit (Anderson et al., 1998; Blakeman et al., 2002; Davidheiser-Kroll et al., 2013), this study provides a particularly clear case where the existence of multiple feeder zones along several major faults controls Zn, Pb, and Zn/Pb grade distribution.

The present study is part of a broader project aiming to reevaluate the role of the crystalline basement, the migration flow path, the driving force, the precipitation mechanism, and the age of sandstone-hosted Pb-Zn mineralization in a structurally constrained geologic framework.

Geologic Setting

The tectonostratigraphic architecture of the Caledonian orogen in Scandinavia resulted from a series of tectonic events during the latest Cambrian through to the Devonian that involved convergence of two plates containing continental lithosphere referred to as Baltica and Laurentia. This convergence culminated with the collision of these two continents during subduction of the margin of Baltica beneath Laurentia. Several allochthonous thrust nappes, comprising rift-related, platformal and foreland basinal sequences derived from Baltica, oceanic arc-related sequences and exotic continental terranes, were thrust eastward onto Precambrian rocks of the Fennoscandian Shield (Fig. 1A, B; Gee, 1975; Roberts and Gee, 1985; Stephens, 1988; Gee et al., 2010).

Gee (1975) and Roberts and Gee (1985) established a systematic nomenclature for the tectonostratigraphy in the Scandinavian Caledonides involving sheets of thrust nappes in ascending order, referred to as the Lower, Middle, Upper, and Uppermost allochthons (Fig. 1B). The Lower allochthon rests above a sole thrust on top of the thin veneer of Ediacaran-Cambrian locally through to Lower Ordovician autochthonous sedimentary rocks that were deposited on the platformal margin to Baltica (Figs. 1, 2). The Middle and Upper Cambrian Alum Shale Formation (Fig. 2) is partly strongly deformed and provided the main decollement overlain by allochthonous thrust sheets throughout the orogen in Scandinavia (Gee, 1975; Roberts and Gee, 1985; Stephens, 1988; Gee et al., 2010). The Laisvall and Vassbo deposits are hosted in sandstone that constitutes part of the Ediacaran-Cambrian autochthonous siliciclastic rock sequence (Figs. 1, 2).

At Laisvall, the autochthonous stratigraphy is well developed and preserved underneath the main decollement in the Alum Shale Formation and the overlying allochthonous thrust sheets (Figs. 2, 3A, D). The Paleoproterozoic basement is composed of granite which formed at 1.8 Ga. The basement is overlain by the Ediacaran-Cambrian Laisberg Formation (35–40 m thick; Nielsen and Schovsbo, 2011) passing upward into the Grammajukku and Middle Cambrian Alum Shale Formations (Ljungner, 1950; Rickard et al., 1979; Willdén, 1980). The Laisberg Formation represents a transgressive, sandstone-dominated sequence (Willdén, 1980; Nielsen and Schovsbo, 2011).

Mineralization occurs as disseminated mottles and bands of galena and/or sphalerite that constitute interstitial epigenetic cement (Christofferson et al., 1979; Rickard et al., 1979; Willdén, 1980) in the porous sandstone paleoaquifers. Calcite, quartz, K-feldspar, fluorite, and barite occur as accessory to locally dominant cement phases. In places, apatite is found intergrown with sphalerite while organic compounds are intergrown with sphalerite or barite (Saintilan et al., 2014). Scarce steeply dipping galena-sphalerite-calcite veinlets cut through the sulfide-cemented sandstone. Mineralization is hosted in two distinct sandstone paleoaquifers; the Lower and Upper Sandstones (Fig. 2, Rickard et al., 1979; Willdén, 1980) of the Laisberg Formation. In the Lower Sandstone, the orebody is between 12 and 27 m thick, locally thinning to 4 m, with Pb grades between 0.1 and 10%. Zn grades are generally below 1%. In the Upper Sandstone, the orebody is 6 to 8 m thick in average, locally up to 11 m thick. Pb grades are between 1 and 4%, locally up to 12%, while Zn grades are between 1 and 5%. The Zn/Pb ratio is about 8/1 in the Upper Sandstone. The Grammajukku Formation, which caps

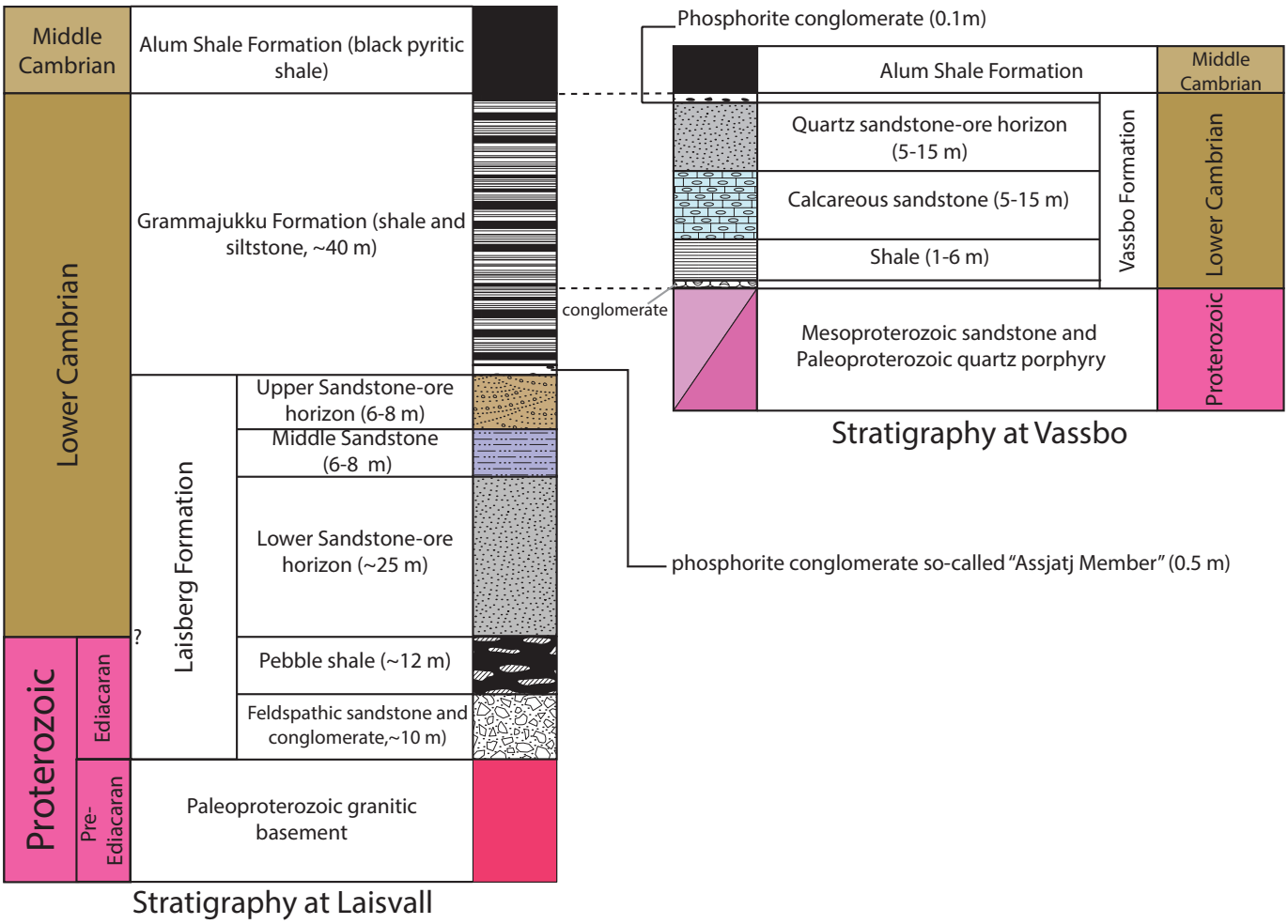

FIG. 2. Stratigraphic columns in the autochthonous sedimentary cover sequences at Laisvall (modified after Rickard et al., 1979; Willdén, 1980; Nielsen and Schovsbo, 2011) and Vassbo (modified after Christofferson et al., 1979; Nielsen and Schovsbo, 2011). Nielsen and Schovsbo (2011) proposed that the Cambrian stratigraphy at Vassbo is coeval with deposition of the Grammajukku Formation in the Laisvall area.

the Upper Sandstone, comprises various shale and siltstone with subordinate sandstone intercalations (Fig. 2). The Alum Shale Formation is composed of black pyritic shale (Ljungner, 1950; Willdén, 1980; Nielsen and Schovsbo, 2011).

The autochthonous sequence at Vassbo (Figs. 2, 4A) corresponds to the Lower Cambrian Vassbo Formation (28–30 m thick) deposited on a peneplained crystalline basement composed of Mesoproterozoic sandstone in the east and acid volcanic or subvolcanic rock (quartz porphyry) dated to 1.7 Ga in the west (Christofferson et al., 1979; Wallin, 1982; Nielsen and Schovsbo, 2011). Two sets of dolerites dated at 1.27 to 1.26 and 0.98 to 0.95 Ga (Central Scandinavian Dolerite Group and Blekinge-Dalarna dolerites; Söderlund et al., 2005), including steeply dipping dikes with NNE–SSW or NW–SE trend and flat-lying sills, are also present in the crystalline basement. These dolerite intrusions were interpreted to reflect back-arc extensional activity (Söderlund et al., 2005). The Lower Cambrian Vassbo Formation is capped by the partly deformed Middle Cambrian Alum Shale Formation (Christofferson et al., 1979; Wallin, 1982). Mineralization is hosted in a quartz sandstone horizon in the upper part of the Vassbo Formation. Some mineralization also occurs in the underlying calcareous sandstone. Mineralization has the same characteristics as the one described above at Laisvall.

Interpretation of Airborne Magnetic Data

Magnetic data and methodology

The use of magnetic data is a geophysical exploration technique based on mapping the subsurface distribution of magnetic minerals (oxides or sulfides). This technique can be a valid approach to mineral exploration either directly for mineral deposits containing magnetic minerals (e.g., magnetite, hematite, pyrrhotite) or indirectly for the ones spatially associated with, for example, faults. Advances in spatial control using global positioning systems (GPS) have not only reduced survey costs but also increased data accuracy (Reeves et al., 1997).

Total magnetization of rock is the vector sum of two components: (1) induced magnetization (proportional in magnitude and generally parallel to the Earth's ambient field), and (2) remnant magnetization (which has a direction and intensity

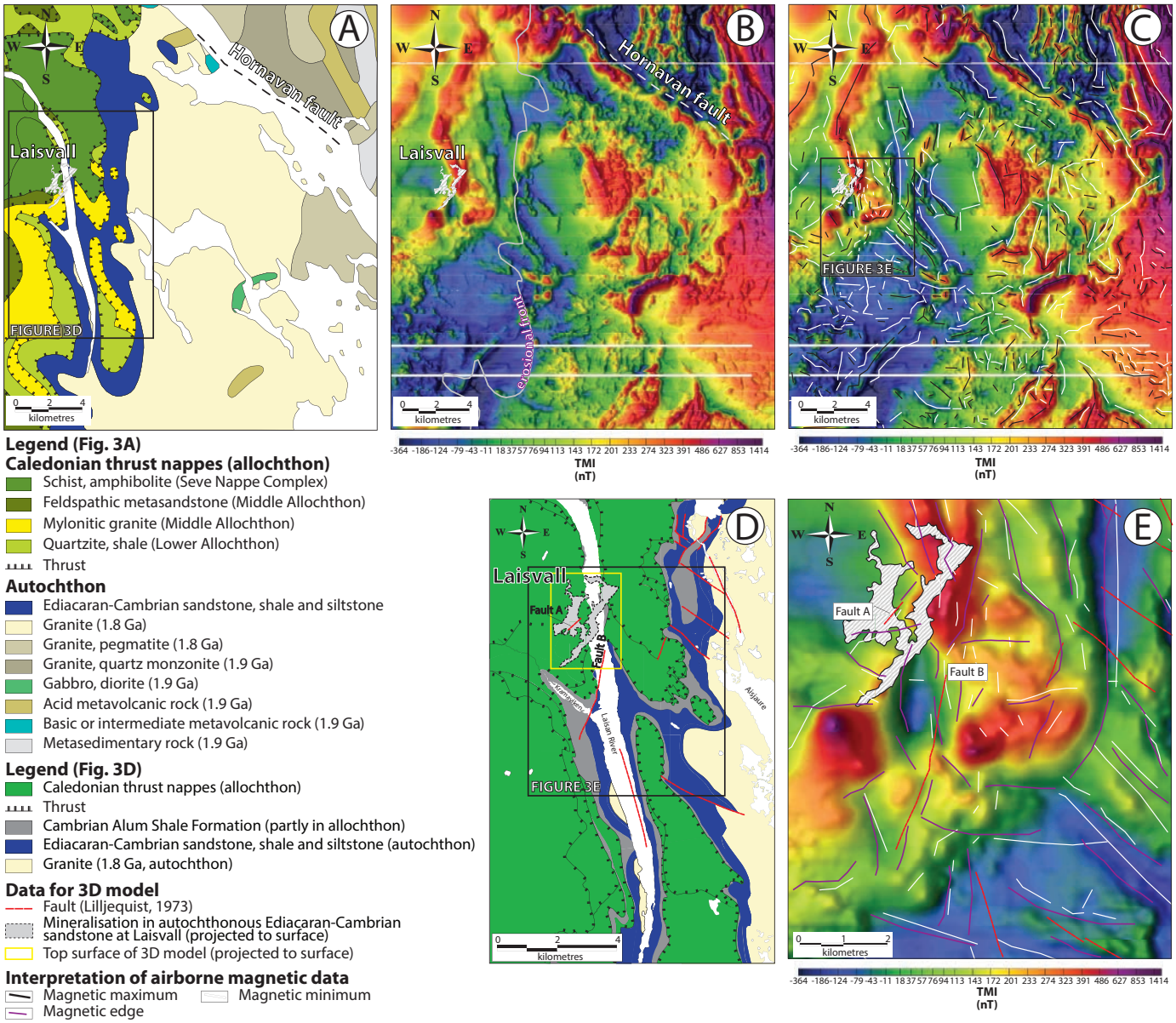

FIG. 3. A. Geologic map of the Caledonian allochthons, the autochthonous sedimentary cover rocks, and the Paleoproterozoic basement in the Laisvall area (modified after acquisition of data from the Geological Survey of Sweden´s bedrock map database of Sweden at the scale 1:1,000,000). The trace of the fault at the ground surface along Lake Hornavan is also shown. B. Total magnetic intensity (TMI) airborne magnetic map of the Laisvall area. The erosional front where Paleoproterozoic crystalline basement is covered by Ediacaran-Cambrian autochthonous sedimentary rocks beneath allochthonous Caledonian thrust sheets (gray line), the projection of the Laisvall ore deposit, and the trace of the fault at the ground surface along Lake Hornavan are also shown. C. Linear magnetic anomalies (magnetic minima and maxima) interpreted using the TMI map. D. Geologic map of the Laisvall area at the ground surface (modified after Lilljequist, 1973). The outline of the Laisvall ore deposit, which is hosted by autochthonous Ediacaran-Cambrian sandstone, and the top surface of the volume selected for modeling work in this study are projected to this surface. E. Detailed view of the spatial relationships between lineaments defined by magnetic minima using the maxima-minima approach and edges from the edge detection approach, the known faults A and B shown in (D), and the ore deposit in the Laisvall area.

dependent on the origin and geologic history of the rock). The intensity of induced magnetization is related to the intensity of the ambient field through the magnetic susceptibility of the rock considered (Hildenbrand et al., 2001). This magnetic susceptibility constant is directly proportional to the modal mineral composition and chemistry of the rock (Hildenbrand et al., 2001).

Rocks have widely varying magnetic properties (Carmichael, 1982; Clark, 1997a, b). At the regional scale, magnetic highs are commonly associated with major igneous provinces in crystalline basement. By contrast, magnetic lows often occur in areas dominated by thick sedimentary basins (e.g., Hildenbrand et al., 2001) or where, for example, igneous rocks are altered and magnetite was replaced by hematite when

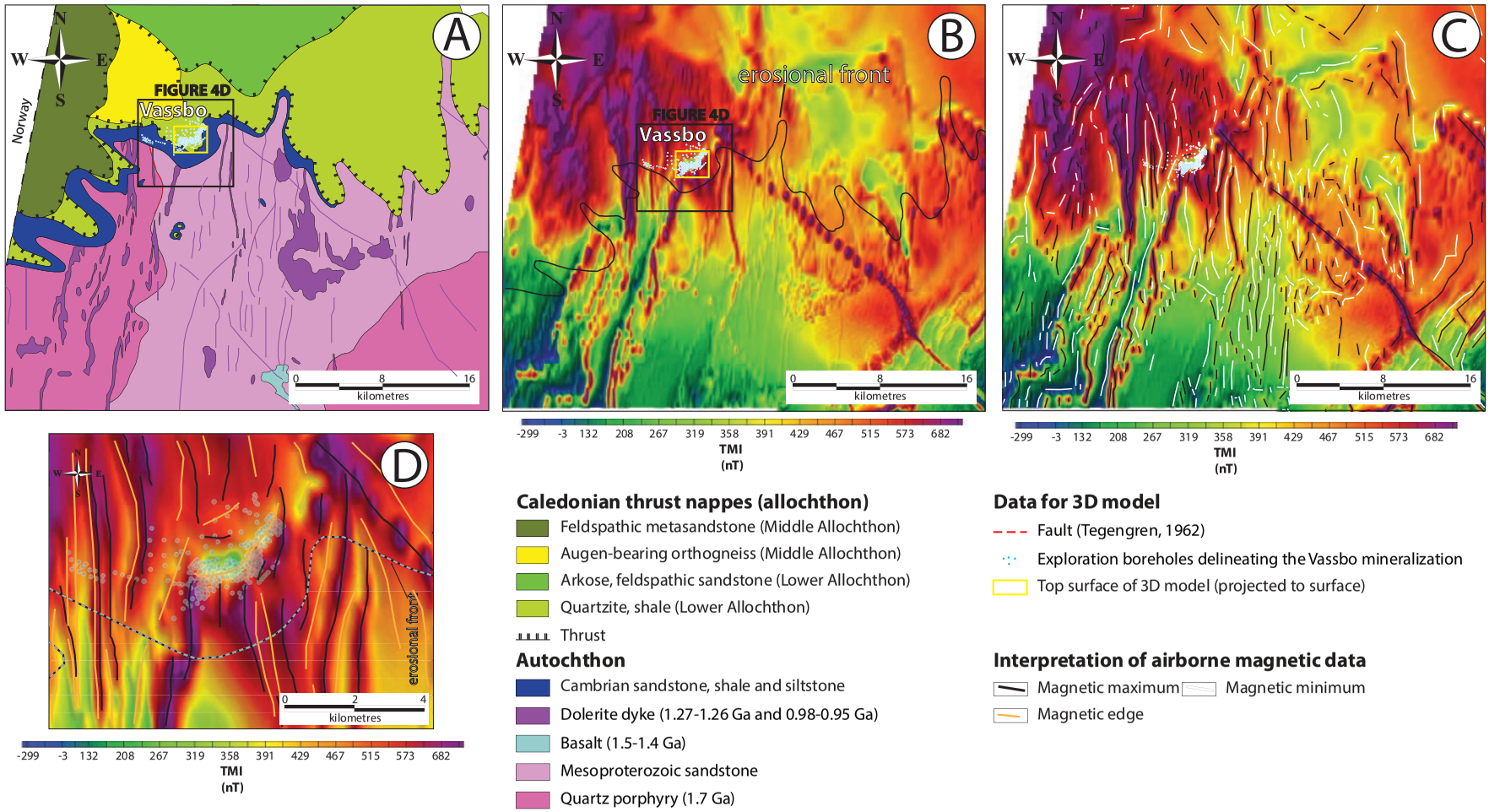

FIG. 4. A. Geologic map of the Vassbo area at the ground surface (modified after Tegengren, 1962, and after the acquisition of data from the Geological Survey of Sweden´s bedrock map database). The purple lines represent inferred dolerite dikes, interpreted solely from geophysical data (Geological Survey of Sweden's bedrock map database). Exploration boreholes delineate the shape of the Vassbo orebody hosted by autochthonous Cambrian sandstone. The top surface of the volume selected for modeling work in this study is also projected to the ground surface. B. TMI airborne magnetic map of the Vassbo area. The erosional front where Proterozoic crystalline basement is covered by Cambrian autochthonous sedimentary rocks beneath allochthonous Caledonian thrust sheets (black line) and the projection of the Vassbo ore deposit are also shown. The strong linear feature with northwest trend that extends as a series of beads strung along a line is an artifact due to survey design (see text for explanation). C. Linear magnetic anomalies (magnetic minima and maxima) interpreted using the TMI map. D. Detailed view of the spatial relationships between lineaments defined by magnetic maxima using the maxima-minima approach and edges from the edge detection approach, and the ore deposit in the Vassbo area.

hydrothermal fluids have migrated along faults. Grant et al. (1985a, b) emphasized that the magnetic response observed in magnetic anomaly maps is influenced by the geometry and depth of the magnetic bodies, their azimuth with regard to magnetic north, and the inclination of the magnetic field at the latitude of the survey. In the neighborhood of mineral deposits, the mineralogical variety and thermal history related to mineral deposits can subsequently affect magnetic properties. The degree of oxidation, alteration, weathering, and metamorphism also affects the magnetic properties of the rock (Hildenbrand et al., 2001). All these combined factors concur to generate complex pictures of magnetic properties in airborne magnetic maps.

Airborne magnetic data, acquired by the Geological Survey of Sweden during 2005 and 2009 in the Vassbo and Laisvall areas, respectively, have been extracted, processed, and interpreted in this study. The geophysical surveys were all carried out in a west-east direction at an altitude of 60 m and the data were acquired at the same resolution of 0.1 nT. However, line and point spacings were different in the Laisvall (200 and 7 m, respectively) and Vassbo (800 and 16 m, respectively) areas (Table 1). As a basis for detailed lineament interpretation, the data were processed by Boliden geophysicists as Geosoft XYZ files and bidirectional gridding was used with a grid cell size equal to the point spacing in each area.

Lineaments defined by magnetic anomalies were systematically identified by drawing lines corresponding to maxima and minima ("maxima-minima approach") in a subjective manner by eye using total magnetic intensity (TMI) and first vertical derivative (FVD) maps. Lineaments defined by magnetic minima that are discordant to main geologic trends defined by magnetic anomalies (alternating maxima and minima considering the maxima-minima approach) have been exposed by dredging or drilled at several places in Sweden and have been shown to represent faults (Henkel and Guzmán, 1977; SKB, 2008, p. 124–128). Lineaments defined by narrow magnetic maxima can assist in the identification of, for example, dolerite dikes that have a high magnetic susceptibility with respect to surrounding rocks. An alternative approach involves the use of analytical signal (AS) and tilt derivative (TD) maps to detect edges along magnetic gradients, which can also help to detect faults (Nabighian et al., 2010, and references therein). Linear features were once again drawn subjectively by eye along major gradients in the magnetic data in AS maps, and these features were checked and proofed in TD maps, and finally referred back into TMI maps.

Table 1. Technical and Survey Characteristics of the Airborne Magnetic Data[1]

Map ID	Location	Survey ID	Survey year	Line spacing/ point spacing (m)
16CDv	Vassbo	FTBC	2005	800/16
26Hno	Laisvall	FXBB	2009	200/7
26Hnv	Laisvall	FXBB	2009	200/7
26Hsv	Laisvall	FXBB	2009	200/7

[1] Data acquired by the Geological Survey of Sweden and were processed as a basis for a detailed lineament interpretation in the Laisvall and Vassbo areas

In summary, this study has adopted both the "maxima-minima approach" and the "edge detection approach" in order to test whether lineaments defined by magnetic anomalies arise from the crystalline basement lying beneath the autochthonous sedimentary cover rocks and allochthonous Caledonian thrust nappes at Laisvall and Vassbo, and to evaluate to what extent these features delineate faults in the basement.

In order to assist with this exercise, magnetic susceptibility values for different geologic units in the crystalline basement, in the sedimentary cover rocks, and in the Caledonian thrust nappes in the Laisvall (Fig. 3A) and Vassbo (Fig. 4A) areas were extracted from the petrophysical database at the Geological Survey of Sweden (Tables 2 and 3, respectively). It is worth noting that the airborne magnetic surveys close to Laisvall and Vassbo were carried over mined-out sphalerite-galena ± pyrite orebodies, i.e., deposits containing nonmagnetic minerals.

Laisvall area

The TMI map over the Laisvall area, including the erosional front where Paleoproterozoic crystalline basement is covered by Ediacaran-Cambrian autochthonous sedimentary rocks beneath allochthonous Caledonian thrust sheets (Fig. 3A), is presented in Figure 3B. The thickness of the allochthonous and autochthonous units amounts to 200 to 300 m (Lilljequist, 1973; Willdén, 1980).

Figure 3C shows the linear magnetic anomalies that were interpreted in the Laisvall area and classified as "magnetic maxima" or "magnetic minima" using the maxima-minima approach. The magnetic lineaments fall into two main sets: (1) N-S to NE-SW and (2) WNW-ESE to NW-SE. Areas where the trend of the lineaments changes abruptly are also observed. The outline of the Laisvall orebodies is spatially associated with one of these areas, the lineament trend changing from NE-SW to NW-SE; the orebodies appear to follow a mainly NE-SW trend (Fig. 3C). There appears to be no break in magnetic anomaly trends or patterns across the erosional front (Fig. 3B). The trends in magnetic anomalies mapped using the maxima-minima approach are the same on both sides of the front and they match the regional NNE-SSW and NW-SE geologic trends in the crystalline basement of the Fennoscandian Shield in the Laisvall area (Fig. 3A, B).

Both the autochthonous sedimentary cover rocks and the Caledonian allochthonous units comprising metamorphosed sedimentary rocks and even mylonitic granite have distinctly lower magnetic susceptibility values than the rocks in the Paleoproterozoic crystalline basement in the Laisvall area (Table 2). In addition, the variable composition of the rocks in the basement is accompanied by variable magnetic susceptibility values (Table 2), which is important for detecting internal structures in the basement. These observations suggest that the rocks in the autochthonous cover and in the allochthonous thrust nappes are not sufficiently magnetic to produce anomalies that mask the signal from the underlying crystalline basement. By consequence, it is inferred that the magnetic data and inferred lineaments are providing information on the geology in the autochthonous crystalline basement. In particular, it is possible to use magnetic anomaly patterns in order to map basement structures beneath the autochthonous sedimentary rocks and Caledonian allochthonous units to the west of their erosional front.

Table 2. Magnetic Susceptibility Data of the Different Rock Types in the Crystalline Basement, the Autochthonous Sedimentary Cover Rocks, and the Caledonian Allochthons in the Laisvall Area[1]

Lithology in the Caledonian allochthons and autochthonous sedimentary rocks	Count (n = x)	Magnetic susceptibility ($\times 10^{-6}$ SI units), median
Schist, amphibolite (Seve Nappe Complex)	7	266.90
Feldspathic metasandstone (Middle Allochthon)	1	364.00
Mylonitic granite (Middle Allochton)	5	231.00
Quartzite, shale (Lower Allochthon)	2	131.20
Ediacaran-Cambrian sandstone, shale, and siltstone	7	37.71
Lithology in the crystalline basement	**Count (n = x)**	**Magnetic susceptibility ($\times 10^{-6}$ SI units), median**
Dolerite dike	4	26090.00
Granite	109	3177.00
Granite, pegmatite	52	3935.50
Granite, quartz monzonite	11	2033.00
Gabbro, diorite	1	11640.00
Acid metavolcanic rock	19	10360.00
Sediment enclave in granite	8	19890.00
Metasedimentary rock	2	59213.00

[1] Data extracted from the petrophysical database at the Geological Survey of Sweden

Table 3. Magnetic Susceptibility Data of the Different Rock Types in the Crystalline Basement, the Autochthonous Sedimentary Cover Rocks, and the Caledonian Allochthons in the Vassbo Area[1]

Lithology in the Caledonian allochthons and autochthonous sedimentary rocks	Count (n = x)	Magnetic susceptibility ($\times 10^{-6}$ SI units), median
Feldspathic metasandstone (Middle Allochthon)	11	90.00
Mylonitic granite (Middle Allochton)	7	720.00
Quartzite, shale (Lower Allochthon)	2	45.00
Cambrian sandstone, shale, and siltstone	1	360.00
Lithology in the crystalline basement	**Count (n = x)**	**Magnetic susceptibility ($\times 10^{-6}$ SI units), median**
Dolerite dike	10	21335.00
Basalt	2	11485.00
Mesoproterozoic sandstone	17	60.00
Quartz porphyry	7	210.00
Acid volcanic rock	4	145.00

[1] Data extracted from the petrophysical database at the Geological Survey of Sweden

The trace of the fault at the ground surface along Lake Hornavan is shown in Figure 3A and B. This regionally significant fault in the Paleoproterozoic crystalline basement defines the contact between 1.8-Ga granite to the south and other crystalline rocks to the north (Fig. 3A). It is identified as a series of magnetic minima with NW-SE trend that are concordant with magnetic maxima (Fig. 3B, C). The 1.8-Ga granite crops out to the south of the Laisvall mine area along the Laisan River (Fig. 3D). It is characterized by steeply dipping to vertical NNW- and NNE-striking fractures and veinlets (up to 1 cm in width), locally filled with quartz and minor pyrite. The granite shows hematite alteration after magnetite on the walls of these fractures.

Figure 3E is a detailed view of the TMI map in the Laisvall area as delineated in Figure 3D. Earlier work identified faults in the Laisvall area using aerial photographs and field studies (Fig. 3D). These faults have two main orientations, NNE-SSW and NW-SE (Lilljequist, 1973). Some faults cut through both the autochthonous Ediacaran-Cambrian cover rocks and the allochthonous thrust nappes (e.g., fault A, Fig. 3D) and were characterized as being related to orogenic collapse (Lilljequist, 1973). As a result of the degree of erosion to the current land surface, some faults are only shown to affect the autochthonous rocks (e.g., fault B, Fig. 3D). Faults A and B show a spatial correlation with magnetic minima that trend NE-SW and NNE-SSW, respectively (Fig. 3E). In addition, the edge detection approach shows that the traces of both faults A and fault B are parallel to one or several straight edges. Since the current work shows that at least some concordant minima correspond to a fault in the Paleoproterozoic crystalline basement, it is inferred that the faults identified by Lilljequist (1973) not only affect both the allochthonous thrust nappes and the autochthonous sedimentary cover rocks but are also rooted downward in the Paleoproterozoic basement.

Vassbo area

The TMI map over the Vassbo area, including the erosional front where Paleoproterozoic and Mesoproterozoic crystalline basement rocks are covered by Cambrian autochthonous sedimentary rocks beneath allochthonous Caledonian thrust sheets (Fig. 4A), is presented in Figure 4B. There are some problems in interpreting this map because of the survey design (Table 1). Data derived from airborne measurements at 60 m above the ground with line spacing of 800 m are problematic for the identification of linear magnetic sources that are shallow. According to Reid (1980), to properly evaluate the magnetic fields produced by two-dimensional magnetic sources (such as dikes and faults), the optimum ratio of line spacing to height above the sources should be 2/1 along lines flown approximately perpendicular to strike. For the present Vassbo survey design, it means that sources need to be at least 340 m below the ground for their anomalies to be properly presented in the magnetic field map. The consequences for shallower anomalies is well presented by the strong linear feature with a northwest trend (Fig. 4B) that extends as a series of beads strung along a line toward the southeast corner of the image. The width of each bead is a function of line spacing. The bidirectional gridding approach, which was used in this study, helps to combat the problem, but also tends to elongate everything in the N-S direction perpendicular to the flightline direction and thus isolate the beads. In addition, E-W linear trends might be difficult to capture with such a survey design. These problems have been kept in mind while examining the regional orientations of linear sources.

Magnetic lineaments were identified using the maxima-minima approach (Fig. 4C) and, additionally, in the vicinity of the mine area, using the edge detection approach (Fig. 4D). They have been classified as belonging to two main sets: (1) NNE-SSW to NNW-SSE and (2) NW-SE to W-E. In some areas, lineaments change in trend from NNE-SSW to WNW-ESE or W-E and, as at Laisvall, the outline of the Vassbo orebody is spatially associated with one such area, which is most clearly expressed by the change in trend of the magnetic edges (Fig. 4D). There appears to be no break in magnetic anomaly trends or patterns across the erosional front. The trends in magnetic anomalies mapped using the maxima-minima approach are the same on both sides of the front and they match the regional N-S and NNE-SSW geologic trends in the crystalline basement in the Vassbo area (Fig. 4).

Table 3 shows that the autochthonous sedimentary cover rocks and the allochthonous metamorphic rocks derived from sedimentary rocks have similar magnetic susceptibilities as the sandstone and felsic igneous rocks in the Proterozoic basement in the Vassbo area. Only the mylonitic granite in the Middle allochthon, with restricted surficial extent, has higher magnetic susceptibilities than these basement lithologies. By contrast, the numerous dolerite dikes and basalt in the crystalline basement have significantly higher magnetic susceptibilities (Table 3) than all the other rock types in the study area. These observations suggest that the signal in the TMI maps is markedly influenced by dolerite dikes and basalt, and that the magnetic data are depicting basement geologic features across the whole study area. In particular, the magnetic maxima and sharp edges in the Vassbo area are coupled to dolerite dikes with NNE-SSW or NW-SE trend, which intruded into the older Proterozoic basement (cf. Fig. 4). Thus, as in the Laisvall area, it is inferred to be possible to use magnetic anomaly patterns in order to map basement structures even beneath the autochthonous sedimentary rocks and Caledonian allochthonous units to the north of their erosional front.

The dolerites can be followed using the magnetic data beneath the overlying allochthonous thrust sheets in the Caledonian orogen (Fig. 4C). Changes in trend along the magnetic maxima (Fig. 4C) and edges (Fig. 4D) are inferred to be related to folding that shows a Z-shaped asymmetry. The folding probably took place during the later stage of the Sveconorwegian orogeny and inside the immediate foreland to this orogenic system (Fig. 1A). In the vicinity of the Vassbo mine, borehole data were available to fine tune the location of a dolerite dike beneath the mine and constrain the folding and hydrothermal alteration of this dike (see "Modeling of Lithologic Units and Ore Grades in Three-Dimensional Space at the Vassbo Strata-Bound Pb-Zn Deposit").

Tegengren (1962) suggested that a regionally significant fault separates the Mesoproterozoic sandstone from the 1.7-Ga quartz porphyry in the crystalline basement (Fig. 4A). On the other hand, no faults have been mapped at the ground surface as being related to the location of dolerite dikes in the basement. Experimental work by Abdelmalak et al. (2012) showed that dikes establish zones with a high frequency of fractures in connection with their emplacement and preferentially intrude along preexisting faults in the basement. Thus, a distinctive bedrock fracture network close to the dolerite dikes is inferred to be present and edges associated with these dikes may not simply represent the boundaries to the dolerite dikes but also faults in the basement.

Modeling of Faults, Lithostratigraphic Units, and Ore Grades in Three-Dimensional Space at the Laisvall Strata-Bound Pb-Zn Deposit

Data and general methodology

The Laisvall deposit was extensively drilled by Boliden AB for brown-field and subsequent near-mine exploration from the 1930s to the 2000s. Approximately 1,200 boreholes were drilled. Geologic and both Pb and Zn grade data in the autochthonous sedimentary rocks were available for 1,120 boreholes, 90% of which are vertical (Fig. 5). Information on the location and character of faults in the mine and in the field was obtained by relogging selected boreholes at the Geological Survey of Sweden core storage facilities in Malå and reinterpreting, where necessary, the existing information from Boliden AB archives and from the literature (Lilljequist *in* Boliden AB unpub. internal reports, 1965, 1968; Carlson *in* Boliden AB unpub. internal reports, 1970; Lilljequist, 1973; Rickard et al., 1979; Lucks, 2004). Key geologic cross sections have been drawn and allowed to identify breaks in the stratigraphy and, in combination with the character of the rocks, in the drill core (e.g., occurrence of core loss, crushed core, probable fault gouge, fracture intensity), provided a further basis for the location of the more important faults.

Modeling of faults, lithostratigraphic units, and ore grades in three-dimensional space at the Laisvall deposit has been carried out inside the area shown in Figure 3D between

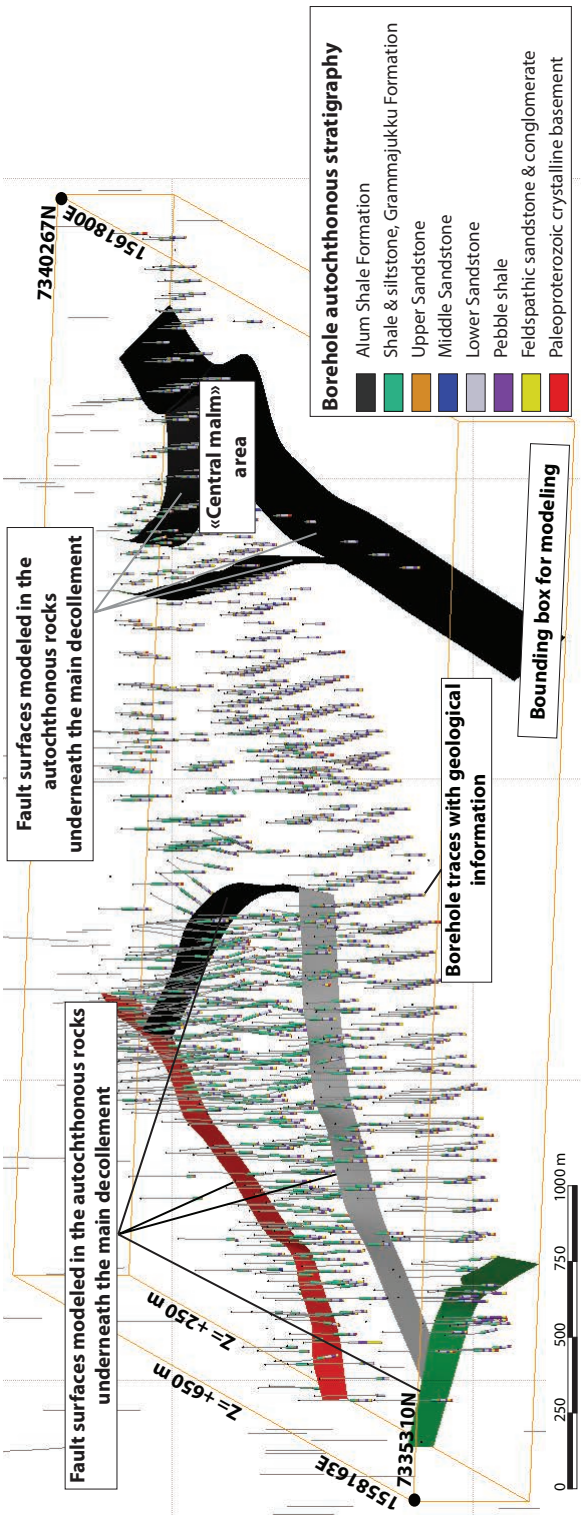

FIG. 5. Leapfrog three-dimensional model view (to north-northeast), showing the borehole database with geologic information at the Laisvall ore deposit inside the bounding box designed for modeling. Fault surfaces were constructed in the autochthonous sedimentary rocks underneath the main decollement in the Alum shale formation using legacy mine data, published literature, and the information along geologic cross sections.

+650- and +250-m elevation, underneath the Middle Cambrian Alum Shale Formation where the main decollement beneath the Lower allochthon in the Caledonian orogen is located (Fig. 5). The model volume extends downward into the upper part of the 1.8-Ga granitic crystalline basement (Fig. 2). The contact to the Alum Shale Formation defines an upper bounding surface in the model volume. The choice of this upper surface was justified by the poor core recovery above the decollement, as well as the fact that numerous parts of drill cores located above this decollement were not systematically preserved and stored. The lower bounding surface was defined by the intersections of boreholes with the basement. The corners of the model volume were set around the most densely drilled area where information on faults in the mine and grade data were available. Delineation of lithostratigraphic units and ore grades in three-dimensional space was carried out using Leapfrog Mining three-dimensional software after having modeled fault surfaces in the autochthonous sedimentary sequence (Fig. 5).

Fault model

Fault surfaces were defined by first constructing a polyline corresponding to the intersection between the upper bounding surface and a given fault, as recognized in the previous work at the mine. Subsequently, the dip, sense of movement, and amount of throw were determined in the key geologic cross sections and during the core logging exercise. Based on the construction of the polyline and the dip information at different levels in the autochthonous sedimentary rocks, the fault surfaces were calculated in three-dimensional space. A plan view at the elevation of the upper bounding surface showing the fault surface intersections with this surface and the intervening structural blocks is presented in Figure 6A. Two of these faults (Kautsky and Nadok faults) were recognized during earlier work in the mine (Lilljequist, 1973; Rickard et al., 1979; Lucks, 2004) and two others (Kramaviken and Niepsurt faults; Fig. 6A) have been identified in this study. Fault segments trend NNE-SSW, NE-SW, NNW-SSE or WNW-ESE to NW-SE. It is suggested that fault A and fault B, which both affected the allochthonous and autochthonous units (Lilljequist, 1973; Fig. 3D, E) and were previously shown to be associated with basement magnetic edges, correspond to parts of the Nadok and Kramaviken faults, respectively, in sandstone in the mine.

The Kautsky fault (Fig. 6) is described as comprising three segments: (1) a NNE-SSW-striking northern segment, (2) a zone of en échelon segments striking N 170° to N 189°, and (3) a NNW-striking southern segment (Lucks, 2004). The fault dips steeply to the west and shows both normal and later reverse senses of displacement and a 30-m throw; it is subsequently cut by low-angle thrusts (Rickard et al., 1979; Lucks, 2004). The location of the Kautsky fault was confirmed in this study on the basis of the occurrence of considerable core loss and fracture networks in drill cores.

Rickard et al. (1979) and Lucks (2004) described the Nadok fault (Fig. 6) as a subvertical, normal fault comprising four segments striking N 019°, N 052°, N 139°, and N 175°. Current work shows that it dips steeply to the west. Furthermore, the northern segment shows a downthrown side to the west with a vertical displacement of 16 to 20 m while the southern

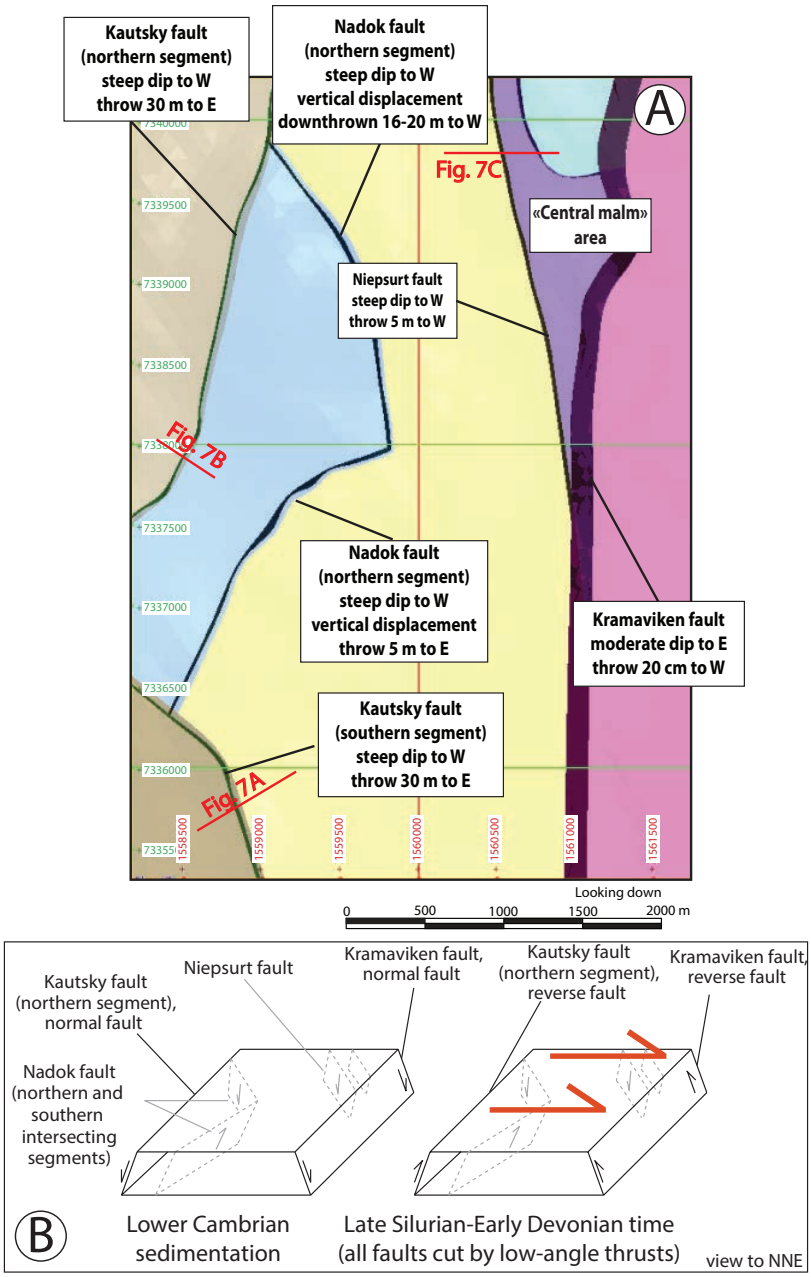

FIG. 6. A. Map view of the upper surface in the bounding modeling box (Fig. 5), showing the tectonic framework of the main faults in the autochthonous sedimentary rocks at the Laisvall ore deposit. Colors indicate the different blocks that were delineated and bounded by the faults. Lithostratigraphic units and ore grades were modeled independently within each fault-bounded block. No modeling work was completed in the brown-colored domains to the west of the two segments of the Kautsky fault due to the paucity of data. The locations of the geological cross sections presented in Figure 7 are shown. B. Interpretative conceptual cartoon of the timing, variable sense of displacement, and formation of the faults at Laisvall.

segment shows a vertical displacement of 5 m to east. This suggests that the block between the northern segment of the Kautsky fault and the two intersecting segments of the Nadok fault was tilted at some stage. Rickard et al. (1979, p. 1263) suggested that the "Nadok fault penetrates the autochthonous sequence from within the basement." The Nadok fault is transected by and predates the Kautsky fault (Rickard et al., 1979; Lucks, 2004).

Lilljequist (1973) suggested that a NNE-striking fault zone with a moderate dip to the east affected the northeastern part of the Laisvall mine (the so-called "Central Malm;" Fig. 5). This fault contains slickenlines indicating reverse movement with a throw of at least 20 cm. In addition, Lilljequist (1973) identified in the field a fault striking NNE, which affected the autochthonous cover rocks on the Kramaviken peninsula along the western shore of the Laisan River (fault B, Fig. 3D). He inferred that the fault in the mine was most probably the continuation of the fault at Kramaviken. The paucity of drill holes between the Central Malm and Kramaviken (Fig. 5) does not enable us to link with confidence these two

structures. However, the fault in the mine was clearly recognized in the core logging and in the constructed geologic cross sections completed in the current work, as Lilljequist (1973) had suggested. We chose to name this fault the Kramaviken fault (Fig. 6A).

Less than 500 m to the west of the Kramaviken fault, a NNW-oriented zone was identified in the present study by significant breaks in stratigraphy and by the concentration of core loss in the autochthonous cover rocks in drill cores in no less than 15 boreholes. In addition, Lucks (2004) had showed, on the basis of unpublished structural maps, that several NNW-striking "minor extensional faults" were concentrated in this part of the mine. This concomitant evidence served as a basis to construct the Niepsurt fault (Fig. 6A). This fault could not be traced in the few boreholes located to the southeast of the Kramaviken fault. It is inferred that the Niepsurt fault predates and is cut by the Kramaviken fault with its reverse sense of movement. A possible minor fault was recognized northeast of the Niepsurt fault through core logging and breaks in stratigraphy. This fault is subparallel to the Niepsurt fault and also terminates against the Kramaviken fault (Fig. 6).

In summary, the Laisvall deposit is bounded by reverse faults on its western and eastern sides with steep dips to the west and east, respectively, and at least one of these faults (the Kautsky fault) moved in a normal sense prior to being active in a reverse mode (Rickard et al., 1979; Lucks, 2004). Faults with a normal sense of movement are sandwiched between the bounding reverse structures. All these steeply dipping structures are cut by low-angle thrusts. This overall architecture could tentatively be interpreted as a minor horst bounded by two major normal faults (e.g., the NNE-SSW-striking and W-dipping northern segment of the Kaustky fault, and the NNE-SSW-striking E-dipping Kramaviken fault) that were subsequently inverted into reverse faults prior to being cut by low-angle thrusts (Fig. 6B).

Model for lithostratigraphic units and the interplay with faults

Several structural blocks emerged when consideration was taken of the three-dimensional spatial distribution of the bounding faults described above (Fig. 6A). Each lithostatigraphic unit in the Laisberg Formation was then modeled independently in each block. The hanging-wall side of the northern and southern segments of the Kautsky fault was omitted from the workflow to model lithostratigraphic units (and ore grades) due to the paucity of continuous geologic and grade data in boreholes in this part of the model volume. The Leapfrog Mining three-dimensional software allowed the extraction of the hanging-wall and footwall contact points of each unit in all the boreholes considered in the model volume (Fig. 5). Within each fault-bounded block, the hanging-wall and footwall surfaces were then computed for each unit from the corresponding contact points and a volume for each lithostratigraphic unit was defined. Building on earlier findings concerning the stratigraphic sequence and sedimentology at Laisvall (Rickard et al., 1979; Willdén, 1980; Lucks, 2004) and the current three-dimensional modeling work, it has been possible to evaluate the relationships between faults and sedimentation and to study the influence of faults on sedimentary facies distribution and thickness variations.

In the southwestern part of the mine (Fig. 6A), the Ediacaran pebble shale horizon is up to 30 to 40 m thick in the southwestern hanging wall of the Kautsky fault. Against this fault and up to ca. 100 m southwest of it, the pebble shale is locally replaced by a succession comprising a few meters of pebble shale overlain by 17 to 19 m of white sandstone resembling the Lower Sandstone, again capped by pebble shale for a few meters (Fig. 7A). Willdén (1980) interpreted this sandstone member to represent a beach in an overall bay environment during the distal glacial conditions proposed for the pebble shale horizon. However, Willdén reported thicknesses of only ca. 3 to 4 m for this sandstone horizon. Higher up in the stratigraphic sequence, in the same area, thickness variations exist in the Middle Sandstone. This unit is 6 to 7 m thick ca. 200 m southwest of the Kautsky fault, and thickens to 9 to 10 m against the fault (Fig. 7A). Breccia, inferred to be fault related in two of the boreholes (LAI 1013 and 1019), is ubiquitous at the bottom of the Middle Sandstone in the northeastern footwall. Immediately northeast of the Kautsky fault, the Middle Sandstone is only 1 to 3 m thick, while 250 m northeast of the fault, it thickens to 12 to 15 m. Significant facies changes are also present across the northern segment of the Kautsky fault in the Lower Sandstone unit, where sandstone passes eastward into shale and siltstone in the hanging wall to the west of the fault. This shale and siltstone unit is completely absent in the Lower Sandstone unit in the footwall to the east. In addition, thickness variations in the Middle and Upper Sandstone units are conspicuous on either side of the northern segment of the Kautsky fault (Fig. 7B).

In summary, these observations indicate variations in facies and thickness at the meter scale of lithostratigraphic units across the Kautsky fault as well as the development of fault-related breccia during the Lower Cambrian in the vicinity of this structure. Facies changes and thickness variations at the meter scale in the Lower, Middle, and Upper Sandstone units are also conspicuous on either side of the Niepsurt fault (Fig. 7C).

Relationships between basement faults and the faults at mine scale

The inset map in Figure 8A serves as the basis to establish some evidence for the relationships between the basement faults identified by the interpretation of airborne magnetic data and the faults found in the mine from mapping and core examination.

The Niepsurt and Kramaviken faults are spatially associated with and show similar orientations as magnetic edges with NNW-SSE and NNW-SSE or NNE-SSW trends, respectively. Similarly, the northern segment of the Nadok fault and the area where this segment meets the southern segment of the same fault are spatially associated with edges that show NE-SW and NW-SE trends, respectively. The southern segment of the Kautsky fault shows the same trend as and is subparallel to an edge with NW-SE trend. The convergence of three edges occurs in the area of intense core loss and fracture density (beige-shaded rectangle in Fig. 8A), where faulting in sandstone is inferred.

These observations suggest a close relationship between basement faults inferred from the magnetic data and the mapped faults in the mine where the basement features

appear to affect the trends of overlying faults in sandstone or interact with them. However, the correspondence is not a simple one-to-one relationship.

Ore grade model

Grade data for Pb and Zn were modeled independently in each fault-bounded block (Fig. 6A) using assayed drill core. Data were filtered for Pb and Zn values exceeding 0.1%. The Laisvall mine has two distinct orebodies in the Laisberg Formation; the Lower Sandstone Pb-Zn and the Upper Sandstone Zn-Pb orebodies (Rickard et al., 1979). Mineralization is dominated by Pb in the Lower Sandstone Pb-Zn orebody (Fig. 8B), with Zn grades generally below 0.5%; there are only four areas where Zn grades are above 1% (marked by purple stars, Fig. 8B). By contrast, both Pb and Zn values are available for the Upper Sandstone Zn-Pb orebody (Fig. 8C). Threshold and bin values for Pb and Zn grades (Fig. 8B, C) are based on variograms of grade distribution in Leapfrog Mining three-dimensional software with localized outliers above 5% Pb and Zn and numerous mineralized zones between 0.1 and 0.5% Pb or Zn. For clarity, five classes between 1 and 5% and above 5%, with a step size of 1%, are displayed for Pb grades. Five classes between 0.1 and 5% are shown for Zn grades.

The main elongation of the Pb-Zn orebodies is NE-SW, along a trend parallel to the southern segment of the Nadok fault, and locally changing to NW-SE (Fig. 8B, C). The Pb grades in the Lower Sandstone Pb-Zn orebody show two additional prominent features (Fig. 8B). First, there is a concentration of the highest Pb grades on either side of and close to the southern segment of the Nadok fault where there are also clear signs of postmineralization faulting (Rickard et al., 1979). Pb grades are between 2 and 5% (and locally >5%) within a 200- to 250-m radius from the fault and they progressively diminish to 1% away from the fault (Fig. 8B). The same area in relationship to the southern segment of the Nadok fault is characterized by three points with Zn grades above 1% (Fig. 8B). Second, Pb grades between the Nadok and Niepsurt faults display a change in mineralization trend from NE-SW to NNW-SSE and then back to NE-SW (Fig. 8B). Higher Zn grades in the Lower Sandstone Pb-Zn orebody are closely linked to this change in mineralization trend. Between the Niepsurt and Kramaviken faults, in the northeastern part of the mine (Central Malm, Fig. 6), a similar NE-SW to NW-SE change in mineralization trend is present with again higher Pb grades close to the faults (Fig. 8B). There are also signs of faulting that displaces mineralization in this part of the mine (Lilljequist, 1973).

The pattern of Pb and Zn grade shells in the Upper Sandstone Zn-Pb orebody is shown in Figure 8C. Pb grades display the same geometry with respect to the southern segment of the Nadok fault as observed in the Lower Sandstone Pb-Zn orebody (Fig. 8C). However, it is important to note that the

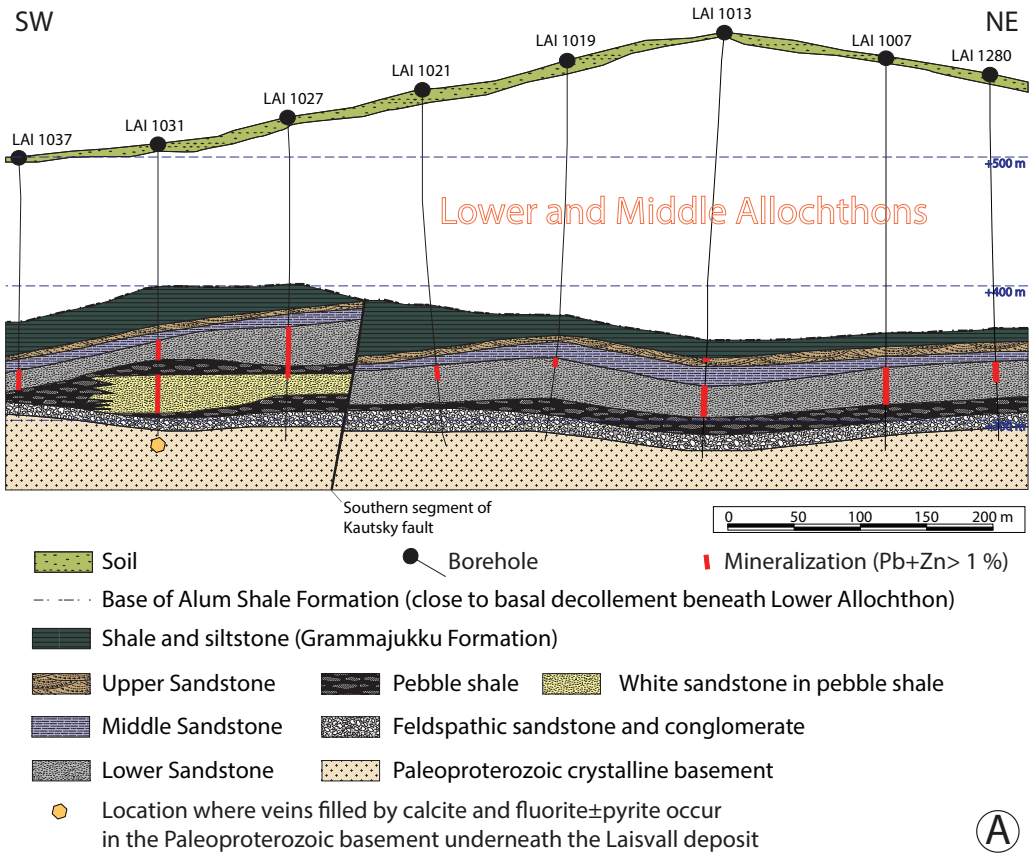

FIG. 7. A. Geologic cross section through the southern segment of the Kautsky fault in the southwestern part of the Laisvall orebody. B. Geologic cross section through the northern segment of the Kautsky fault in the western part of the Laisvall orebody. C. Geologic cross section through the Niepsurt fault in the northeastern part of the Laisvall orebody.

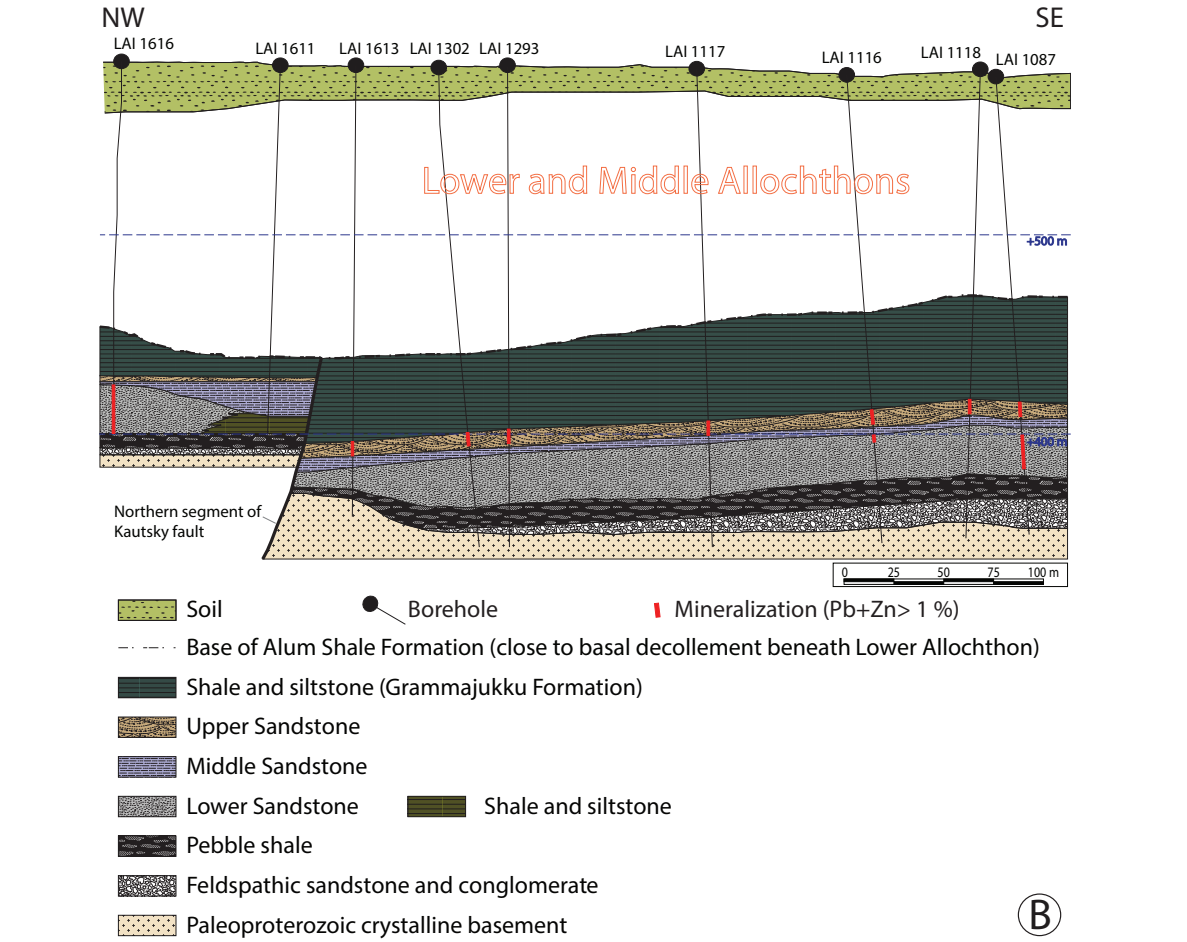
NW
SE
LAI 1616
LAI 1611
LAI 1613
LAI 1302
LAI 1293
LAI 1117
LAI 1116
LAI 1118
LAI 1087
Lower and Middle Allochthons
+500 m
+400 m
Northern segment of Kautsky fault
0 25 50 75 100 m
Soil
Borehole
Mineralization (Pb+Zn> 1 %)
Base of Alum Shale Formation (close to basal decollement beneath Lower Allochthon)
Shale and siltstone (Grammajukku Formation)
Upper Sandstone
Middle Sandstone
Lower Sandstone
Shale and siltstone
Pebble shale
Feldspathic sandstone and conglomerate
Paleoproterozoic crystalline basement
B

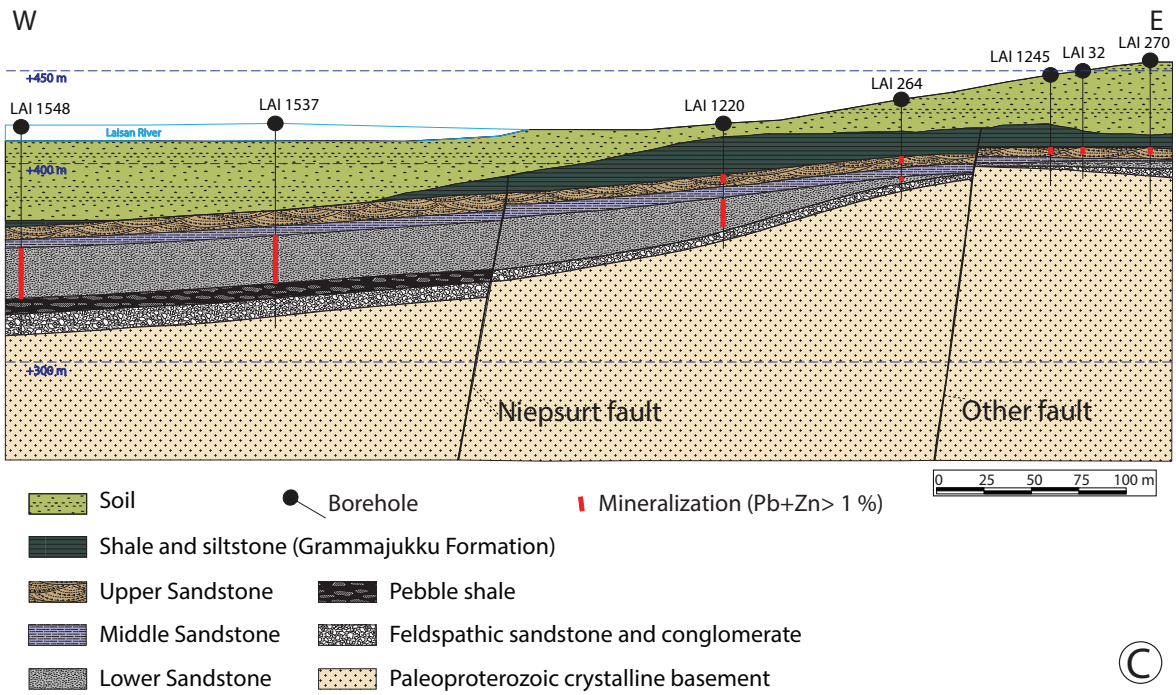
W
E
+450 m
LAI 1548
LAI 1537
LAI 1220
LAI 264
LAI 1245
LAI 32
LAI 270
Laisan River
+400 m
+300 m
Niepsurt fault
Other fault
0 25 50 75 100 m
Soil
Borehole
Mineralization (Pb+Zn> 1 %)
Shale and siltstone (Grammajukku Formation)
Upper Sandstone
Pebble shale
Middle Sandstone
Feldspathic sandstone and conglomerate
Lower Sandstone
Paleoproterozoic crystalline basement
C

FIG. 7. *(Cont.)*

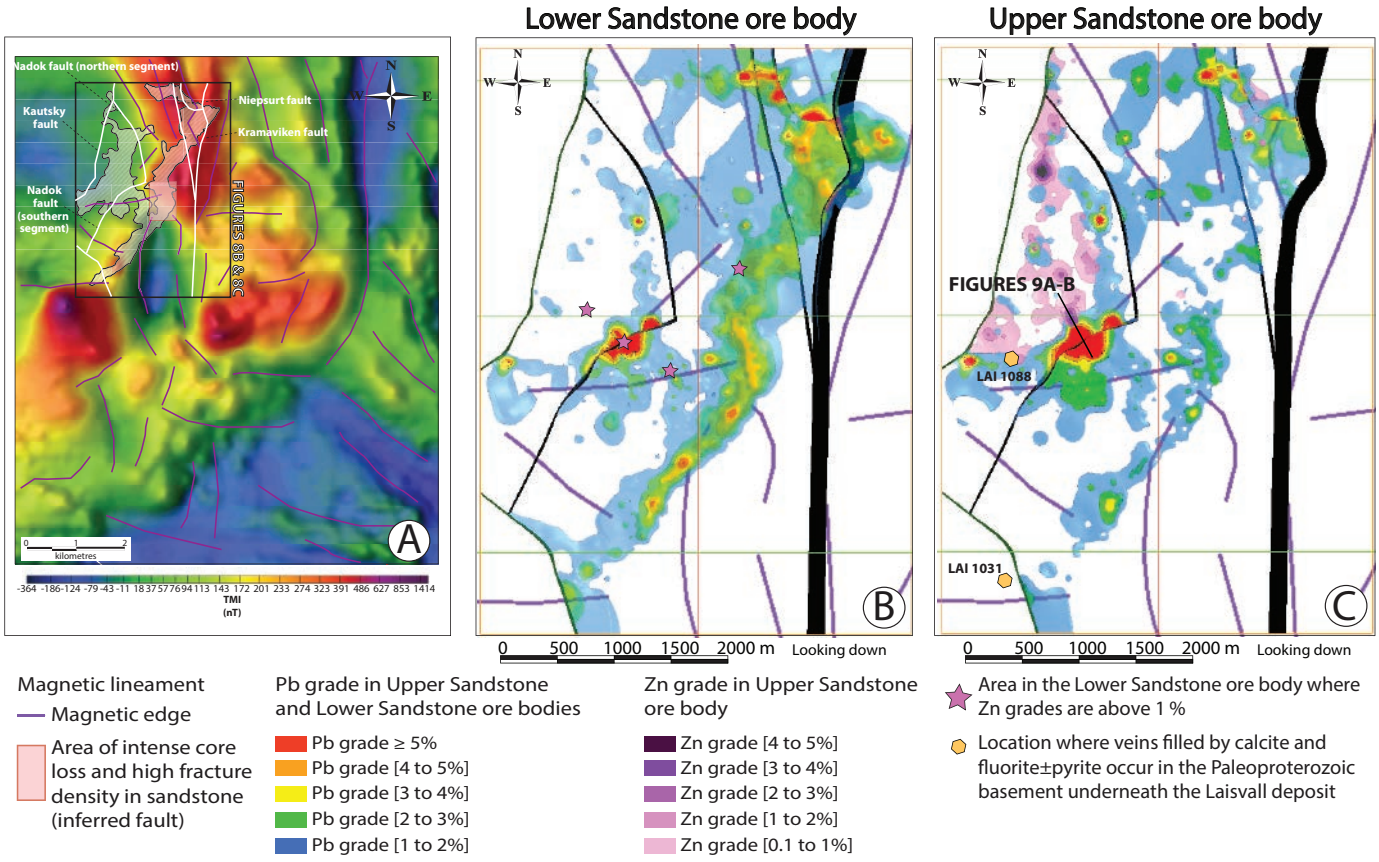

FIG. 8. A. Same map view as in Figure 3E showing the spatial relationship between lineaments defined by edges along magnetic gradients (purple lines) and the faults (white lines) at the Laisvall ore deposit as presented in Figure 6. B. Map view of the same surface as that shown in Figure 6 showing the relationship between faults, lineaments defined by edges along magnetic gradients, and Pb-Zn grades modeled at the Lower Sandstone orebody. C. Same map view as in Figure 8B showing the relationship between faults, lineaments defined by edges along magnetic gradients, and Pb-Zn grades modeled in the Upper Sandstone orebody.

grade shells between 2 and 5% (and locally >5%) are wider than the respective grade shells in the Lower Sandstone Pb-Zn orebody (Fig. 8B, C). In addition, the same general NE-SW trend and change in mineralization trend is seen for the Pb grade shells between the Nadok and Niepsurt faults, even if it is less well delineated and only concerns Pb values between 1 and 3% (Fig. 8C). The volume where the mineralization trend for Pb grades changes abruptly from NE-SW to NNW-SSE in the Lower and Upper Sandstone orebodies is spatially linked to the zone of higher fracture intensity and higher frequency of core loss (inferred fault, Fig. 8A). In the northeastern part of the mine, Pb grades display the same conspicuous spatial relationship to faults as in the Lower Sandstone Pb-Zn orebody (Fig. 8C). By corollary with the conclusion drawn in the previous section, there is not only a spatial relationship between some basement faults inferred from the magnetic data and the mapped faults in the mine, but the inferred basement faults are spatially related to the ore grade variations in sandstone, i.e., to the change in mineralization trend associated with the area of high fracture density and high frequency of core loss (Fig. 8A).

The geometry of the Pb grade shells in the Lower and Upper Sandstone orebodies and the Upper Sandstone orebody adjacent to the southern segment of the Nadok fault is shown in Figure 9A. The Pb grades define a fault-rooted, funnel-shape geometry in both orebodies where Pb grades splay out from the base of the sandstone paleoaquifers, from the fault toward the hanging wall of the two sandstone horizons at the contact with the individual aquitards (i.e., the Middle Sandstone and Grammajukku Formation, respectively). The same funnel-shape geometry, with the highest Zn grades clearly occurring at the hanging wall, is observed in the Upper Sandstone at the contact with the Grammajukku Formation (Fig. 9B)

Zn grade shells in the Upper Sandstone orebody display a conspicuous pattern that is best observed in relationship to the southern segment of the Nadok fault (Figs. 8C, 9A, B). Zn grades are highest in the structural block bounded by the Kautsky and Nadok faults (Fig. 6A). Lucks (2004) suggested that Zn mineralization was located west of the Pb mineralization in this part of the mine. Our work shows that Zn mineralization occurs to the northwest of the Pb mineralization and that the volume with higher Zn grades (2–4% grade shells) in the Upper Sandstone orebody is shifted about 120 m to the northwest of the volume with higher Pb grades on the northern hanging wall side of the Nadok fault. Only Zn grades between 0.1 and 1% occur close to the fault on its hanging-wall side. By contrast, the highest Zn grades on the footwall side of the Nadok fault are spatially consistent with the highest

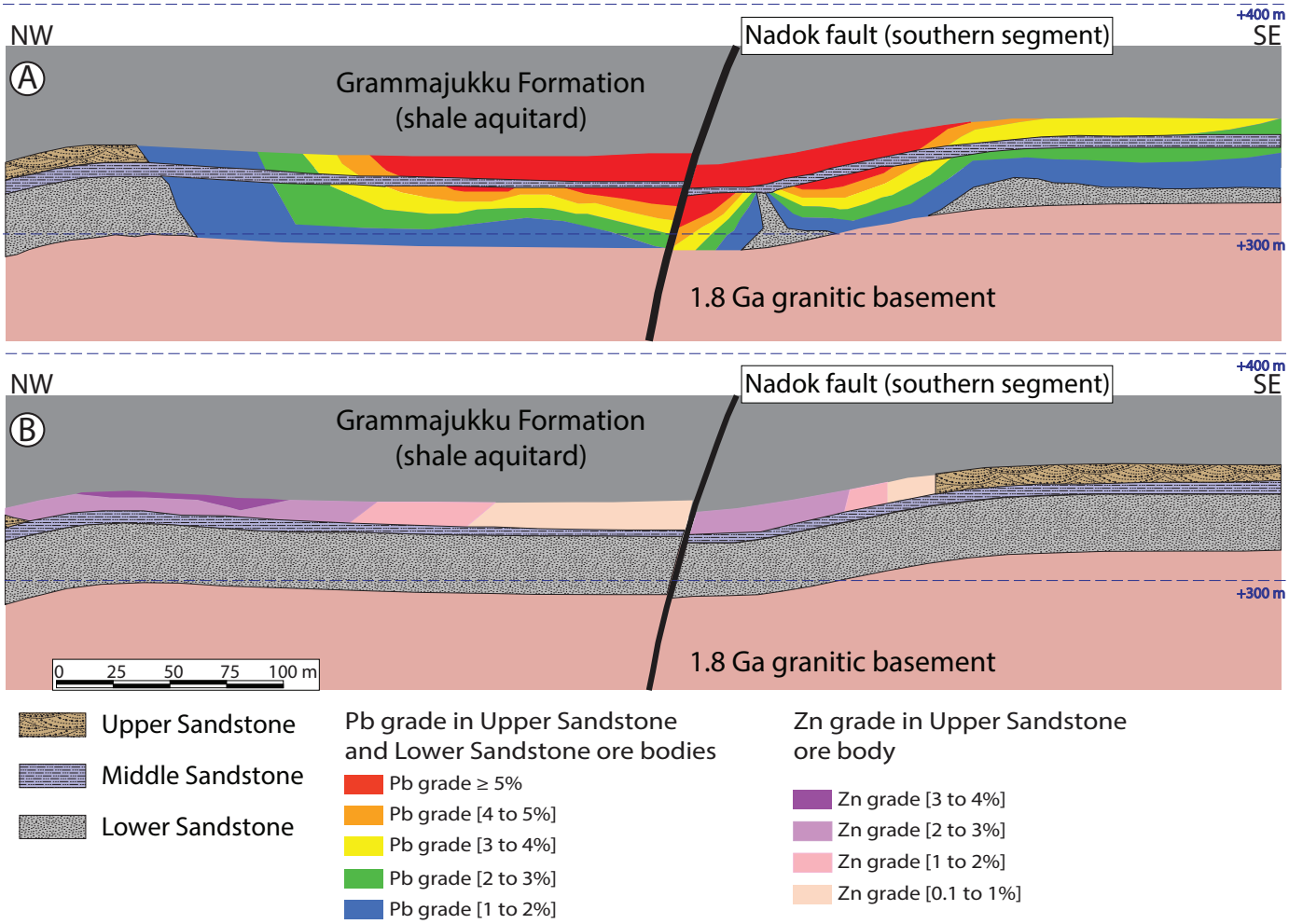

FIG. 9. Ore grades along a NW-SE cross section through the Nadok fault at Laisvall. A. Distribution of Pb grades in the Upper Sandstone and Lower Sandstone ore horizons. B. Distribution of Zn grades in the Upper Sandstone ore horizon.

Pb grades. While Pb grades are proximal to the Niepsurt fault (and its secondary minor fault) in the Upper Sandstone orebody in the northeastern part of the Laisvall mine (Fig. 8C), Zn grades are more distal away from this fault in an easterly direction.

In summary, Pb and Zn grades appear to show funnel-shape geometry both in the Upper and Lower Sandstone orebodies as recognized in a NW-SE section across the Nadok fault (Fig. 9A, B). In particular (1) Pb grades are the highest closer to the fault and diminish away from it; (2) in contrast to the Pb grades, the highest Zn grades are more distal away from the fault; (3) within a given sandstone paleoaquifer, the highest Pb and/or Zn grades occur at the hanging wall at the contact with the overlying aquitard; (4) as suggested by Lucks (2004), the Upper and Lower Sandstone orebodies thin gradually toward the west and northwest.

Zn/Pb ratios in the Lower and Upper Sandstone orebodies

The Zn/Pb patterns in the the Upper and Lower Sandstone orebodies are shown in Figures 10 and 11, respectively. Where sphalerite was not visible or not recognized in borehole, Zn content was not systematically analyzed. Zn and Pb content data in single borehole sections are consequently only available for 4,184 sections in the Lower Sandstone orebody and 2,179 sections in the Upper Sandstone orebody out of the total of 6,919 sections for which Pb data were available.

Box plot diagrams for the Zn/Pb data are presented for the the Upper and Lower Sandstone orebodies (Figs. 10D and 11D, respectively). The median and Q_3 values correspond to the 50th and 75th percentile, respectively, and were chosen for showing the gradual increase in Zn/Pb ratio by progressively displaying all values below these percentile values (Figs. 10B, C, 11B, C). The study of Zn/Pb ratios in Zn-Pb sediment-hosted deposits proved an effective method in defining feeder areas associated with low Zn/Pb ratios (e.g., Silvermines, Mount Isa, McArthur River, Sullivan, and Tara; Large, 1980; Taylor, 1984; Davidheiser-Kroll et al., 2013). Considering the Pb-dominated Lower Sandstone orebody and the Zn-dominated Upper Sandstone orebody, this method should in theory reveal isolated high Pb areas (where Zn/Pb is less than 1) and outward zoning into Zn-rich areas (where Zn/Pb is higher than 1) in the Laisvall mine.

The Lower Sandstone orebody is characterized by three main areas with variable Zn/Pb patterns (Fig. 10A-C): (1) A

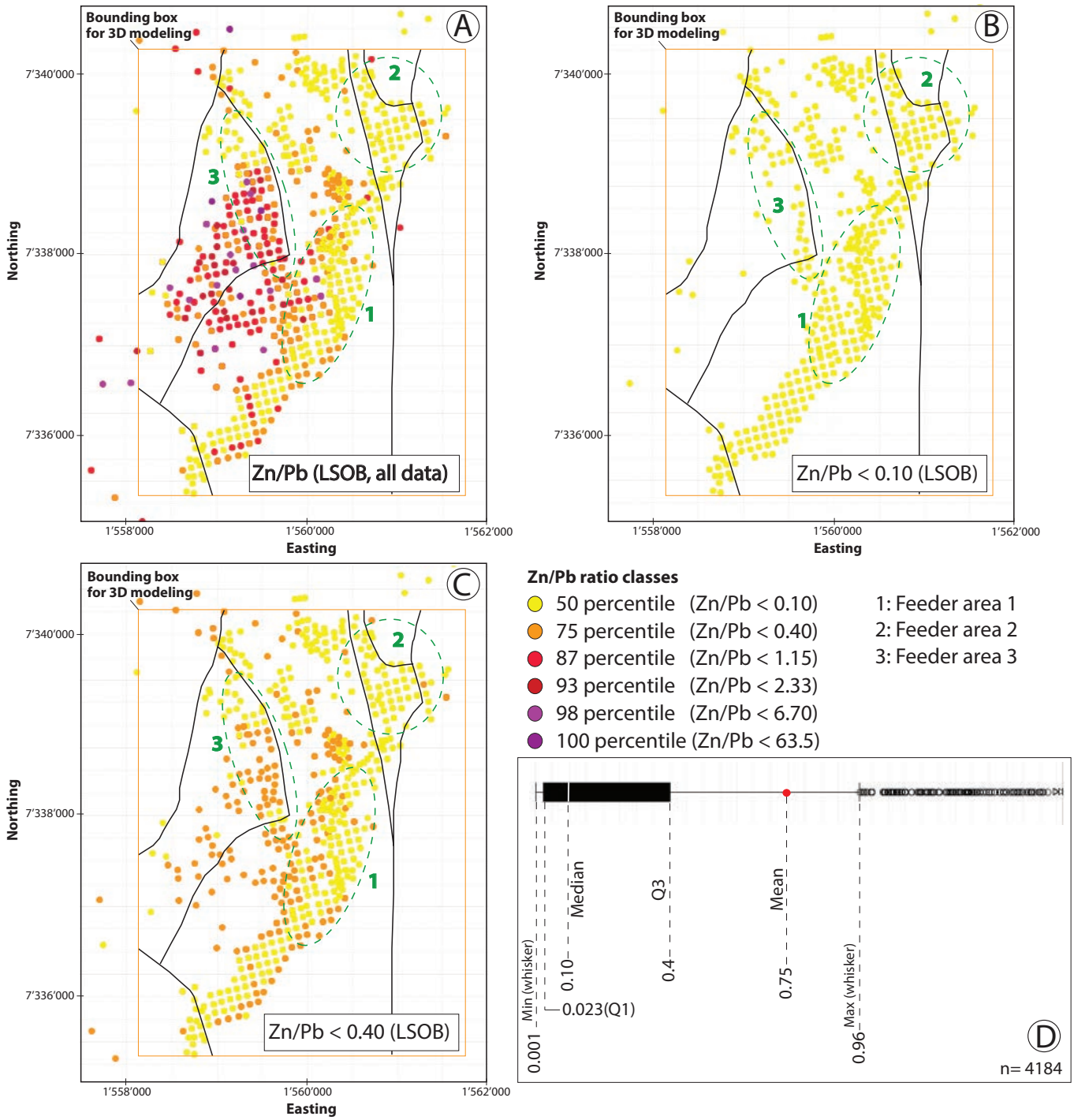

FIG. 10. A. Zn/Pb ratios for mineralized sections (n = 4,184) in the Lower Sandstone orebody at Laisvall. The traces of the faults identified in the three-dimensional model (see Fig. 6) are shown as black lines. B. Panel showing Zn/Pb ratios below the 50th percentile (Zn/Pb <0.10). Three main high lead areas are identified (dashed green ellipsoids). C. Panel showing Zn/Pb ratios below the 75th percentile (Zn/Pb <0.40), displaying progressive growth of Zn richer areas from the locations of mineralized fluid input identified in (B). D. Tukey box plot of mineralized sections (n = 4,184) in the Lower Sandstone orebody. The top and bottom of the box, and the median, mean, lower and upper whisker values are shown.

main mineralized Area 1 between the northern and southern Nadok, Niepsurt, Kramaviken, and southern Kaustky faults with Zn/Pb ratios below the 50th and 75th percentile. Area 1 corresponds to a NNE-SSW trend where we identified a high density of core loss in drill cores despite no fault having been documented previously (Fig. 8A). Area 1 is characterized by a progressive increase in Zn/Pb ratio (75th percentile) on both sides of the mineralized segment (Fig. 10C); (2) The Central Malm area (Area 2) located between the Niepsurt and Kramaviken faults, characterized by Zn/Pb ratios below the

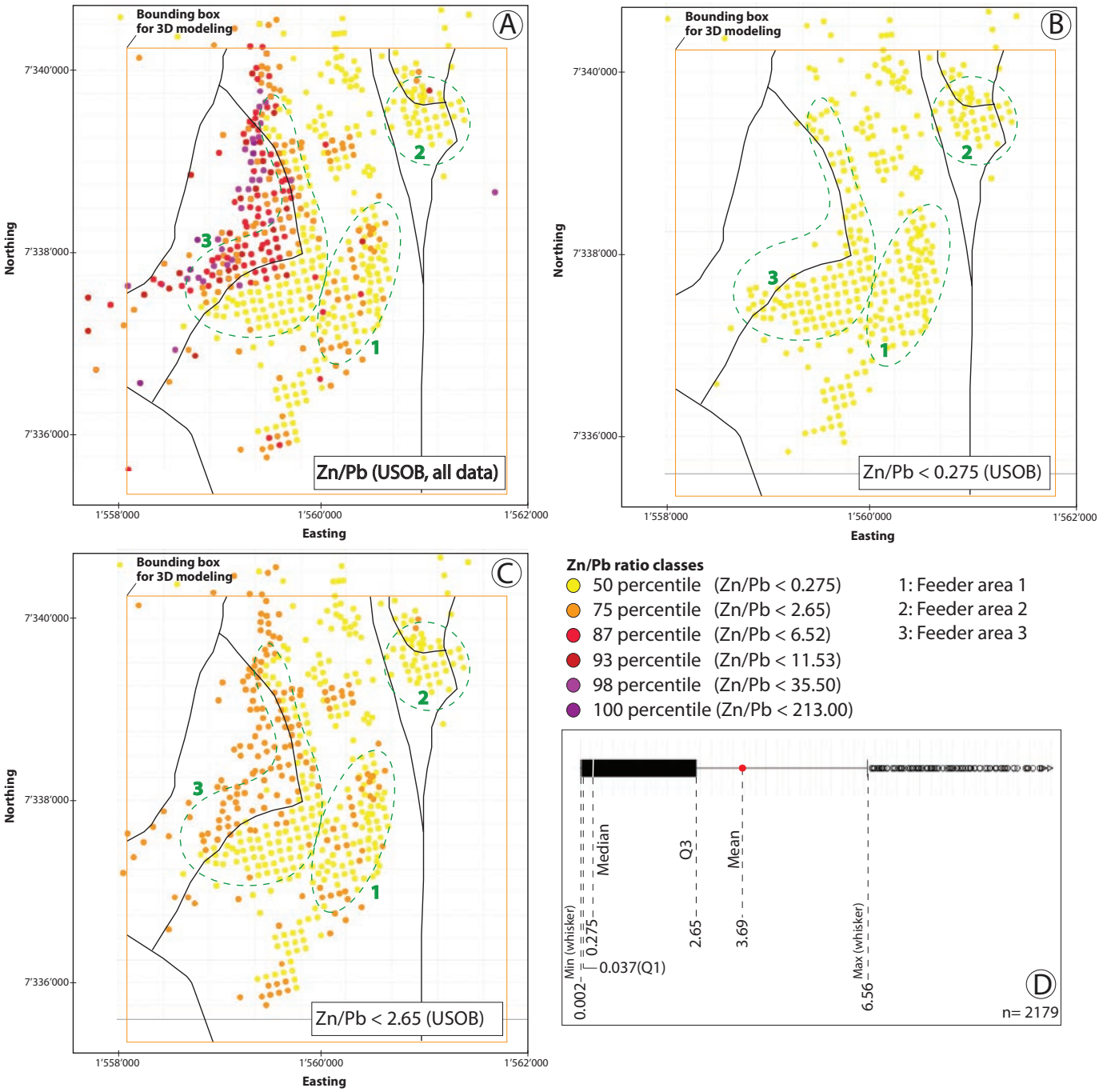

FIG. 11. A. Zn/Pb ratios for mineralized sections (n = 2,179) in the Upper Sandstone orebody at Laisvall. The traces of the faults identified in the three-dimensional model (see Fig. 6) are shown as black lines. B. Panel showing Zn/Pb ratios below the 50th percentile (Zn/Pb <0.275). Three main high lead areas are identified (dashed green ellipsoids). C. Panel showing Zn/Pb ratios below the 75th percentile (Zn/Pb <2.65), displaying progressive growth of Zn richer areas from the locations of mineralized fluid input identified in (B). D. Tukey box plot of mineralized sections (n = 2,179) in the Upper Sandstone orebody. The top and bottom of the box, and the median, mean, lower and upper whisker values are shown.

50th percentile. The Central Malm area does not show any increase in Zn/Pb ratio above 0.10; (3) Zn/Pb ratios mostly above the 75th percentile in Area 3 between the northern Kautsky, the northern and southern Nadok faults. Area 3 is somehow related to the hanging-wall sides of the segments of the Nadok fault. This area is characterized by a systematic increase in Zn/Pb ratio, up to the highest Zn/Pb ratios (Fig. 10A).

This suggests the following three feeder areas: (1) Area 1 characterized by low but increasing Zn/Pb ratios (below 0.4) in a highly fractured area, (2) the Central Malm area (Area 2) characterized by low Zn/Pb ratio (below 0.10) between the

Niepsurt and Kramaviken faults, and (3) Area 3 characterized by low to high Zn/Pb ratios on the hanging wall of the northern and southern segments of the Nadok fault. Area 1 might actually be the main feeder area in the Lower Sandstone orebody.

The Upper Sandstone orebody is also characterized by three main areas with variable Zn/Pb patterns (Fig. 11A-C): (1) the same Area 1 as identified in the Lower Sandstone orebody though being almost only characterized here by Zn/Pb ratios below the 50th percentile and less mineralized than in the Lower Sandstone orebody, (2) the Central Malm area only characterized by Zn/Pb ratios below the 50th percentile (Area 2), and (3) a main mineralized area (Area 3) where Zn/Pb ratios below the 50th percentile spread out on the footwall side of the southern and northern Nadok faults. In addition, Zn/Pb ratios below the 75th percentile are more systematically located on the hanging-wall side of these faults. This hanging-wall side locates almost exclusively all Zn richer areas characterized by Zn/Pb ratios above the 75th percentile.

The three feeder areas identified in the Lower Sandstone orebody are also recognized in the Upper Sandstone orebody: (1) Area 1 characterized by low Zn/Pb ratios (below 0.275), (2) the Central Malm area (Area 2) characterized by low Zn/Pb ratio (below 0.275) between the Niepsurt and Kramaviken faults; and (3) Area 3 characterized by low Zn/Pb ratios (below 0.275) on the footwall side of the segments of the Nadok fault and, increasing Zn/Pb ratios on the hanging-wall side of these faults. In contrast to the Lower Sandstone orebody where the main feeder area was Area 1 and to a lesser extent the Central Malm area, the two segments of the Nadok fault are suggested to represent the main feeder for the Zn-dominated mineralization in the Upper Sandstone orebody.

Mineralized steeply dipping fractures in the sandstone horizons and the basement beneath the Laisvall deposit

In the sandstone horizons at the Laisvall deposit, steeply dipping fractures striking NW to WNW and NNE to NE are filled with calcite and fluorite (Rickard et al., 1979), less commonly with pyrite and chalcopyrite (Lilljequist *in* Boliden AB unpub. internal reports, 1965). North-northeast-striking galena-filled tension fractures have also been observed (Rickard et al., 1979). During the core logging exercise carried out in the present study, steeply dipping galena-calcite ± sphalerite veins were commonly observed in the Lower Sandstone orebody. Such veins are scarce in the Upper Sandstone orebody where, instead, galena-coated fractures are common.

In boreholes LAI 1031 and 1088, we encountered subvertical veins filled with calcite-fluorite ± pyrite ± chalcopyrite in the Paleoproterozoic basement beneath the Laisvall mine. These veins are braided and approximately 0.5 to 1.0 cm thick. Borehole LAI 1031 is located in the hanging wall and 200 m southwest of the southern segment of the Kautsky fault while borehole LAI 1088 is situated in the hanging wall and 250 m northwest of the southern segment of the Nadok fault (Figs. 7A, 8C). These calcite-fluorite-sulfide veins in the basement are characterized by sharp vein walls. The outer part of the veins consists of coarse-grained, green fluorite intergrown with coarse-grained calcite. Granitic country-rock xenoliths are present. Toward the central part of the vein, large crystals of coarse-grained calcite rest in a groundmass of purple fluorite enclosing brecciated calcite fragments. Pyrite and chalcopyrite are present within both carbonate and fluorite. The vein in borehole LAI 1088 is situated below a center of higher Zn grades in the Upper Sandstone orebody (Fig. 8C). Together with the interpretation of basement structures and metal grade distribution in sandstone, these veins have significant implications for the understanding of the pathways that conveyed the hydrothermal mineralizing fluids to favorable sandstone horizons (see discussion below).

Modeling of Lithologic Units and Ore Grades in Three-Dimensional Space at the Vassbo Strata-Bound Pb-Zn Deposit

Data and methodology

The Vassbo deposit was explored and mined by Boliden AB and 846 boreholes were drilled. All boreholes are vertical. More than 90% of these boreholes have geologic and grade data for both Pb and Zn. Mineralization is hosted by the quartz sandstone horizon in the Vassbo Formation located underneath and in direct contact with the Middle Cambrian Alum Shale Formation (Fig. 2C). Some Pb mineralization also occurs in the first few centimeters of the underlying calcareous sandstone (Christofferson et al., 1979; this study). Our investigations and core logging revealed that many boreholes were not analyzed for Zn, where pale yellow sphalerite was previously mistaken for carbonate cement or sections with brown mottles of sphalerite were simply overlooked (e.g., boreholes VAI 112 and VAI 117). For this reason, the Zn grade distribution might not be totally representative. As at Laisvall, the main decollement marking the base of the Lower Allochthon is located within the Alum Shale Formation, and the lowermost few centimeters (5–10 cm) of the Alum Shale Formation still belong to the stratigraphy in the autochthonous cover sequence. The modeling of lithologic units and ore grades in three-dimensional space has been carried out beneath the base of the Alum Shale Formation inside the area shown in Figure 4A between +620- and +500-m elevation (Fig. 12).

The boreholes at Vassbo are rather short (50–100 m) and usually only penetrated the quartz sandstone ore horizon and the underlying calcareous sandstone. Only 55 boreholes were drilled through the stratigraphically lower units in the Vassbo Formation into the Proterozoic basement. A block model in three-dimensional space (Fig. 12) has been constructed for the quartz sandstone ore horizon and the underlying calcareous sandstone unit, using the same methodology as described earlier for the lithostratigraphic units in the Laisberg Formation at Laisvall. Based on the 55 boreholes that reached the basement, the geologic and structural maps from the archives at Boliden AB and digital information of the bedrock geology at the ground surface supplied by the Geological Survey of Sweden, modeling of the spatial distribution of lithologic units in the basement beneath the Vassbo mine was also completed (Fig. 13A, B). In contrast to Laisvall, where information on faults and structural data exist, virtually no data on such geologic features are available at Vassbo. As a consequence, it has not been possible to construct faults and fault-bounded blocks prior to the modeling of lithologic units and ore grades in three-dimensional space.

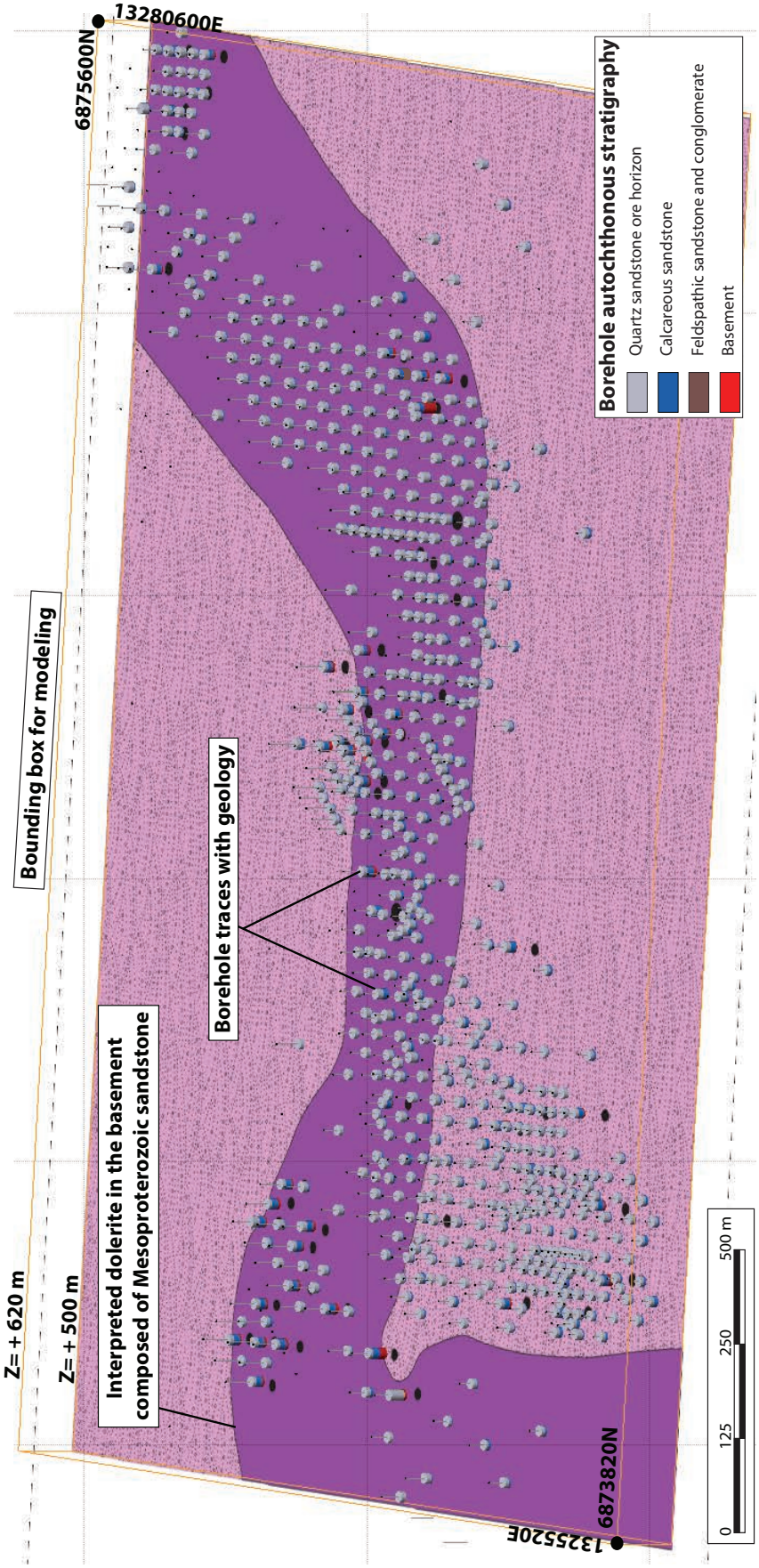

FIG. 12. Leapfrog three-dimensional model view (to north) showing the borehole database with geologic information at the Vassbo orebody. The spatial distribution of the lithologic units in the basement beneath the Vassbo deposit is shown on the surface at +500-m elevation in the model. Note how the distribution of the boreholes, which delineate the extent of the orebody within the bounding box used for modeling, follows the form of the dolerite dike (see also Christoffersen et al., 1979). The boreholes that were used to interpret the outline of the dolerite dike that intruded into the Mesoproterozoic sandstone in the basement are projected as black ellipses on the basement lithologies.

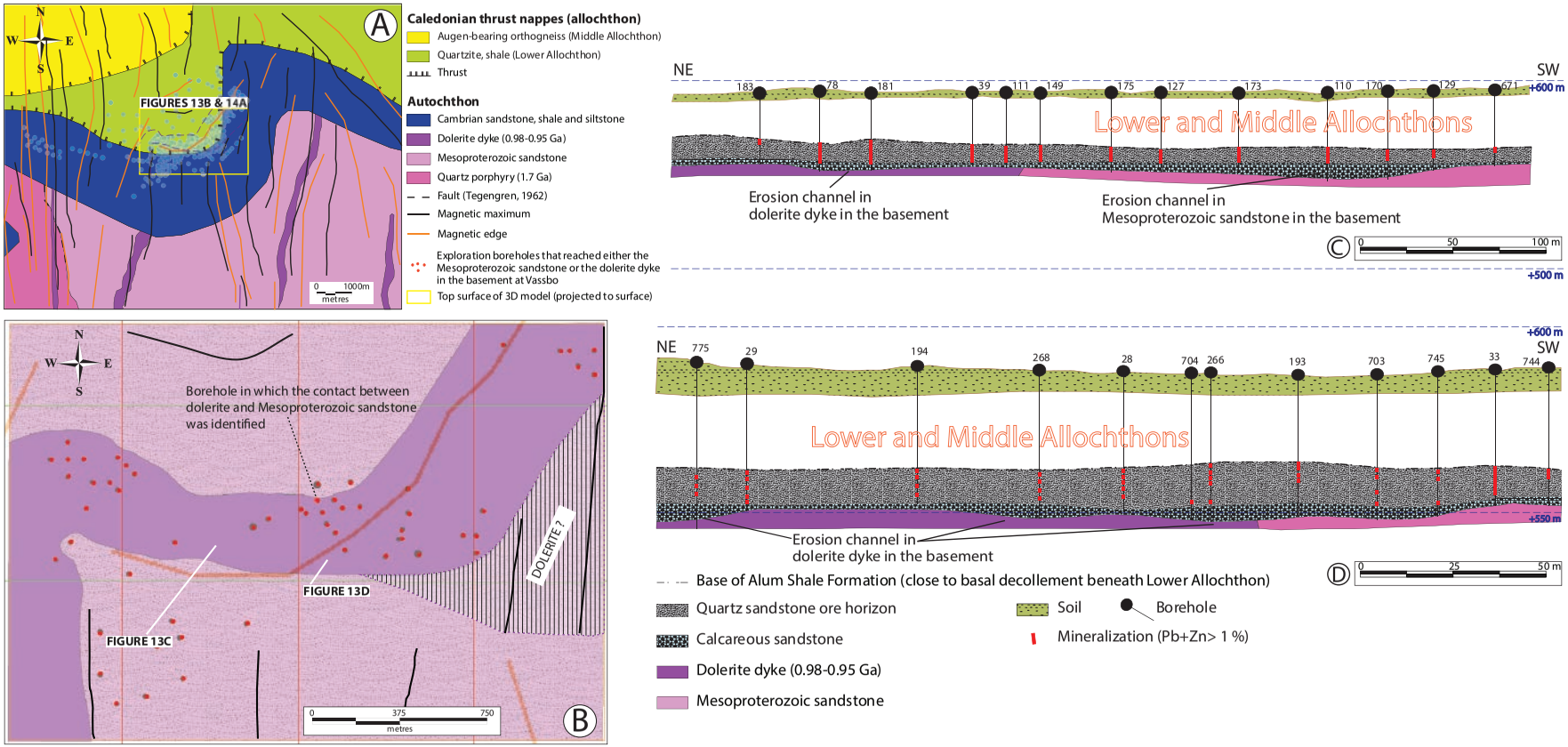

FIG. 13. A. Same map view in the neighborhood of the Vassbo orebody (outlined by exploration boreholes) as in Figure 4A, showing the spatial relationship between dolerite dikes in the Proterozoic basement and lineaments defined by magnetic maxima (black line) and edges along magnetic gradients (orange line). B. Interpreted geologic map of the bottom surface in the bounding box (Fig. 12), showing the spatial relationship between lineaments defined by magnetic maxima (black line) and edges along magnetic gradients (orange line) and the dolerite dike in the basement underneath the Vassbo orebody. The locations of the 55 boreholes that were drilled into the basement are also shown. The shape of the dolerite dike in the basement is based on geologic evidence using limited basement intersections in boreholes and is not overinterpreted. C. Geologic cross section through the western part of the Vassbo orebody. D. Geologic cross section through the eastern part of the Vassbo orebody.

Relationships between magnetic edge, dolerite dike, and fault in the basement

The basement beneath the Vassbo mineralization is composed of a dolerite dike that intruded into Mesoproterozoic sandstone (Figs. 12, 13). It is part of the 0.98- to 0.95-Ga swarm of dolerites with high magnetic susceptibility referred to as the Blekinge-Dalarna dolerites (Söderlund et al., 2005).

The modeled dolerite dike is deformed along a Z-shaped fold structure which probably formed during the Sveconorwegian orogeny (Fig. 13A, B). The western side of this folded dolerite dike is spatially associated with a N-S-trending magnetic maximum that lies close to the interpreted contact between the dike and the Mesoproterozoic sandstone. On the other hand, two NNE-SSW-trending magnetic maxima are almost parallel to the eastern edge of the dike and the contact with the sandstone. Given the relative paucity of boreholes that were drilled into the basement, there is some degree of uncertainty in the position of the dolerite dike (Fig. 13B). Given the high magnetic susceptibility value for dolerite (Table 3), it is arguable that the eastern limb of the dolerite could be extended farther east where the two NNE-SSW maxima trend. The same argument is valid for the western limb where the contact between the dike and the Mesoproterozoic sandstone could be moved a few meters to the east, and for the northern contact of the dike. In its current state, the shape of the dolerite dike in the basement is based on geologic evidence using limited basement intersections in boreholes and is not overinterpreted.

This dike also correlates with a curved magnetic edge with a change in trend from NNE-SSW to the west of the Vassbo deposit to E-W and NE-SW farther to the east. The segments of the magnetic edge with NNE-SSW and E-W trends lie parallel to the contact between the dolerite dike and the Mesoproterozoic sandstone while the segment with NE-SW trend lies within the modeled dolerite dike (Fig. 13B). It remains unclear whether or not this segment of the magnetic edge is a fault. Furthermore, apart from the data from the few boreholes where the contact between the dolerite dike and Mesoproterozoic sandstone was identified (Fig. 13B), little information is available on the orientation of this steeply dipping dike to better constrain the fold geometry. The dolerite dike in the basement in the Vassbo area was, at least partly, more deeply eroded than the surrounding Mesoproterozoic sandstone prior to Cambrian sedimentation (Christofferson et al., 1979; this study).

Model for lithologic units

The basal conglomerate in the overlying Vassbo Formation (Fig. 2) is polymict and is absent above the dolerite dike in the basement. In particular, in the mineralized area, the basal conglomerate unit is commonly absent and the dike is in erosive contact with the calcareous sandstone. The conglomerate is replaced by a facies composed of weathered fragments of dolerite, locally cemented by calcite (Christofferson et al., 1979; this study). The basal conglomerate passes laterally to the northwest of the Vassbo mine into thicker feldspathic sandstone (Nielsen and Schovsbo, 2011). The 1- to 6-m-thick shale unit with accessory silt and sandstone layers that overlies the basal conglomerate in the Vassbo Formation (Fig. 2) is not present in the mineralized area. This unit was either not deposited there or was eroded during deposition of the sediments of the calcareous sandstone in the mine area. Approximately 3 km to the northwest of the Vassbo mine, this shale unit is consistently 5 m thick or more (Christofferson et al., 1979).

The calcareous sandstone is consistently thicker above the channels eroded in the dolerite dike and the Mesoproterozoic sandstone (Fig. 13C, D). The geometry of the hanging wall of the calcareous sandstone unit shows that the area was leveled prior to deposition of the overlying quartz sandstone that hosts Pb-Zn mineralization, since the calcareous sandstone was also deposited above higher grounds of Mesoproterozoic sandstone on the sides of the eroded dike (Fig. 13C, D). Christofferson et al. (1979) reported that the contact between the quartz sandstone and the underlying calcareous sandstone is sharp and shows erosional features.

The ore-bearing quartz sandstone shows thickness variations from 6 to 13 m (Fig. 13C, D). Christofferson et al. (1979) suggested that the quartz sandstone is thicker due to basement depressions coincident with the location of dolerite dikes. We question this interpretation, since the lithologic model constructed here shows that the quartz sandstone is not directly thicker above former basement depressions filled with calcareous sandstone, irrespective of whether these basement depressions are located in the dolerite dike or the Mesoproterozoic sandstone (Fig. 13C, D). Indeed, thinning of the quartz sandstone can even be observed above some of the channels filled with calcareous sandstone, and the quartz sandstone is laterally thicker away from these channels. In addition, we have observed that the relative thickening of the quartz sandstone tends to spatially correspond to the areas of change in trend of lineaments along the Z-shaped fold structure in the basement.

Ore grade model

Modeling of ore grades was carried out in the same manner as at Laisvall (cf. subsections "Data and general methodology" and "Relationships between basement faults and the faults at mine scale" in the section above). The Vassbo mineralization in the quartz sandstone ore horizon comprises three segments; two NE-SW-striking segments on the western and eastern parts of the deposit, and a central segment oriented WNW-ESE (Fig. 14A). Christofferson et al. (1979) referred to this as a Z-shaped orebody. Our observations show that the geometry of the orebody follows the shape of the fold with Z asymmetry defined by the dolerite dike in the underlying basement (Figs. 13B, 14A).

The current work shows that the highest Pb grades splay out from the base of the quartz sandstone ore horizon and toward its hanging wall at the contact with the overlying Alum Shale Formation, building several funnel-shape orebodies (Fig. 14B-D) similar to those recognized at Laisvall. The richest orebodies are located close to or in the hinges of the probably late Sveconorwegian fold structure defined by the dolerite dikes in the basement (Fig. 14A, B). In addition, the mineralization follows the shape of the magnetic edge and is located on its southern side. If this edge represents a fault in the folded dolerite dike in the basement, this could illustrate the pathway along which mineralizing fluids were conveyed (Fig. 14).

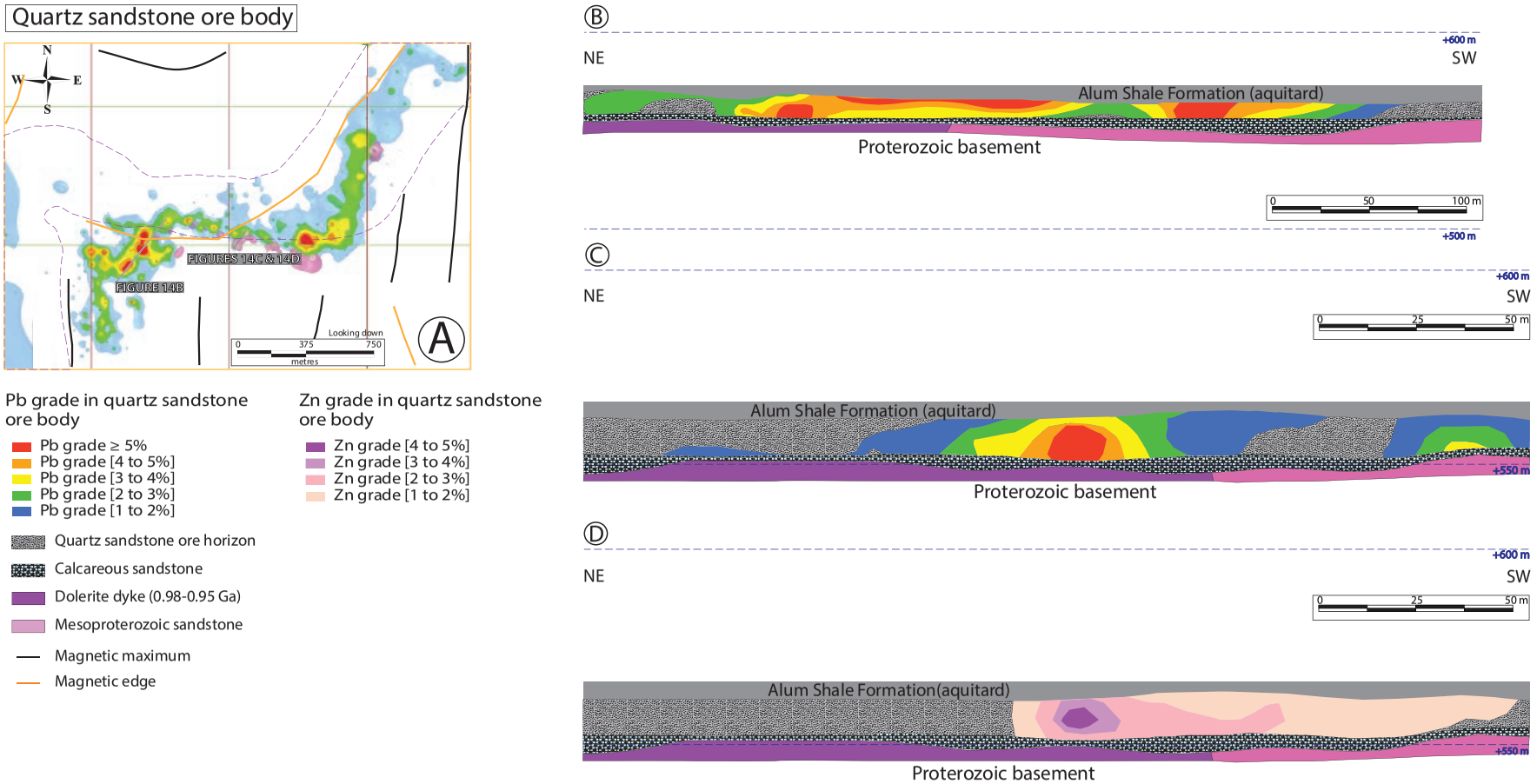

FIG. 14. A. Map view of the bottom surface in the bounding modeling box (Fig. 12), showing the relationship between magnetic maxima (black line), magnetic edges (orange line), the folded dolerite dike, and the Pb-Zn grades modeled in the quartz sandstone orebody at Vassbo. B. Distribution of Pb grades in the quartz sandstone orebody in the same geological cross section as that presented in Figure 13C. C. Distribution of Pb grades in the quartz sandstone orebody in the same geologic cross section as that presented in Figure 13D. D. Distribution of Zn grades in the quartz sandstone orebody in the same geologic cross section as that presented in Figure 13D.

By contrast, as Christofferson et al. (1979) observed, higher Zn grades are mainly located on the southern edge of the WNW-ESE Pb-mineralized segment of the orebody (Fig. 14A). We also identified higher Zn grade centers which lie in the northeastern part of each NE-SW segment of the orebody (Fig. 14A). As for Pb grades, Zn grades (Fig. 14D) splay out in the quartz sandstone from its base to its hanging wall in a funnel shape. In contrast to the Pb grades, the highest Zn grades are only situated at the hanging wall of the quartz sandstone.

Mineralized fractures in the sandstone and the basement beneath the Vassbo deposit

During the core logging exercise carried out in the current study, steeply dipping fractures with varying mineralogy were encountered in the quartz sandstone ore horizon at Vassbo. Fractures are commonly filled with galena and pyrite, locally also with barite; sphalerite is scarce. Cores from these vertical boreholes were not oriented. As a consequence, it was not possible to determine the orientation of these steeply dipping fractures.

Tegengren (1962) described fracture sets striking N 35° E, N 75° W, and N 15° W (minor) that intersect the autochthonous Cambrian sandstone in the Vassbo mine. Christofferson et al. (1979) confirmed a major vertical fracture system striking WNW-ESE to be ubiquitous in the mine and a second set striking NE-SW at a high angle to this system. The shape of the Vassbo deposit closely follows the orientation of these two fracture systems. The same array of fractures exists in the Proterozoic basement at Vassbo (Tegengren, 1962).

Discussion

Origin and timing of faulting in sandstone at Laisvall

Ljungner (1943) and Willdén (1980) suggested that a paleotopography existed in the basement with an overall NNW-SSE trend comprising a group of "residual hills" with abrupt flanks ("Laisan" and "Peak Islands"), the trend being dissected by NE-SW lineaments in the Ljungner Gap (Ljungner, 1943; Willdén, 1980). According to Willdén (1980), other highs with N-S to NNW-SSE trend existed to the northeast and southwest, (e.g., "Jutas" and"Niobe Islands," respectively). The facies changes from sandstone- to shale-dominated areas during deposition of the Lower Sandstone was explained by Willdén (1980) as the result of hydrodynamic variations governed by basement paleotopography.

As first proposed by Willdén (1980), building on earlier findings by Ljungner (1943, 1950), Nielsen and Schovsbo (2011, p. 258) summarized that the basement paleotopographic architecture at Laisvall was more "complicated than elsewhere due to the presence of local basement highs some 50 m or more above the surrounding sub-Cambrian peneplain." Willdén (1980) utilized the Assjatj Member (Fig. 2) as reference for restoring the strata to their pretectonic position. However, the Assjatj Member is not always present in the Laisvall mine area and, on the basis of the core logging work completed in this study, it is apparent that this phosphorite-pebble conglomerate does not occur systematically above the Upper Sandstone at the base of the Grammajukku Formation. It often lies within the lowest part of the Grammajukku Formation, even as much as 50 to 100 cm above the lower contact with the Upper Sandstone. In addition, there are several phosphorite-pebble conglomerate horizons within the Grammajukku Formation (Nielsen and Schovsbo, 2011; this study). Furthermore, the Grammajukku Formation is disturbed by second-order low-angle thrust tectonics above the decollement. The tectonic complexity together with the existence of several phosphorite-pebble conglomerate horizons suggests that the choice of the Assjatj Member as marker horizon for the restoration of strata to their pretectonic position is questionable.

The geometry of the sedimentary units revealed by the three-dimensional modeling carried out in the present work (e.g., Fig. 7), including the presence of feldspathic sandstone and conglomerate on top of granite crystalline basement at the suggested location of Willdén's "hills" (Fig. 7C), is not compatible with a model influenced by the basement paleotopography. Our findings are consistent instead with a crystalline basement peneplained during the Neoproterozoic and completely flat at the dawn of the Cambrian following birth of the continent Baltica, as proposed by Nielsen and Schovsbo (2011). The facies distribution and thickness variations in combination with the occurrence of fault-related breccia suggest sedimentation controlled by synsedimentary block faulting on this peneplained basement. Such faulting had already been suggested by Ljungner (1943), Carlson (Boliden AB, unpub. internal reports, 1970), and Lilljequist (1973) in the Laisvall area. However, the main stream of workers disregarded this hypothesis. This synsedimentary tectonic activity is suggested to have taken place prior to postsedimentation and postmineralization faulting along, for example, the Nadok and Kautsky faults (Rickard et al., 1979; Lucks, 2004; this study).

A correlation between certain magnetic edges and faults in the Ediacaran-Cambrian sedimentary cover rocks was presented in Figure 8A. It is apparent that there is a clear spatial association between basement faults inferred from the magnetic data and major faults observed in the mine. Since magnetic lineaments depict structures that are located within the Paleoproterozoic basement, we propose that synsedimentary, postsedimentation, and postmineralization faulting that affected the Ediacaran-Cambrian sedimentary cover rocks find their origin in the basement through reactivation of preexisting structures and the triggering of block faulting in the basement.

Link between basement structure, mineralized fractures, and metal grades at the Laisvall and Vassbo strata-bound Pb-Zn deposits

Laisvall: Lilljequist (Boliden AB, unpub. internal reports, 1965, 1973) conducted a systematic survey of mesoscopic faults and fractures in the autochthonous sedimentary rocks and in the Paleoproterozoic basement at and surrounding the Laisvall ore deposit. This work showed that the orientations of the regionally important faults in the area are similar to the different sets of mesoscopic faults and fractures in the mine area.

The current work has described how, in the Laisvall mine, the highest Pb and Zn grades delineate orebodies and orebody trends controlled by faults (Fig. 8B, C). The change in trend of the Pb grade mineralization in the Lower Sandstone orebody and Upper Sandstone orebody, from NE-SW to NNW-SSE, remarkably matches the area of intense core loss and the

change in strike of the Nadok fault from NE-SW along the southern segment of the fault to NNW-SSW along its northern segment (Fig. 8). The main feeder fault zone in the Upper Sandstone orebody is suggested to be along the segments of the Nadok fault. Mineralization in the Lower Sandstone orebody is suggested to be rooted, on the one hand, in the area characterized by high density of core loss and, on the other, in the area between the Niepsurt and Kramaviken faults. Fluids with variable Zn/Pb ratios might have been present in the Upper and Lower Sandstone orebodies.

The spatial relationship between magnetic edges, mineralization trends, faults and fracture sets in the Laisvall mine suggests that mineralized fracture trends coincide with regional fault orientations in the Paleoproterozoic basement. On this basis, it is suggested that the basement-steered, synsedimentary structures also acted subsequently as conduits that conveyed the metal-bearing fluids to favorable locations where the autochthonous sandstones were mineralized at an economically significant level. The mineralizing fluids followed NNE-SSW to NE-SW and NNW-SSE steeply dipping faults and fractures that are observed in the basement and in the autochthonous sedimentary rocks in the Laisvall area. The veins in the basement beneath the Laisvall mine filled with calcite-fluorite ± pyrite ± chalcopyrite, described in the current work, as well as the steeply dipping mineralized fractures in the sandstone described previously (e.g., Lilljequist *in* Boliden AB unpub. internal reports, 1965, Rickard et al., 1979) and summarized above, provide some illustration of these pathways.

These findings are similar to those made at the southeastern Missouri sandstone-hosted Pb-Zn deposits (Clendenin et al., 1989, 1994, and references therein), and particularly at the Navan Irish-type Zn-Pb deposit (Anderson et al., 1998; Blakeman et al., 2002; Davidheiser-Kroll et al., 2013) where faults of the Dublin basin, which triggered synsedimentary block movement and conditioned sedimentation, also acted as conduits for the mineralizing fluids at a later time. Existence of multiple feeder zones along several major faults at Navan (Anderson et al., 1998) was highlighted by Zn, Pb, and Zn/Pb distribution (Blakeman et al., 2002; Davidheiser-Kroll et al., 2013).

The inferred orebody morphology, in particular the fault-rooted funnel shape (e.g., the southern segment of the Nadok fault, Fig. 9A, B), first confirms that migration of ore-bearing fluids was controlled by faults and, second, provides some indications of the precipitation process discussed briefly below.

Vassbo: In the Vassbo area, the geometry of the orebody follows the shape of a fold with Z asymmetry defined by a dolerite dike in the underlying basement (Figs. 13B, 14A). No faults have been mapped at the ground surface as being related to the location of dolerite dikes in the basement. Although there is some uncertainty concerning whether or not the magnetic edge in the vicinity of the deposit (Figs. 13B, 14A) is a fault, the dikes presumably provided areas with a high frequency of fractures in connection with their emplacement and possibly even preferentially intruded along preexisting faults in the basement.

Abdelmalak et al. (2012) discussed the effect of dike propagation mode on surface deformation through two-dimension laboratory models. They identified two types of intrusion morphologies which exhibit two evolutional stages. During the first stage, a vertical dike is formed and its propagation is controlled by both shear deformation and opening of tensile cracks. During the second stage, the dike can either rotate and form an inclined sheet dipping between 45° and 65°, or the dike tip interacts with tensile cracks formed at the earlier stage. This fracture pattern controls the subsequent propagation of the dike toward the surface. Given the lack of field evidence due to thick Quaternary glacial till overburden, the conclusions of the experimental work by Abdelmalak et al. (2012) are proposed to illustrate the kind of fracture pattern and morphology linked to the dolerite dike in the basement beneath the Vassbo deposit.

Given the similarity in shapes of the Vassbo mineralized body and the fold structure in the basement as well as the close relationship between the hinges of the fold structure and the location of the highest Pb grade centers, we propose that the mineralization at Vassbo is also closely linked to the structures in the Proterozoic crystalline basement. The mineralization at Vassbo also follows the shape of the magnetic edge and is located on its southern side. If, as discussed above, this edge represents a fault in the folded dolerite dike, this could represent the pathway along which the mineralizing fluids were conveyed (Fig. 14).

Since the fracture patterns described above (cf. "Mineralized fractures in the sandstone and the basement beneath the Vassbo deposit" in the section above") in the basement and sedimentary cover rocks bear close similarities in orientation and mineralogy (e.g., Tegengren, 1962; Christofferson et al., 1979), it is proposed that there is a connection between these fracture systems, if not even reactivation of fractures in the basement during and/or after deposition of the Ediacaran-Cambrian rocks. By analogy with Laisvall, including the funnel geometry of the orebodies (Fig. 14B-D), it is inferred that these fractures acted as conduits that conveyed the metal-bearing fluids to favorable locations for mineralization.

Funnel-shape morphology

Modeling work in three-dimensional space shows prominent fault-rooted funnel-shape orebodies at Laisvall. At Vassbo, similar funnel-shape mineralization is situated close to the hinges of the folded dolerite dike in the crystalline basement. The orebodies of both deposits also share a similar metal distribution pattern with Pb-rich cores proximal to the faults or fold hinges and a Zn-rich shell more distal from these structures. The funnel-shape ore geometry may reflect the fault-rooted migration path and the metal precipitation mechanism.

In both deposits, the highest Pb and Zn grades occur at the top of sandstone paleoaquifers in a similar manner as the variation in grades and paleoaquifer settings recognized in several carbonate-hosted MVT Zn-Pb deposits (e.g., San Vicente deposit in Peru; Fontboté and Gorzawski, 1990; Topla-Mežica deposits in Slovenia; Spangenberg and Herlec, 2006). This geometry is suggestive of a sour gas trap that accumulated at the top of paleoaquifers due to density. This gas provided H_2S by thermogenic sulfate reduction to the metal-bearing fluids and triggered subsequent precipitation of Pb-Zn sulfides (e.g., Anderson and references therein, 2008). Thermogenic sulfate reduction is compatible with the few so far available sulfur

stable isotope data on Pb and Zn sulfides at Laisvall (Rickard et al., 1979, 1981).

Conclusions

This multidisciplinary study has recognized the primary role of structures in the basement beneath two major sandstone-hosted Pb-Zn deposits along the Caledonian front, Laisvall, and Vassbo, in localizing and constraining not only the sedimentary facies distribution of the host sandstone but also the feeders of Pb-Zn mineralization at these deposits.

Linear anomalies have been identified in high-resolution airborne magnetic data and these anomalies correspond to geologic features in the Proterozoic basement. Furthermore, the Laisvall and Vassbo strata-bound Pb-Zn deposits are both spatially associated with areas of change in the trend of the magnetic lineaments. Magnetic lineaments, trending either N-S to NE-SW and WNW-ESE to NW-SE in the Laisvall area, and NNE-SSW to NNW-SSE and NW-SE to W-E in the Vassbo area, were identified.

In the Laisvall area, individual magnetic edges can be correlated with faults in the Ediacaran-Cambrian sedimentary cover rocks that are interpreted to extent downward into faults in the underlying Proterozoic basement. The reactivation of these basement structures is expressed higher up in the Ediacaran-Cambrian sedimentary cover rocks as newly formed structures with Phanerozoic displacement. In individual faults of the sets (NE-SW to N-S and WNW-ESE to NW-SE) synsedimentary block movement has been recognized. The highest Pb and Zn grades in Laisvall delineate orebodies and orebody trends that follow these faults. An input of mineralizing fluids with probably variable Zn/Pb ratios has been suggested at several feeder fault locations in the deposit area. Areas where the faults change strike contain some of the largest and richest orebodies.

In the Vassbo area, the geometry of the ore deposit follows the shape of a fold defined by a dolerite dike in the basement. No faults have been mapped at the ground surface as being related to the location of dolerite dikes in the basement. However, it is inferred that the emplacement of these dikes produced a fracture network or was driven by preexisting basement structures.

The main orebodies in both deposits display a funnel geometry, fault rooted in Laisvall and located close to the hinges of folded dolerite dike in the basement in Vassbo. Metal distribution patterns are also similar in both deposits and are characterized by Pb-rich cores proximal to the basement-steered structures, while Zn-rich shells are more distal relative to these structures. The funnel-shaped ore geometry is interpreted to reflect a fault-rooted migration path and the metal precipitation mechanism.

In both deposits, the highest Pb and Zn grades occur at the top of sandstone paleoaquifers in a similar manner as the variation in grades and paleoaquifer settings recognized in several carbonate-hosted MVT Zn-Pb deposits. This geometry is suggestive of a sour gas trap that accumulated at the top of paleoaquifers due to density. This gas provided H_2S by thermogenic sulfate reduction to the metal-bearing fluids and triggered precipitation of Pb-Zn sulfides.

The combined evidence from the interpretation of the airborne magnetic data, the structural analysis, and the three-dimensional modeling of the orebodies, including their metal distribution, suggests that the basement faults reactivated during the Ediacaran-Cambrian sedimentation, acted as feeders for the metal-bearing fluids to favorable locations for mineralization, and localized deformation during postsedimentary and postmineralization tectonics. These findings provide support to Romer's hypothesis (1992), mainly based on lead isotope geochemistry, of a large-scale ore-bearing fluid migration through the basement enabled by reactivation of Proterozoic basement structures.

The present contribution defines and constrains the structural framework for the Laisvall and Vassbo deposits. It demonstrates that sandstone-hosted Pb-Zn Laisvall-type deposits can be added to the list of sediment-hosted Zn-Pb deposit types that were shown to be structurally controlled (e.g., Leach et al., 2005, and references therein). This framework can now be used for the interpretation work in current ongoing geochronological and geochemical studies that should help to define a broader genetic model for the Laisvall-type deposits.

Acknowledgments

This research is financially supported by Boliden AB (Sweden) and the Swiss National Foundation (SNF, Switzerland, FN 146 353). The Geological Survey of Sweden (SGU) has also provided financial and logistic support for much of the fieldwork in Sweden. The staff at SGU in Malå, especially Jerry Hedström, is thanked for their help at the national core archive and for the supply of past reports. The authors are grateful to Boliden AB via Hans Årebäck (former Exploration manager) for financial and logistic support for the work carried out in Boliden and to the staff working at the core archive in Boliden for their help in supplying drill cores. We would also like to acknowledge the contribution of Mikko Mali and Bertil Sandström (Geophysicist and Chief Geophysicist, respectively, at Boliden AB) for the production of the diverse geophysical maps and for the constructive discussions on the interpretation of airborne magnetic data, and also the assistance of Ildiko Antal (SGU) who helped with the extraction of the provided petrophysical data from the database at SGU. The authors also appreciate the contribution and motivating comments by David Leach during a poster presentation at the SEG Conference in Lima (Peru) in September 2012. The review on the use and interpretation of airborne magnetic data by V.J.S. Grauch (US Geological Survey) and the constructive suggestions and criticisms by John Ashton (Boliden Tara Mines Ltd.) helped significantly to improve the quality of the manuscript. Motivating remarks and comments by the editor Larry Meinert and the associate editor John Slack are also acknowledged.

REFERENCES

Abdelmalak, M.M., Mourgues, R., Galland, O., and Bureau, D., 2012, Fracture mode analysis and related surface deformation during dike intrusion: Results from 2D experimental modeling: Earth and Planetary Science Letters, v. 359–360, p. 93–105.

Anderson, G.M., 2008, The mixing hypothesis and the origin of Mississippi Valley-type ore deposits: Economic Geology, v. 103, p. 1683–1690.

Anderson, I.K., Ashton, J.H., Boyce, A.J., Fallick, A.E., and Russell, M.J., 1998, Ore depositional process in the Navan Zn-Pb deposit, Ireland: Economic Geology, v. 93, p. 535–563.

Bjørlykke, A., and Sangster, D.F., 1981, An overview of sandstone lead deposits and their relation to red-bed copper and carbonate-hosted lead-zinc deposits: Economic Geology 75th Anniversary Volume, p. 179–213.

Blakeman, R.J., Ashton, J.H., Boyce, A.J., Fallick, A.E., and Russell, M.J., 2002, Timing of interplay between hydrothermal and surface fluids in the Navan Zn + Pb orebody, Ireland: Evidence from metal distribution trends, mineral textures, and $\delta^{34}S$ analyses: Economic Geology, v. 97, p. 73–91.

Carmichael, R.S., 1982, Handbook of physical properties of rocks: Boca Raton, Florida, CRC Press, v. 2, 345 p.

Christofferson, H.C., Wallin, B., Selkman, S., and Rickard, D.T., 1979, Mineralization controls in the sandstone lead-zinc deposits at Vassbo, Sweden: Economic Geology, v. 74, p. 1239–1249.

Clark, D.A., 1997a, Magnetic properties of rocks and minerals: Journal of Australian Geology and Geophysics, v. 17, p. 5–10.

——1997b, Magnetic petrophysics and magnetic petrology—aids to geological interpretation of magnetic surveys: AGSO Journal of Australian Geology and Geophysics, v. 17, p. 83–103.

Clendenin, C.W., Niewendorp, C.A., and Lowell, G.R., 1989, Reinterpretation of faulting in Southeast Missouri: Geology, v. 17, p. 217–220.

Clendenin, C.W., Niewendorp, C.A., Duane, M.J., and Lowell, G.R., 1994, The paleohydrology of Southeast Missouri Mississippi Valley-type deposits: Interplay of faults, fluids, and adjoining lithologies: Economic Geology, v. 89, p. 322–332.

Davidheiser-Kroll, B., Boyce, A.J., Ashton, J.H., Blakeman, R., and Geraghty, J., 2013, How did it get there? Searching for "the feeder" at the Navan Zn + Pb deposit, Ireland: Mineral deposit research for a high-tech world: Biennial SGA Meeting, 12th, 12–15 August 2013, Uppsala, Sweden, Proceedings, ISBN 978-91-7403-2079, p. 616–619.

Fontboté, L., and Gorzawski, H., 1990, Genesis of the Mississippi Valley-type Zn-Pb deposit of San Vicente, Central Peru: Geologic and isotopic (Sr, O, C, S, Pb) evidence: Economic Geology, v. 85, p. 1402–1437.

Gee, D.G., 1975, A tectonic model for the central part of the Scandinavian Caledonides: American Journal of Science, v. 275A, p. 468–515.

Gee, D.G., Guezou, J.-C., Roberts, D., and Wolff, F.C., 1985, The central-southern part of the Scandivian Caledonides, *in* Gee, D.G., and Sturt, B.A., eds., The Caledonide orogen-Scandinavia and related areas: New York, J. Wiley, and Sons, p. 109–134.

Gee, D.G., Fossen, H., Henriksen, N., and Higgins, A.K., 2008, From the early Paleozoic platforms of Baltica and Laurentia to the Caledonide orogen of Scandinavia and Greenland: Episodes, v. 31, p. 1–8.

Gee, D.G., Juhlin, C., Pascal, C., and Robinson, P., 2010, Collisional orogeny in the Scandinavian Caledonides (COSC): Geologiska Föreningens i Stockholm Förhandlingar, v. 132, p. 29–44.

Grant, F.S., 1985a, Aeromagnetics, geology, and ore environments, I. Magnetite in igneous, sedimentary, and metamorphic rocks—an overview: Geoexploration, v. 23, p. 303–333.

——1985b, Aeromagnetics, geology, and ore environments, II. Magnetite and ore environments: Geoexploration, v. 23, p. 335–362.

Grip, E., 1954, Blymalmen vid Laisvall, dess geologi och jämförelse med några utländska förekomster: Geologiska Föreningens i Stockholm Förhandlingar, v. 76, p. 357–380 (in Swedish).

Henkel, H., and Guzmán, M., 1977, Magnetic features of fracture zones: Geoexploration, v. 15, p. 173–181.

Hildenbrand, T.G., Berger, B., Jachens, R.C., and Ludington, S., 2001, Utility of magnetic and gravity data in evaluating regional controls on mineralization: Examples from the Western United States: Reviews in Economic Geology, v. 14, p. 75–109.

Large, D.E., 1980, Geological parameters associated with sediment-hosted submarine exhalative Pb-Zn deposit: An empirical model for mineral exploration: Geologisches Jahrbuch, ser. D, v. 40, p. 59–129.

Leach, D.L., Sangster, D.F., Kelley, K.D., Large, R.R., Garven, G., Allen, C.R., Gutzmer, J., and Walters, S., 2005, Sediment-hosted lead-zinc deposits: A global perspective: Economic Geology 100th Anniversary Volume, p. 561–607.

Lilljequist, R., 1973, Caledonian geology of the Laisvall area, southern Norbotten, Swedish Lappland: Stockholm, Geological Survey of Sweden, C 691, 43 p.

Ljungner, E., 1943, Deformation der Gebirgsoberfläche unter dem kaledonischen Gebrigsrand in Lappland: Geologische Rundschau, v. 34, p. 180–196 (in German).

——1950, Urbergsytans form vid Fjällranden: Geologiska Föreningens i Stockholm Förhandlingar, Bd 72, H 3 (in Swedish).

Lucks, T.J., 2004, Controls on the ore distribution of the Laisvall deposit, Sweden: Ph.D. thesis, Cardiff, United Kingdom, University of Cardiff, 269 p.

Nabighian, M., Grauch, V., Hansen, R., LaFehr, T., Li, Y., Peirce, J., Phillips, J., and Ruder, M., 2010, Magnetic exploration methods, *in* Society of Exploration Geophysicists, 9. Magnetic exploration methods: Geophysics Today, p. 183–213.

Nielsen, A.T., and Schovsbo, N.H., 2011, The Lower Cambrian of Scandinavia: Depositional environment, sequence stratigraphy and paleogeography: Earth-Science Reviews, v. 107, p. 207–310.

Reeves, C.V., Redford, S.W., and Milligan, P.R., 1997, Airborne geophysics—old methods, new images: Geophysics and Geochemistry at the Millenium: Prospectors and Developers Association of Canada, Exploration 97, Fourth Decennial Conference on Mineral Exploration, Toronto, Ontario, GEOF/X, Proceedings, p. 13–30.

Reid, A.B., 1980, Aeromagnetic survey design: Geophysics, v. 45, p. 973–976.

Rickard, D.T., Willdén, M.Y., Marinder, N.E., and Donnelly, T.H., 1979, Studies on the genesis of the Laisvall sandstone lead-zinc deposit, Sweden: Economic Geology, v. 74, p. 1255–1285.

Rickard, D.T., Coleman, M.L., and Swainbank, I., 1981, Lead and sulfur isotopic compositions of galena from the Laisvall sandstone lead-zinc deposit, Sweden: Economic Geology, v. 76, p. 2042–2046.

Roberts, D., and Gee, D.G., 1985, An introduction to the structure of the Scandinavian Caledonides, *in* Gee, D.G., and Sturt, B.A., eds., The Caledonide orogen—Scandinavia and related areas: Chichester, Wiley, p. 55–68.

Romer, R., 1992, Sandstone-hosted lead-zinc mineral deposits and their relation to the tectonic mobilization of the Baltic Shield during the Caledonian orogeny, a reinterpretation: Mineralogy and Petrology, v. 47, p. 67–85.

Saintilan, N.J.D., Fontboté, L., Spangenberg, J., Samankassou, E., and Stephens, M.B., 2014, The Laisvall and Vassbo sandstone-hosted Pb-Zn deposits along the eastern front of the Scandinavian Caledonides: An example of phosphorous-rich sulfide-mineralized Cambro-Ordovician sour gas reservoirs: Mineral Deposit Studies Group, 37th Annual Winter Meeting, 6–7 January 2014, University of Oxford, UK, p. 70.

SKB, 2008, Site description of Forsmark at completion of the site investigation phase: SDM-Site Forsmark: Stockholm, Swedish Nuclear Fuel and Waste Management Company Report TR-08-05, 545 p. http:/www.skb.se/publications.

Söderlund, U., Isachsen, C., Bylund, G., Heaman, L., Patchett, P.J., Vervoort. J.D., and Andersson, U.B., 2005, U-Pb baddeleyite ages and Hf, Nd isotope chemistry constraining repeated mafic magmatism in the Fennoscandian Shield from 1.6 to 0.9 Ga: Contributions to Mineralogy and Petrology, v. 150, p. 174–194.

Spangenberg, J.E., and Herlec, U., 2006, Hydrocarbon biomarkers in the Topla-Mežica zinc-lead deposits, northern Karavanke/Drau Range, Slovenia: Paleoenvironment at the site of ore formation: Economic Geology, v. 101, p. 997–1021.

Stephens, M.B., 1986, Stratabound sulfide deposits in the Central Scandinavian Caledonides: IAGOD Symposium and Nordkallot Project Meeting, 7th, Excursion Guide 2, Ca 60, Uppsala, Sweden, Geological Survey of Sweden, 68 p.

——1988, The Scandinavian Caledonides: A complexity of collisions: Geology Today, v. 4, p. 20–26.

Taylor, S., 1984, Structural and paleotopographic controls of lead-zinc mineralization in the Silvermines orebodies, Republic of Ireland: Economic Geology, v. 19, p. 529–548.

Tegengren, F.R., 1962, Vassbo blymalmfyndighet och dess geologiska inramning: Geological Survey of Sweden, Serie 586, årsbok 56, no. 2 (in Swedish).

Wallin, B., 1982, Sedimentology of the Lower Cambrian sequence at Vassbo, Sweden: Ph.D. thesis, Acta Universitatis Stockholmiensis, Stockholm Contributions in Geology, 1982, v. 39 (1), 111 p.

Willdén, M.Y., 1980, Paleoenvironment of the autochthonous sedimentary rocks sequence at Laisvall, Swedish Caledonides: Ph.D. thesis, Stockholm, Sweden, Stockholms Universitets Geologiska Institutionen, 100 p.

——2004, The Laisvall sandstone-hosted Pb-Zn deposit: Geological overview: Society of Economic Geologists Guidebook Series, v. 33, p. 115–127.

Zachrisson, E., 1980, Aspects of stratabound base metal mineralization in the Swedish Caledonides: Geological Survey of Ireland Special Paper 5, p. 41–61.

CHAPTER 2

A Middle Ordovician Age for the Laisvall Sandstone-Hosted Pb-Zn Deposit, Sweden: A Response to Early Caledonian Orogenic Activity

Saintilan, N.J., Schneider, J., Stephens, M.B., Chiaradia, M., Kouzmanov, K., Wälle, M., and Fontboté, L., A Middle Ordovician Age for the Laisvall Sandstone-Hosted Pb-Zn Deposit, Sweden: A Response to Early Caledonian Orogenic Activity: ECONOMIC GEOLOGY, *in press*.

A Middle Ordovician Age for the Laisvall Sandstone-Hosted Pb-Zn Deposit, Sweden: A Response to Early Caledonian Orogenic Activity

Nicolas J. Saintilan[1], Jens Schneider[2], Michael B. Stephens[3,4], Massimo Chiaradia[1], Kalin Kouzmanov[1], Marküs Wälle[5], Lluís Fontboté[1]

[1]*Section of Earth and Environmental Sciences, University of Geneva, Rue des Maraîchers 13, 1205 Geneva, Switzerland*

[2]*Department of Mineralogy, Technische Universität Bergakademie Freiberg, Brennhausgasse 14, 09596 Freiberg, Germany*

[3]*Geological Survey of Sweden (SGU), Box 670 SE-751 28 Uppsala, Sweden*

[4]*Department of Civil, Environmental and Natural Resources Engineering, Division of Geosciences, Luleå University of Technology, SE-971 87 Luleå, Sweden*

[5]*Institute of Geochemistry and Petrology, ETH Zürich, Clausiusstrasse 25, CH-8092 Zürich, Switzerland*

Corresponding author:

Nicolas J. Saintilan
nicolas.saintilan@unige.ch
Tel: +41 22 379 66 97
Fax: +41 22 379 32 10

Ten sphalerite separates isolated from mineralized samples in proximal and distal positions relative to the proposed main feeder fault systems at the Laisvall deposit were used to obtain an absolute age determination of this world-class Pb-Zn deposit hosted by autochthonous Ediacaran to lower Cambrian sandstone and located currently along the erosional front of the Scandinavian Caledonides in northern Sweden. Residue and leachate fractions of each separate were obtained using the crush-leaching technique. All samples correspond to sphalerite formed using sulfur derived from thermochemical sulfate reduction, three of them from disseminated ore in the Lower Sandstone, two from the disseminated ore in the Upper Sandstone, and five from steeply-dipping galena-sphalerite-calcite veinlets interpreted in previous works as remobilization of disseminated ores. The ID-TIMS data yield an overall complex Rb-Sr isotope pattern with two distinct trends in the $^{87}Sr/^{86}Sr$ vs. $^{87}Rb/^{86}Sr$ isochron diagram. The three sphalerite residues of disseminated mineralization from the Lower Sandstone orebody show Rb-Sr isotope systematics indicative of undisturbed primary precipitates, and yield an isochron model age of 467 ± 5 Ma (MSWD = 1.4). Since the isochron is based on three points, the obtained age is to be considered as preliminary. Yet, the obtained age is fully consistent with geologic evidence reported by previous authors and pointing to Middle Ordovician timing of ore formation.

The ID-TIMS data were complemented by LA-ICPMS analyses on the same sphalerite samples. The data support the hypothesis that the measured ID-TIMS Rb and Sr contents in these sphalerite residues are held in the sphalerite structure itself and are not related to micro-inclusions. The most viable hypothesis, in agreement with published work, is that during rapid growth, sphalerite may incorporate up to ~600 ppt to ~1 ppm Rb and up to a few ppm Sr ions from the hydrothermal fluids in its structure.

By contrast, the second trend in the $^{87}Sr/^{86}Sr$ vs. $^{87}Rb/^{86}Sr$ space defined by most other sphalerite residues and corresponding inclusion fluid leachates from the Upper Sandstone orebody and the veinlet samples is too steep to account for a realistic isochron age determination. This steep linear trend is interpreted to represent a post-mineralization disturbance involving fluids rich in Sr. This disturbance of the Rb-Sr isotope system is consistent with the presence of the steeply-dipping galena-sphalerite-calcite veinlets and the fact that the Upper Sandstone is, in places, tectonically disrupted because of its proximity to the basal Caledonian décollement. The attempt to date the Granberget deposit, located in tectonically disrupted allochthonous units inside the Caledonian orogen, failed, because the Rb-Sr isotope systematics of the three analyzed sphalerite samples are also disturbed.

The obtained Middle Ordovician (467 ± 5 Ma) mineralization age at Laisvall can be interpreted as a far-field foreland response to an early Caledonian arc-continent collision and the subsequent development of a foreland basin. Basinal brines formed in the foredeep of the orogen could be conveyed cratonward, interact with permeable Baltica crystalline basement rocks, and resurge as metal-bearing fluids in sandstone at Laisvall along reactivated Paleoproterozoic crystalline basement faults. Mixing of metal-bearing brines with hydrocarbon and H_2S-rich fluids in Ediacaran to lower

Cambrian sandstone may explain the initial Sr isotope signature ($^{87}Sr/^{86}Sr$ = 0.715900 ± 60) of the isochron intersect.

Introduction

The sandstone-hosted Pb-Zn deposit at Laisvall (64.3 million metric tons of ore at 4.0% Pb, 0.6% Zn, and 9.0 g/t Ag), currently located along the erosional front of the Scandinavian Caledonides in northern Sweden (Fig. 1A), was discovered in 1939. Mining operations started in 1941 (Grip, 1954) and lasted until its closure in 2001. The timing of this Pb-Zn mineralization has been discussed with some controversy (cf., Rickard et al., 1979; 1981; Rickard, 1983; Bjørlykke and Sangster, 1981; Bjørlykke et al., 1991; Romer, 1992; Kendrick et al., 2005) and geochronological work had not been carried out prior to the current study.

Rickard et al. (1979) characterized the Laisvall deposit as epigenetic mineralization in sandstone, resulting from the mixing of migrating metal-rich brines with H_2S-rich fluid hosted in porous sandstone. This epigenetic model was supported by Kendrick et al. (2005) who provided evidence for extensive fluid-basement interaction before mineralization. Kendrick et al. (2005) also suggested that the mineralizing process involved basinal brine dominated fluids influenced by subsequent fluid interaction with organic-matter in the subsurface. Recently, Saintilan et al. (2015) proposed that Paleoproterozoic basement faults at Laisvall were reactivated during Ediacaran to lower Cambrian sedimentation and subsequently acted as feeders of the metal-bearing fluids, providing support to Romer (1992) who invoked fluid migration through basement structures in the genesis of Laisvall and similar mineral deposits presently located along the erosional front of the Scandinavian Caledonides (e.g., Osen, Vassbo; Fig. 1A). By contrast, Bjørlykke and Sangster (1981) proposed an early diagenetic model based on groundwater transport of metals from the underlying basement under stable tectonic conditions although, subsequently, Bjørlykke et al. (1991) placed the formation at a later stage involving sedimentary brines.

The lack of absolute age determinations for Laisvall-type mineralization has markedly contributed to the genetic controversy. Grip (1960) proposed a genetic relationship between epigenetic mineralization and Caledonian overthrusting with mineralizing solutions derived from the "inner part of the Caledonian range" (p. 158). Geologic and geochemical evidence led Gee (1972) and Rickard et al. (1975, 1979) to propose that mineralization at Laisvall probably occurred after the deposition of the middle Cambrian to Lower Ordovician Alum Shale Formation that represents an impermeable cap-rock above the strata-bound mineralization in sandstone. Rickard et al. (1979) related mineralization at Laisvall to Caledonian tectonics and suggested that mineralization predated the "great Caledonian nappes emplacement" (p. 1277) during the early Devonian. Rickard et al. (1979) maintained that some sets of joints "related to the Caledonian trend" (p. 1278) were filled at the same time as the disseminated strata-bound mineralization in sandstone, possibly in early Silurian time. Rickard (1983)

later suggested that basinal brines might have been supplied to the depositional site at Laisvall during the "beginning of the Caledonian orogeny" (p. 456), which, based on the polyphase Caledonian orogenic evolution proposed by Gee (1972) and Sturt (1978), was placed by Rickard (1983) during "upper Cambrian to Lower Ordovician" time (p. 456).

The hypothesis of ore formation driven by early Caledonian tectonic activity receives additional support by the similarity of the lead isotopic signature of galena in disseminated mineralization hosted by Lower Ordovician limestone in the Boda area (Fig. 1A) and Laisvall-type mineralization (Wickman et al., 1963; Gee, 1972). This geochemical evidence led Gee (1972) to propose that epigenetic Pb mineralization was of Middle Ordovician age or younger. Kesler (1994) concluded that epigenetic mineralization at Laisvall had already been emplaced prior to the end of Ordovician time, i.e., before the dismantling of the hydrological system related to Caledonian thrust tectonics.

The aim of the current study is to present an absolute age for the Laisvall deposit by using sphalerite Rb-Sr isotope dilution thermal ionization mass spectrometry systematics (ID-TIMS). In order to better constrain the siting of Rb and Sr in sphalerite and to strengthen the viability of Rb-Sr isotope geochronology age determination in this mineral, we use a multidisciplinary approach that combines Rb-Sr isotope determinations with LA-ICPMS analyses of the Rb and Sr contents in inclusion-free and inclusion-bearing sphalerite.

Representative sphalerite samples were selected from the following mineralization types (Fig. 1A): (i) the two strata-bound orebodies in the autochthonous Lower Sandstone (Pb-Zn) and Upper Sandstone (Zn-Pb) at Laisvall; (ii) the strata-bound Granberget Zn-Pb mineralization in sandstone of the lowermost allochthonous units inside the Caledonian orogen, located about 200 km south of Laisvall; and (iii) the Åkerlandet calcite-fluorite-Zn±Pb sulfide vein deposit, located in the Paleoproterozoic basement about 35 km to the east of the erosional front of the Scandinavian Caledonides. The latter is part of a group of calcite-galena vein deposits that were proposed to be co-genetic with strata-bound sandstone-hosted Pb-Zn deposits of the Laisvall type (e.g., Johansson and Rickard, 1984). Additionally, whole-rock Sr isotope geochemistry and X-ray fluorescence analyses were performed on crystalline basement and unconformably overlying siliciclastic rocks from the autochthonous stratigraphy at Laisvall.

This paper will be complemented soon by two companion articles that, respectively, explain the role of organic matter in mineralization and refine a genetic model for the Laisvall deposit, and, propose a re-evaluation of the source(s) of metals in mineralization at Laisvall and in basement-hosted calcite-galena vein deposits.

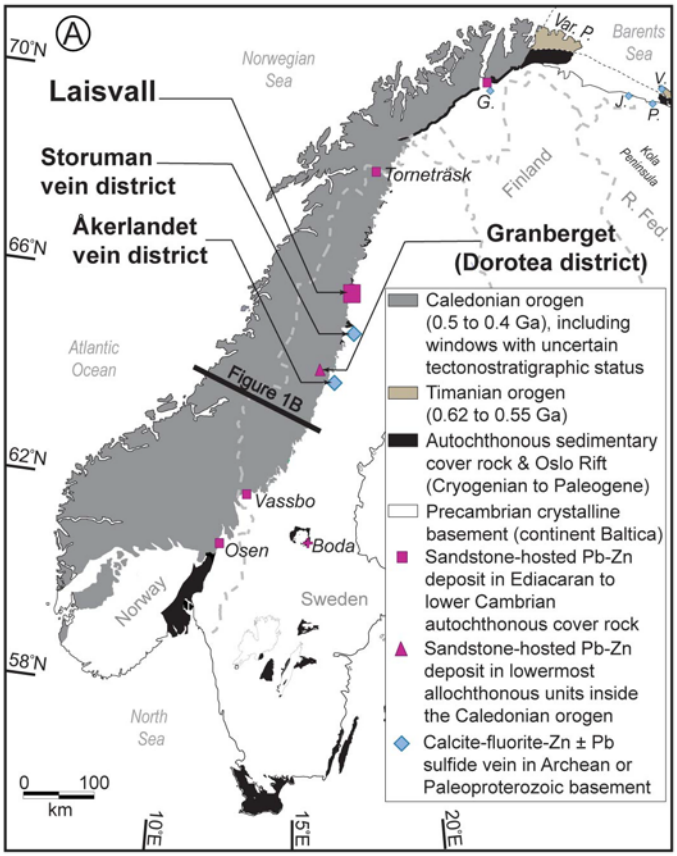

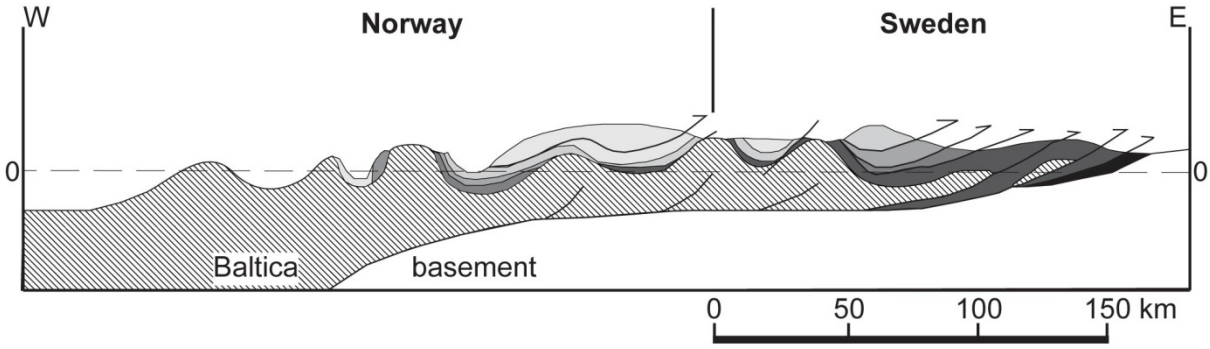

Middle and Upper Allochthons

- Köli Nappe Complex (outboard terranes)
- Seve Nappe Complex (schist, paragneiss, amphibolite)
- Särv Nappe (feldspathic sandstone, dolerite)
- Mylonitic granite, feldspathic sandstone

Lower Allochthon and Autochthon

- Baltoscandian sedimentary cover (allochthonous & autochthonous)
- Baltica basement (allochthonous & autochthonous)

B

Fig. 1 (previous page) A. Simplified geologic map of Scandinavia (modified after Roberts and Siedlecka, 2002; Gee et al., 2008 and Bergman et al., 2012). The locations of: (i) sandstone-hosted Pb-Zn deposits in Ediacaran to lower Cambrian siliciclastic sedimentary rock, both in the autochthonous cover rocks to the crystalline basement and in the lowermost allochthonous units in the Caledonian orogen (after Zachrisson, 1980; Stephens, 1986), (ii) calcite-fluorite-Zn±Pb sulfide vein-type mineralization in Paleoproterozoic crystalline basement in the Åkerlandet and Storuman areas, northern Sweden, (iii) similar vein-type mineralization in Paleoproterozoic basement rocks in northern Norway (e.g., G.: Gurrogaissa), in Archean basement rocks in northern Norway and Russia (e.g., J.: Jakobselv, P.: Peuravuono), and in rocks of the Timanian orogen in Russia (e.g., V.: Vaitolahti) (after Gee, 1972; Sundblad, 1990) are shown. Abbrevations: R. Fed.: Russian Federation; Var. P.: Varanger Peninsula. B. Cross-section through the central part of the Caledonide orogen in Sweden and Norway (modified after Gee et al., 2010).

Geologic setting

Geologic framework

In the central and northern parts of Sweden, the crystalline basement is composed of Paleoproterozoic and Archean rocks belonging to a 2.0–1.8 Ga orogenic system (Svecokarelian orogen), and subordinate late Paleoproterozoic–early Neoproterozoic (1.7–0.9 Ga) sedimentary, volcanic and intrusive rocks. The basement is overlain unconformably by a thin cover of Ediacaran to lower Cambrian, locally through Lower Ordovician, autochthonous sedimentary rocks that were deposited on the western (present-day coordinates) stable platformal margin of the Baltica continent (Bergman et al., 2012; Fig. 1A). Along the northeastern (present-day coordinates) continental margin of Baltica, in the Varanger and Kola Peninsulae along the Barents Sea parts of Norway and Russia (Fig. 1A), sedimentation onto Archean and Paleoproterozoic crystalline basement rocks commenced in the early Cryogenian and continued in the Ediacaran (Roberts and Siedlecka, 2002). Sedimentation occurred in an elongate basin controlled by important NW–SE faults along pre-existing, deep-seated anisotropies in the basement (Roberts and Siedlecka, 2002). These sedimentary rocks are tectonically juxtaposed against folded and metamorphosed rocks belonging to the c. 620 to 550 Ma Timanian orogen (Roberts and Siedlecka, 2002; Pease et al., 2008; Fig. 1A).

To the west, rocks belonging to both continental margins and the Timanian orogen are overlain by thrust sheets belonging to the c. 500 to c. 400 Ma Caledonian orogen (Gee, 1975; Roberts and Gee 1985; Bergman et al., 2012; Figs. 1A and B). In the present study, the term "Caledonian" is used to characterize tectonic events that took place during the time interval between late Cambrian (c. 500 Ma) and Middle Devonian (c. 395 Ma); the term "pre-Caledonian" is used for events that occurred prior to 500 Ma.

The Caledonian orogen in present-day Scandinavia resulted from a polyphase orogenic evolution (Gee, 1972; Sturt, 1978; Dallmeyer and Gee, 1986). A foreland basin developed as a response to the collision of Baltica with an outboard island arc, with the collision producing a mountain belt comprising mixed accreted Neoproterozoic continental rocks and oceanic material. These continental supracrustal rocks, preserved c. 10 km northwest of Laisvall in the allochthonous nappes referred to as the Seve Nappe Complex, contain eclogites that were exhumed to high crustal levels at c. 490 to 460 Ma (Dallmeyer and Gee, 1986; Santallier, 1988; Stephens, 1988; Kullerud et

al., 1990; Gromet et al., 1996; Greiling and Garfunkel, 2007; Root and Corfu, 2012). This early continent-arc collision and foreland basin development preceded the closure of the Iapetus Ocean and terminal continent-continent (Laurentia-Baltica) collision, which probably began at c. 450 Ma during the latest part of the Ordovician, and continued through the Silurian into Devonian time with final emplacement of the Caledonian thrust nappes (Gee, 1975; Stephens, 1988; Gee et al., 2010; Root and Corfu, 2012).

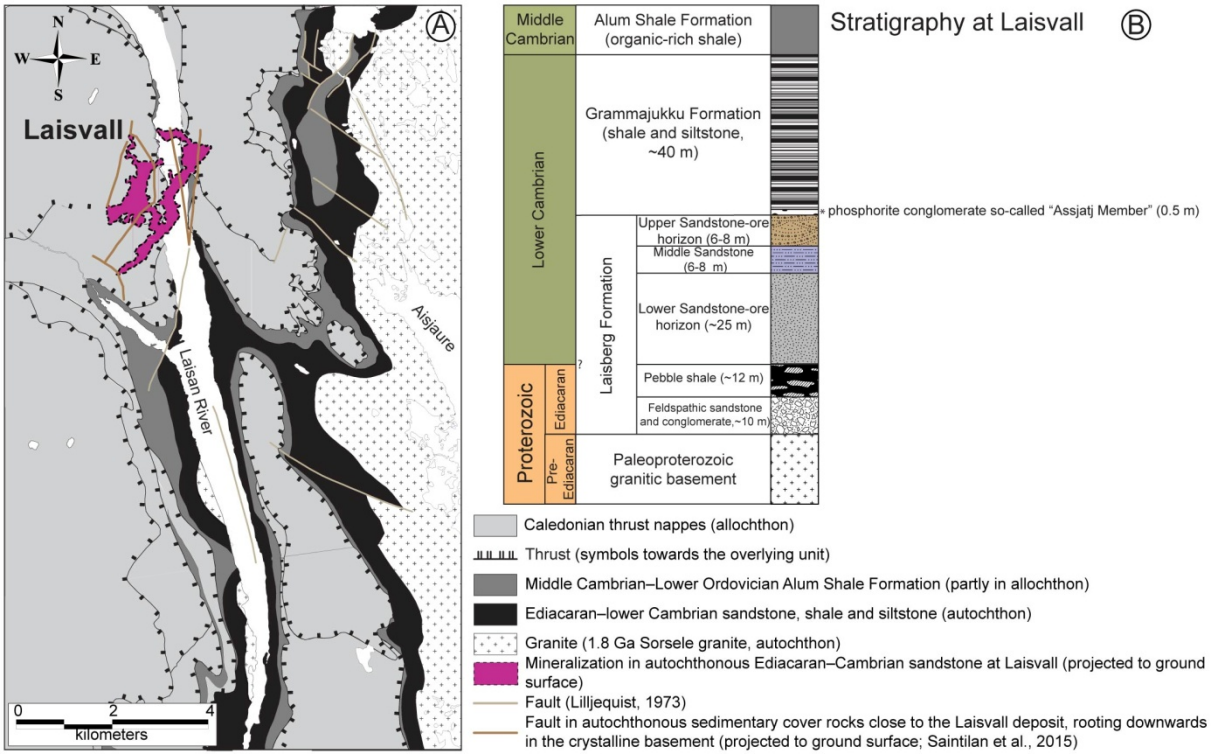

Fig. 2 A. Geologic map of the Caledonian allochthons, autochthonous sedimentary cover rocks and Paleoproterozoic crystalline basement in the Laisvall area (modified after Lilljequist, 1973 and Bergman et al., 2012). The projection of the Laisvall orebodies to ground surface is also shown. B. Stratigraphic column of the autochthonous sedimentary cover sequence above Paleoproterozoic basement at Laisvall (modified after Rickard et al., 1979; Willdén, 1980; Nielsen and Schovsbo, 2011). The age of the Sorsele granite at Laisvall is after Skiöld (1988).

Strata-bound sandstone-hosted Pb-Zn deposit in autochthonous sedimentary cover rocks and lowermost allochthonous units

Strata-bound Pb-Zn sulfide mineralization hosted by Ediacaran to lower Cambrian siliciclastic sedimentary rocks in autochthonous sequences beneath the Caledonian thrust nappes includes the Osen, Vassbo, Laisvall and Torneträsk deposits and related minor occurrences (Fig. 1A; Christofferson et al., 1979; Rickard et al., 1979; Zachrisson, 1980; Bjørlykke and Sangster, 1981; Stephens, 1986). Similar sandstone-hosted mineralization occurs in the lowermost allochthonous units inside the Caledonian orogen and includes the Granberget, Bellviksberg, and Lövstrand deposits in the Dorotea district (Fig. 1A; Årebäck, 2003; Ayrault, 2008; Chelle-Michou, 2008; Saintilan, 2010).

At Laisvall (Fig. 2A), the autochthonous stratigraphy (Fig. 2B) overlying the Paleoproterozoic (1.8 Ga) granite basement (Skiöld, 1988; Bergman et al., 2012) is approximately 100 m thick and is preserved underneath the main Caledonian décollement in the Alum Shale Formation and the overlying allochthonous thrust sheets. The sequence of autochthonous sedimentary cover rocks comprises the 35 to 40 m-thick Ediacaran to lower Cambrian Laisberg Formation (Willdén, 1980; Nielsen and Schovsbo, 2011) passing upward into the lower Cambrian Grammajukku Formation and the lowermost part of the middle Cambrian to Lower Ordovician Alum Shale Formation (Ljungner, 1950; Rickard et al., 1979; Willdén, 1980; Thickpenny, 1984).

The Laisberg Formation (Fig. 2B) represents a transgressive, sandstone-dominated sequence (Willdén, 1980; Nielsen and Schovsbo, 2011). Epigenetic, disseminated, mottled or banded galena-sphalerite cement mineralization is hosted in two sandstone paleoaquifers, the Lower and Upper Sandstones (Rickard et al., 1979; Willdén, 1980; Saintilan et al., 2015). Calcite, quartz, barite, K-feldspar and fluorite occur as accessory to locally dominant pre-mineralization cements (Rickard et al., 1979; Lindblom, 1986; Saintilan et al., 2014a). A detailed paragenetic sequence of Pb-Zn sulfide mineralization at Laisvall and Raman spectrometry studies of solid and fluid inclusions in sphalerite indicate the local presence of fluorapatite inclusions in sphalerite (Saintilan et al., 2014a). Early diagenetic fluorapatite, in places abundant, is found in cements of the Upper Sandstone. In addition, a new generation of aggregated euhedral to subhedral fluorapatite has been found to be co-genetic within sphalerite (Saintilan et al., 2014a). Organic compounds (i.e., solid organic matter) are intergrown with sphalerite or included in barite (Saintilan et al., 2014a) and hydrocarbons were optically-recognized in fluid inclusions in sphalerite (Lindblom, 1986). These observations are consistent with the results of the work by Rickard et al. (1975) suggesting that the mineralizing fluids contained petroleum-like compounds.

In places, steeply-dipping galena-sphalerite-calcite veinlets cut through both the Lower Sandstone and Upper Sandstone orebodies (Rickard et al., 1979; Saintilan et al., 2015). At Laisvall, parts of the mineralization in the autochthonous sedimentary cover rocks were affected by reverse faults and some mineralization has been incorporated in the lowermost allochthonous thrust sheets (Rickard et al., 1979; Saintilan et al., 2015). These observations suggest that the mineralization pre-dated the middle Silurian to Lower Devonian (post-430 Ma and pre-397 Ma) emplacement of the Caledonian thrust nappes (Stephens, 1988; Gee et al., 2008; Corfu et al., 2014). Similar observations were made at the Vassbo deposit (Christofferson et al., 1979; Saintilan et al., 2015).

The Grammajukku Formation (Willdén, 1980) overlies a thin phosphorite pebble conglomerate horizon at the top of the Laisberg Formation (Fig. 2B). It consists of shale and siltstone with subordinate sandstone intercalations. The overlying Alum Shale Formation (Fig. 2B) comprises mainly black and gray, laminated, organic matter rich mudstone and shale with high total organic carbon contents (1 to 22 wt.% TOC) that could have constituted hydrocarbon source rocks (Thickpenny, 1984). This formation builds a regionally extensive cap rock sealing the hydrodynamic

system above the sandstone paleoaquifers that host the Laisvall deposit. Early diagenetic calcite concretions within the black shales of the Alum Shale Formation in southern Sweden were dated at 509.8 ± 5.1 Ma using U-Pb geochronology (Israelson et al., 1996), an age proposed for the upper Cambrian (Cohen et al., 2013) and in line with the proposed time of deposition of the Alum Shale Formation from middle Cambrian to locally Lower Ordovician using paleontological data (cf. Andersson et al., 1985). Deposition of ≥200 m Lower Ordovician limestone (Gee et al., 2013) caused the "final stage of sediment compaction of the semi-consolidated Alum Shale Formation" and "significant changes in the pore water regime of shale" (Israelson et al., 1996, p. 158). These limestones are not preserved at Laisvall.

At Granberget in the Dorotea district (Fig. 1A), the autochthonous stratigraphy is less than 10 m thick, comprises shale and siltstone, and lacks porous sandstone units, in sharp contrast to the autochthonous stratigraphy at Laisvall. In places, the Alum Shale Formation occurs in direct contact with Paleoproterozoic basement (Gee et al., 1978; Thickpenny, 1984; Saintilan, 2010). Mineralization, not observed in the autochthonous rocks, occurs in clay-matrix, clast-supported, coarse-grained feldspathic sandstone/arkose and conglomerate in the lowermost allochthonous units formed during the Caledonian orogeny. It consists mainly of sphalerite and galena cementing quartz and feldspar detrital grains, similar to that at Laisvall. Fluorapatite is not observed. Disseminated mineralization is tectonically disrupted by subvertical faults, cut by steeply-dipping galena-sphalerite-calcite veinlets, and all these structures are in turn cut by low-angle thrusts (Årebäck, 2003; Saintilan, 2010).

Calcite-galena vein deposits in the basement

Moorbath and Vokes (1963), Wickman et al. (1963), Grip (1967, 1973), Gee (1972), Johansson and Rickard (1984), Lindahl and Bjørlykke (1988), and Sundblad (1990) report the existence of several calcite-galena vein deposits in the Paleoproterozoic and Archean basement of Baltica. Several of these vein deposits occur 10 to 35 km east of the current erosional front of the Scandinavian Caledonides in Sweden and Norway (Fig. 1A). In addition, veins comprising either quartz-calcite-barite-galena-sphalerite or only calcite-galena (Sundblad, 1990) are found along the shoreline of the Kola Peninsula in Norway and Russia (Fig. 1A). In all cases, lead isotope studies suggest that Pb in galena was derived from local Precambrian basement rocks (Johansson, 1983a; Johansson and Rickard, 1984; Lindhal and Bjørlykke, 1988; Sundblad, 1990; Romer and Wright, 1993; Billström et al., 2012).

Along the erosional front of the Scandinavian Caledonides, calcite-fluorite- Zn ± Pb sulfide vein deposits in the Storuman and Åkerlandet districts (Fig. 1A) are hosted by Paleoproterozoic (1.9 Ga) metasedimentary rocks intruded by Revsund granite (1.8 Ga), and Paleoproterozoic (1.9 Ga) migmatitic paragneiss and homogeneous leucocratic granite, respectively (Bergman et al., 2012). The vein deposits are located in brittle structures along shear zones with N–S to NE–SW trends and both strike-slip and dip-slip components of movement (Billström et al., 2012; Saintilan et al., 2012).

Johansson (1983b, 1984) and Billström et al. (2012) proposed that these vein deposits formed by the mixing of a hot (160–200°C) saline hydrothermal fluid with a cooler (< 70°C), less saline fluid.

Sample selection and analytical procedures

Sample selection for Rb-Sr isotope systematics and characterization

Sphalerite samples from the orebodies at Laisvall were taken from the two distinct types of mineralization at the deposit: disseminated sphalerite mineralization as cement in sandstone, referred to hereafter as disseminated samples; and steeply-dipping galena-sphalerite-calcite veinlets discordant to the disseminated mineralization, referred to hereafter as veinlet samples. The sampling included: (i) two disseminated and three veinlet samples from the Upper Sandstone orebody; (ii) three disseminated and two veinlet samples from the Lower Sandstone orebody (Table 1). Several sphalerite generations have been distinguished petrographically and by means of sulfur isotope data (Saintilan et al., 2014a, b). All samples belong to the main sphalerite generation characterized by heavy $\delta^{34}S$ values from 27.0 to 34.0‰, indicating H_2S produced by thermochemical sulfate reduction (cf. Rickard, 1983; Saintilan et al., 2014a, b) involving hydrocarbons (cf. Rickard et al, 1975; Lindblom, 1986; Saintilan et al., 2014c). The sampling procedure avoided earlier-stage generations that formed by replacement of early diagenetic framboidal pyrite and euhedral diagenetic pyrite ($\delta^{34}S$ values from –11.0 to –6.0‰, and from 21.0 to 31.0‰, respectively; Saintilan et al., 2014a, b). The samples were collected from drill cores stored at the Geological Survey of Sweden (SGU) in Malå and at the Boliden AB core archive in Boliden, Sweden. The ten samples were selected in profiles in proximal and distal positions relative to the Nadok fault and Central Malm fault systems (Table 1), which are interpreted as having been main feeder systems for mineralization (Saintilan et al., 2015).

In addition, three disseminated samples from the Granberget deposit were taken from drill core archived in Boliden (Table 1). Furthermore, one intensely mineralized sphalerite-rich calcite-fluorite-sulfide vein sample was selected at Åkerlandet for analysis from the old adit in a previously operated small-scale quarry within the main mineralized area along a shear zone. Given the close proximity between the Granberget deposit and the basement-hosted Åkerlandet vein deposit (Fig. 1A), the original goal was to combine the Rb-Sr systematics of these samples in a regression to study the possible genetic link between these two deposits.

Thin sections of all samples were studied by transmitted and reflected light microscopy. The paragenetic sequence and the relationships between the pre-sphalerite stage cements, the accessory mineral phases, and the sphalerite-stage mineral associations have been established for Laisvall and presented elsewhere (Saintilan et al., 2014a). Carbon-coated, polished thick sections of two representative disseminated samples from both the Lower and Upper Sandstone orebodies at Laisvall (~100 µm thick) and of the sample from Åkerlandet (~30 µm thick) were utilized for electron microprobe and subsequent LA-ICPMS analyses.

Portions of all samples (Table 1) were crushed using a hydraulic press and sieved. Following heavy liquid separation of the 315–125 μm size fractions, the heavy mineral fractions were handpicked under a binocular microscope to obtain about 75 mg sphalerite aliquots for Rb-Sr isotope analysis.

Table 2 lists the samples selected from key stratigraphic units at Laisvall for whole-rock and Sr isotope geochemical analyses. Samples of granite, collected from drill core pieces or basement outcrops in the field, were crushed and milled using an automated grinder with a built-in agate mortar. Other drill core samples include black (11LAI16-2) and dark-gray shale (11LAI45) from the Alum Shale Formation, and a green shale (11LAI26) from the Grammajukku Formation. In addition, a sphalerite-mineralized sample (11LAI03-2) was taken from the lower part of the phosphorite conglomerate at the contact with the underlying sphalerite±galena-mineralized Upper Sandstone orebody (Fig. 2B), and a poorly galena-mineralized sample (11LAI03-1) was collected from the upper part of this conglomerate in contact with the green shale belonging to the Grammajukku Formation.

Whole-rock X-ray fluorescence (XRF) analyses were performed for major, minor and trace elements (including Rb and Sr) on these samples, using an Axios Advanced 4.0 kW X-ray fluorescence spectrometer at the University of Lausanne, Switzerland.

Mineral chemistry of sphalerite

Major and minor elements in sphalerite (S, Zn, Fe, Mn, Cu, Se, Ag, Cd and In) were quantified in the thick sections by electron microprobe analysis (EMPA, JEOL 8200 electron Superprobe) at the University of Lausanne, Switzerland. Operating conditions were set to an acceleration voltage of 20 kV, a beam current of 40 nA, and a counting time of 20 seconds for peak and 2x10 seconds for background. Se, Ag and In were systematically below detection limit in all samples, and Cu was detected and quantified only rarely. Data for S, Mn, Fe, Cu, Zn and Cd were averaged using the geometric mean per sample and reported with 1σ standard deviations.

LA-ICPMS analyses of trace elements in sphalerite were conducted using a 193 nm ArF Excimer laser with an energy-homogenized beam profile coupled with the ELAN 6100 DRC ICP quadrupole mass spectrometer (QMS) at ETH Zürich, Switzerland (Günther et al., 1997; Heinrich et al., 2003). Table 3 provides a summary of the elements analyzed and the analytical conditions and data acquisition parameters. The ablation rate for sphalerite was between 0.1 and 0.2 μm/pulse. By adjusting an aperture in the laser beam path, the optical imaging system permits visual positioning of ablation points and the use of different pit diameters (30-60 μm) at constant energy densities. The samples were loaded, along with the synthetic polymetallic sulfide standard MASS-1 (Wilson et al., 2002) and the SRM 610 glass NIST standard, in a 1 cm^3 ablation cell on a modified Zeiss petrographic microscope. P, Rb and Sr were quantified using the SRM 610 glass NIST external standard; for quantification of all other elements, the MASS-1 standard was used. Data reduction was carried out using the SILLS software (Guillong et al., 2008) and using the Zn content, known from electron microprobe analyses, as an internal standard.

Si was used to monitor inclusions of hydrothermal quartz in sphalerite, while P was used to monitor the presence of fluorapatite inclusions in sphalerite or of fluorapatite lining sphalerite crystals along contacts with detrital quartz and quartz overgrowths in the host sandstone at Laisvall (Fig. 3). In order to optimize the LA-ICPMS analyses using ablation crater diameters of 30–60 μm, an effort was made to pre-select sphalerite volumes free of obvious fluorapatite, quartz, galena or other solid and fluid inclusions by combining SEM-CL imaging with transmitted and reflected light microscopy (Fig. 3). However, such inclusions may not have been avoided in all instances. Representative single-spot spectra chosen from the complete dataset, showing both smooth and irregular profiles, are shown in Figure 4. Since the spot sizes used for LA-ICPMS analyses were greater than many of these inclusions, the ablation profiles are not invariably homogenous at the scale of the ablation spots (Figs. 4A and B). Aside from such inclusions, the analyzed samples show rather homogeneous ablation profiles for other elements.

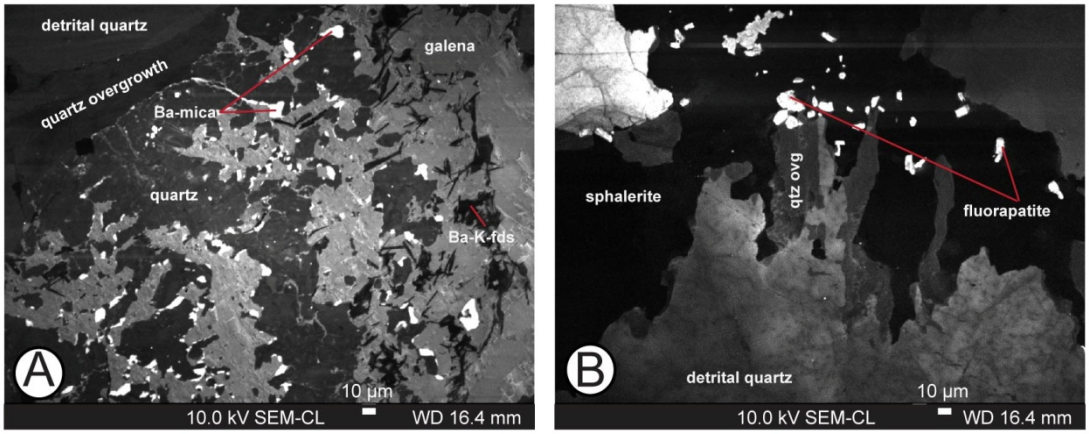

Fig. 3 Scanning electron microscope, cathodoluminescence mode (SEM-CL) images of galena-mineralized (A) and sphalerite-mineralized (B) sandstone at Laisvall, showing details of diagenetic quartz overgrowth (qtz ovg) on detrital quartz grains, as well as later co-genetic Ba-mica and Ba-bearing K-feldspar inclusions in galena, and co-genetic fluorapatite inclusions in sphalerite.

Table 1. ocation and geologic setting of "disseminated" and "veinlet" sphalerite samples from the orebodies at Laisvall and at the Granberget deposit, and the sphalerite sample from the basement-hosted Åkerlandet vein deposit selected for Rb-Sr isotope geochemistry. The δ^{34}S VCDT isotope compositions (± 0.3‰) of the sphalerite aliquots are after Saintilan et al. (2014a). n.a.: not analyzed.

Deposit	Sample	Mineral phase (δ^{34}S VCDT)	Type	Location and geologic setting
Laisvall, Upper Sandstone orebody	**12 LAI 12**	Sphalerite δ^{34}S = 29.0‰	Disseminated	Beige, disseminated sphalerite in borehole 1647 ~20 m to the north of the northern segment of the Kautsky fault (distal, north-west of the Nadok fault)
	12 LAI 52	Sphalerite δ^{34}S = 29.2‰	Disseminated	Mottled mineralization with different colours of sphalerite (yellow and orange) in borehole 280 on the Nadok fault
Laisvall, Lower Sandstone orebody	**12 LAI 03**	Sphalerite δ^{34}S = 31.5‰	Disseminated	Typical interstitial mottled mineralization. Located ~50 m to the south-east of the northern segment of the Kautsky fault in borehole 1610 (distal, north-west of the Nadok fault)
	12 LAI 53	Sphalerite δ^{34}S = 29.1‰	Disseminated	Located on the Nadok fault in borehole 280. Typical mottled mineralization
	11 LAI 33	Sphalerite δ^{34}S = 28.2‰	Disseminated	Located in borehole 1580, a few meters to the north of the densely fractured area in the Lower Sandstone, where the mineralization makes an inflection point changing direction from NE–SW to NW–SE (distal, east of the Nadok fault)
Laisvall, veinlets in Upper Sandstone orebody	**12 LAI 43**	Sphalerite δ^{34}S = 28.3‰	Veinlet	Steeply-dipping galena-sphalerite-calcite veinlets in borehole 258, ~25 m north of the small fault between the Niepsurt and Kramaviken faults (Central Malm)
	12 LAI 44-1 & -2	Sphalerite δ^{34}S = 29.8‰	Veinlet	Several veinlets at same location as 12 LAI 43
Laisvall, veinlets in Lower Sandstone orebody	**12 LAI 14**	Sphalerite δ^{34}S = 29.4‰	Veinlet	Steeply-dipping galena-sphalerite-calcite veinlet on the northern segment of the Kautsky fault
	12 LAI 84	Sphalerite δ^{34}S = n. a.	Veinlet	Steeply-dipping galena-sphalerite-calcite veinlet on the northern segment of the Kautsky fault

Table 1. (cont.)

Granberget	**BRB 50**	Sphalerite $\delta^{34}S$ = 17.2‰	Disseminated	Main mineralized lens (Saintilan, 2010)
	BRB 56	Sphalerite $\delta^{34}S$ = 14.1‰	Disseminated	Mineralization in secondary lenses above a low-angle thrust above the main lens (Saintilan, 2010)
	BRB 58	Sphalerite $\delta^{34}S$ = 19.3‰	Disseminated	
Åkerlandet vein deposit	**12 AKE 01**	Sphalerite $\delta^{34}S$ = 0.1‰	Basement-hosted vein	Calcite-fluorite vein with brecciated sphalerite-quartz-adularia clasts

Table 2. Whole-rock samples selected in the stratigraphy at Laisvall (Fig. 2B) for major, minor and trace element geochemistry as well as radiogenic Sr isotope geochemistry.

Sample number	Rocktype
11LAI16-2	Black shale with pyrite in the Alum Shale Formation
11LAI45	Grey shale with organic matter in the Alum Shale Formation
11LAI26	Green shale in the Grammajukku Formation
11LAI03-1	Phosphorite polymictic conglomerate, poorly galena-mineralized
11LAI03-2	Phosphorite polymictic conglomerate with interstitial sphalerite
11BAS01	Granite (1.8 Ga) in the crystalline basement
11BAS02	Granite (1.8 Ga) in the crystalline basement
11BAS03	Granite (1.8 Ga) in the crystalline basement
11BAS04	Granite (1.8 Ga) in the crystalline basement
11BAS05	Granite (1.8 Ga) in the crystalline basement
11BAS06	Granite (1.8 Ga) in the crystalline basement

Table 3. LA_ICPMS machine and data acquisition parameters.

Excimer 193 nm ArF laser Compex 110I	Sphalerite
Output energy	20 mJ
Homogeneous energy density on sample	~5 J/cm^2
Repetition rate	5 Hz
Ablation mode	Single hole
Crater sizes	30-60 µm
Ablation cell	In-house built glass chamber with anti-reflection coated silica glass window
Perkin Elmer ELAN 6100 DRC	
Rf-power	1550 W
Detector mode	Dual
Quadrupole setting time	3 ms
Nebulizer gas flow	0.79 l/min Ar
Auxiliary gas flow	0.85 l/min Ar
Plasma gas flow	15.5 l/min Ar
Carrier gas flow	1.1 l/min He
Additional gas flow	5 ml/min H_2
Data acquisition parameters	
Sweeps per reading	1
Readings per replicate	300
Replicates	1
Dwell time per isotope	30 ms for Ga, Rb, Sr 10 ms for all others
Points per peak	1 per measurement
Oxide production rate	tuned to <0.5 % ThO
Isotopes analyzed	^{28}Si, ^{31}P, ^{32}S, ^{55}Mn, ^{57}Fe, ^{65}Cu, ^{66}Zn, ^{69}Ga, ^{77}Se, ^{85}Rb, ^{88}Sr, ^{109}Ag, ^{111}Cd, ^{115}In, ^{118}Sn, ^{121}Sb, ^{208}Pb

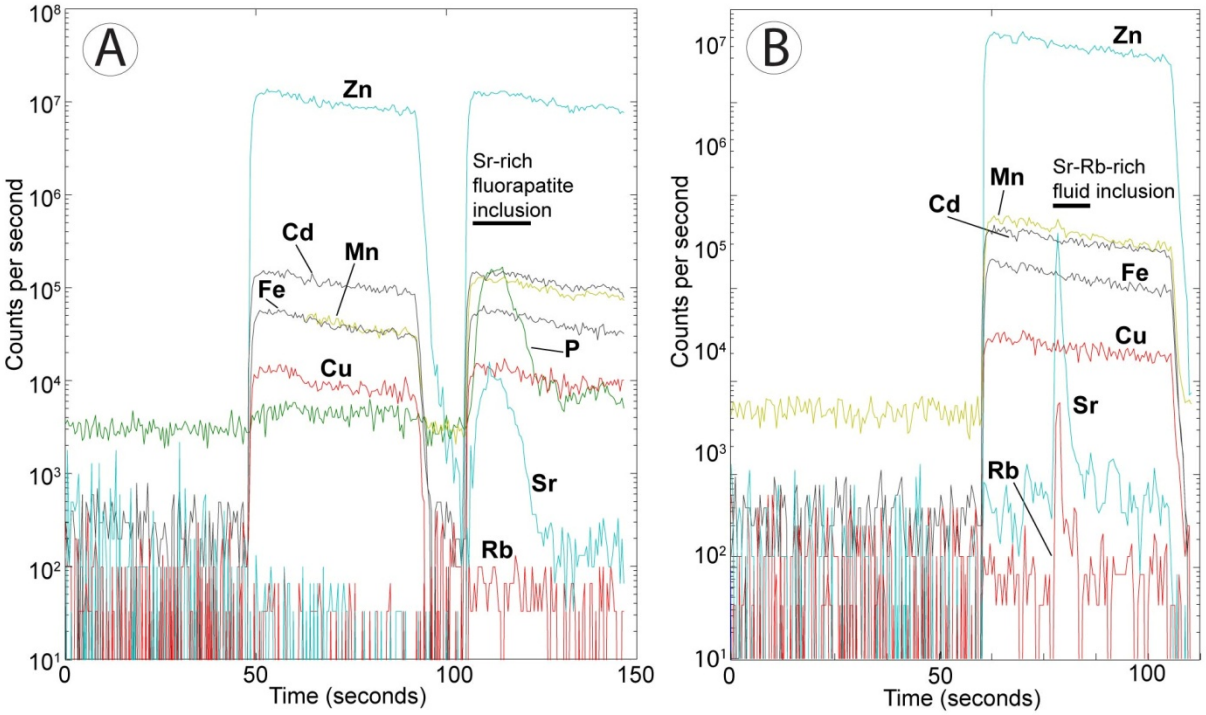

Fig. 4 Representative single-spot LA-ICPMS spectra for Rb, Sr, P, and major elements (previously determined by EMPA) in sphalerite in the Upper Sandstone orebody at Laisvall. A. The spectrum is composed of two successive single-spot analyses within the same sphalerite crystal. Note the presence of Sr-rich fluorapatite inclusion at the beginning of the second analysis. B. Sphalerite with representative heterogeneous distribution of Sr and Rb in sphalerite. Note the presence of a Sr- and Rb-rich fluid inclusion in the central part of the spectrum (see text for discussion). Spectra similar to Fig. 4B exist for sphalerite in the Lower Sandstone orebody.

Rb-Sr isotope analysis of sphalerite and whole-rock samples

The sphalerite separates were leached in 2 N HCl and 2 N HF (15 min. each) to remove carbonate, phosphate or silicate (cf. Schneider et al. 1999). The separates were then repeatedly washed and ultrasonified in deionized water. The wet separates were crushed using a pre-cleaned boron carbide mortar and pestle for 2 to 5 minutes and ~1.5 ml of deionized water was added after crushing in order to sample the liberated fluid inclusions. Care was taken to grind the aliquots thoroughly to minimize the possibility of contributions from unopened fluid inclusions (Pettke and Diamond, 1996). The leachate (L) was recovered from the residual sphalerite, hereafter referred to as residue or R by repeated centrifuging. The first supernate was kept as the fluid inclusion leachate sample and a known weight of a mixed tracer containing highly enriched ^{87}Rb and ^{84}Sr was added to these solutions.

The residual sphalerite powders were again leached and sonified in 2 N HCl and 2 N HF (15 min. each), with repeated water washes in between until neutral reaction of the supernate. All washes were discarded. The residues were transferred to pre-weighed Teflon vials and dried overnight. Subsequently, the sample containers were allowed to cool and reweighed to obtain the sample weights. The sphalerite residues were then totally spiked using a mixed ^{87}Rb-^{84}Sr tracer solution and dissolved in 6 N HCl on a hot plate.

Rubidium and strontium were separated with 3 N HNO_3 using EICHROM Sr resin on 50 µl Teflon microcolumns, following the methods of Deniel and Pin (2001). The first 600 µl of HNO_3 wash were collected for Rb collection. The Rb cuts from sphalerite residues were further purified using standard cation-exchange procedures (Birck, 1986), whereas no additional Rb separation was necessary for the fluid inclusion liquids. Sr was stripped from the columns with 1 ml of deionized water. For thermal ionization mass spectrometry of spiked sphalerite Rb and Sr (ID-TIMS), Sr was loaded with a $TaCl_5$-HF-H_3PO_4 solution (Birck, 1986) onto W single filaments. Rb was loaded with 2 N HNO3 onto the evaporation ribbon of a Ta double-filament assemblage.

Between 100 and 150 mg of powdered whole-rock samples were prepared and dissolved following the procedure described in Chiaradia et al. (2011). Strontium was separated from the rock matrix using EICHROM Sr resin before being converted into 5 ml solutions of 2% HNO_3.

All isotopic measurements of the Rb and Sr cuts from sphalerite residues and leachates were performed on Thermo Fisher TRITON (ID-TIMS), while Sr isotope ratios of whole-rock samples were determined by multicollector ICP-MS (NEPTUNE) in static mode using the virtual amplifier mode at the University of Geneva, Switzerland. Details relative to procedural blank corrections and in-run and external fractionation corrections are given in Appendix 1. A $^{87}Sr/^{86}Sr$ ratio of 0.721269 ± $1.4*10^{-5}$ (2σ) is reported as 0.721269 ± 14.

Rb-Sr model isochron regressions were calculated after Ludwig (2003) using the ISOPLOT/Ex version 3.00 program. For iterative planar paleomixing line regressions according to Schneider et al. (2003), an internal FORTRAN subroutine «MIXING LINE 3 D» was used. The decay constant used for the age calculations was $\lambda^{87}Rb = 1.42 \times 10^{-11} a^{-1}$ (Steiger and Jäger, 1977), and errors on Rb-Sr model ages are quoted at the 2σ level. The goodness of fit of linear and planar regressions has been tested by means of the MSWD parameter (Wendt and Carl, 1991).

Results

Minor and trace-element distribution in sphalerite from disseminated samples

Major and minor element concentrations of sphalerite samples are provided in Appendix 2. The full LA-ICPMS dataset of minor and trace-elements in sphalerite, including 60 single-spot analyses in the Laisvall samples and 31 single-spot analyses in the Åkerlandet sample, is reported in Appendix 3. Apatite inclusions were identified by P and Sr peaks in the ablation profiles (Fig. 4A). The presence of parts of the ablated samples rich in or devoid of Rb- and Sr-rich fluid inclusions in sphalerite is readily identified in ablation profiles (Figs. 4B). In ablated samples devoid of fluid inclusion, Sr and Rb contents in sphalerite do not correlate with the distribution of the principal trace metals (e.g., Zn, Mn, Fe, Cu, and Cd; Figs. 4A and B).

Rb-Sr isotope systematics of sphalerite

The results of Rb and Sr isotope analyses for sphalerite samples are shown in Table 4. The Rb and Sr elemental concentrations of the sphalerite residues (R) obtained in the three analyzed deposits display wide ranges (0.015 to 2.6 ppm Rb and 0.071 to 3.017 ppm Sr). Except for one sample from the Lower Sandstone orebody at Laisvall, which has a high Rb content of 2.601 ppm, Rb contents remain below 0.4 ppm, whereas Sr shows greater variations, with several Laisvall sphalerite residues showing high contents of Sr (2.121 to 3.017 ppm). In general, the Rb and Sr elemental concentrations of the sphalerite residues obtained in the three analyzed deposits are consistent with other published Rb-Sr data for sulfides (see Reesman, 1968; Medford et al., 1983; Nakai et al., 1990, 1993; Brannon et al., 1991, 1992; Nelson et al., 2002, Christensen et al., 1995a, b; Yang and Zhou, 2001). See also Rb and Sr concentrations found in sphalerite and other sulfides in Mississippi Valley-type (MVT) deposits, e.g., from Pine Point, Northwest Territories, Canada (Medford et al., 1983) and from the Immel Mine/Coy Mine, Mascot-Jefferson MVT district, eastern Tennessee (Nakai et al., 1990; 1993). Rb and Sr concentrations of fluid inclusion leachates are not reported because the total amount of trapped fluid in the samples cannot be determined.

The sphalerite samples have $^{87}Rb/^{86}Sr$ ratios between 0.141 and 7.25, with most ratios being lower than 0.6. All sphalerite samples show moderately radiogenic $^{87}Sr/^{86}Sr$ ratios between 0.7191 and 0.7645 (Table 4). On a $^{87}Sr/^{86}Sr$ vs. $^{87}Rb/^{86}Sr$ correlation (isochron) diagram including the three studied deposits (Fig. 5A), the sphalerite residues scatter widely and do not define an all-sample Rb-Sr isochron. Remarkable internal contrasts in the Rb-Sr isotope systematics are found between the two following groups of samples: (i) the three disseminated samples from the Lower Sandstone orebody at Laisvall, one disseminated sample (12LAI52 R) from the Upper Sandstone orebody, and the Åkerlandet vein sample; (ii) the other sphalerite samples from the Upper Sandstone orebody, the veinlet samples from the Lower Sandstone orebody at Laisvall, and the disseminated samples from the Granberget deposit.

In a $^{87}Sr/^{86}Sr$ vs. $^{87}Rb/^{86}Sr$ diagram, the three disseminated residues from the Lower Sandstone orebody plot along a line of moderate slope which can be interpreted to represent a three-point isochron (Fig. 5B); the slope corresponds to an age of 467 ± 5 Ma (Mean Square Weighted Deviation, MSWD = 1.4, with an initial $^{87}Sr/^{86}Sr$ ratio of 0.715900 ± 60). Since the isochron is based on three points, the obtained age is to be considered preliminary. These residues do not plot as a mixing array but remain scattered in a $^{87}Sr/^{86}Sr$ vs. $1/^{86}Sr$ diagram (Fig. 6A). The results suggest that the original Rb-Sr system in the disseminated sphalerite mineralization in the Lower Sandstone orebody has been preserved. The three corresponding fluid inclusion leachates plot slightly above this model isochron, reflecting limited post-mineralization disturbance. The disseminated residue 12LAI52 (R) from the Upper Sandstone orebody also plots slightly above this model isochron.

For the given number of sphalerite residues from the Lower Sandstone orebody (n = 3) and considering their true and limited analytical errors (Table 4), the goodness of fit in terms of MSWD indicates that these sphalerite residues are age concordant in the sense of the isochron model. This

interpretation is supported by leachate sample 12LAI03 (L) which has the least radiogenic $^{87}Sr/^{86}Sr$ ratio (0.717892 ± 3) of the entire sample set and, therefore, most probably represents the pristine isotopic fluid composition.

Table 4. Rb-Sr isotopic composition of residues and corresponding leachates of sphalerite samples from the Lower Sandstone and Upper Sandstone orebodies (disseminated samples) and remobilization veinlets (veinlet samples) at the Laisvall deposit, from the sandstone-hosted Granberget deposit and from the basement-hosted Åkerlandet vein deposit. *Rb and Sr concentrations of fluid inclusions are not reported because the total amount of trapped fluid in the samples is not know. [1]: Leachate BRB58 was lost.

	$^{87}Rb/^{86}Sr$	2σ	$^{87}Sr/^{86}Sr$	2σ 10^{-6}	Rb [ppm]	2σ	Sr [ppm]	2σ
Crushed-leached sphalerite residues (R)								
Laisvall Upper Sandstone								
12 LAI 12 R	0.2572	0.0038	0.726134	2	0.1339	0.0017	1.5090	0.0197
12 LAI 52 R	1.3499	0.0193	0.727203	4	0.1677	0.0021	0.3600	0.0047
Laisvall Lower Sandstone								
12 LAI 03 R	0.4946	0.0071	0.719191	4	0.0973	0.0012	0.5695	0.0074
11 LAI 33 R	4.9872	0.0715	0.748900	17	0.3194	0.0041	0.1860	0.0024
12 LAI 53 R	7.2453	0.1173	0.764457	6	2.6007	0.0364	1.0443	0.0136
Veinlet in Laisvall Upper Sandstone								
12 LAI 43 R	0.1570	0.0025	0.726391	2	0.1149	0.0016	2.1211	0.0277
12 LAI 44 R (1)	0.2600	0.0038	0.726294	24	0.1025	0.0013	1.1426	0.0149
12 LAI 44 R (2)	0.1699	0.0024	0.725305	3	0.1624	0.0021	2.7714	0.0363
Veinlet in Laisvall Lower Sandstone								
12 LAI 14 R	0.4654	0.0520	0.739143	10	0.0303	0.0026	0.1892	0.0025
12 LAI 84 R	0.2626	0.0038	0.737266	8	0.0323	0.0004	0.3568	0.0047
Granberget								
BRB 50 R	0.4991	0.0074	0.746848	89	0.2243	0.0029	1.3051	0.0173
BRB 56 R	0.1416	0.0020	0.729805	5	0.0154	0.0002	0.3144	0.0041
BRB 58 R	0.2667	0.0038	0.744350	14	0.2771	0.0035	3.0170	0.0394
Åkerlandet								
AKE-1 R	1.1129	0.0158	0.723380	8	0.0274	0.0004	0.0713	0.0009
Fluid inclusion leachates (L)*								
Laisvall Upper Sandstone								
12 LAI 12 L	0.1025	0.0015	0.723846	4	-	-	-	-
12 LAI 52 L	0.1290	0.0019	0.722199	3	-	-	-	-
Laisvall Lower Sandstone								
12 LAI 03 L	0.1265	0.0018	0.717892	3	-	-	-	-
11 LAI 33 L	1.2249	0.0229	0.727581	20	-	-	-	-
12 LAI 53 L	1.1512	0.0165	0.732624	5	-	-	-	-
Veinlet in Laisvall Upper Sandstone								
12 LAI 43 L	0.0959	0.0014	0.727287	6	-	-	-	-

12 LAI 44 L (1)	0.2635	0.0038	0.722985	4	-	-	-	-
12 LAI 44 L (2)	0.1130	0.0016	0.725883	3	-	-	-	-
Veinlet in Laisvall Lower Sandstone								
12 LAI 14 L	0.1736	0.0025	0.740630	3	-	-	-	-
12 LAI 84 L	0.1508	0.0022	0.738577	3	-	-	-	-
Granberget[1]								
BRB 50 L	0.1133	0.0017	0.745676	24	-	-	-	-
BRB 56 L	0.1177	0.0017	0.733489	4	-	-	-	-
Åkerlandet								
AKE L	0.1424	0.0020	0.720009	4	-	-	-	-

The sphalerite residue from the Åkerlandet calcite-galena basement-hosted vein also plots close to the above-mentioned line of moderate slope and would fall on the three-point model isochron defined by the sphalerite residues from the Lower Sandstone orebody at Laisvall (cf. Figs. 5B and 5C). A combined four-point model isochron (Fig. 5C) would yield an age of 468 ± 5 Ma with an essentially identical MSWD and initial $^{87}Sr/^{86}Sr$ ratio as those of the three-point isochron for the Lower Sandstone disseminated mineralization. The Åkerlandet fluid inclusion leachate plots close to leachate 12LAI03 (L), and similarly, slightly above this model isochron, reflecting limited post-mineralization disturbance. These results are intriguing when taking into account the different geologic settings and the distance between the Åkerlandet and Laisvall deposits, as discussed in more detail below.

All other fluid inclusion leachates and the corresponding residues (i.e., from the Upper Sandstone orebody at Laisvall, from the Granberget deposit, and from two veinlet samples in the Lower Sandstone orebody are positively correlated (r = 0.785) and plot along a steep linear trend with MSWD >10 000 (Fig. 5A). The slope of this line corresponds to an unrealistic age (2.65 Ga), far in excess of the age of rocks hosting the deposits. Schneider et al. (2003) successfully evaluated a method that enables the dating of Sr isotopic disequilibrium in hydrothermal alteration assemblages by reconstruction of hypothetical two-component paleomixing lines in $^{87}Sr/^{86}Sr$ vs. $1/^{86}Sr$ space from Rb-Sr analytical data, using an iterative planar regression approach. However, application of this method to the sphalerite residues analyzed in this study does not yield statistically robust binary paleomixing lines for any realistic age (calculated ages are in excess of 3.0 Ga). As discussed below, this trend probably reflects post-mineralization event(s) that affected and disturbed the Rb-Sr systems of both the inclusion fluids and their host minerals in most samples from the Upper Sandstone, in the veinlet samples of the Lower Sandstone orebodies, and in all samples from Granberget.

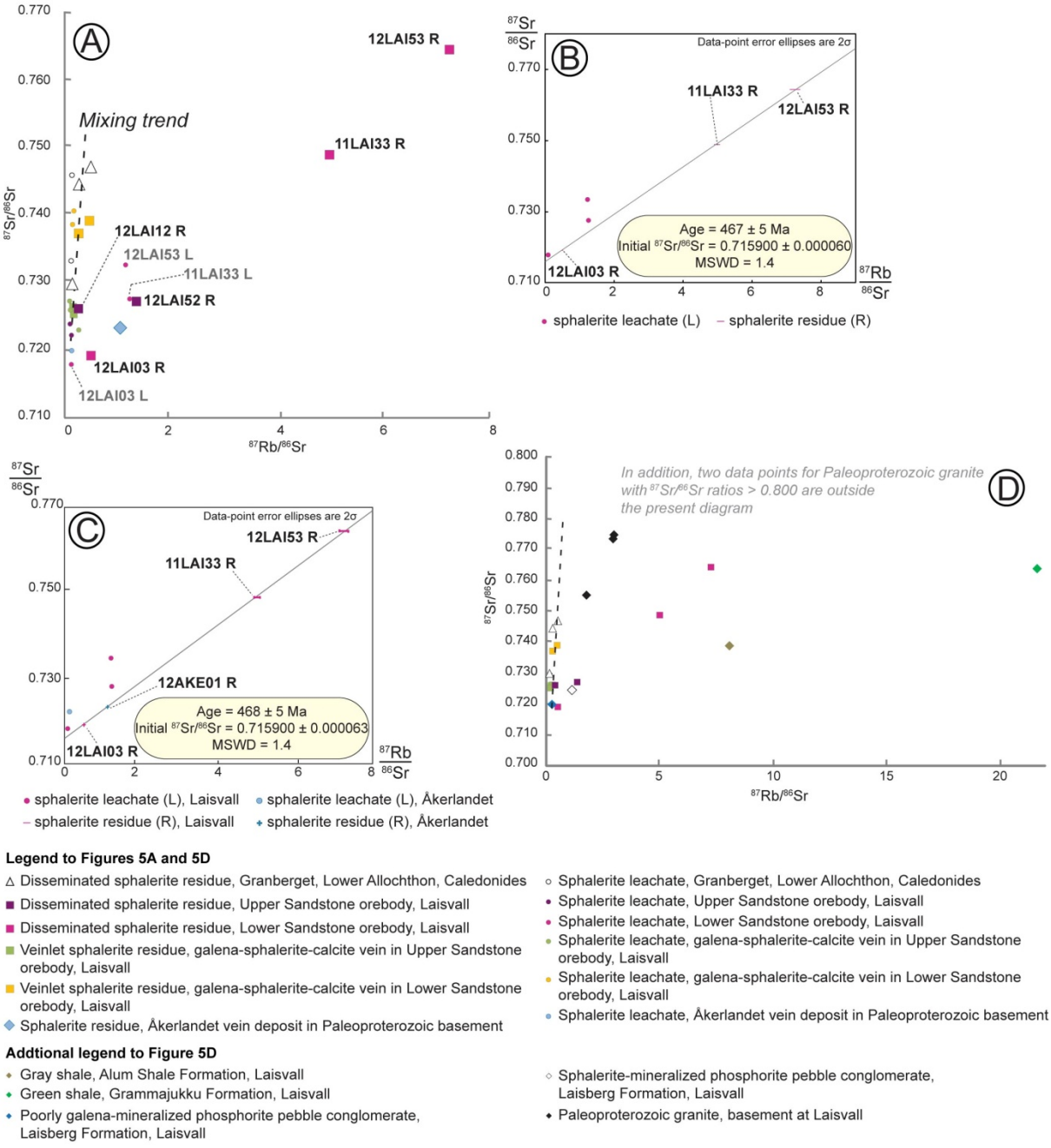

Fig. 5 A. $^{87}Sr/^{86}Sr$ vs. $^{87}Rb/^{86}Sr$ diagram for sphalerite disseminated residues and complementary leachates from the Lower Sandstone and Upper Sandstone orebodies, from remobilization veinlets at the Laisvall deposit, from the sandstone-hosted Granberget deposit, and from the Åkerlandet vein deposit in Paleoproterozoic basement. B. Rb-Sr isochron diagram for disseminated sphalerite samples (n = 3) from the Lower Sandstone orebody at Laisvall. 2σ values are provided in Table 4. C. Rb-Sr isochron diagram for disseminated sphalerite samples from the Lower Sandstone orebody at Laisvall and the sphalerite residue from the Åkerlandet vein deposit in Paleoproterozoic basement (n = 4). 2σ values are provided in Table 4. D. $^{87}Sr/^{86}Sr$ vs. $^{87}Rb/^{86}Sr$ diagram for sphalerite disseminated residues from the Lower Sandstone and Upper Sandstone orebodies, from remobilization veinlets at the Laisvall deposit, and from the sandstone-hosted Granberget deposit. Data points with the Rb-Sr isotopic composition of granite (1.8 Ga) in the Paleoproterozoic basement, in the phosphorite pebble conglomerate of the Laisberg Formation, in the green shale of the Grammajukku Formation, and in the gray shale of the overlying Alum Shale Formation at Laisvall are also shown. Two data points for Paleoproterozoic granite with $^{87}Rb/^{86}Sr$ ratios above 20 and $^{87}Sr/^{86}Sr$ ratios between 1.2 and 1.4 plot outside the present diagram but define a statistically-robust regression line with the other granite samples. See text for further discussion.

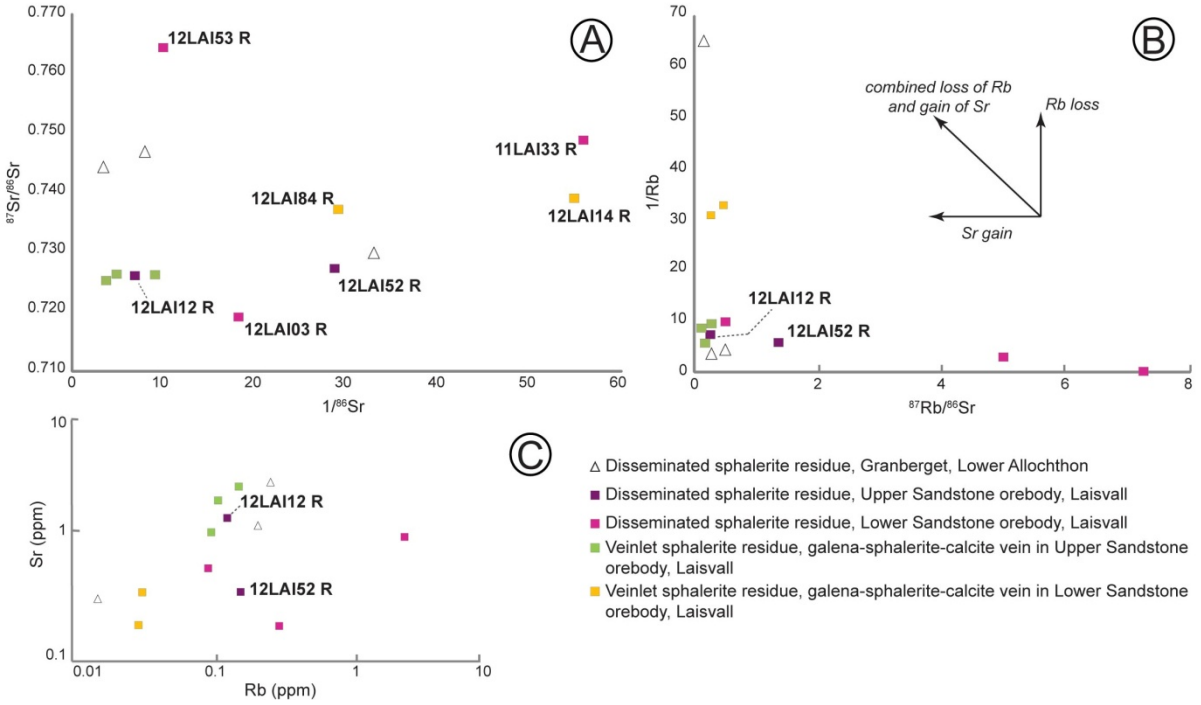

Fig. 6 A. $^{87}Sr/^{86}Sr$ vs. $1/^{86}Sr$ diagram for residues of disseminated sphalerite samples from the Lower Sandstone and Upper Sandstone orebodies, from remobilization veinlets at the Laisvall deposit, and from the sandstone-hosted Granberget deposit. 2σ values are provided in Table 4. B. 1/Rb vs. $^{87}Rb/^{86}Sr$ diagram for the same residues of sphalerite as shown in Fig. 6A. The alignment of the residues of disseminated sphalerite samples from the Lower Sandstone orebody is a consequence of isochronism identified in Fig. 5B. 2σ values are provided in Table 4. C. Sr vs. Rb diagram showing the ppm contents of these elements in the same residues of sphalerite as included in Fig. 6A. 2σ values are provided in Table 4.

Geochemistry and Sr isotope composition of the crystalline basement and the autochthonous sedimentary cover sequence at Laisvall

XRF analyses of oxides and trace elements in dark-gray shale from the Alum Shale Formation, in green shale from the Grammajukku Formation, and in variably mineralized polymictic phosphorite conglomerate beneath the Grammajukku Formation are given in Appendix 4. Dark-gray and green shales have relatively high K_2O (2.1 and 5.6 wt%, respectively) and P_2O_5 contents (0.2 and 0.3 wt%, respectively). The P_2O_5 enrichment is probably linked to numerous phosphorite pebble horizons present in green shale in the Grammajukku Formation (Nielsen and Schovsbo, 2011; Saintilan et al., 2015), whereas high K_2O contents are probably related to feldspar-rich silt inliers (cf. Willdén, 1980). Both shale samples are characterized by rather high Rb and Sr contents. The Rb content of dark-gray shale is about three times lower than that of green shale (111 and 372 ppm, respectively), whereas Sr contents are similar in both shale units (40 and 50 ppm, respectively). The samples of poorly mineralized sub-horizons in polymictic phosphorite pebble conglomerate have Sr contents of 122 and 77 ppm and Rb contents of 10 and 30 ppm, respectively. The sphalerite-mineralized sample has three times the Rb content of the galena-mineralized sample, but much lower Sr content.

The strontium isotope data and the Rb and Sr concentrations of the rock units that underlie and overlie the mineralized sandstone units in the stratigraphy at Laisvall are presented in Table 5. Black shale with pyrite and gray shale have present-day $^{87}Sr/^{86}Sr$ ratios of 0.721269 ± 14 and 0.739333 ± 14, respectively, whereas underlying green shale has a $^{87}Sr/^{86}Sr$ ratio of 0.764182 ± 16. Correction of these $^{87}Sr/^{86}Sr$ ratios for radiogenic growth back to the presumed depositional age yields unrealistically low values < 0.7020 (even for 200 to 300 Ma).

The samples of poorly mineralized phosphorite pebble conglomerates have $^{87}Sr/^{86}Sr$ ratios of 0.720336 ± 14 and 0.724978 ± 14, respectively. Due to their low Rb/Sr ratios, these radiogenic values cannot be explained solely by decay of the original Rb, which would have yielded $^{87}Sr/^{86}Sr$ values around 0.715 when corrected for a presumed sedimentation age of ~530 Ma. For this reason, it is proposed that both samples have experienced hydrothermal overprints.

Two granite samples with chlorite-altered amphibole have comparable, moderately radiogenic present-day $^{87}Sr/^{86}Sr$ ratios of ~0.774 as well as $^{87}Rb/^{86}Sr$ ratios and elemental concentrations. By contrast, reddened granite samples with hematite veinlets have highly radiogenic strontium ratios ($^{87}Sr/^{86}Sr$ of 1.188594 ± 20 and 1.286898 ± 20) while relatively fresh granite samples have relatively low $^{87}Sr/^{86}Sr$ ratios (0.743031 ± 14 and 0.755376 ± 16). A best-fit line (MSWD = 35, apparent initial $^{87}Sr/^{86}Sr$ = 0.72) defined by the granite data points in $^{87}Sr/^{86}Sr$ vs. $^{87}Rb/^{86}Sr$ space (Fig. 5D) yields a slope corresponding to an apparent age of 1330 ± 70 Ma, which may indicate an alteration event. Applying calculated Rb/Sr ratios for the 1.8 Ga granite samples, all analyzed granite samples of the Paleoproterozoic basement progressively arrive at unrealistically low $^{87}Sr/^{86}Sr$ ratios.

Discussion

Siting of Rb and Sr in sphalerite and implications for Rb-Sr isochron geochronology

Benchmark studies (e.g., Christensen et al., 1996; Pettke and Diamond, 1996) explained in detail why Rb-Sr direct dating of sphalerite is significant and identified the main analytical pitfalls to be avoided. However, the connection between some MVT mineralization and orogenic phases based on Rb-Sr ages on sphalerite, e.g., the East Tennessee MVT district and the Acadian orogeny (Kesler and Carrigan, 2002 and references therein), has been questioned (Leach et al., 2001, 2002). Given the discrepancies in certain ore districts between Rb-Sr ages (e.g., Schneider et al., 2002; Heijlen et al., 2003) and paleomagnetic ages (e.g., Symons et al., 1995), Bradley and Leach (2003) and Bradley et al. (2004) raised doubts around the Rb-Sr dating of sphalerite and were concerned by the possible contamination by carbonate and clay inclusions present in sphalerite. On the other hand, Kesler et al. (2004) questioned the validity of paleomagnetic ages, which are often similar to or younger than Rb-Sr isotope ages, potentially reflecting late fluid events which may have reset paleomagnetic ages.

Recent studies provide examples of concordance between Rb-Sr ages and the ages determined by using other geochronologic isotopic systems. For instance, Re-Os geochronometry on bitumen

coatings on sulfide mineralization at the Polaris Zn-Pb deposit yielded an age in agreement with Rb-Sr sphalerite and paleomagnetic ages for the mineralization (Selby et al., 2005 and references therein). Schneider et al. (2007) presented concordant Re-Os and Rb-Sr ages from direct dating of sulfide phases at the Kipushi deposit, DR Congo. Chesley et al. (1994) has also presented Sm-Nd ages on fluorite in the Illinois-Kentucky fluorite district in agreement with Rb-Sr ages on sphalerite from the possibly related Upper Mississippi Valley district (Brannon et al., 1992).

The critical issue of the siting of Rb and Sr in sphalerite, i.e., in its lattice or hosted by fluid and/or solid inclusions, was discussed in detail in the 1990´s by Nakai et al. (1990, 1993), Brannon et al. (1991, 1992), Christensen et al. (1996), and Pettke and Diamond (1996). Brannon et al. (1991) showed that Rb/Sr ratios of sphalerite in several MVT deposits were similar to those of associated K-feldspar or clay minerals. Their investigations showed that sparse K-feldspar inclusions constituted less than 0.1 % of their host sphalerite. On the basis of Rb and Sr geochemical data on K-feldspar, they concluded that sphalerite isochronism is not an artifact of leaching of K-feldspar, and that mixing between K-feldspar and other components with lower Rb/Sr ratio could not have produced the sphalerite isochrons obtained in their studies.

Ablation profiles for sphalerite analyzed in this study (Figs. 4A and B) show that Rb and Sr concentrations are two orders of magnitude higher in the analyzed volume of sphalerite containing micrometer-scale fluid inclusions than in inclusion-free sphalerite. These in-situ analyses confirm the findings by Pettke and Diamond (1996) that Rb-Sr isotope analyses of sphalerite residues are highly sensitive to minute amounts of unopened fluid inclusions, given that trapped hydrothermal fluids may have high Sr and high Rb contents. The relative similarity of Rb and Sr contents in sphalerite residues determined by ID-TIMS (Table 4), and Rb and Sr contents of inclusion-free sphalerite determined by LA-ICPMS (Appendix 3) favors the hypothesis that the obtained Rb and Sr values in sphalerite residues correspond to the contents of these elements in inclusion-free parts where they are held within the crystalline sphalerite structure.

Similarly, LA-ICPMS data for inclusion-free sphalerite in the Lower Sandstone orebody define a straight line with a slope of 0.020 ± 0.002 (2σ) on a Rb vs. Sr diagram (Fig. 7A). This positive correlation is interpreted to be intrinsic to sphalerite in which the Rb-Sr was not disturbed by post-mineralization processes. By contrast, the data for inclusion-free sphalerite in the Upper Sandstone orebody show greater scatter, in particular at low values of Rb or Sr, and only part of the data points define a straight line with a slope of 0.045 ± 0.018 (2σ) on a Rb vs. Sr diagram (Fig. 7B). This scatter may be an additional indication that the Rb-Sr isotope system in sphalerite in the Lower Sandstone was preserved whereas that in the Upper Sandstone was disturbed.

A diagram showing Sr vs. P contents in "inclusion-free" sphalerite data (Fig. 7C) shows that there is no apparent correlation between Sr and P in the analyzed samples from the Lower Sandstone orebody at Laisvall and from the Åkerlandet vein deposit. About half the data for sphalerite from the Upper Sandstone orebody at Laisvall do not show an apparent correlation between Sr and P; however,

other data for high P contents (> ~50 ppm) show a moderate positive correlation. The absence of a correlation between Sr and P in sphalerite from the Lower Sandstone orebody at Laisvall and from the Åkerlandet vein deposit, and in places in sphalerite from the Upper Sandstone orebody suggests that, in these samples, Sr contents are not related to micrometer-scale inclusions of fluorapatite or another P-bearing mineral phase but rather originate from the sphalerite lattice itself. Conversely, the moderate positive correlation between Sr and P in sphalerite with P contents above ~50 ppm in the Upper Sandstone orebody suggests that some Sr might be contributed by micrometer-scale P-bearing phases (e.g., fluorapatite). Rb-Sr systematics in sphalerite mineralization with co-genetic fluorapatite is not understood yet. However, the failure to obtain an absolute date for mineralization in the Upper Sandstone orebody is apparently not related to the presence of this fluorapatite co-genetic with sphalerite, but to the later disturbance of the Rb-Sr system, as discussed below.

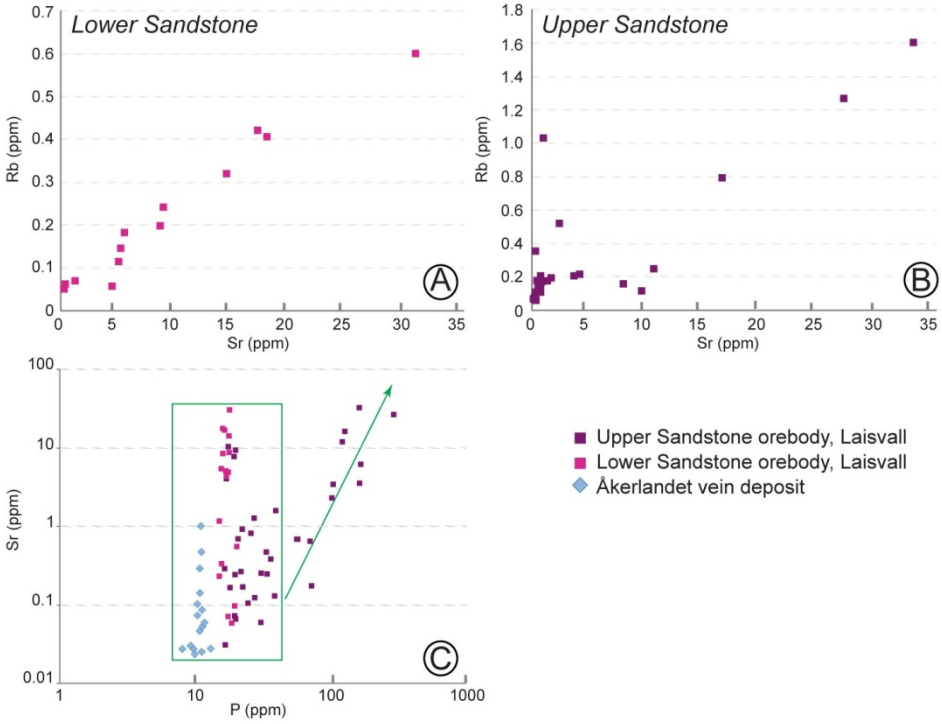

Fig. 7 A. Rb vs. Sr diagram for the ppm contents of these elements in sphalerite in the Lower Sandstone orebody at the Laisvall deposit, determined by LA-ICPMS analyses. B. Rb vs. Sr diagram for the ppm contents of these elements in sphalerite in the Upper Sandstone orebody at the Laisvall deposit, determined by LA-ICPMS analyses. C. Sr vs. P diagram for the ppm contents of these elements in sphalerite in the Lower Sandstone and Upper Sandstone orebodies at the Laisvall deposit, and in sphalerite at the Åkerlandet vein deposit, determined by LA-ICPMS analyses.

Nakai et al. (1993), Pettke and Diamond (1996) and Christensen et al. (1996) argued that it is unlikely that Rb and Sr occupy a zinc site in the sphalerite crystal structure, given the much higher ionic radii of Rb and Sr relative to Zn. Sb concentrations in sphalerite in the Lower Sandstone orebody at Laisvall, determined by LA-ICPMS in the present study (Appendix 3), show a weak positive correlation with Rb contents, whereas the correlation is very weak or absent in the Upper Sandstone (data in Saintilan, 2015). Sn contents show no correlation with Rb in either orebody at Laisvall.

Similarly, Rb does not correlate with Ga in any of the orebodies (Appendix 3). These results suggest that the proposed charge-coupled substitution 2 $Zn^{2+} \leftrightarrow Rb^{+} + Me^{3+}$ (e.g., Me: Sb, Sn, Ga; Pettke and Diamond, 1996) is not a likely mechanism for the incorporation of Rb in the analyzed sphalerite.

In conclusion, the LA-ICPMS and ID-TIMS data are consistent with the hypothesis that Rb and Sr are held in the sphalerite structure. Our data suggest also that fluorapatite inclusions and the coupled substitution cannot explain the observed Rb and Sr contents in fluid inclusion-free sphalerite. At the present state of knowledge, the most viable explanation could be that Rb and Sr are located in octahedral voids in the sphalerite structure itself (Fig. 8), as proposed by Pettke and Diamond (1996).

Christensen et al. (1996) emphasized that fine-grained colloform sphalerite (e.g., at Pine Point: Nakai et al., 1993; at Polaris: Christensen et al., 1995b) characterized by elevated $^{87}Rb/^{86}Sr$ ratios of up to 10 had a higher potential to be successfully dated. Pettke and Diamond (1996) and Christensen et al. (1996) invoked disequilibrium kinetics during crystal growth, favoring partitioning of low-concentration trace elements, which have $D^{crystal/liquid} << 1$ (e.g., Rb and Sr), to explain the possible concentration of Rb and Sr during rapid precipitation of colloform or fine-grained sphalerite. At Laisvall, evidence for rapid crystal growth of sphalerite was documented by Lindblom (1986). Indeed, fine-grained sphalerite disseminated residues in the orebodies at Laisvall, in particular the three disseminated residues from the Lower Sandstone, have elevated $^{87}Rb/^{86}Sr$ ratios of up to 7 (Table 4). These petrographic and geochemical evidences offer additional explanations for why an isochron could be obtained for these samples.

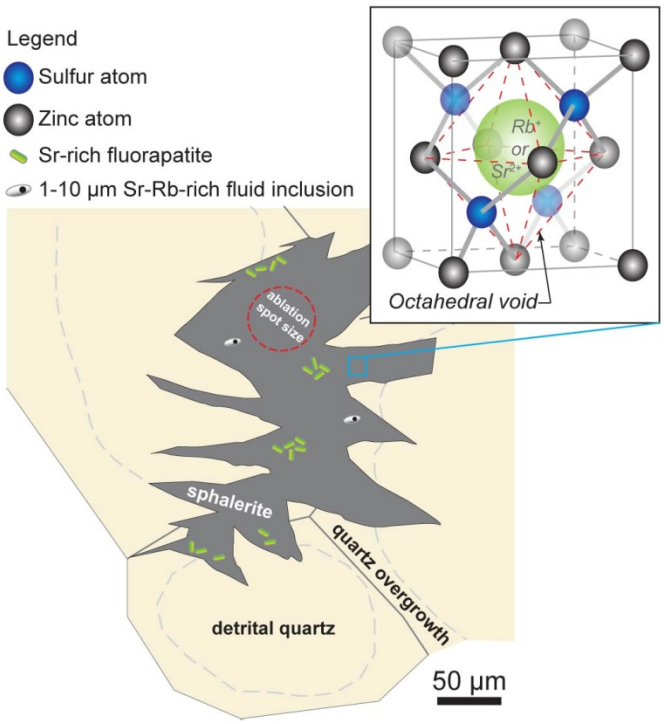

Fig. 8 Sketch of typical epigenetic sphalerite mineralization with H_2S derived from thermochemical sulfate reduction at Laisvall. The sphalerite cement was precipitated in sandstone, interstitially to partly-dissolved etched detrital quartz and diagenetic quartz overgrowths. The types of solid and fluid inclusions in sphalerite are shown, complemented by a sketch of sphalerite crystal structure with the proposed siting of Rb and Sr in octahedral voids.

Interpretation of the results from the Åkerlandet vein deposit

The original Rb-Sr systematics in the sphalerite sample from the Åkerlandet vein deposit also seems to have been preserved. The data can be interpreted in at least two ways (Fig. 9A), both being geological meaningful. The regional-scale implications of the alternative Hypotheses #1 and 2 are discussed further below.

Hypothesis #1: As indicated above, a 4-point isochron defined by the disseminated residues from the Lower Sandstone orebody at Laisvall and the residue from the Åkerlandet vein deposit yields an age of 468 ± 5 Ma (Fig. 5C), similar to the age of 467 ± 5 Ma from the 3-point isochron defined by the disseminated residues from the Lower Sandstone orebody. At a first view, it may appear surprising that data from the Åkerlandet and Laisvall deposits, separated by a distance of 250 km (Fig. 1A), lie along the same regression line. However, the Åkerlandet mineralization is located only 35 km east of the Granberget deposit (Fig. 1A), which in turn, shares many similarities with the disseminated mineralization Laisvall. Given our working hypothesis stated above that the Laisvall and Granberget deposits were formed coevally by fluids driven during the same large-scale tectonic event, it is geologically plausible that the Laisvall and Åkerlandet deposits, despite the distance between them, are also coeval and that the model age of 468 ± 5 Ma obtained from the 4-point Rb-Sr isochron is justified. According to Hypothesis #1, the Laisvall, Åkerlandet, and Granberget deposits could all have formed as a response to the tectonic event discussed below (in the section devoted to the age determination of the Laisvall deposit). Furthermore, the Åkerlandet vein system could represent an equivalent to feeders of metal-rich brines for Laisvall-type mineralization, as has been proposed by previous authors (e.g., Johansson and Rickard, 1984).

Hypothesis #2: An alternative hypothesis is that the Åkerlandet residue lies along the 3-point isochron of disseminated sphalerite mineralization in the Lower Sandstone because of a fortuitous coincidence. If so, the following possibility merits some exploration.

Billström et al. (2012) presented a tentative four-point Rb-Sr isochron age of 531 ± 6.5 Ma (early Cambrian; initial $^{87}Sr/^{86}Sr$ = 0.716560 ± 660) for sphalerite residues (MSWD = 2.4) from the basement-hosted Ersmarksberget, Svärtträsk and Gubbträsk vein deposits in the Storuman district, 100 km north of Åkerlandet (Fig. 1A). These authors described calcite-fluorite-Zn-Pb sulfide mineralization at Ersmarksberget and Gubbträsk along brittle structures partly discordant to the regional ductile fabric. Given the similarities in mineralogy, texture, and tectonic structures in the host basement rocks at the Ersmarksberget, Gubbträsk, and Åkerlandet deposits (Billström et al., 2012; Saintilan et al., 2012), it seems reasonable to try to combine our Åkerlandet data with those published for the Ersmarksberget and Gubbträsk deposits by Billström et al. (2012).

The regression of the sphalerite residue aliquots from the Ersmarksberget and Gubbträsk deposits with our aliquot from Åkerlandet yields a recalculated four-point isochron model age of 544 ± 4 Ma (late Ediacaran; Fig. 9B; MSWD = 1.9, initial $^{87}Sr/^{86}Sr$ = 0.714770 ± 150). One fluid inclusion leachate corresponding to the Ersmarksberget vein deposit has a $^{87}Sr/^{86}Sr$ ratio close to the obtained initial

$^{87}Sr/^{86}Sr$ ratio of our recalculation, while the other leachate from Ersmarksberget and those from the Gubbträsk and Åkerlandet vein deposits plot slightly above this model isochron, reflecting limited secondary disturbance (Fig. 9B). According to Hypothesis #2, an age of 544 ± 4 Ma could be proposed, which is close to the Rb-Sr isochron age of 531 ± 6.5 Ma of Billström et al. (2012).

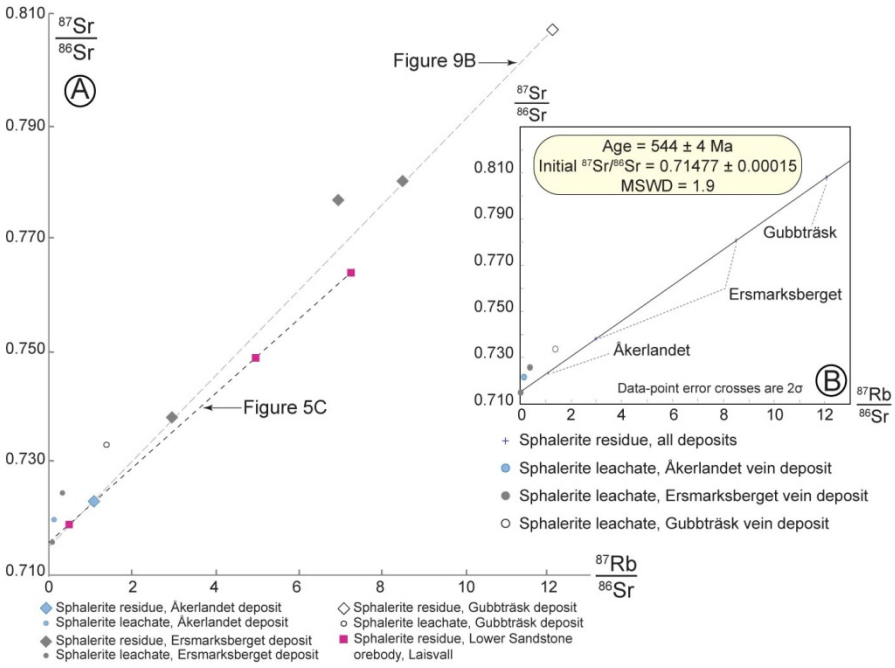

Fig. 9 A. $^{87}Sr/^{86}S$ vs. $^{87}Rb/^{86}Sr$ diagram for sphalerite residues and complementary leachates from several samples of calcite-fluorite-Zn±Pb sulfide vein-type mineralization in Paleoproterozoic basement along the erosional front of the Scandinavian Caledonides: (i) the Ersmarksberget and Gubbträsk deposits in the Storuman district (data after Billström et al., 2012), (ii) the Åkerlandet deposit (this study). The sphalerie residues from the Lower Sandstone orebody at Laisvall are shown for reference. The dashed lines represent the model isochron (n = 4) combining disseminated residues from the Lower Sandstone orebody at Laisvall and the data from Åkerlandet (black dashed line; Fig. 5C), and the model isochron (n = 4) for only the basement-hosted vein deposits (gray dashed line; Fig. 9B). See text for further explanation. B. Recalculated isochron model age diagram (n = 4) for residues and corresponding leachates of sphalerite samples from the basement-hosted Ersmarksberget and Gubbträsk vein deposits and the basement-hosted Åkerlandet vein deposit.

Nature and origin of the disturbance of the Rb-Sr systematics in sphalerite in the Upper Sandstone at Laisvall and at the Granberget deposit

As discussed above, all analyzed samples except three disseminated samples from the Lower Sandstone orebody, one disseminated sample from the Upper Sandstone orebody at Laisvall, and the Åkerlandet vein sample are disturbed in the Rb-Sr isotope systematics and plot on a strikingly different isotopic trend in the $^{87}Sr/^{86}Sr$ vs. $^{87}Rb/^{86}Sr$ space (Fig. 5A). This trend indicates various degrees of disturbance of the original Rb-Sr system, both in residues and leachates of these samples (Fig. 5A), that prevented isochron model age determination for the Upper Sandstone disseminated samples, the Upper Sandstone and Lower Sandstone veinlet samples, and for the Granberget disseminated samples. Taking into account that disseminated mineralization in the Upper Sandstone

orebody appears to have been remobilized in steeply-dipping galena-sphalerite-calcite veinlets (cf. Rickard et al., 1979; Saintilan et al., 2015) and that the Upper Sandstone is close to the basal Caledonian décollement, it is not surprising that the Rb-Sr system in disseminated samples in the Upper Sandstone has been disturbed during post-mineralization events. Failure to determine the age of the disseminated Granberget mineralization is also not surprising, bearing in mind that the mineralization is tectonically disrupted by subvertical faults, cut by steeply-dipping galena-sphalerite-calcite veinlets, and that all of these structures are cut, in turn, by low-angle thrusts (Årebäck, 2003; Saintilan, 2010).

Linear trends, defined by sphalerite fluid inclusion leachates plotting steeper than or deviating from isochrons of corresponding sphalerite residues, were observed by, for example, Christensen et al. (1995b), Schneider et al. (1999, 2007) and Nelson et al. (2002), and have generally been interpreted to reflect mixtures of "primary and secondary" fluids (e.g., ore-bearing fluids and later fluids). Sherlock et al. (2005) documented certain detrital K-feldspar grains in sandstone paleoaquifers at Laisvall that show outer rims with *in-situ* ^{40}Ar–^{39}Ar ages of 453 ± 8 Ma to 403 ± 6 Ma (Upper Ordovician to Early Devonian). These ages are younger than our 467 ± 5 Ma Rb-Sr sphalerite age for disseminated mineralization in the Lower Sandstone at Laisvall. Sherlock et al. (2005) suggested that tectonically-induced fluid flow was responsible for the precipitation of the outer rims around some K-feldspar grains. As discussed in the section on geologic setting above, the period defined by the *in-situ* ^{40}Ar–^{39}Ar ages of 453 ± 8 Ma to 403 ± 6 Ma is characterized by continuous tectonic convergence related to the terminal continent-continent (Laurentia-Baltica) collision, as well as subsequent orogenic collapse and the formation of intra-orogenic basins. This fluid migration may have also caused the post-mineralization disturbance of the Rb-Sr systems by Sr-rich fluids, the nature of which is described below.

All disseminated and veinlet residues from the Upper Sandstone orebody (excluding the relatively undisturbed disseminated residue 12LAI52 R) and the veinlet samples from the Lower Sandstone orebody (12LAI14 R and 12LAI84 R) define an array in the $^{87}Sr/^{86}Sr$ vs. $1/^{86}Sr$ diagram (Fig. 6A) in which the Upper Sandstone orebody sphalerite residues are biased towards high contents of common Sr. The same samples in the 1/Rb vs. $^{87}Rb/^{86}Sr$ diagram (Fig. 6B) systematically show very low $^{87}Rb/^{86}Sr$ ratios. A Sr vs. Rb diagram (Fig. 6C) shows that the disseminated residues in the Upper Sandstone have rather similar Rb contents, but the disturbed residue 12LAI12 contains four times more Sr than the relatively undisturbed residue 12LAI52 and falls in the field of the veinlet samples in the Upper Sandstone orebody (Tables 1 and 4). In addition, the disturbed residue 12LAI12 has a low $1/^{86}Sr$ ratio, a slightly lower $^{87}Sr/^{86}Sr$, but a markedly lower $^{87}Rb/^{86}Sr$ ratio than residue 12LAI52. The Rb and Sr budget of the disturbed residue 12LAI12 being similar to that of the veinlets, it can be suggested that this isotopic composition was acquired through an input of Sr during remobilization that produced the steeply-dipping galena-sphalerite-calcite veinlets in the Upper

Sandstone. The Granberget disseminated residues appear to have been affected by a similar input of Sr (Figs. 5A, 6B, and 6C).

These results and steep linear disturbance trend discussed above are compatible with a gain of Sr during post-mineralization event(s). Figure 5D shows the isotopic composition of possible Sr sources in the stratigraphy at Laisvall that could be responsible for the disturbance of the Rb-Sr system with the mixing of: (i) very radiogenic Sr ($^{87}Sr/^{86}Sr$ > 0.750), probably mobilized from the Paleoproterozoic crystalline basement; and (ii) less radiogenic Sr, released from a sedimentary source with a Sr composition close to that of galena-poor phosphorite pebble conglomerate deposited on top of the Upper Sandstone paleoaquifer ($^{87}Sr/^{86}Sr$ ~ 0.725: Table 5). The Sr isotopic composition of the two samples of shale overlying the Laisvall sandstone paleoaquifers (Table 5, Fig. 5D) is not compatible with these shales having been a Sr reservoir involved in this steep mixing trend.

Early Caledonian foreland basin evolution and the age of strata-bound and disseminated mineralization in the Lower Sandstone at Laisvall

A 467 ± 5 Ma (Middle Ordovician) age for mineralization at Laisvall is geologically plausible (Fig. 10A). Logically, the same applies for the combined four-point model isochron with an age of 468 ± 5 Ma, using Hypothesis #1 above.

In details, a tectonic response to the development of the early Caledonian foreland basin could have involved the reactivation of faults in the Paleoproterozoic crystalline basement (Gee, 1972; Saintilan et al., 2015) in the vicinity of the forebulge (Fig. 10A), i.e., the so-called “hinge-zone” of Gee (1972). Basinal brines in the foredeep to the northwest could have been conveyed cratonward to the southeast and resurged as metal-bearing fluids along reactivated basement faults at Laisvall (Rickard et al., 1979, Romer, 1992; Saintilan et al., 2015). The initial Sr isotope signature (Fig. 5B) indicated by the three-point isochron ($^{87}Sr/^{86}Sr$ = 0.715900 ± 60) is much higher than the Sr isotopic composition of Cambrian–Ordovician seawater that ranged between 0.707 and 0.709 (Veizer et al., 1999). This initial high Sr isotopic composition can be explained as having resulted from the mixing of brines with hydrocarbon and H_2S-rich fluids in sandstone (Rickard et al., 1975, 1979; Lindblom, 1986; Saintilan et al., 2014b, c). The brines would have acquired metals during cratonward migration and interaction with permeable Baltica basement rocks (Wickman et al., 1963; Rickard et al., 1981; Romer, 1992; Kendrick et al., 2005; Saintilan et al., 2015). A link between MVT mineralization and reactivation of large-scale basement structures, during the development of a foreland basin in connection with collisional tectonics, has also been proposed in the case of the Ellesmerian orogen and the Polaris MVT deposit and for the Ouachita orogen and the Southeastern Missouri MVT district (Bradley and Leach, 2003 and references therein).

Remnants of the early Caledonian foreland basin are now preserved in the lower allochthonous Caledonian nappes in Sweden and Norway and this >260 km-wide foreland basin can be traced with a NNE–SSW trend for at least 500 km along the Caledonian orogen (Gee, 1972;

Stephens, 1988; Karis, 1998; Greiling and Garfunkel, 2007; Gee et al., 2013). The basin had a well-defined eastern external margin that moved progressively towards the foreland during Lower to Middle Ordovician time (Garfunkel and Greiling, 2002; Greiling and Garfunkel, 2007). Greiling and Garfunkel (2007) proposed a location for this external margin ~20 km west from the present-day location of the Laisvall deposit during the Lower Ordovician. This margin ceased to migrate towards the foreland and the basin deepened instead during the Middle Ordovician (Greiling and Garfunkel, 2007); the proposed age for Laisvall mineralization at 467 ± 5 Ma suggests a possible link with this basin deepening.

Estimates for the depth and sediment thickness within the basin are difficult to assess (Greiling and Garfunkel, 2007). Turbidite sedimentation in Lower to Middle Ordovician time documents basin subsidence that, in turn, implies increased orogenic load (Greiling and Garfunkel, 2007). The overall tectonic evolution resulted in shallow-marine carbonate sedimentation along the forebulge during the Middle Ordovician, with these strata being progressively overstepped subsequently by a turbidite and shale sequence to the northwest. Increased turbidite and shale sedimentation continued and prevailed laterally northwestward in the deepening basin. The sediment fill amounted to ~500 m, and several hundred meters of water depth were reached between shallow carbonate intervals (Fig. 10A; Karis, 1998; Greiling and Garfunkel, 2007). This tectonic setting and the upward-deepening sedimentary succession are similar to the conditions described by Bradley and Leach (2003, their Fig. 3) in their sequential model for an arc-passive margin collision and the foredeep-forebulge-foreland situation of the Ouachita orogen in North America. This “arc-passive margin collision provides all of the key ingredients for MVT mineralization in a single chain of events” (p. 664; Bradley and Leach, 2003).

According to the model in the present study, the passive margin of Baltica with organic-rich shale in the regionally extensive Alum Shale Formation and underlying Ediacaran to Cambrian siliclastic rocks was already buried in the foreland basin during the Lower Ordovician and overlain by the additional load of the orogenic wedge (Karis, 1998; Greiling and Garfunkel, 2007). For this reason, it is proposed that the burial in the foredeep provided conditions for hydrocarbon generation from organic-rich shale. Subsequently, hydrocarbon migration (Rickard et al., 1975; 1979; Lindblom, 1986; Saintilan et al., 2014c) could have taken place from the basin in the northwest southeastward towards the forebulge. Hydrocarbon accumulation in sandstone paleoaquifers contributed to the generation of reduced sulfur via thermochemical sulfate reduction (Rickard et al., 1975; Rickard, 1983; Saintilan et al., 2014a, b; Saintilan et al., 2015).

Table 5. Rb and Sr contents (ppm) and Sr isotopic composition of whole-rock samples selected in the stratigraphy at Laisvall. "-": not available.

Sample	Stratigraphy	Alteration	Rb (ppm)	Sr (ppm)	$^{87}Rb/^{86}Sr$	2σ	$^{87}Sr/^{86}Sr$	$2\sigma\ 10^{-6}$
11LAI16-2	Black shale with pyrite in the Alum Shale Formation		-	-	-	-	0.721269	14
11LAI45	Grey shale with organic matter in the Alum Shale Formation		111	40.1	8.05	0.24	0.739333	14
11LAI26	Green shale in the Grammajukku Formation		372	49.8	21.64	0.65	0.764182	16
11LAI03-1	Phosphorite polymictic conglomerate, poorly galena-mineralized		10	122	0.24	0.01	0.720336	14
11LAI03-2	Phosphorite polymictic conglomerate with interstitial sphalerite		30	76.8	1.13	0.03	0.724978	14
11BAS01	Granite (1.8 Ga) in the crystalline basement	Chlorite alteration	149	148	2.93	0.09	0.773616	16
11BAS02	Granite (1.8 Ga) in the crystalline basement	Reddened, hematite veins	245	31.2	23.94	0.72	1.188594	20
11BAS03	Granite (1.8 Ga) in the crystalline basement	Chlorite alteration	153	150	2.97	0.09	0.774925	16
11BAS04	Granite (1.8 Ga) in the crystalline basement	Reddened, hematite veins	217	22	30.15	0.90	1.286898	20
11BAS05	Granite (1.8 Ga) in the crystalline basement	Slightly altered (reddened)	-	-	-	-	0.743031	14
11BAS06	Granite (1.8 Ga) in the crystalline basement	Slightly altered (reddened)	134	221	1.76	0.05	0.755376	16

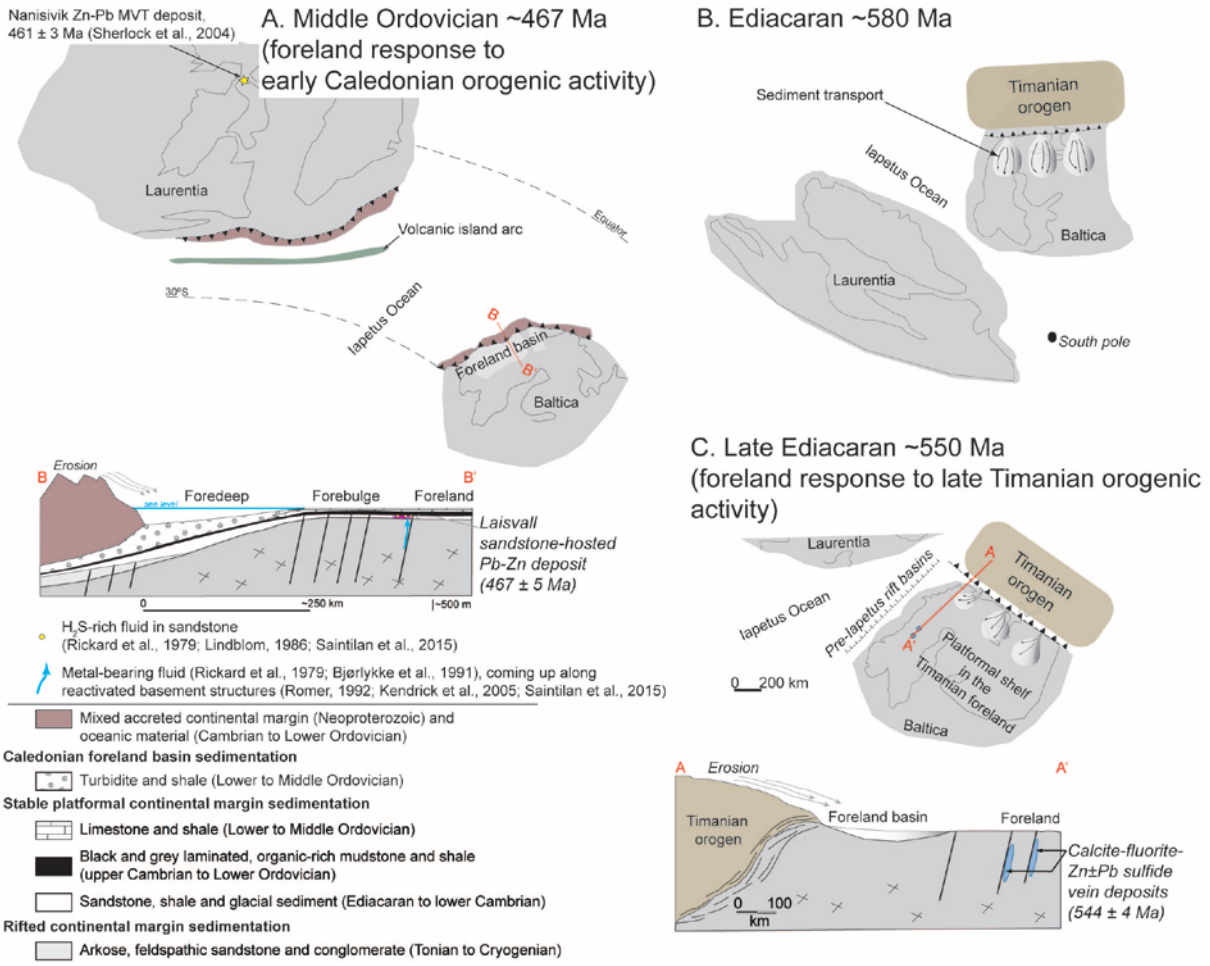

Fig. 10 (previous page) Cartoons showing the series of tectonic events between Ediacaran and Middle Ordovician time, with focus on Baltica. The paleogeography of Laurentia is shown for reference. A. Middle Ordovician (~467 Ma). The proposed ~467 Ma age for mineralization at Laisvall is coeval with the deepening of the foreland basin during the Middle Ordovician. See text for further discussion. It is interesting that the Nanisivik Zn-Pb Mississippi Valley-type deposit is suggested to have formed at 461 ± 3 Ma in Mesoproterozoic sedimentary rock in the basement of Laurentia beneath Cambrian to Ordovician transgressive sedimentary rock sequences (Sherlock et al., 2004). The general structural framework and the paleogeography of Laurentia and the Iapetus Ocean are drawn after Mac Niocaill et al. (1997), while the structural framework and paleogeography of Baltica are drawn after Stephens (1988) and Mac Niocaill et al. (1997). B. Ediacaran (~580 Ma). Continental drift between Baltica and Laurentia and opening of the Iapetus Ocean, development of a platformal shelf over much of Baltica, and formation of a foreland basin to the Timanian orogen (~620 to 550 Ma; after Svenningsen, 2001; Remizov and Pease, 2004; Kirkland et al., 2011; Andresen et al., 2014). Paleogeography is drawn after Pease et al. (2008). C. Late Ediacaran (~550 Ma). Waning stage of the Timanian orogeny with proposed basement-hosted calcite-fluorite-Zn±Pb vein-type mineralization at 544 ± 4 Ma. Paleogeography is drawn after Pease et al. (2008).

Re-evaluation of the relationship between the Laisvall deposit and calcite-galena vein mineralization in the Baltica basement

Hypothesis #1: A possible genetic link between the Laisvall deposit and basement-hosted calcite-galena veins.

The 468 ± 5 Ma age derived from the 4-point isochron defined by the disseminated residues from the Lower Sandstone orebody at Laisvall and the residue from the Åkerlandet vein deposit

suggests that these deposits are coeval, supporting the hypothesis of Johansson and Rickard (1984) that certain vein deposits may represent feeder traces of metal-bearing fluids in the crystalline basement for Laisvall-type mineralization. If this hypothesis is correct, it also implies that there are several phases of basement-hosted vein-type mineralization in the Baltica basement, given the significantly older age of c. 531 Ma for the calcite-galena vein deposits in Paleoproterozoic basement in the Storuman district (Billström et al., 2012). Moorbath and Vokes (1963), Wickman et al. (1963), and Johansson and Rickard (1984) documented that all these basement-hosted calcite-galena vein deposits are characterized by radiogenic lead in galena. A hypothesis of diachronous and polyphase hydrothermal vein-type activity would be in accordance with the mobilization of radiogenic lead at the scale of the Fennoscandian Shield, coinciding with multiple tectonic reactivation of old fault zones in the foreland of several orogens (including the ~0.5 to 0.4 Ga Caledonian orogen, the ~1.1 to 0.9 Ga Sveconorwegian orogen, and the ~2.0 to 1.8 Ga Svecokarelian orogen) or rifts (e.g., the Oslo Rift at ~280 Ma). Polyphase hydrothermal vein-type activity has been documented, for instance, in the Black Forest in southwestern Germany, where five generations of hydrothermal veins in Variscan basement with ages between Permian and Miocene have been distinguished (Staude et al., 2009 and references therein).

Hypothesis #2: A possible late Timanian origin for some basement-hosted calcite-galena vein deposits

The recalculated four-point isochron for calcite-galena vein-type mineralization in the Paleoproterozoic basement, obtained by combining our Åkerlandet data with those for the Ersmarksberget and Gubbträsk deposits in the Storuman district (Billström et al., 2012), yields a late Ediacaran age of 544 ± 4 Ma. This age is close to the original lower Cambrian age of 531 ± 6.5 Ma obtained by Billström et al. (2012). Migration of hydrothermal fluids in the basement in the 525 to 548 Ma range could be related to a far-field tectonic response to the Timanian orogeny (Figs. 10B and 10C; cf. Roberts and Siedlecka, 2002; Roberts and Olovyanishnikov, 2004; Pease et al., 2008). According to this hypothesis, hydrothermal vein mineralization could have taken place in the Timanian foreland (cf. Remizov and Pease, 2004; Pease et al., 2008; Andresen et al., 2014) as a consequence of tectonic activity along the northeastern margin of Baltica.

Conclusions

This study provides the first absolute age determination of the Pb-Zn Laisvall deposit hosted by autochthonous Ediacaran to lower Cambrian sandstone. Ten crushed and leached sphalerite separates were obtained from mineralized sandstone samples in proximal and distal positions relative to the proposed main feeder fault systems at the Laisvall deposit. All separates correspond to sphalerite that precipitated using reduced sulfur derived from thermochemical sulfate reduction, the

main reduced sulfur source at Laisvall. A Rb-Sr isochron model age of 467 ± 5 Ma was obtained from three sphalerite residues sampled from the Lower Sandstone sphalerite disseminated mineralization. Yet, the obtained age is consistent with geologic evidence reported by previous authors pointing to a Middle Ordovician timing of ore formation.

LA-ICPMS analyses on the same sphalerite samples support the hypothesis that the measured ID-TIMS Rb and Sr contents in these sphalerite residues are held in the sphalerite structure itself and are not related to micro-inclusions. The most viable explanation, in agreement with Pettke and Diamond (1996) and Christensen et al. (1996), is that Rb and Sr ions from hydrothermal fluids may be incorporated into the structure of sphalerite, possibly in octahedral voids, during rapid crystal growth.

Dating of samples from the Laisvall Upper Sandstone orebody probably failed due to post-mineralization disturbance of the Rb-Sr isotope systematics. The Upper Sandstone mineralization is located close to the basal Caledonian décollement (c. 430 to 397 Ma, i.e., middle Silurian–Lower Devonian time) and was therefore more probably disrupted tectonically than the Lower Sandstone mineralization. Post-mineralization disturbance may also explain the failure to date steeply-dipping galena-sphalerite-calcite veinlets in the Upper and Lower Sandstone orebodies, which are interpreted to be in part remobilization of disseminated mineralization. Most data obtained from sphalerite residues and corresponding inclusion fluid leachates from these samples define a trend in the $^{87}Sr/^{86}Sr$ vs. $^{87}Rb/^{86}Sr$ diagram too steep to account for a realistic isochron age determination. The pattern in a 1/Rb vs. $^{87}Rb/^{86}Sr$ diagram and LA-ICPMS analyses of Rb and Sr contents in sphalerite suggest that the disturbance of the Rb-Sr isotope systematics involved an admixture of Sr-rich fluids.

Similarly, the attempt to date disseminated sandstone-hosted mineralization at the Granberget deposit in the lower allochthonous units in the Caledonian orogen was not successful. At Granberget, mineralization is tectonically disrupted by subvertical faults cut by steeply-dipping galena-sphalerite-calcite veinlets. All of these structures are cut in turn by low-angle thrusts. This tectonic setting can explain the observed disturbance of the Rb-Sr isotope systematics of the three analyzed sphalerite samples.

A mineralization age for Laisvall at 467 ± 5 Ma corresponds to a far-field foreland response to an early Caledonian arc-continent collision and the subsequent development of a foreland basin. Basinal brines formed in the foredeep of the orogen could have been conveyed cratonward and then resurged as metal-bearing fluids in sandstone at Laisvall along reactivated Paleoproterozoic crystalline basement faults. Mixing of brines, which according to other works acquired metals during migration and interaction with permeable Paleoproterozoic basement rocks, with hydrocarbon- and H_2S-rich fluids in Ediacaran to lower Cambrian sandstone may explain the initial Sr isotope signature ($^{87}Sr/^{86}Sr$ = 0.715900 ± 60) of the isochron intersect.

The Rb-Sr systematics of a sphalerite sample at the basement-hosted calcite-fluorite-Zn±Pb sulfide Åkerlandet vein deposit seems to have been preserved. The obtained data are compatible with two hypotheses, both of which are geologically meaningful. A 4-point isochron combining data from

the Lower Sandstone orebody at Laisvall and the residue from the Åkerlandet vein deposit would yield an age of 468 ± 5 Ma, similar to the proposed 467 ± 5 Ma age for mineralization in the Lower Sandstone orebody at Laisvall. This hypothesis would give credit to the suggestion by Johansson and Rickard (1984) that, for Laisvall-type mineralization, this vein deposit may represent traces of metal-bearing fluids guided by feeders in the crystalline basement. Bearing in mind the age of sphalerite mineralization of 531 ± 6.5 Ma obtained by Billström et al. (2012) for the Storuman vein district, this difference in age of sphalerite precipitation would imply that basement-hosted vein-type mineralization in the Baltica basement is polyphase. Alternatively, regression of sphalerite data for the Åkerlandet vein deposit with the geologically and mineralogically similar basement-hosted Ersmarksberget and Gubbträsk vein deposits in the Storuman district would yield a recalculated Rb-Sr isochron model age of 544 ± 4 Ma, which is close to the Rb-Sr isochron age of 531 ± 6.5 Ma of Billström et al. (2012). According to this second hypothesis, mineralization could be a far-field tectonic response to the Timanian orogeny along the northeastern margin of Baltica.

Acknowledgments

This research has been financially supported by Boliden AB (Sweden) and the Swiss National Science Foundation (SNF, Switzerland, FN 146 353). The Geological Survey of Sweden (SGU) also provided financial and logistical support for much of the fieldwork in Sweden, and the staff at SGU in Malå is thanked for their help at the national core archive. The authors are grateful to Boliden AB including Hans Årebäck (former exploration manager) and Rodney L. Allen (Manager Geology Research and Development) for financial and logistical support for the work carried out in Boliden and also stimulating discussions. We acknowledge the help of the staff working at the core archive in Boliden in the supply of drill cores. Cyril Chelle-Michou (University of Geneva) is acknowledged for constructive discussions concerning hydrothermal fluid circulation and orogenic systems in general. A. Bjørlykke and D.T. Rickard are thanked for their detailed reviews and very helpful comments toward clarifying many aspects of the manuscript. We would also like to acknowledge the thorough and pertinent reviews of associate editor Alex Brown and the editorial work of editor Larry Meinert.

References

Andersson, A., Dahlman, B., Gee, D., and Snall, S., 1985, The Scandinavian alum shales: Geologic Survey of Sweden, Ser. Ca 56, 86 p.

Andresen, A., Agyei-Dwarko, N.Y., Kristoffersen, M., and Hanken, N.-M., 2014, A Timanian foreland basin setting for the late Neoproterozoic–Early Paleozoic cover sequences (Dividal Group) of northeastern Baltica, *in* Corfu, F., Gasser, D., and Chew, D.M., eds., New Perspectives on the Caledonides of Scandinavia and Related Areas: London, Geologic Society Special Publication 390, p. 157-175.

Ayrault, S., 2008, Geology and mineral resources of the Lövstrand Pb (-Zn) mineralization, Dorotea area, north-central Sweden [Master thesis]: Luleå, Luleå University of Technology, Sweden, 55 p.

Årebäck, H., 2003, The Granberget Pb-Zn deposit, Dorotea district, Västerbotten: Unpublished Boliden AB internal report.

Bergman, S., Stephens, M.B., Andersson, J., Kathol, B., and Bergman, T., 2012, Geologic map of Sweden: Geologic Survey of Sweden, scale 1:1 000 000, 1 sheet.

Billström, K., Broman, C., Schneider, J., Pratt, W., and Skogsmo, G., 2012, Zn-Pb ores of Mississippi Valley-type in the Lycksele-Storuman District, Northern Sweden: A possible rift-related Cambrian mineralising event: Minerals, v. 1, p.169-207.

Birck, J. L., 1986, Precision K-Rb-Sr isotopic analysis: application to Rb-Sr chronology: Chemical Geology, v. 56, p. 73-83.

Bjørlykke, A., and Sangster, D.F., 1981, An overview of sandstone lead deposits and their relation to red-bed copper and carbonate-hosted lead-zinc deposits: ECONOMIC GEOLOGY 75th Anniversary Volume, p.179-213.

Bjørlykke, A., Sangster, D.F., and Fehn, U, 1991, Relation between high heat-producing (HHP) granites and strata-bound lead-zinc deposits, in Pagel, M., and Leroy, J.-L., eds., Source, transport and deposition of metals: Balkema, Rotterdam, p. 257-260.

Bradley, D.C., and Leach, D.L., 2003, Tectonic controls of Mississippi Valley-type lead-zinc mineralization in orogenic forelands: Mineralium Deposita, v. 38, p.652-667.

Bradley, D. C., Leach, D. L., Symons, D., Emsbo, P., Premo, W., Breit, G., and Sangster, D. F., 2004, Reply to Discussion on ‘‘Tectonic controls of Mississippi Valley-type lead–zinc mineralization in orogenic forelands’’ by S.E. Kesler, J.T. Christensen, R.D. Hagni, W. Heijlen, J.R. Kyle, K.C. Misra, P. Muchez, and R. van der Voo, Mineralium Deposita: Mineralium Deposita, v. 39, p. 515-519.

Brannon, J.C., Podosek, F.A., Viets, J.G., Leach, D.L., Goldhaber, M., and Rowan, E.L., 1991, Strontium isotopic constraints on the origin of ore-forming fluids of the Viburnum Trend, southeast Missouri: Geochimica et Cosmochimica Acta, v. 55, p.1407-1419.

Brannon, J.C., Podosek, F.A., and Mclimans, R.K., 1992, Alleghenian age of the Upper Mississippi Valley zinc lead deposit determined by Rb-Sr dating of sphalerite: Nature, v. 356, p. 509-511.

Chelle-Michou, C., 2008, Geology and mineralization of the Bellviksberg sandstone-hosted Pb-Zn deposit, Dorotea area, Sweden [Master thesis]: Luleå, Luleå University of Technology, Sweden, 54 p.

Chesley, J.T., Halliday, A.N., Kesler, S.E., Spry, P.G., 1994, Direct dating of Mississippi Valley-type mineralization: use of Sm-Nd in fluorite: ECONOMIC GEOLOGY, v. 89, p. 1192-1199.

Chiaradia, M., Müntener, O., and Beate B., 2011, Enriched basaltic andesites from mid-crustal fractional crystallization, recharge, and assimilation (Pilavo Volcano, Western Cordillera of Ecuador): Journal of Petrology, v. 22, p. 1107-1141.

Christensen, J. N., Halliday, A. N., Vearncombe, J. R., and Kesler, S. E., 1995a, Testing models of large-scale crustal fluid flow using direct dating of sulfides: Rb-Sr evidence for early dewatering and formation of Mississippi Valley-type deposits, Canning Basin, Australia: ECONOMIC GEOLOGY, v. 90, p. 877-884.

Christensen, J.N., Halliday, A.N., Kesler, S.E., Liegh, K.E., and Randell, R.N., 1995b, Direct dating of sulfides by Rb-Sr–a critical test using the Polaris Mississippi Valley-type Zn-Pn deposit: Geochimica et Cosmochimica Acta, v. 59, p. 5191-5197.

Christensen, J.N., Halliday, A.N., and Kesler, S.E., 1996, Rb-Sr dating of sphalerite and the ages of Mississippi Valley-type Zn-Pb deposits: Society of Economic Geologists, Special Publication 4, p. 527-535.

Christofferson, H.C., Wallin, B., Selkman, S., Rickard, D.T., 1979, Mineralization controls in the sandstone lead-zinc deposit at Vassbo, Sweden: ECONOMIC GEOLOGY, v. 74, p. 1239-1249.

Cohen, K.M., Finney, S.C., Gibbard, P.L., and Fan, J.-X., 2013 (updated), The ICS International Chronostratigraphic Chart: Episodes, v. 36, p. 199-204.

Corfu, F., Andersen, T.B., and Gasser, D., 2014, The Scandinavian Caledonides: main features, conceptual advances and critical questions, *in* Corfu, F., Gasser, D., and Chew, D.M., eds., New Perspectives on the Caledonides of Scandinavia and Related Areas: London, Geologic Society Special Publication 390, p. 9-43.

Dallmeyer, R.D., and Gee, D.G., 1986, $^{40}Ar/^{39}Ar$ mineral dates from retrogressed eclogites within the Baltoscandian miogeocline: Implications for a polyphase Caledonian orogenic evolution: Geologic Society of America Bulletin, v. 97, p. 26-34.

Deniel, C., and Pin, C., 2001, Single-stage method for the simultaneous isolation of lead and strontium from silicate samples for isotopic measurements: Analytica Chimica Acta, v. 426, p. 95-103.

Garfunkel, Z., and Greiling, R.O., 2002, The implications of foreland basins for the causative tectonic loads: EGU Stephan Mueller Special Publication Series, v. 1, p. 3-16.

Gee, D.G., 1972, The regional geologic context of the Tåsjö uranium project, Caledonian front, Central Sweden: Geologic Survey of Sweden, Årsbok 66 2, Ser C, 671, 37 p.

Gee, D.G., 1975, A tectonic model for the central part of the Scandinavian Caledonides: American Journal of Science, v. 275A, p. 468-515.

Gee, D.G., Kumpulainen, R., and Thelander, T., 1978, The Tåsjö décollement, Swedish Caledonides: Sverige Geologiska Undersökning ser. C742, p.1-35.

Gee, D.G., Fossen, H., Henriksen, N., and Higgins, A.K., 2008, From the Early Paleozoic platforms of Baltica and Laurentia to the Caledonide Orogen of Scandinavia and Greenland: Episodes, v. 31, p. 1-8.

Gee, D.G., Juhlin, C., Pascal, C., and Robinson, P., 2010, Collisional orogeny in the Scandinavian Caledonides (COSC): Journal of the Geologic Survey of Sweden (GFF), v. 132, p.29-44.

Gee, D.G., Ladenberger, A., Dahlqvist, P., Majka, J., Be'eri-Shlevin, Y., Frei, D., and Thomsen, T., 2013, The Baltoscandian margin detrital zircon signatures of the central Scandes, *in* Corfu, F., Gasser, D., and Chew, D.M., eds., New Perspectives on the Caledonides of Scandinavia and Related Areas: London, Geologic Society Special Publication 390, p. 131-155.

Greiling, R.O., and Garfunkel, Z., 2007, An Early Ordovician (Finnmarkian?) foreland basin and related lithospheric flexure in the Scandinavian Caledonides: American Journal of Science, v. 307, p. 527-553.

Grip, E., 1954, Blymalmen vid Laisvall, dess geologi och jämförelse med några utländska förekomster: Geologiska Föreningens i Stockholm Förhandlingar (GFF), v. 76, p. 357-380 (in Swedish).

Grip, E., 1960, The lead deposits of the eastern borders of the Caledonides in Sweden. 21st International Geological Congress, Copenhagen, Norden 16, p. 149-159.

Grip, E., 1967, On the genesis of the lead ores of the eastern border of the Caledonides in Scandinavia: Society of Economic Geologists Monograp 3, p. 208-218.

Grip, E., 1973, Sulfimalm i fjällkedjan och i det baltiska kambriska flackhavsområdet, *in* Grip, E., and Frietsch, R., eds., Malm i Sverige 2, Norra Sverige, Stockholm, Almqvist and Wiksell, p. 10-66 (in Swedish).

Gromet, L.P., Sjöström, H., Bergman, S., Claesson, S., Essex, R.M., Andreasson, P.G., and Albrecht, L., 1996, Contrasts in ages of metamorphism in the Seve Nappes: U-Pb results from the central and northern Swedish Caledonides: Journal of the Geologic Survey of Sweden (GFF), v. 118, p. 36-38.

Guillong, M., Meier, D.L., Allan, M.M., Heinrich, C.A., and Yardley, B.W.D., 2008, SILLS: a Matlab-based program for the reduction of Laser Ablation ICP-MS data of homogeneous materials and inclusions, *in* Sylvester, P., ed., Laser-ablation-ICPMS in the earth sciences : current practices and outstanding issues: Vancouver, B.C., Mineralogical Association of Canada, p. 328–333.

Günther, D., Frischknecht, R., Heinrich, C.A., and Kahlert, H.J., 1997, Capabilities of an Argon Fluoride 193 nm excimer laser for laser ablation inductively coupled plasma mass spectrometry microanalysis of geologic materials: Journal of Analytical Atomic Spectrometry, v. 12, p. 939-944.

Heijlen, W., Muchez, P., Banks, D.A., Schneider, J., Kucha, H., and Keppens, E., 2003, Carbonate-hosted Zn-Pb deposits un Upper Silesia, Poland: Origin and evolution of mineralizing fluids and constraints on genetic models: ECONOMIC GEOLOGY, v.98, p. 911-932.

Heinrich, C.A., Pettke, T., Halter, W.E., Aigner-Torres, M., Audétat, A., Günther, D., Hattendorf, B., Bleiner, D., Guillong, M., and Horn, I., 2003, Quantitative multi-element analysis of minerals, fluid and melt inclusions by laser-ablation inductively-coupled-plasma mass-spectrometry: Geochimica et Cosmochimica Acta, v. 67, p. 3473-3497.

Israelson, C., Halliday, A.N., and Buchardt, B., 1996, U-Pb dating of calcite concretions from Cambrian black shales and the Phanerozoic time scale: Earth and Planetary Science Letters, v. 141, p.153-159.

Johansson, Å., 1983a, Lead isotope composition of Caledonian sulfide-bearing veins in Sweden: ECONOMIC GEOLOGY, v. 78, p. 1674-1688.

Johansson, Å., 1983b, Composition of sphalerite in some Swedish Pb-Zn bearing veins, *in* Lindblom, S., ed., Annual report of the ore research group, Stockholm University, p. 151-166.

Johansson, Å., 1984, Fluid inclusion and stable isotope studies on some Caledonian sulfide-bearing veins in Sweden: ECONOMIC GEOLOGY, v. 79, p. 1736-1748.

Johansson, Å., and Rickard, D.T., 1984, Isotope composition of Phanerozoic ore leads from the Swedish Segment of the Fennoscandian Shield: Mineralium Deposita, v. 19, p. 249-255.

Karis, L., 1998, Jämtlands östliga fjällberggrund, in Beskrivning till berggrundskartan över Jämtlands län, Del 2: Fjälldelen, Sveriges Geologiska Undersökning, Series Ca 53:2, p. 6-184 (in Swedish).

Kendrick, M.A., Burgess, R., Harrison, D., and Bjørlykke, A., 2005, Noble gas and halogen evidence for the origin of Scandinavian sandstone-hosted Pb-Zn deposits: Geochimica et Cosmochimica Acta, v. 69, p. 109-129.

Kesler, S.E., 1994, Mississippi Valley-Type deposits in continental margin basins: Lessons from the Appalachian-Caledonian orogen, *in* Fontboté, L., Boni, M., eds., Sediment-hosted Zn-Pb ores: Berlin Heidelberg, Springer-Verlag, Society for Geology Applied to Mineral Deposits, Special Publication 10, p. 89-103.

Kesler, S.E. and Carrigan, C.W., 2002, Discussion on „Mississippi Valley-type lead–zinc deposits through geologic time: Implications from recent age-dating research“: Mineralium Deposita, v. 37, p. 800-802.

Kesler, S. E., Chesley, J. T., Christensen, J. N., Hagni, R. D., Heijlen, W., Kyle, J. R., Muchez, Ph., Misra, K. C., and van der Voo, R., 2004, Discussion of ‘‘Tectonic controls of Mississippi Valley-type lead-zinc mineralization in orogenic forelands’’ by D.C. Bradley and D.L. Leach: Mineralium Deposita, v. 39, p. 512-514.

Kirkland, C., Bingen, B., Whitehouse, M., Beyer, E., and Griffin, W.L., 2011, Neoproterozoic paleogeography in the North Atlantic Region: interferences from the Akkajaure and Seve Nappes of the Scandinavian Caledonides: Precambrian Research, v. 186, p. 127-146.

Kullerud, K., Stephens, M.B., and Zachrisson, E., 1990, Pillow lavas as protoliths for eclogites: evidence from a late Precambrian–Cambrian continental margin, Seve Nappes, Scandinavian Caledonides: Contributions to Mineralogy and Petrology, v. 99, p. 344-351.

Leach, D.L., Bradley, D.C., Lewchuk, M.T., Symons, D.T.A., de Marsily, G., and Brannon, J., 2001, Mississippi Valley-type lead-zinc deposits through geologic time: Implications from recent age-dating research: Mineralium Deposita, v. 36, p. 711-740.

Leach, D. L., Bradley, D. C., Lewchuck, M., Symons, D. T. A., Premo, W., Brannon, J., and de Marsily, G., 2002, Reply to discussion on „Mississippi Valley-type lead–zinc deposits through geologic time: Implications from recent age-dating research“ by S. E. Kesler and C. W. Carrigan: Mineralium Deposita, v. 37, p. 803–805.

Lindahl, I., and Bjørlykke, A., 1988, The Geitvann lead-copper (-zinc) mineralization, Porsangerhalvøya, Finnmark, northern Norway: Norsk Geologisk Tidsskrift, v. 68, p. 125-131.

Lindblom, S., 1986, Textural and fluid inclusion evidence for ore deposition in the Pb-Zn deposit at Laisvall, Sweden: ECONOMIC GEOLOGY, v. 81, p. 46-64.

Lilljequist, R., 1973, Caledonian geology of the Laisvall area, Southern Norbotten, Swedish Lappland: Geologic Survey of Sweden, serie C, nr 691, årsbok 67, nr 10, scale 1:50 000, 1 sheet.

Ljungner, E., 1950, Urbergsytans form vid Fjällranden: Journal of the Geologic Survey of Sweden (GFF), Bd 72, H 3 (in Swedish)

Ludwig, K. R., 2003, User's manual for Isoplot 3.00: a geochronological toolkit for Microsoft Excel (No. 4).

Mac Niocaill, C., Van der Pluijm, B.A., and Van der Voo R., 1997, Ordovician paleogeography and the evolution of the Iapetus ocean: Geology, v. 25, p. 159-162.

Medford, G.A., Maxwell, R.J., and Armstrong, R.L., 1983, $^{87}Sr/^{86}Sr$ ratio measurements on sulfides, carbonates, and fluid inclusions from Pine Point, Northwest Territories, Canada: An $^{87}Sr/^{86}Sr$ ratio increase accompanying the mineralizing process: ECONOMIC GEOLOGY, v. 78, p. 1375-1378.

Moorbath, S., and Vokes, F.M., 1963, Lead isotope abundance studies occurrences in Norway: Norsk Geologisk Tidtskrift, v. 43, p. 283-343.

Nakai, S., Halliday, A.N., Kesler, S.E., Jones, H.D., 1990, Rb-Sr dating of sphalerites from Tenessee and the genesis of Mississippi Valley-type ore deposits: Nature, v. 346, p. 354-357.

Nakai, S., Halliday, A.N., Kesler, S.E., Jones, H.D., Kyle, J.R., and Lane, T.E., 1993, Rb-Sr dating of sphalerites from Mississippi Valley-type (MVT) ore deposits: Geochimica et Cosmochimica Acta, v.57, p. 417-427.

Nelson, J., Paradis, S., Christensen, J., and Gabites, J., 2002, Canadian Cordilleran Mississippi Valley-type deposits: A case for Devonian-Mississippian back-arc hydrothermal origin: ECONOMIC GEOLOGY, v. 97, p. 1013-1036.

Nielsen, A.T., and Schovsbo, N.H., 2011, The Lower Cambrian of Scandinavia: Depositional environment, sequence stratigraphy and paleogeography: Earth-Science Reviews, v. 107, p. 207-310.

Pease, V., Daly, J.S., Elming, S.-Å., Kumpulainen, R., Moczydłowska, M., Puchkov, V., Roberts, D., Saintot, A., and Stephenson, R., 2008, Baltica in the Cryogenian, 850–360 Ma: Precambrian Research, v. 160, p. 46-65.

Pettke, T., and Diamond, L., 1996, Rb-Sr dating of sphalerite based on fluid inclusion-host mineral isochrons: a clarification of why it works: ECONOMIC GEOLOGY, v. 91, p. 951-956.

Reesman, R.H., 1968, The Rb-Sr analyses of some sulfide mineralization: Earth and Planetary Science Letters, v. 5, p. 23-26.

Remizov, D., and Pease, V., 2004, The Dzela complex, Polar Urals, Russia: a Neoproterozoic island arc, in Gee, D.G., and Pease, V., eds., The Neoproterozoic Timanide orogen of eastern Baltica, Geologic Society of London, Memoirs, v. 30, p. 107-123.

Rickard, D.T., 1983, Precipitation and mixing mechanisms in Laisvall-type sandstone Pb-Zn deposits, *in* Kirsvarsanyi, G., Hagni, R., Pratt, W., and Koening, J.W., eds., Proceedings of the International Conference on Mississippi Valley Type Lead-Zinc Deposits: Rolla, Missouri, 1983

Rickard, D.T., Willdén, M., Mårde, Y., and Ryhage, R., 1975, Hydrocarbons associated with lead-zinc oresat Laisvall, Sweden: Nature, v. 255, p. 131-133.

Rickard, D.T., Willdén, M.Y., Marinder, N.E., and Donnelly, T.H., 1979, Studies on the genesis of the Laisvall sandstone lead-zinc deposit, Sweden: ECONOMIC GEOLOGY, v. 74, p.1255-1285.

Rickard, D.T., Coleman, M., and Swainbank, I., 1981, Lead and sulfur isotopic compositions of galena from the Laisvall sandstone lead-zinc deposit, Sweden: ECONOMIC GEOLOGY, v. 76, p. 2042-2046.

Roberts, D., and Gee, D.G., 1985, An introduction to the structure of the Scandinavian Caledonides, *in* Gee, D.G., Sturt, B.A., eds., The Caledonide orogen – Scandinavia and related areas: New York, Wiley, p. 56-68.

Roberts, D., and Siedlecka, A., 2002, Timanian orogenic deformation along the northeastern margin of Baltica, Northwest Russia and Northeast Norway, and Avalonian–Cadomian connections: Tectonophysics, v. 352, p. 169-184.Romer, R., 1992, Sandstone-hosted lead-zinc mineral deposits and their relation to the tectonic mobilization of the Baltic Shield during the Caledonian orogeny, a reinterpretation: Mineralogy and Petrology, v. 47, p.67-85.

Roberts, D., and Olovyanishnikov, V., 2004, Structure of the Timanide orogen, in Gee, D.G., and Pease, V., eds., The Neoproterozoic Timanide orogen of eastern Baltica, Geologic Society of London, Memoirs, v. 30, p. 47-57.

Romer, R.L., 1992, Sandstone-hosted Pb-Zn mineral deposits and their relation to the tectonic mobilization of the Baltic Shield during the Caledonian orogeny–a reinterpretation: Mineralogy and Petrology, v. 47, p. 67-85.

Romer, R.L., Wright, J.E., 1993, Lead mobilization during tectonic reactivation of the western Baltic Shield: Geochimica et Cosmochimica Acta, v. 57, p. 2555-2570.

Root, D., and Corfu, F., 2012, U-Pb geochronology of two discrete Ordovician high-pressure metamorphic events in the Seve Nappe Complex, Scandinavian Caledonides: Contribution to Mineralogy and Petrology, v. 163, p. 769-788.

Saintilan, N.J., 2010, The Granberget Pb-Zn deposit in the Dorotea district - Drilling activities 2009. Unpublished Boliden AB internal report.

Saintilan, N.J., 2015, Key controls, age, source of metals and role of hydrocarbons on the origin of Laisvall-type Pb-Zn deposits and their relationship to calcite-fluorite-Zn±Pb sulfide vein-type mineralization in Baltica basement (Sweden): PhD thesis, University of Geneva, Geneva, Switzerland.

Saintilan, N.J., Stephens, M.B., Fontboté, L., and Lundstam, E., 2012, Reactivation of fault zones in Precambrian crystalline basement and the location of strata-bound, sandstone-hosted Pb-Zn deposits along the

front of the Scandinavian Caledonides, Sweden: Integrated exploration and ore deposits, Society of Economic Geologist 2012 Conference - 23-26 September 2012, Lima, Perú, Abstracts.

Saintilan, N.J., Fontboté, L., Spangenberg, J.E., Samankassou, E., Stephens, M.B., 2014a, The Laisvall and Vassbo sandstone-hosted Pb-Zn deposits along the eastern front of the Scandinavian Caledonides: An example of phosphorous-rich sulfide-mineralized Cambro-Ordovician sour gas reservoirs: Mineral Deposit Studies Group, 37th Annual Winter Meeting – 6-7 January 2014, University of Oxford, UK, Abstracts, p. 70.

Saintilan, N.J., Stephens, M.B., Spangenberg, J.E., Fontboté, L., and Lundstam, E., 2014b, Proterozoic basement structures and thermogenic sulfate reduction-derived H_2S as key controls on economic Laisvall-type Pb-Zn deposits, eastern erosional front of the Scandinavian Caledonides, Sweden: Building Exploration Capability for the 21st Century, Society of Economic Geologist 2014 Conference – 27-30 September 2014, Keystone, Colorado, USA, Abstracts.

Saintilan, N.J., Spangenberg, J.E., Fontboté, L., and Stephens, M. B., 2014c, Migration of extrinsic organic compounds and sources of H_2S in the Pb-Zn sandstone-hosted Laisvall deposit, Caledonian front, Sweden: Swiss Geoscience Meeting 2014, Fribourg, Switzerland, Abstracts.

Saintilan, N.J., Stephens, M.B., Lundstam, E., and Fontboté, L., 2015, Control of reactivated basement structures on sandstone-hosted Pb-Zn deposits along the Caledonian Front, Sweden: Evidence from airborne magnetic field data, structural analysis and ore grade modeling: ECONOMIC GEOLOGY, v. 110, p. 91-117.

Santallier, D.S., 1988, Mineralogy and crystallization of the Seve eclogites in the Vuoggatjålme area, Swedish Caledonides of Norrbotten: Journal of the Geologic Society of Sweden (GFF), v. 110, p. 89-98.

Schneider, J., Haack, U., Hein, U.F., and Germann, A., 1999, Direct Rb/Sr dating of sandstone-hosted sphalerites from strata-bound Pb-Zn deposits in the northern Eifel, NW Rhenish Massif, Germany, *in* Stein, H. J., Hannah, J. L., eds., Timing and duration of ore-forming processes: Contributions from radiometric dating, *in* Stanley, C.J., ed., Mineral deposits: Processes to processing, Proceedings 5th Biennial SGA Meeting and the 10th Quadrennial IAGOD Symposium, London, 22-25 August, 1999, p. 1287-1280.

Schneider, J., Heijlen, W., Muchez, Ph. and Haack, U., 2002, Rb-Sr dating of sphalerites from Pomorzany, Upper Silesia (Poland): Abstracts of the 12th Annual V.M. Goldschmidt Conference, Davos, Switzerland 18 - 23 August: Geochimica Cosmochimica Acta, v. 66, (Suppl. 1): A 683.

Schneider, J., Haack, U., and Stedingk, K., 2003, Rb-Sr dating of epithermal vein mineralization stages in the eastern Harz Mountains (Germany) by paleomixing lines: Geochimica et Cosmochimica Acta, v. 67, p. 1803-1819.

Schneider, J., Melcher, F., and Brauns, M., 2007, Concordant ages for the giant Kipushi base metal deposit from direct Rb-Sr and Re-Os dating of sulfides: Mineralium Deposita, v. 42, p. 791-797.

Selby, D., Creaser, R.A., Dewing, K., and Fowler, M., 2005, Evaluation of bitumen as a ^{187}Re–^{187}Os geochronometer for hydrocarbon maturation and migration: A test case from the Polaris MVT deposit, Canada: Earth and Planetary Science Letters, v.235, p. 1-15.

Sherlock, R.L., Lee, J.K., and Cousens, B.L., 2004, Geologic and geochronologic constraints on the timing of mineralization at the Nanisivik zinc-lead Mississippi Valley-type deposit, northern Baffin Island, Nunavut, Canada: ECONOMIC GEOLOGY, v. 99, p. 279-293.

Sherlock, S.C., Lucks, T., Kelley, S.P., Barnicoat, A., 2005, A high resolution record of multiple diagenetic events: Ultraviolet laser microprobe Ar/Ar analysis of zoned K-feldspar overgrowths: Earth and Planetary Science Letters, v. 238, p. 329-341.

Skiöld, T., 1988, Implications of new U-Pb zircon chronology to early Proterozoic crustal accretion in northern Sweden: Precambrian Research, v. 38, p. 147-164.

Staude, S., Bons, P.D., and Markl, G., 2009, Hydrothermal vein formation by extension-driven dewatering of the middle crust: An example from SW Germany: Earth and Planetary Science Letters, v. 286, p. 387-395.

Steiger, R., and Jäger, E., 1977, Subcommission on geochronology: convention on the use of decay constants in geo-and cosmochronology: Earth and planetary science letters, v. 36, p. 359-362.

Stephens, M.B., 1986, Strata-bound sulfide deposits in the Central Scandinavian Caledonides, *in* 7th IAGOD Symposium and Nordkallot project meeting, Excursion Guide n°2, Ca 60, Geologic Survey of Sweden, Uppsala, Sweden, 68 p.

Stephens, M.B., 1988, The Scandinavian Caledonides: a complexity of collisions: Geology Today, v. 4, p.20-26.

Sturt, B.A., 1978, The Norwegian Caledonides: Geological Survey of Canada Paper, v. 78, p. 13-16.

Sundblad, K., 1990, Precambrian metal sources in sulfide deposits in the northernmost part of the Scandes: Journal of the Geologic Society of Sweden (GFF), v. 111, p. 415-418.

Svenningsen, O.M., 2001, Onset of seafloor spreading in the Iapetus Ocean at 608 Ma: precise age of the Sarek Dyke Swarm, northern Swedish Caledonides: Precambrian Research, v. 110. p. 241-254.

Symons, D.T.A., Sangster, D.F., and Leach, D.L., 1995, A Tertiary age from paleomagnetism for Mississippi Valley-type zinc-lead mineralization in Upper Silesia, Poland: Economic Geology, v. 90, p. 782-794.

Thickpenny, A., 1984, The sedimentology of the Swedish alum shales: London, Geologic Society Special Publications 15, p. 511-525.

Veizer, J., Ala, D., Azmy, K., Bruckschen, P., Buhl, D., Bruhn, F., Carden, G.A.F., Diener, A., Ebneth, S., Godderis, Y., Jasper, T., Korte, C., Pawellek, F., Podlaha, O.G., and Strauss, H., 1999, $^{87}Sr/^{86}Sr$, $\delta^{13}C$ and $\delta^{18}O$ evolution of Phanerozoic seawater: Chemical Geology, v. 161, p. 59-88.

Wendt, I., and Carl, C., 1991, The statistical distribution of the mean squared weighted deviation: Chemical Geology: Isotope Geoscience Section, v. 86, p. 275-285.

Wickman, F.E., Blomqvist, N.G., Geijer, P., Parwel, A., Ubisch, H.V., and Welin, E., 1963, Isotopic constitution of ore lead in Sweden: Arkiv f. Min. Gel., v. 3, p. 193-257.

Willdén, M.Y., 1980, Paleoenvironment of the autochthonous sedimentary rocks sequence at Laisvall, Swedish Caledonides [PhD thesis]: Stockholm, Sweden, Stockholms Universitets Geologiska Institutionen, 100 p.

Wilson, S.A., Ridley, W.I., Koenig, A.E., 2002, Development of sulfide calibration standards for the laser ablation inductively- coupled plasma mass spectrometry technique: Journal of Analytical Atomic Spectrometry, v. 17, p. 406–409.

Yang, J. H., and Zhou, X. H., 2001, Rb-Sr, Sm-Nd, and Pb isotope systematics of pyrite: Implications for the age and genesis of lode gold deposits: Geology,v. 29, p. 711-714.

Zachrisson, E., 1980, Aspects of strata-bound base metal mineralization in the Swedish Caledonides, *in* Vokes, F.M., Zachrisson, E., eds., Review of Caledonian-Appalachian strata-bound sulfide deposits: Geologic Survey of Ireland, Special Paper 5, v. 41-61.

CHAPTER 3

Unconventional lead source in the metal endowment of sediment-hosted mineral deposits: the contribution from shale hydrocarbon source rocks

This manuscript is co-authored by Nicolas J. Saintilan, Massimo Chiaradia, Cyril Chelle-Michou, Jorge E. Spangenberg, Michael B. Stephens, and Lluís Fontboté. Data tables and an extended description of methods and analytical protocols are given in the Data Repository. The mention Saintilan et al. (*in press*) refers to Chapter 2.

Unconventional lead source in the metal endowment of sediment-hosted mineral deposits: the contribution from shale hydrocarbon source rocks

Nicolas J. Saintilan[1], Massimo Chiaradia[1], Cyril Chelle-Michou[1], Jorge E. Spangenberg[2], Michael B. Stephens[3,4], and Lluís Fontboté[1]

[1]Section of Earth and Environmental Sciences, University of Geneva, Rue des Maraîchers 13, 1205, Geneva, Switzerland

[2]Institute of Earth Surface Dynamics, University of Lausanne, Building Geopolis, 1015 Lausanne, Switzerland

[3]Geological Survey of Sweden (SGU), Box 670 SE-751 28 Uppsala, Sweden

[4]Division of Geosciences, Luleå University of Technology, SE-971 87 Luleå, Sweden

ABSTRACT

A lead isotope survey of ore (n = 47) and whole rock (n = 11) samples was carried out at the world-class, sandstone-hosted, Mississippi Valley-type Laisvall Pb-Zn deposit, Sweden. Calculation of lead source model ages for this Middle Ordovician deposit (467 ± 5 Ma, Rb-Sr geochronology on sphalerite consistent with geologic constraints) suggests that the line defined by the lead isotopic composition of Pb-Zn sulfides, in a conventional $^{207}Pb/^{204}Pb$ vs. $^{206}Pb/^{204}Pb$ diagram, corresponds to a mixing line for which a lead source is needed in addition to the conventional source from basement rocks. By using the Pb isotopic composition of separate HCl-HNO_3 leachate and HF-HNO_3 residue whole rock fractions from metal-rich shale hydrocarbon source rock (Alum Shale Formation), granite basement samples and K-feldspar in the granite, the following lead sources were constrained: (1) Mainly radiogenic Pb leached from basement rocks; (2) subordinate but significant input of low-radiogenic Pb derived from shale hydrocarbon source rocks in the Alum Shale Formation. This low-radiogenic end-member results from the leaching of the following components in these shale source rocks: (i) HCl-HNO_3 leachable organic molecules providing organo-metallic Pb; (ii) microscopic fragments of K-feldspars; and (iii) pyrite ± other sulfides. While the radiogenic Pb leached from crystalline basement rocks is consistent with other data and the standard MVT model for the transport of metals as chloride complexes in basinal brines, the

low-radiogenic Pb end-member requires other mechanisms. Most of the reduced sulfur for mineralization upon mixing with metal-bearing brines was produced via thermochemical sulfate reduction with characteristic high δ^{34}S values in pools of hydrocarbons accumulated as petroleum-aqueous phase systems in sandstone paleoaquifers. Hydrocarbons had been produced by shale source rocks in the Alum Shale Formation and had migrated into sandstone paleoaquifers. A working hypothesis suggests that the low-radiogenic Pb end-member is mainly contributed by Pb-bearing organic molecules in this petroleum-aqueous phase system derived from anomalously metal-rich shale of the Alum Shale Formation.

INTRODUCTION

Organic compounds (e.g., hydrocarbons) are involved in several instances in the formation at low temperatures (<200°C) of sediment-hosted deposits (e.g., Mississippi Valley-type MVT deposits, Cu sandstone-hosted deposits; Spangenberg and Macko, 1998; Box et al., 2012; Hayes et al., 2012; Saintilan et al., *submitted to Mineralium Deposita, current Chapter 4*). Liquid or gaseous hydrocarbons acted as reductant during thermochemical sulfate reduction (TSR) in MVT and Cu sandstone-hosted deposits with high δ^{34}S values and containing bitumen, whereas crude oil and related organic matter directly supplied reduced sulfur in MVT deposits with low δ^{34}S values (Anderson, 1991; Kesler et al., 1994; Hayes et al., 2012; Saintilan et al., *submitted to Mineralium Deposita, current Chapter 4*).

In cases where hydrocarbons were produced from shale source rocks with high metal contents (e.g., U, Mo, Ni, V, Hg, Pb, Zn; Pašava, 1996) and these hydrocarbons were subsequently involved in mineralizing process of sediment-hosted deposits, the question may be rightly asked if such hydrocarbon source rocks may have contributed indirectly via the hydrocarbon system (i.e., petroleum and associated aqueous phase) to the metal endowment of mineral deposits. Given that only petroleum liquids with high asphaltic content have the potential to contribute Zn and more rarely Pb in sufficient concentrations for ore formation (> 10 ppm; Manning and Giże, 1993), the possibility has been invoked that, in a petroleum-aqueous phase system, Pb and Zn partition preferentially into the aqueous phase where they may form metallo-organic complexes (e.g., metal-carboxylate; Parnell, 1988; Manning and Giże, 1993; Filby, 1994; Giordano and Kharaka, 1994; Giordano, 2002; Greenwood et al., 2013).

This working hypothesis is applied to the case study of the Laisvall sandstone-hosted Pb-Zn MVT deposit (64 Mt at 4 %Pb, 0.6 %Zn) currently located along the erosional front of the Caledonian orogen, Sweden. Exogenous hydrocarbon migrated from metal-rich (e.g., 10–200 ppm Pb; Thickpenny, 1984) shale source rocks in the Alum Shale Formation buried in the foredeep of the early Caledonian basin into sandstone where they accumulated in traps in forebulge setting. These hydrocarbons participated in the supply of reduced sulfur via TSR for Pb-Zn sulfide precipitation (Saintilan et al., *submitted to Mineralium Deposita, current Chapter 4*).

There is a general consensus that oxidized basinal brines act as a transport medium for Pb and Zn and supply the bulk of metals in MVT deposits. According to widely accepted hypotheses, basinal fluids of high salinity and low H_2S content acquire metals as the result of alteration of metal-bearing solid phases in local basement and basal detrital rocks, chloride-metal complexes being the dominant transport agent for Pb and Zn (e.g., Dixon et al., 1990; Goldhaber et al., 1995; Hanor, 1996; Leach et al., 2005).

In the current contribution and to our knowledge for the first time, by using lead isotope geochemistry of sulfides and whole rock at Laisvall, an example is presented of (1) lead being extracted from shale hydrocarbon source rock, (2) making a subordinate but significant contribution in complement to the main supply of metals by the above-mentioned evolved and basement-interacted basinal brines in the formation of this MVT deposit (cf. Saintilan et al., *submitted to Mineralium Deposita, current Chapter 4*).

Pb-Zn MINERALIZATION IN SANDSTONE AND THE ROLE OF ORGANIC-RICH SHALE

In the central and northern parts of Sweden, the crystalline basement (Fig. 1) is dominated by Paleoproterozoic rocks included in the 2.0 to 1.8 Ga Svecokarelian orogen (Bergman et al., 2012). These rocks are overlain unconformably by Ediacaran to Cambrian, locally through to Lower Ordovician, autochthonous sedimentary cover rocks that were deposited on the western passive margin to the continent Baltica (Gee, 1975; Bergman et al., 2012). The cover rocks are overlain in turn to the west by thrust sheets belonging to the 0.5 to 0.4 Ga Caledonian orogen (Gee, 1975; Roberts and Gee 1985; Bergman et al., 2012). At Laisvall, the autochthonous stratigraphy that overlies the Paleoproterozoic (c. 1.8 Ga) granite basement is preserved underneath a décollement along middle Cambrian to Lower Ordovician organic-rich mudstone and shale units (Alum Shale Formation) with overlying allochthonous thrust sheets (Rickard et al., 1979; Saintilan et al., 2015). Strata-bound, epigenetic, disseminated galena-sphalerite mineralization is hosted in two sandstone paleoaquifers capped by the regionally extensive Alum Shale Formation (Rickard et al., 1979; Willdén, 1980; Saintilan et al., 2015).

The Laisvall deposit formed during the Middle Ordovician (467 ± 5 Ma) as a response to early Caledonian orogenic activity (Saintilan et al., *in press*). Ore formation resulted from the mixing of (1) metal-bearing evolved basinal brines in the Caledonian foredeep which acquired metals during cratonward migration along permeable channelways and interaction with crystalline basement rocks and erosional products; with (2) a pool of hydrogen sulfide produced in sandstone during thermochemical sulfate reduction (TSR) aided by exogenous hydrocarbons which had migrated cratonward and accumulated in favorable traps in permeable Ediacaran to Cambrian sandstone. Hydrocarbons were produced from source rocks in the middle Cambrian to Lower Ordovician Alum Shale Formation buried

in the Caledonian foredeep (Rickard et al., 1975, 1979, 1981; Lindblom, 1986; Kendrick et al., 2005; Saintilan et al., *to be submitted to Mineralium Deposita, current Chapter 4*).

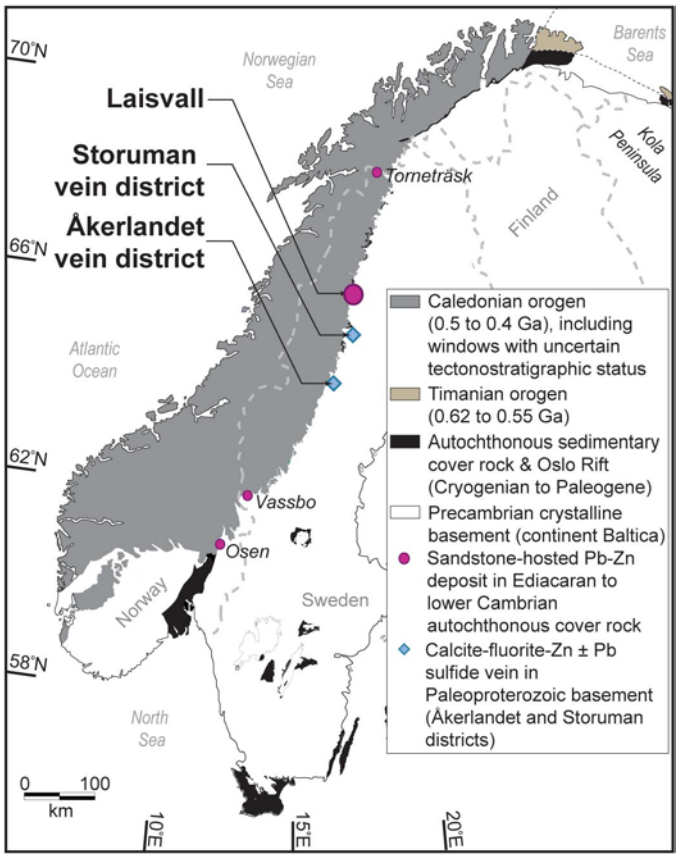

FIG. 1 Simplified geologic map of Scandinavia showing the location of sandstone-hosted Pb-Zn deposits in Ediacaran to lower Cambrian sandstone and calcite-fluorite-Zn ± Pb sulfide vein-type deposits in Paleoproterozoic crystalline basement, current erosional front of the Caledonian orogen, Sweden (modified after Saintilan et al., *in press).*

The Alum Shale Formation contains, in part, horizons with high contents of total organic carbon (1–22 wt.% TOC), Pb (10–200 ppm) and other metals (e.g., Ni, V, Mo, U, Zn; Thickpenny, 1984; Pašava, 1996). The kerogen structure of the Alum Shale Formation consists primarily of algal organic matter (Bharati et al., 1991). Reducible metals are fixed as sulfides or associated with organic matter. Iron is completely sulfidized as pyrite in shales with TOC > 5 wt.% (Leventhal, 1991). Silicate minerals in shale are illite, quartz and K-feldspar fragments in the range of 5 to 15 wt.% (Thickpenny, 1984). Lead in the Alum Shale Formation could be leached from (1) microscopic K-feldspar fragments that are erosional products of crystalline rocks in Baltica basement (cf. Nielsen and Schovsbo, 2011); (2) sulfides (e.g., pyrite) in organic-rich shale; (3) metal porphyrins (see below).

During diagenesis of organic matter in sediments, the central Mg^{2+} cation coordinated to the porphin ring structure of macromolecules (e.g., chlorophyll) is replaced by divalent metals (e.g. Pb^{2+}; Callot et al., 1990; Filby, 1994; Manning and Giże, 1993). The resulting metal geoporphyrins accumulate

in kerogen and are released during catagenesis into the asphaltene and NSO fraction (polar compounds containing heteroatoms of nitrogen, sulfur and oxygen) of bitumen and oil (Tissot and Welte, 1984; Filby, 1994). In addition, porphyrin acids are metallated and adsorbed in ion-exchange sites along clay interlayers in shale (Filby, 1994; Manning and Giże, 1993).

VEIN DEPOSITS IN BASEMENT ROCKS OF BALTICA, FENNOSCANDIAN SHIELD

The Åkerlandet calcite-fluorite-Zn ± Pb sulfide vein deposit (Johansson, 1980) is located 35 km to the east of the erosional front of the Caledonian orogen, central Sweden, in Paleoproterozoic (1.9 Ga) migmatitic paragneiss belonging to the crystalline basement (Fig. 1; Bergman et al., 2012). Similar vein deposits (Billström et al., 2012) occur 75 km to the north in the Storuman district (Fig. 1) in Paleoproterozoic (2.0–1.9 Ga) metasedimentary rocks intruded by 1.8 Ga granite (Bergman et al., 2012). Zn-Pb sulfide mineralization at Åkerlandet, which is older than (Ediacaran) or possibly coeval with mineralization at Laisvall (Saintilan et al., *in press*), formed by oxidizing and slightly acidic hydrothermal fluids transporting metals and leaching H_2S from sulfides in local basement rocks (Saintilan et al., ***Chapter 5***). Subsequent calcite and fluorite precipitated from basement-interacted, organic-matter interacted, reduced and alkaline hydrothermal fluids (Saintilan et al., ***Chapter 5***).

MATERIAL AND METHODS

Galena aliquots from mineralized samples from the Laisvall deposit (n = 42) and Åkerlandet district (n = 6) were analyzed for their Pb isotopic composition. Additional lead aliquots were obtained from sphalerite samples at these deposits (n = 6) during Rb-Sr-Pb column chemistry (Saintilan et al., *in press*). This dataset was complemented with published Pb isotope data of galena and sphalerite aliquots from vein deposits in the Storuman district (Billström et al., 2012).

Following the protocol by Chiaradia and Fontboté (2003), the Pb isotopic composition of leachate and residue whole rock fractions (Fig. 2) were obtained from samples from the Alum Shale Formation (n = 5) with TOC from 0.38 to 2.80 wt.%, basement granite samples (n = 6) and K-feldspar separated from the granite samples (n = 7).

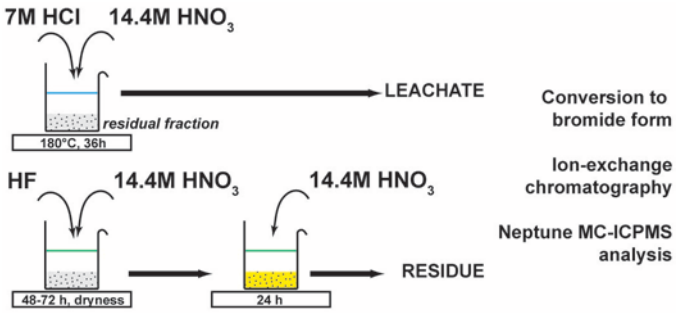

FIG. 2 Protocol for determination of the Pb isotopic composition of leachate and residue whole rock fractions (after Chiaradia and Fontboté, 2003).

LEAD ISOTOPE COMPOSITION AND SOURCE MODEL AGES

Data points for Laisvall and each district of vein deposits define separate clusters in a $^{207}Pb/^{204}Pb$ vs. $^{206}Pb/^{204}Pb$ diagram, with the cluster from Laisvall being characterized by less radiogenic isotope compositions than the vein deposit clusters (Fig. 3). Sulfides from Laisvall define a line with slope 0.1124 that is distinct from the line defined by sulfides from the combined vein deposits with slope 0.1364. In contrast to the conclusions by Johansson and Rickard (1984), Duane and de Wit (1988) and Romer (1992), these results suggest that the Laisvall and vein deposits do not fall on the same line. The lines defined by sulfides at Laisvall and in vein deposits could represent separate paleoisochrons or, alternatively, a paleoisochron and a mixing line between two isotopically discrete lead sources.

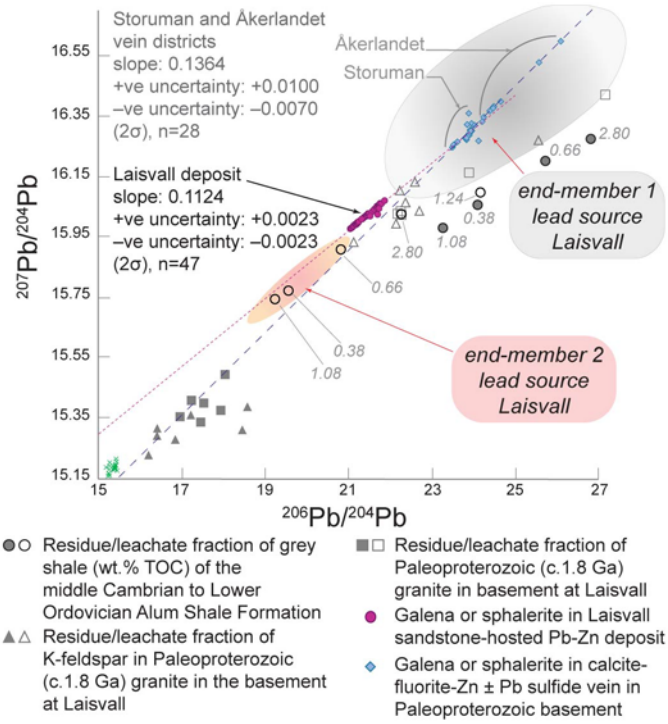

FIG. 3 $^{207}Pb/^{204}Pb$ vs. $^{206}Pb/^{204}Pb$ plot of residues and leachates of Paleoproterozoic crystalline basement rock, corresponding K-feldspar crystals and middle Cambrian to Lower Ordovician organic-rich shale at Laisvall, and of sulfides from the Laisvall deposit and basement-hosted vein-type deposits in the Storuman and Åkerlandet districts. Numbers in grey indicate the total organic carbon content (wt% TOC) of each shale sample from which residue and leachate fractions were obtained. The residue of shale sample with 1.24 wt% TOC plots outside the diagram with a $^{206}Pb/^{204}Pb$ ratio of 90. The lead isotope composition of volcanic-hosted massive sulfide deposits in the Paleoproterozoic Skellefte district (after Billström and Vivallo, 1994), shown by green crosses, is not a lead source for the Laisvall deposit. Unlike sulfides, the current Pb isotope compositions of whole rock residue-leachate fractions may be slightly more radiogenic than at the time of vein-type or Laisvall-type mineralization due to U and Th decay. An artifact of laboratory HNO_3 treatment may be the partial oxidation of some kerogen moieties, which could explain the more radiogenic signature of two leachates with TOC > 1 wt% (comprising low radiogenic organo-metallic Pb and high radiogenic Pb from U decay), close to that of shale residues.

We calculated lead source model ages (T) for a range of mineralization ages (t, when the $^{235}U/^{238}U$ ratio had a different value than at present) between 400 and 600 Ma, consistent with the published Rb-Sr sphalerite isochron ages for the Laisvall deposit (467 ± 5 Ma; Saintilan et al., *in press*) and vein deposits (548 to 463 Ma; Billström et al., 2012; Saintilan et al., *in press*). The equation of the slope (m) of a paleoisochron is:

$$m = \left(\frac{^{207}Pb}{^{206}Pb}\right)^{*} = \frac{1}{137.818} \times \left(\frac{e^{\lambda_{235}\mathrm{T}} - e^{\lambda_{235}\mathrm{t}}}{e^{\lambda_{238}\mathrm{T}} - e^{\lambda_{238}t}}\right) \qquad (A)$$

Since galena and sphalerite contain virtually no uranium and thorium, their lead isotopic composition approximates the common lead composition at the time of precipitation. For mineralization ages between 400 and 600 Ma, the source of lead in the vein deposits has a model age between 1.8 and 2.1 Ga while the source of lead at Laisvall has an invariably younger model age between 1.4 and 1.7 Ga

(Fig. 4). Considering the range of Rb-Sr sphalerite ages for the vein deposits, the lead source model age of 2.1 to 1.8 Ga is consistent with the geologic age of the crystalline basement rocks. On the other hand, mineralization at Laisvall at 467 ± 5 Ma implies a lead source model age of c. 1.61 to 1.52 Ga. This age is inconsistent with any known rock unit in the part of the Baltica basement around Laisvall. Thus, the line for sulfides at Laisvall more likely represents a mixing line for which another lead source is needed in addition to basement rocks.

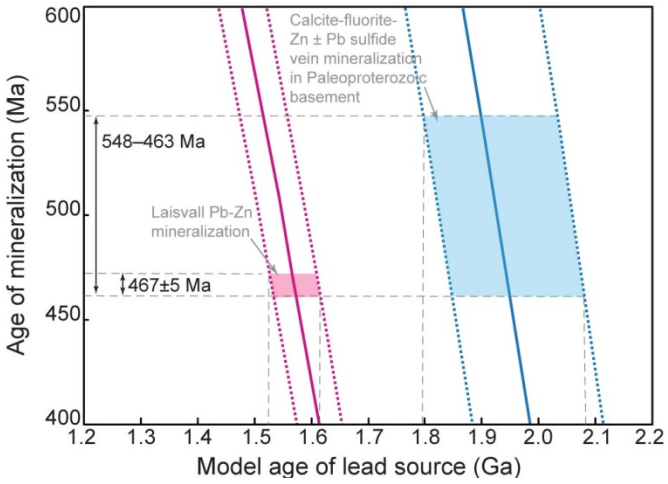

FIG. 4 Model age of lead source vs. timing of mineralization between 400 and 600 Ma for the Laisvall deposit and the vein-type deposits in the Storuman and Åkerlandet districts.

DISCUSSION AND CONCLUSION

Residues of Paleoproterozoic granite basement and corresponding K-feldspar crystals at Laisvall cluster in a narrow isotopic field (Fig. 3). Residues are systematically less radiogenic than corresponding leachates. The individual residue-leachate pairs have ages between 2.0 and 1.8 Ga consistent with the age of the rocks. Leachates from granite and K-feldspar fall on or close to the more radiogenic side of the Laisvall sulfide line. Thus, these could represent an important Pb source for this deposit. The lead isotopic composition of the vein deposits is compatible with that of the leachates from granite and K-feldspar with variable high μ values ($^{238}U/^{204}Pb$).

Three shale HCl-HNO_3 leachates from the Alum Shale Formation fall close to the Laisvall sulfide line on the side of lower radiogenic values and might represent a second Pb source (Fig. 3). The shale residues are more radiogenic than the corresponding leachates.

In the laboratory, bitumen is dissolved by organic solvents (e.g., dichloromethane) while kerogen is obtained by subsequent acidification by HF-HCl (e.g., Spangenberg and Macko, 1998; Spangenberg et al., 2014). Since uranium mineralization in the Alum Shale Formation occurs as uraniferous ± Zr ± Y phospho-silicate complexes intimately associated with kerogen (Lecomte et al., 2013), the residue fraction, obtained with a mixture of concentrated HF and HNO_3 (Chiaradia and Fontboté, 2003), contains

common Pb from undissolved kerogen and bitumen, and radiogenic lead from uranium decay. The isotopic composition of the shale residue fractions does not fall on the Laisvall line implying that low-radiogenic organo-metallic Pb and radiogenic Pb from U decay in kerogen did not contribute to the composition of Pb-Zn sulfides at Laisvall.

We conclude that the lead isotopic composition of sulfides at Laisvall is compatible with two lead sources involving (Figs. 3 and 5):

(1) Mainly radiogenic Pb leached from crystalline basement rocks by basinal brines resurging as metal-bearing fluids in sandstone along reactivated Paleoproterozoic crystalline basement faults (Saintilan et al., 2015, *submitted to Mineralium Deposita, current Chapter 4*);

(2) a subordinate input of low-radiogenic Pb with bulk composition derived from the leaching of the following components in metal-rich shale hydrocarbon source rocks of the Alum Shale Formation: (i) HCl-HNO_3 leachable organic molecules providing organo-metallic Pb; (ii) microscopic fragments of K-feldspars; and (iii) pyrite ± other sulfides.

A working hypothesis considers that the main contributors to this low-radiogenic end-member are Pb-bearing organic compounds in the petroleum-aqueous phase system in sandstone that were derived from Pb-bearing organic molecules in the Alum Shale Formation and migrated with liquid hydrocarbons. Given that hydrocarbons from the Alum Shale Formation were relatively heavy (cf. Saintilan et al., *submitted to Mineralium Deposita, current Chapter 4*), the metal content in petroleum accumulated in sandstone might have been relatively high due to high asphaltic content. Additional research work is currently being carried out by adapting the protocol by Chiaradia and Fontboté (2003) to produce whole rock leachable fractions of shale hydrocarbon source rocks using organic solvents. This procedure aims to determine the Pb isotope composition of extractable organic matter in organic-rich shale of the Alum Shale Formation in order to compare it to the isotopic composition of HCl-HNO_3 leachates of organic-rich shale that defines the low-radiogenic Pb end-member of the Laisvall sulfide line in the current study.

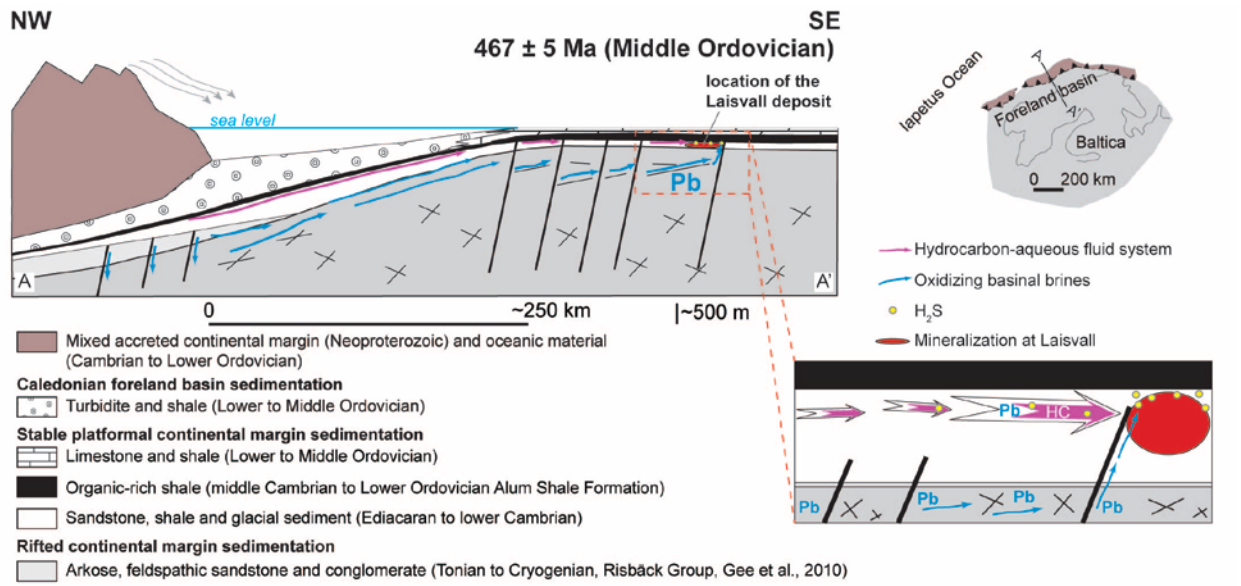

FIG. 5 Lead sources for the formation of the Laisvall sandstone-hosted Pb-Zn deposit (modified after Saintilan et al., *submitted to Mineralium Deposita, current Chapter 4*).

ACKNOWLEDGMENTS

This research is financially supported by Boliden AB (Sweden), the Swiss National Foundation (SNF, Switzerland, FN 146 353) and the Geological Survey of Sweden.

REFERENCES

Anderson, G.M., 1991, Organic maturation and ore precipitation in Southeast Missouri: Economic Geology, v. 86, p. 909-926.

Barth, T., and Bjørlykke, K., 1993, Organic acids from source rock maturation: generation potentials, transport mechanisms and relevance for mineral diagenesis: Applied Geochemistry, v. 8, p. 325–337.

Bergman, S., Stephens, M.B., Andersson, J., Kathol, B., and Bergman, T., 2012, Geological map of Sweden: Geological Survey of Sweden, scale 1:1 000 000, 1 sheet.

Bharati, S., Patience, R.L., Larter, S.R., Standen, G., and Poplett, I.J.F., 1995, Elucidation of the Alum Shale kerogen structure using a multi–disciplinary approach: Organic Geochemistry, v. 23, p. 1043–1058.

Billström, K., Broman, C., Schneider, J., Pratt, W., and Skogsmo, G., 2012, Zn-Pb ore of Mississippi-Valley Type in the Lycksele–Storuman District, Northern Sweden: A possible rift–related Cambrian mineralization event: Minerals, v. 1, p. 169–207.

Billström, K., and Vivallo, W., 1994, Synvolcanic mixing of ore lead and the development of lead isotopic provinces in the Skellefte district, Sweden: Mineralium Deposita, v. 29, p. 111-119.

Box, S.E., Syusyura B., Seltmann, R., Creaser, R.A., Dolgopolova, A., and Zientek, M.L., 2012b, Dzhezkazgan and associated sandstone copper deposits of the Chu-Sarysu Basin, Central Kazakhstan: Economic Geology Special Publication 16, p. 303-328.

Callot, H. J., Ocampo, R., Albrecht, P., 1990, Sedimetary porphyrins: correlation with biological precursors: Energy & Fuels, v. 4, p. 635–639.

Chiaradia, M., and Fontboté, L., 2003, Separate lead isotope analyses of leachate and residue fractions: implications for metal source tracing in ore deposit studies: Mineralium Deposita, v. 38, p. 185–195.

Dixon, P.R., LeHuray, A.P., and Rye, D.M., 1990, Basement geology and tectonic evolution of Ireland as deduced from Pb isotopes: Geological Society of London Journal, v. 147, p. 121–132.

Duane, M.J., and de Wit, M.J., 1988, Pb-Zn ore deposits of the northern Caledonides: Products of continental-scale fluid mixing and tectonic expulsion during continental collision: Geology, v. 16, p. 999–1002.

Filby, R. H., 1994, Origin and nature of trace element in crude oils, bitumens and kerogens: implications for correlation and other geochemical studies, *in* Parnell, J., ed., Geofluids: Origin, Migration and Evolution of Fluids in Sedimentary Basins: London, Geological Society Special Publication 78, p. 203–219.

Gee, D.G., 1975, A tectonic model for the central part of the Scandinavian Caledonides: American Journal of Science, v. 275A, p. 468–515.

Giordano, T. H., 2002. Transport of Pb and Zn by carboxylate complexes in basinal ore fluids and related petroleum-field brines at 100°C: the influence of pH and oxygen fugacity: Geochemical Transactions, v. 3, p. 56–72.

Giordano, T. H., Kharaka, Y. K., 1994. Organic ligand distribution and speciation in sedimentary basin brines, diagenetic fluids and related ore solutions, *in* Parnell, J., ed., Geofluids: Origin, Migration and Evolution of Fluids in Sedimentary Basins: London, Geological Society Special Publication 78, p. 175–202.

Goldhaber, M.B., Church, S.E., Doe, B.R., Aleinikoff, J.N., Brannon J.C., Podosek, F.A., Mosier, E.L., Taylor, C.F., and Gent, C.A., 1995, Lead and sulfur isotope investigation of Paleozoic sedimentary rocks from the Southern Midcontinent of the United States: Implications for paleohydrology and ore genesis of the Southeast Missouri lead belts: Economic Geology, v. 90, p. 1875–1910.

Greenwood, P. F., Brocks, J.J., Grice, K., Schwark, L., Jaraula, C.M.B., Dick, J.M., and Evans, K.A., 2013, Organic geochemistry and mineralogy. I. Characterization of organic matter associated with metal deposits: Ore Geology Reviews, v. 50, p. 1–27.

Hanor, J.S., 1996, Controls on the solubilization of lead and zinc in basinal brines: Society of Economic Geologists, Special Publication 4, p. 483-500.

Hayes, T.S., Landis, G.P., Whelan, J.F., Rye, R.O., and Moscati, R.J., 2012, The Spar Lake strata-bound Cu-Ag deposit formed accross a mixing zone between natural gas and metals-bearing brine: Economic Geology, v. 107, p. 1223-1249.

Huseby, B., Barth, T., and Ocampo, R., 1996, Porphyrins in Upper Jurassic source rocks and correlations with other source rock descriptors: Organic geochemistry, v. 25, p. 273–294.

Johansson, Å., 1980, Fluid inclusion thermometry on calcite, sphalerite and fluorite from the Åkerlandet vein, Västerbotten County, Sweden, *in* Rickard, D., ed., Annual report of the ore research group, p. 188-200.

Johansson, Å., and Rickard, D.T., 1984, Isotope composition of Phanerozoic ore leads from the Swedish Segment of the Fennoscandian Shield: Mineralium Deposita, v. 19, p. 249-255.

Kendrick, M.A., Burgess, R., Harrison, D., and Bjørlykke, A., 2005, Noble gas and halogen evidence for the origin of Scandinavian sandstone-hosted Pb-Zn deposits: Geochimica et Cosmochimica Acta, v. 69, p. 109–129.

Kesler, S.E., Jones, H.D., Furman, F.C., Sassen, R., Anderson, W.H., and Kyle, J.R., 1994, Role of crude oil in the genesis of Mississippi Valley-Type deposits: Evidence from the Cincinnati arch: Geology, v. 22, p. 609–612.

Leach, D.L., Sangster, D.F., Kelley, K.D., Large, R.R., Garven, G., Allen, C.R., Gutzmer, J., and Walters, S., 2005, Sediment-hosted Pb-Zn deposits: A global perspective: Economic Geology 100th Anniversary Volume, p. 561–607.

Leventhal, J. S., 1991, Comparison of organic geochemistry and metal enrichment in two black shales: Cambrian Alum Shale of Sweden and Devonian Chattanooga Shale of United States: Mineralium Deposita, v. 26, p. 104-112.

Lindblom, S., 1986, Textural and fluid inclusion evidence for ore deposition in the Pb-Zn deposit at Laisvall, Sweden: Economic Geology, v. 81, p. 46-64.

Lecomte, A., Cathelineau, M., Michels, R., and Brouand, M., 2013, Uranium mineralization in the Alum Shale Formation (Sweden): Mineral deposit research for a high-tech world, Proceedings of the 12th Biennial SGA Meeting, 12-15 August 2013, Uppsala, Sweden, Abstracts, p. 1654–1656.

Machel, H.G., 2001, Bacterial and thermochemical sulfate reduction in diagenetic settings–old and new insights: Sedimentary Geology, v. 140, p. 143–175.

Manning, D.A.C., and Giże, A., 1993, The role of organic matter in ore transport processes, *in* Engel, M.H., and Macko, S.A., eds., Organic geochemistry, Topics in Geobiology: New York, Plenum Press, v. 11, p. 547–563.

Nielsen, A.T., Schovsbo, N.H., 2011, The Lower Cambrian of Scandinavia: Depositional environment, sequence stratigraphy and paleogeography: Earth-Science Reviews, v.107, p.207-310.

Parnell, J. 1988. Metal enrichments in solid bitumens: a review: Mineralium Deposita, v. 23, 191–199.

Pašava, J., 1996, A group of papers devoted to the metallogeny of black shales – Preface: Economic Geology, v. 91, p. 1-3.

Rickard, D.T., 1983, Precipitation and mixing mechanisms in Laisvall-type sandstone Pb-Zn deposits, *in* Kirsvarsanyi, G., Hagni, R., Pratt, W., and Koening, J.W., eds., Proceedings of the International Conference on Mississippi Valley Type Lead-Zinc Deposits: Rolla, Missouri, 1983.

Rickard, D.T., Willdén, M., Mårde, Y., and Ryhage, R., 1975, Hydrocarbons associated with Pb–Zn ores at Laisvall, Sweden: Nature, v. 255, p. 131–133

Rickard, D.T., Willdén, M.Y., Marinder, N.E., and Donnelly, T.H., 1979, Studies on the genesis of the Laisvall sandstone lead–zinc deposit, Sweden: Economic Geology, v. 74, p. 1255–1285.

Rickard, D.T., Coleman, M., and Swainbank, I., 1981, Lead and sulfur isotopic compositions of galena from the Laisvall sandstone lead-zinc deposit, Sweden: Economic Geology, v. 76, p. 2042-2046.

Roberts, D., and Gee, D.G., 1985, An introduction to the structure of the Scandinavian Caledonides, *in* Gee, D.G., Sturt, B.A., eds., The Caledonide Orogen–Scandinavia and related areas: Chichester, Wiley, p. 55–68.

Romer, R., 1992, Sandstone-hosted Pb-Zn mineral deposits and their relation to the tectonic mobilization of the Baltic Shield during the Caledonian orogeny, a reinterpretation: Mineralogy and Petrology, v. 47, p.67–85.

Saintilan, N.J., Stephens, M.B., Spangenberg, J.E., Fontboté, L., and Lundstam, E., 2014a, Proterozoic basement structures and thermogenic sulfate reduction-derived H_2S as key controls on economic Laisvall-type Pb-Zn deposits, eastern erosional front of the Scandinavian Caledonides, Sweden: Building Exploration Capability for the 21st Century, Society of Economic Geologist 2014 Conference – 27-30 September 2014, Keystone, Colorado, USA, Abstracts.

Saintilan, N.J., Spangenberg, J.E., Fontboté, L., and Stephens, M. B., 2014b, Migration of extrinsic organic compounds and sources of H_2S in the Pb-Zn sandstone-hosted Laisvall deposit, Caledonian front, Sweden: Swiss Geoscience Meeting 2014, Fribourg, Switzerland, Abstracts.

Saintilan, N.J., Stephens, M.B., Lundstam, E. & Fontboté, L., 2015, Control of reactivated basement structures on sandstone–hosted Pb–Zn deposits along the Caledonian Front, Sweden: Evidence from airborne magnetic field data, structural analysis and ore grade modeling: Economic Geology, v. 110, p. 91-117.

Saintilan, N.J., Schneider, J., Stephens, M.B., Chiaradia, M., Kouzmanov, K., Wälle, M., and Fontboté, L., *in press*, A Middle Ordovician age for the Laisvall sandstone-hosted Pb-Zn deposit, Sweden: A response to early Caledonian orogenic activity: Economic Geology.

Saintilan, N.J., Spangenberg, J., Samankassou, E., Kouzmanov, K., Chiaradia, M., Stephens, M.B., Fontboté, L., A refined genetic model for the Laisvall and Vassbo Mississippi Valley-type sandstone-hosted deposits, Sweden: constraints from paragenetic studies, organic geochemistry, and S, C, N and Sr isotope data: *submitted to Mineralium Deposita* (***Chapter 4***).

Spangenberg, J.E., and Macko, S.A., 1998, Organic geochemistry of the San Vicente Zn-Pb district, eastern Pucará Basin, Peru: Chemical Geology, v. 146, p. 1–23.

Spangenberg, J.E., Bagnoud–Velásquez, M., Boggiani, P.C., Gaucher, C., 2014, Redox variations and bioproductivity in the Ediacaran: Evidence from inorganic and organic geochemistry of the Corumbá Group, Brazil: Gondwana Research, v. 26, p.1186-1207.

Tissot, B.P., and Welte, D.H., 1984, Petroleum formation and occurrence: Berlin, Springer Verlag, 2nd Ed.

Thickpenny, A., 1984, The sedimentology of the Swedish alum shales, *in* Stow, D.A.V., and Piper, D.J.W., eds., Fine-grained sediments: London, Geological Society Special Publications 15, p. 511–525.

Willdén, M.Y., 1980, Paleoenvironment of the autochthonous sedimentary rocks sequence at Laisvall, Swedish Caledonides [PhD thesis]: Stockholm, University of Stockholm, 100 p.

CHAPTER 4

A refined genetic model for the Laisvall and Vassbo Mississippi Valley-type sandstone-hosted deposits, Sweden: constraints from paragenetic studies, organic geochemistry, and S, C, N and Sr isotope data

This manuscript was to Mineralium Deposita. It is co-authored by Nicolas J. Saintilan, Jorge E. Spangenberg, Elias Samankassou, Kalin Kouzmanov, Massimo Chiaradia, Michael B. Stephens and Lluís Fontboté.

A refined genetic model for the Laisvall and Vassbo Mississippi Valley-type sandstone-hosted deposits, Sweden: constraints from paragenetic studies, organic geochemistry, and S, C, N and Sr isotope data

Nicolas J. Saintilan[1], Jorge E. Spangenberg[2], Elias Samankassou[1], Kalin Kouzmanov[1], Massimo Chiaradia[1], Michael B. Stephens[3,4], Lluís Fontboté[1]

[1]*University of Geneva, Department of Earth and Environmental Sciences, Rue des Maraîchers 13, 1205 Geneva, Switzerland*

[2]*Institute of Earth Surface Dynamics, University of Lausanne, Building Geopolis, 1015 Lausanne, Switzerland*

[3]*Geological Survey of Sweden (SGU), Box 670 SE-751 28 Uppsala, Sweden*

[4]*Department of Civil, Environmental and Natural Resources Engineering, Division of Geosciences, Luleå University of Technology, SE-971 87 Luleå, Sweden*

Corresponding author:

Nicolas J. Saintilan

nicolas.saintilan@unige.ch

+41 22 379 66 97

+41 22 379 32 10

Abstract

We refine the previously proposed two-fluid mixing model for the Laisvall (recently published Rb-Sr mineralization age of 467 ± 5 Ma) and Vassbo Mississippi Valley-type deposits hosted in Ediacaran to Cambrian sandstone, Sweden. The study of pre-mineralization cements revealed authigenic monazite, fluorapatite and anatase in the Upper Sandstone at Laisvall, reflecting anoxic conditions during diagenesis in sandstone influenced by the euxinic character of the overlying carbonaceous middle Cambrian to Lower Ordovician Alum Shale Formation ($\delta^{13}C_{org}$ = –33.0 to –29.5‰, $\delta^{15}N_{org}$ = 1.5 to 3.3‰, 0.33 to 3.03 wt.% C, 0.02 to 0.08 wt.% N). The available porosity for epigenetic mineralization, including that produced by subsequent partial dissolution of pre-Pb-Zn sulfide calcite and barite cements, was much higher in calcite- and barite-cemented sandstone paleoaquifers (29 %, QEMSCAN mapping) than in those mainly cemented by quartz (8 %). A major change in the Laisvall plumbing system is recognized by the transition from barite cementation to Pb-Zn sulfide precipitation in sandstone. Ba-bearing, reduced, and neutral fluids had a long pre-mineralization residence time (highly radiogenic $^{87}S/^{86}Sr$ ratios of 0.718 to 0.723) in structures in basement. As a result of an early Caledonian arc-continent collision and development of a foreland basin, fluids migrated cratonward. Reactivated basement structures at Laisvall were first used by these Ba-bearing fluids, which were expelled from their host structures into overlying sandstone where they deposited barite upon mixing with a sulfate pool ($\delta^{34}S$ values = 14 to 33‰). Subsequently, slightly acidic metal-bearing brines originally contained in pre-Ediacaran rift sediments in the foredeep of the early Caledonian foreland basin migrated through the same plumbing system. The bulk of Pb-Zn mineralization proceeded from the mixing of these brines with a pool of H_2S (average $\delta^{34}S$ values = 24 to 29‰) produced via thermochemical sulfate reduction (TSR) and oxidation of hydrocarbons in sandstone. Other minor H_2S sources are identified. Upward migration and fluctuation of the hydrocarbon-water interface with formation of H_2S along it explain the shape of the orebodies splaying out like smoke from a chimney, and conspicuous alternating layers of galena and sphalerite. Intimate intergrowth of bitumen with sphalerite suggests that subordinate amounts of H_2S might have been produced by TSR during Pb-Zn mineralization. Representative gas chromatograms of the saturated hydrocarbon fraction from organic-rich shale and from both mineralized and barren sandstone samples indicate that hydrocarbons migrated from source rocks in the Alum Shale Formation buried in the foredeep into sandstone, where they accumulated in favorable traps in the forebulge setting.

Keywords Pb-Zn mineralization, Laisvall, sandstone, Cambrian, bitumen, hydrocarbon, Alum shale, S, C, N stable isotopes, Caledonian

Introduction

Sandstone-hosted Pb-Zn deposits are considered a sub-type of Mississippi Valley-type (MVT) deposits dominated by carbonate host rocks in Phanerozoic sedimentary sequences (Leach et al. 2005). Although fewer examples than their carbonate-hosted counterparts are known, sandstone-hosted deposits have been significant mineral resources in several countries (e.g., Jinding deposit, China, 200 Mt at 6.1 % Zn and 1.3 % Pb; Xue et al., 2007; Laisvall deposit, Sweden, 64 Mt at 4 % Pb, 0.6 % Zn, 9 g/t Ag; Årebäck and Jonsson pers. comm. 2010). The current study focuses on the Laisvall and Vassbo deposits (Sweden) hosted by Ediacaran to Cambrian sandstone presently located along the erosional front of the Caledonian orogen in Sweden and Norway (Fig. 1a). The world-class Laisvall deposit and the much smaller Vassbo deposit (Fig. 1a, 3.2 Mt, 5.7 % Pb, 0.3 % Zn, 18 g/t Ag; Jonsson pers. comm. 2010) were mined for 60 years (1941–2001) and 22 years (1960–1982), respectively.

Extensive research on carbonate-hosted MVT deposits recognized that deposits within a single district usually have a distinctive combination of ore assemblages, ore controls, host rocks, alteration, and isotope and geochemical features (e.g., Gerdemann and Meyers 1972; Lyle 1977; Gregg 1985; Voss and Hagni 1985; Rowan 1986; Spangenberg et al. 1995, 1996; Jones et al. 1996; Leach et al. 2001; Bradley and Leach 2003; Leach et al. 2005; Anderson 2008; Leach et al. 2010; Heijlen et al. 2003).

The aim of the current study is to refine and present new aspects of the genetic model for the Laisvall and Vassbo deposits, with the ambition, inspired by the work carried out on carbonate-hosted MVT deposits over 40 years, to document the distinctive features of Laisvall-type deposits. We present a stepwise genetic model for the Laisvall deposit in the geodynamic evolution of the western (present-day coordinates) Baltica margin in upper Cambrian to Middle Ordovician time.

The model has been constructed by combining the results of the current work with: (i) previous studies dealing with fluid inclusion microthermometry in sphalerite and barite at Laisvall (Lindblom 1986), noble gas and halogen evidence from barite and sulfides at Laisvall and Vassbo (Kendrick et al. 2005), and earlier results of sulfur and radiogenic lead isotope studies of sulfides (Rickard et al. 1979, 1981; Rickard 1983; Romer 1992); (ii) the recent findings on the control of reactivated Proterozoic basement structures on the location and genesis of the Laisvall and Vassbo deposits, in particular as feeders for metal-bearing brines (Saintilan et al. 2015); and (iii) sphalerite Rb-Sr geochronology and geochemistry pointing to ore formation at Laisvall in the Middle Ordovician (467 ± 5 Ma) in a forebulge setting as a response to early Caledonian arc-continent collision and development of a foreland basin (Saintilan et al. *in press*).

A multi-disciplinary approach has been applied in the current work and includes mineralogical and paragenetic investigations, sulfur isotope ratios ($\delta^{34}S$) of sulfides and barite, radiogenic Sr isotope composition of pre-Pb-Zn sulfide stage barite, stable isotope composition of kerogen of potential hydrocarbon shale source rock ($\delta^{13}C_{org}$ and $\delta^{15}N_{org}$), and chemical characterization of hydrocarbons by gas chromatography–mass spectrometry in the ore, sandstone host-rocks and shale source rocks. This

study focused on the diagenetic history and ore mineral precipitation processes in sandstone by distinguishing between pre-mineralization cements and sulfide-stage mineral phases. These petrographic data were complemented by petrographically-constrained isotopic composition of these cements, and a re-evaluation of published noble gas and halogen data to unravel the transient nature and origin of hydrothermal fluids between the pre-sulfide and sulfide stages. The source and nature of hydrocarbons, which were suggested to be involved in the mineralizing process by participating to the supply of H_2S by thermochemical sulfate reduction (Rickard et al. 1975, 1979; Rickard 1983), was constrained.

Geologic setting

Caledonian orogen, autochthonous sedimentary cover rocks and Baltica basement

In the central and northern parts of Sweden, the crystalline basement is composed of Paleoproterozoic and Archean rocks belonging to a 2.0 to 1.8 Ga orogenic system (Svecokarelian orogen), and subordinate late Paleoproterozoic to early Neoproterozoic (1.7–0.9 Ga) sedimentary, volcanic and intrusive rocks (Bergman et al. 2012; Fig. 1a). A thin cover of Ediacaran to Cambrian, locally through to Lower Ordovician, sedimentary siliciclastic rocks were deposited unconformably on the crystalline basement of the western (present-day coordinates) stable platformal margin to the continent Baltica (Bergman et al. 2012; Fig. 1a). The sedimentary cover rocks are overlain in turn by thrust sheets belonging to the c. 500 to 400 Ma Caledonian orogen (Gee 1975; Roberts and Gee 1985; Bergman et al. 2012; Fig. 1a).

The Caledonian orogen resulted from a polyphase orogenic evolution (Gee 1972; Sturt 1978; Dallmeyer and Gee 1986). A foreland basin developed as a response to the collision of Baltica with an outboard island arc followed by exhumation of high-pressure rocks, including eclogites, during an early stage of the orogeny in the upper Cambrian and Lower to Middle Ordovician (Dallmeyer and Gee 1986; Santallier 1988; Stephens 1988; Kullerud et al. 1990; Gromet et al. 1996; Root and Corfu 2012). This early arc-continent collision and development of a foreland basin preceded the closure of the Iapetus Ocean and the terminal continent-continent (Laurentia-Baltica) collision, which initiated during the latest part of the Ordovician (c. 450 Ma), and continued through the Silurian and into Devonian time with emplacement of the Caledonian thrust nappes (Gee 1975; Stephens 1988; Gee et al. 2010; Root and Corfu 2012; Fig. 1b).

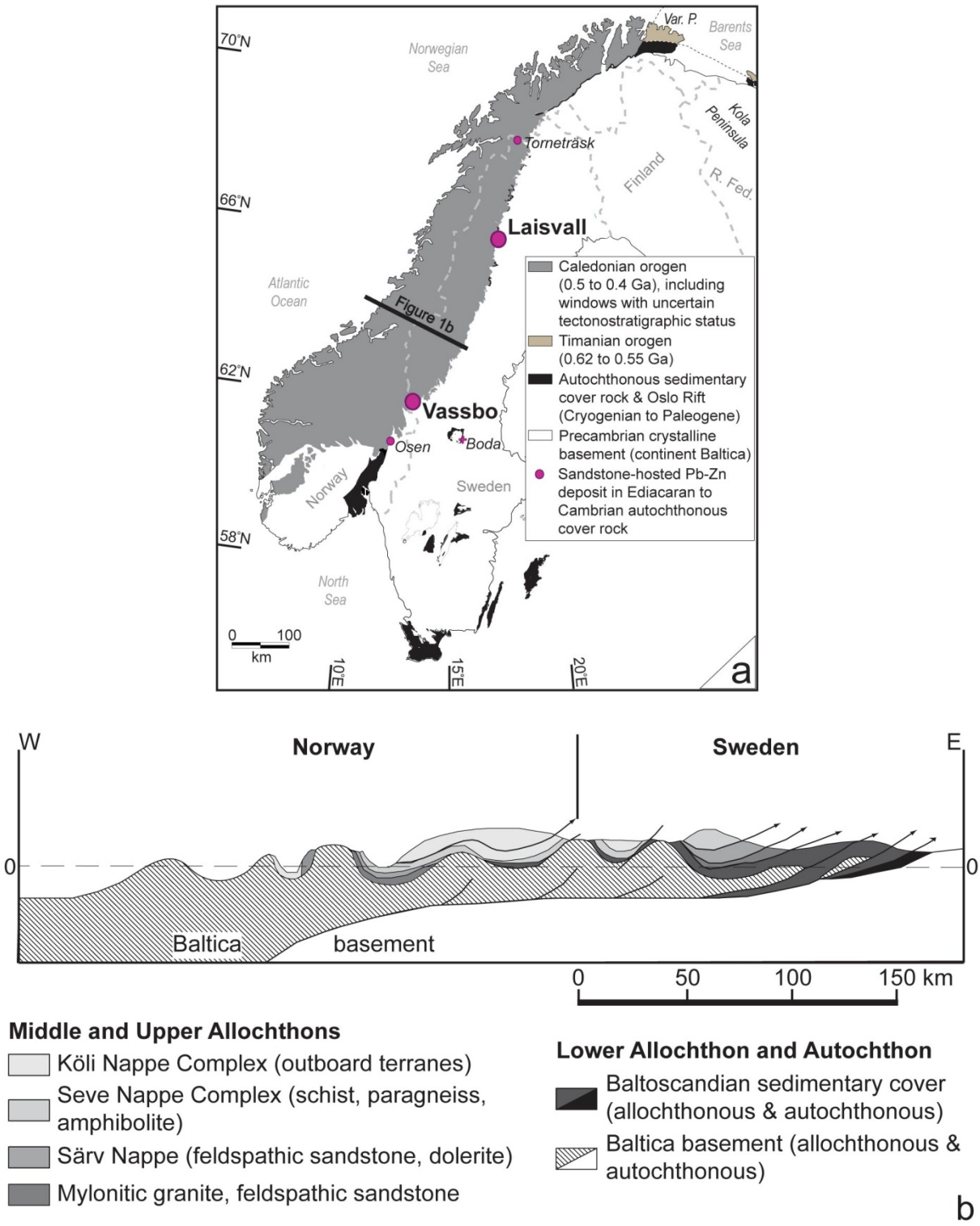

Fig. 1 a. Simplified geological map of Scandinavia (modified after Roberts and Siedlecka, 2002; Gee et al., 2008; Bergman et al., 2012; Saintilan et al., *in press*). The locations of sandstone-hosted Pb-Zn deposits in autochthonous Ediacaran to Cambrian siliciclastic cover rocks to the crystalline basement are shown (Abbrevations: R. Fed.: Russian Federation; Var. P.: Varanger Peninsula). The Boda Pb deposit is hosted by Lower Ordovician limestone ~125 km SE of the erosional front of the Caledonian orogen. b. Cross-section through the central part of the Caledonian orogen in Sweden and Norway (modified after Gee et al., 2010).

Sandstone-hosted Pb-Zn deposits in autochthonous sedimentary cover rocks

At Laisvall (Fig. 2a), the sequence of autochthonous siliciclastic rocks overlying the Paleoproterozoic (1.8 Ga) granite basement (Skiöld 1988; Bergman et al. 2012) is c. 100 m thick and is preserved underneath the main décollement to the Caledonian thrust sheets within the Alum Shale Formation. The autochthonous stratigraphy comprises the 35 to 40 m-thick Ediacaran to lower Cambrian Laisberg Formation (Willdén 1980; Nielsen and Schovsbo 2011) passing upward into the lower Cambrian Grammajukku Formation and the lowermost part of the middle Cambrian to Lower Ordovician Alum Shale Formation (Ljungner 1950; Rickard et al. 1979; Willdén 1980; Thickpenny 1984).

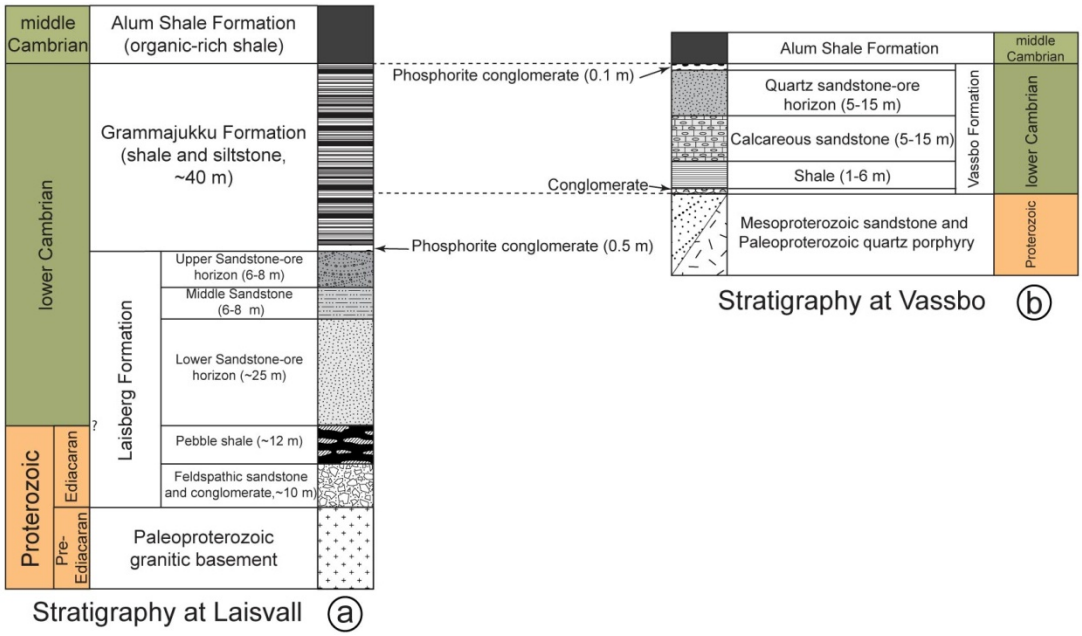

Fig. 2 a. Stratigraphic columns of the autochthonous sedimentary cover sequence at Laisvall (modified after Rickard et al., 1979; Willdén, 1980; Nielsen & Schovsbo, 2011). b. Stratigraphic column of the autochthonous sedimentary cover sequence at Vassbo (modified after Christofferson et al., 1979; Nielsen & Schovsbo, 2011). Nielsen and Schovsbo (2011) proposed that the Cambrian stratigraphy at Vassbo is coeval with deposition of the Grammajukku Formation in the Laisvall area.

The Laisberg Formation (Fig. 2a) represents a transgressive, sandstone-dominated sequence (Willdén 1980; Nielsen and Schovsbo 2011). The formation terminates in a thin phosphorite pebble conglomerate in erosive contact with underlying sandstone. Epigenetic, disseminated, mottled galena ± sphalerite mineralization is hosted in two sandstone paleoaquifers, the Lower and Upper Sandstones (Rickard et al. 1979; Willdén 1980; Saintilan et al. 2015). Ore minerals mainly cement detrital quartz, subordinate K-feldspar (absent in the Upper Sandstone), and minor clay, monazite, zircon, apatite and biotite (Rickard et al. 1979; Christofferson et al. 1979; Willdén 1980; Lindblom 1986; this study). In places, mineralization in the Upper Sandstone and Lower Sandstone orebodies occurs as steeply-dipping galena-sphalerite-calcite veinlets (cf. Rickard et al. 1979; Saintilan et al. 2015). Steeply-dipping calcite-fluorite ± pyrite veinlets were found in the granite basement in close proximity to the southern segments of the Nadok and Kaustky faults (Saintilan et al. 2015).

The Laisberg Formation is capped by the local Grammajukku Formation and the regionally-extensive Alum Shale Formation (Fig. 2a; Willdén 1980; Thickpenny 1984; Nielsen and Schovsbo 2011). The Grammajukku Formation comprises shale and siltstone with subordinate sandstone intercalations (Willdén 1980) whereas the Alum Shale Formation mainly consists of black and grey laminated, organic-rich shale (1 to 22 wt.% total organic carbon TOC; Thickpenny 1984). Deposition of ≥ 200 m Lower Ordovician limestone (Gee et al. 2013) caused a final stage of sediment compaction of the Alum Shale Formation, changing its pore water regime (Israelson et al. 1996). These limestones were not preserved at Laisvall.

At Vassbo (Fig. 2b), the peneplained crystalline basement is composed of Mesoproterozoic sandstone in the east and, in the west, felsic volcanic or subvolcanic rock (quartz porphyry) dated at 1.7 Ga (Christofferson et al. 1979; Wallin 1982; Nielsen and Schovsbo 2011). Steeply-dipping dolerite dykes and flat-lying sills, dated at 1.27–1.26 Ga and 0.98–0.95 Ga (Central Scandinavian Dolerite Group and Blekinge-Dalarna dolerites, respectively; Söderlund et al. 2005) occur in the basement. The lower Cambrian Vassbo Formation, which is equivalent in age with the upper part of the Grammajukku Formation at Laisvall (Nielsen and Schovsbo 2011), unconformably overlies the Proterozoic basement and is capped by the partly allochthonous Alum Shale Formation (Christofferson et al. 1979; Wallin 1982). As at Laisvall, Lower Ordovician limestones were not preserved at Vassbo. Galena and sphalerite mineralization is hosted in a quartz ± K-feldspar sandstone horizon in the upper part of the Vassbo Formation (referred to as "sandstone at Vassbo" or "sandstone orebody at Vassbo" hereafter). Minor galena mineralization is also present in the first few centimeters of the underlying calcareous sandstone. The highest Pb and Zn grades occur at the top of sandstone paleoaquifers at Laisvall and Vassbo (Saintilan et al. 2015).

Material and methods

Drill cores stored at the Geological Survey of Sweden (SGU) in Malå or at the Boliden Mineral core archive in Boliden (Sweden) were sampled as follows: (i) 57 samples from the Upper Sandstone and Lower Sandstone orebodies at Laisvall (including 4 samples with steeply-dipping galena-sphalerite-calcite veinlets); (ii) eight samples from the sandstone orebody at Vassbo, (iii) one sample of shale with pyrite at the base of the Grammajukku Formation at the contact with underlying Upper Sandstone at Laisvall, and (iv) one sample of pyrite-rich grey shale in the Alum Shale Formation at Vassbo. At Laisvall, the samples were selected in profiles at proximal and distal positions relative to the Nadok fault and Central Malm fault systems, which have been interpreted as feeder systems for mineralization (Saintilan et al. 2015). After petrographic investigations, aliquots of these samples were utilized for determination of the sulfur isotope composition of sulfides and barite, and strontium isotope composition of barite. An additional separate of phosphorite pellets in the phosphorite conglomerate at Laisvall (Fig. 2a) was obtained from drill core samples using a microdrill and processed for strontium isotope analyses.

In addition, thirteen drill core samples and one outcrop sample were taken from the stratigraphy at Laisvall for organic geochemical analyses: (i) Eleven shale samples from the Grammajukku and Alum Shale Formations; (ii) two mineralized sandstone samples from the Upper and Lower Sandstones; and (iii) one barren Lower Sandstone sample from outcrops located ~ 5 km to the southeast of the mined area. The shale samples are representative of the stratigraphy upward from the base of the Grammajukku Formation to the uppermost autochthonous part of the Alum Shale Formation at Laisvall. The uppermost sample of black organic-rich shale (ASF 11) was sampled at the top of a few centimeter-thick limestone horizon within the Alum Shale Formation (cf. Thickpenny 1984). Shale sample ASF4 was split in three subsamples (ASF4-0, ASF4-1 and ASF4-2). These samples correspond to the first meter of organic-rich shale in the autochthonous part of the Alum Shale Formation at Laisvall above the contact with the Grammajukku Formation. Hydrocarbons were extracted from ASF4-1 and ASF4-2, and from the three sandstone samples.

Thin sections of all samples were studied using transmitted and reflected light microscopy and a Cl8200 MK5-optical cathodoluminescence microscope with a cold cathode that was mounted on a petrographical microscope. The beam conditions were set at 15 kV and 50 to 60 mA with an unfocused beam of approximately 1 cm in an observation chamber with a residual pressure of 80 mTorr. Samples were not coated. Twenty representative thin sections were mounted on an aluminum stub with double-sided conductive carbon tape. A c. 25 nm thin coating of carbon was deposited on the samples by low vacuum sputter prior to imaging with a Jeol JSM 7001F Scanning Electron Microscope (SEM, Section of Earth and Environmental Sciences, University of Geneva, Switzerland). Investigation of solid black inclusions in barite, calcite and fluorite, and dark fluid inclusions in sphalerite in three samples from Laisvall was carried out by Raman spectrometry at the University of Geneva using a LABRAM confocal Raman microspectrometer with a 532.8-nm He-Ne laser coupled to a B40 Olympus microscope with a 50× objective. Barite and sphalerite fragments from these samples were then mounted on an aluminum stub and coated with gold (c. 10 nm) before investigation using SEM on back-scattered electron mode (BSE) and energy-dispersive X-ray analysis (EDX).

Three representative thin sections were selected for QEMSCAN® imagery and analysis: (i) a sample from the Upper Sandstone orebody in which phosphorous- and/or REE-bearing minerals were investigated in particular; and (ii) two samples from the Lower Sandstone orebody at Laisvall and the sandstone orebody at Vassbo in which the distribution of the cementing phases (quartz, calcite, barite, Pb-Zn sulfides) and their relationships were studied. Automated bulk-rock mineral analysis and textural imaging of the studied samples were performed using an FEI QEMSCAN® Quanta 650F facility at the Section of Earth and Environmental Sciences, University of Geneva, Switzerland. The system is equipped with two Bruker QUANTAX light-element energy dispersive X-ray spectrometers. Analyses were conducted at high vacuum, accelerating voltage of 25 kV, and probe current of 10 nA on carbon-coated samples. FieldImage operating mode (Pirrie et al. 2004) was used for analyses. X-ray spectra acquisition time was 10 ms per pixel, using a point-spacing of 5 µm. Up to 285 individual

fields were measured in each sample, with 1500 pixels per field. Data processing was performed using the iDiscover software package. The final products consist of high-quality spatially resolved and fully quantified mineralogical maps enabling basic image analysis, including particle size and shape distribution, mineral assemblages and mineral proportion definitions.

For sulfur isotope studies, all samples were crushed using a hydraulic press and sieved. Following heavy liquid separation of the 315 to 125 µm size fractions, the heavy mineral fractions were handpicked under a binocular microscope to obtain sulfide (galena, sphalerite and pyrite) and barite aliquots. All aliquots (n = 163 and 25 duplicates) were subsequently powdered using an agate mortar and pestle, and analyzed for the stable sulfur isotope composition by elemental analysis and isotope ratio mass spectrometry (EA-IRMS) at the University of Lausanne, Switzerland. The EA-IRMS analyses were done using a Carlo Erba 1108 elemental analyzer connected to a Thermo Fisher Delta V stable isotope ratio mass spectrometer that was operated in the continuous He flow mode. The stable isotope composition of sulfur is reported in the delta (δ) notation as the per mil (‰) deviation of the isotope ratio ($^{34}S/^{32}S$) relative to the VCDT standard. The precision of the EA-IRMS analyses, evaluated by replicate measurements of laboratory standards (barite, sphalerite, and pyrite) and international reference materials (sphalerite, silver sulfide) is better than ± 0.2‰ (1σ).

Barite and phosporite pellet aliquots were attacked with HCl 6M in screw-sealed Teflon vials on a hot plate at 140°C for several hours. The solutions were centrifuged and the supernatant was recovered and transferred to Teflon vials, where it was dried down on a hot plate. The residue was re-dissolved in a few drops of 14 M HNO_3 and dried down again, before Sr separation from the matrix using a Sr-Spec resin. The Sr separate was re-dissolved in 5 ml of ~2% HNO_3 solutions and ratios were measured using a Thermo Neptune PLUS Multi-Collector ICP-MS in static mode. The $^{88}Sr/^{86}Sr$ (8.375209) ratio was used to monitor internal fractionation during the run. Interferences at masses 84 (^{84}Kr), 86 (^{86}Kr) and 87 (^{87}Rb) were also corrected in-run by monitoring ^{83}Kr and ^{85}Rb. The SRM987 standard was used to check external reproducibility, which on the long-term (more than 100 measurements during one year) was ± 10 ppm. The internally corrected $^{87}Sr/^{86}Sr$ values were further corrected for external fractionation. A $^{87}Sr/^{86}Sr$ ratio of $0.721269 \pm 1.4x10^{-5}$ is reported as 0.721269 ± 14.

The samples for organic geochemical analyses were prepared and analyzed in the Stable Isotope and Organic Geochemistry Laboratories at the University of Lausanne (Switzerland) using procedures described previously (Spangenberg and Herlec 2006; Spangenberg et al. 2014). To remove the weathered material and any contamination from packing and handling, the rocks were cut in slabs with a water-cooled saw. The slabs were cleaned with deionized water (>18MΩ resistance), analytical grade acetone and ethanol, and dried at 50°C for 24 hours. The cleaned slabs were crushed in a thoroughly cleaned hydraulic press and powdered to <125 µm by short grinding periods in an agate ring grinder mill. The powders were stored in pre-annealed (at 450°C for four hours) aluminum disposable canisters and aluminum foil sheets prior to organic geochemical analyses. Total bitumen (extractable organic matter, EOM) was obtained from an aliquot (100 to 200 g) of the powdered

samples by refluxing with dichloromethane (DCM) for six days, with a change of solvent after the first two days. The DCM fractions were combined, gently evaporated to 1 mL, and passed through an activated copper column to remove elemental sulfur. The solvent was passively evaporated to near dryness, and extracts with 0.5 mL DCM stored in 2 mL vials at +4 °C until required for analyses. The extracts were separated into two fractions (aliphatic and aromatic hydrocarbons) using silica/alumina gel liquid chromatography.

Chemical characterization of the aliphatic hydrocarbons was performed by gas chromatography–mass spectrometry (GC–MS), using an Agilent Technologies gas chromatograph HP 6890 coupled to a HP 5973 quadrupole mass selective detector (MSD) with HP-5MS fused-silica capillary column (60 m length, 0.25 mm internal diameter, coated with 0.10 μm 5%-diphenyl–95% dimethyl-polysiloxane as stationary phase) and helium as carrier gas. An aliquot normalized to the extracted aliquot size was introduced in a splitless injector at 280 °C. After an initial period of 7 min at 70 °C, the column was heated to 280 °C at 5 °C/min followed by an isothermal period of 20 min. The MSD was operated in the electron impact mode at 70 eV, source temperature of 250 °C, emission current of 1 mA and multiple-ion detection with a mass range from 50 to 700 a.m.u. Compound identifications were made by comparison with synthetic standards, GC retention times, interpretation of mass spectrometric fragmentation patterns and literature mass spectra. The absence of measurable recovered bitumen in two procedure blanks indicates that no detectable laboratory contaminations were introduced into the samples.

Carbon and nitrogen stable isotope analyses of the total organic carbon were performed on the eleven shale samples. The powdered samples were acidified (1M HCl) for removal of inorganic carbon, rinsed thoroughly with deionized water, filtered, dried overnight, and stored in pre-annealed beakers. The organic fraction of the solid residues was mostly kerogen, and an aliquot submitted to carbon and nitrogen isotope analyses by EA-IRMS. The C and N isotope compositions are reported in the delta (δ) notation as the per mil (‰) deviation of the ($^{13}C/^{12}C$) and ($^{15}N/^{14}N$) isotope ratios relative to the VPDB and N_2 in AIR standards, respectively. The reproducibility of the EA-IRMS measurements for C and N is better than ± 0.1‰ and ± 0.3‰ (1σ), respectively. The TOC (wt.% C) and TON (wt.% N) of each sample was determined by integration of the corresponding EA-IRMS measurement of the carbon and nitrogen isotope composition.

Fig. 3 (next page) Mineral assemblages and paragenetic sequences of the Upper Sandstone and Lower Sandstone orebodies (USOB and LSOB) at Laisvall and the sandstone orebody at Vassbo. Relative timing is from left to right. Monazite at Vassbo is scarce and has not been shown. It is suggested that it occupies a similar paragenetic position in the quartz sandstone at Vassbo as in the Upper Sandstone orebody at Laisvall.

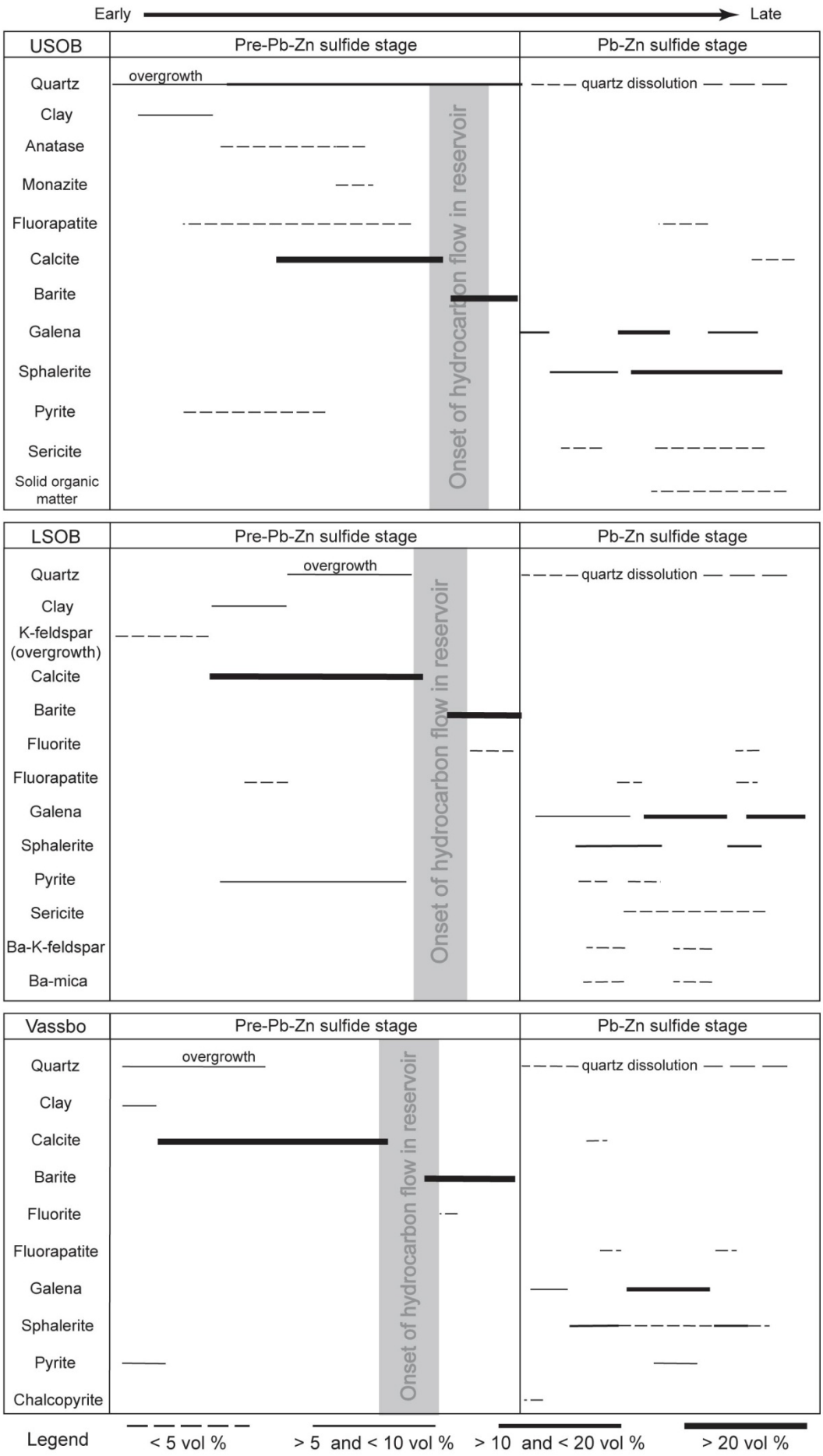
Early
Late
USOB
Pre-Pb-Zn sulfide stage
Pb-Zn sulfide stage
Quartz
overgrowth
quartz dissolution
Clay
Anatase
Monazite
Fluorapatite
Calcite
Barite
Galena
Sphalerite
Pyrite
Sericite
Solid organic matter
Onset of hydrocarbon flow in reservoir
LSOB
Pre-Pb-Zn sulfide stage
Pb-Zn sulfide stage
Quartz
overgrowth
quartz dissolution
Clay
K-feldspar (overgrowth)
Calcite
Barite
Fluorite
Fluorapatite
Galena
Sphalerite
Pyrite
Sericite
Ba-K-feldspar
Ba-mica
Onset of hydrocarbon flow in reservoir
Vassbo
Pre-Pb-Zn sulfide stage
Pb-Zn sulfide stage
Quartz
overgrowth
quartz dissolution
Clay
Calcite
Barite
Fluorite
Fluorapatite
Galena
Sphalerite
Pyrite
Chalcopyrite
Onset of hydrocarbon flow in reservoir
Legend
< 5 vol %
> 5 and < 10 vol %
> 10 and < 20 vol %
> 20 vol %

Results

Paragenetic sequences in paleoaquifers at the Laisvall and Vassbo deposits

Figure 3, which includes data from previous work (cf. Lindblom, 1986; Lucks, 2004), summarizes the relative timing of the authigenic mineral phases that formed in the Upper Sandstone and Lower Sandstone orebodies at Laisvall and the sandstone orebody at Vassbo. These minerals are anatase, hydrothermal monazite and fluorapatite whereas cements are sulfides (galena, sphalerite, and pyrite), calcite, barite, quartz, K-feldspar and fluorite (Figs. 4, 5, 6, 7). At the two deposits, a "pre-Pb-Zn sulfide stage" and a "Pb-Zn sulfide stage" have been distinguished.

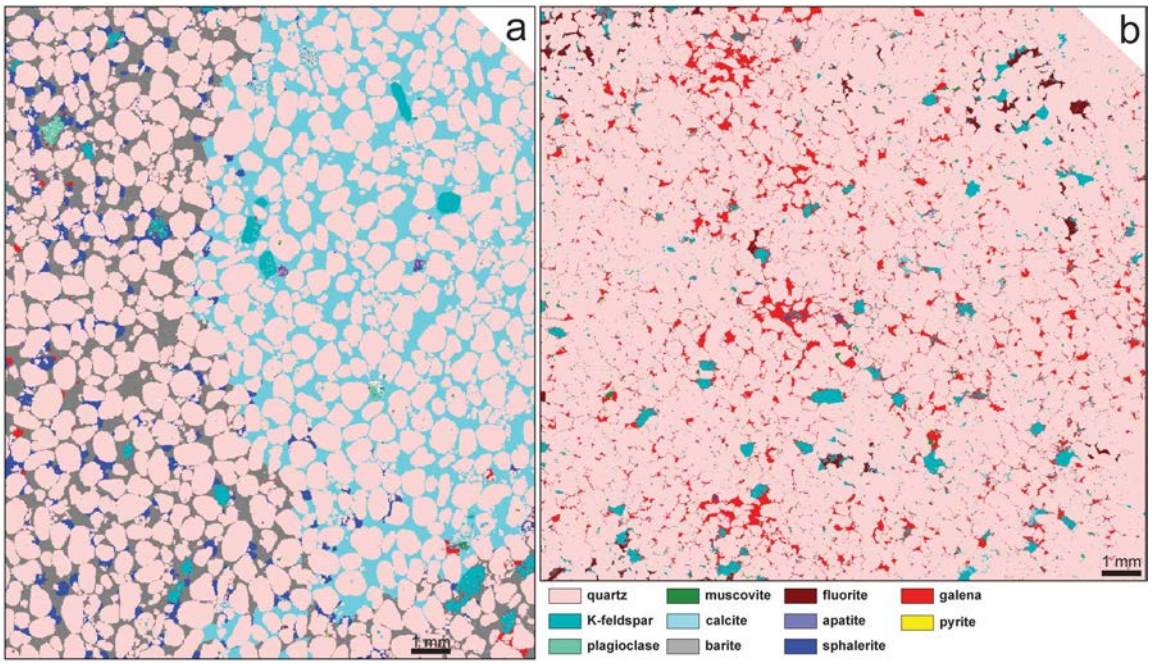

Fig. 4 a. QEMSCAN image of the sandstone orebody at Vassbo. b. QEMSCAN image of a quartz-galena-fluorite ± barite ± calcite cemented part of the Lower Sandstone at Laisvall.

Pre-Zn-Pb sulfide stage

Quartz and calcite cemented the sandstone paleoaquifers (Figs. 3, 4, 5a, 5b and 5c) prior to and locally coeval with barite ± fluorite precipitation (Figs. 5c, 5d and 5e), minerals which locally replaced calcite. QEMSCAN mapping shows that calcite is locally manganiferous. Fluorite is a minor pre-Pb-Zn-sulfide stage cement (<5 vol.%; Figs. 3 and 4b) in the Lower Sandstone orebody at Laisvall and in the sandstone orebody at Vassbo where it is coeval with barite precipitation and locally replaced calcite (e.g., borehole LAI 110 in the Central Malm area, Lower Sandstone orebody; Saintilan et al., 2015); fluorite is scarce in the Upper Sandstone orebody. Pyrite is frequently framboidal and occurs also as aggregates of euhedral diagenetic pyrite.

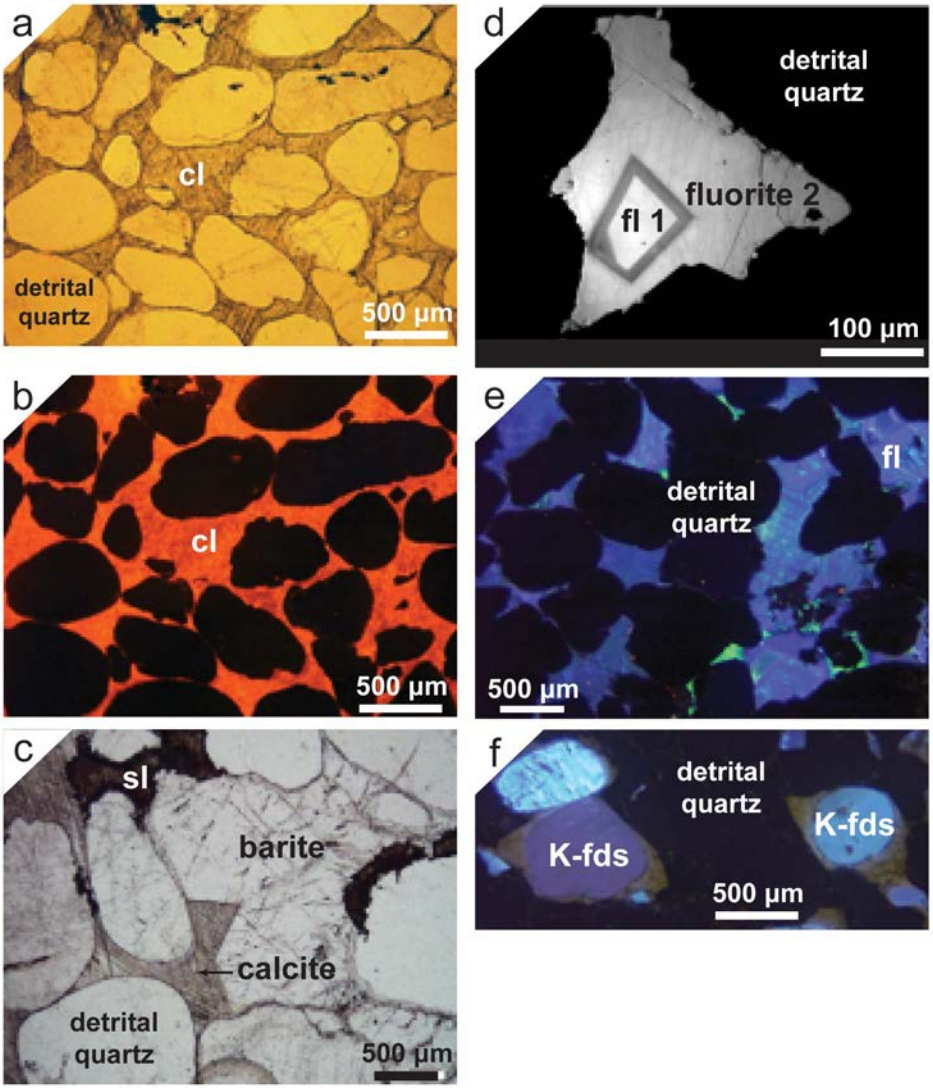

Fig. 5 a. Diagenetic calcite (cl) cement in the sandstone orebody at Vassbo (transmitted-light microscopy). b. Same field observation as in Fig. 5a: optical cathodoluminescence image of the diagenetic calcite cement. The orange-tint and QEMSCAN image analyses suggest some compositional zoning between calcite and Mn-calcite. c. Diagenetic calcite and subsequent barite cements in the sandstone orebody at Vassbo (transmitted-light microscopy). Sphalerite precipitated after reductive dissolution of barite. d. Fluorite cement in the Lower Sandstone at Laisvall (scanning electron microprobe image, cathodoluminescence mode, SEM-CL). There is evidence for two generations of fluorite growth: (1) euhedral fluorite (fl) suggestive of rather stable hydrodynamic conditions, (2) anhedral fluorite with complex crystallinity. e. Optical cathodoluminescence image of a fluorite-cemented zone (blue-green tints) of the Lower Sandstone at Laisvall. f. Details of detrital K-feldspar and their Ba-bearing overgrowths (yellowish tint) in the Lower Sandstone at Laisvall.

In the Upper Sandstone orebody, anatase and hydrothermal monazite form a P-REE-Ti mineral assemblage associated with quartz overgrowths and pyrite. Anatase typically coats detrital quartz, detrital zircon and detrital monazite and is locally included in quartz overgrowths (Fig. 6a). Hydrothermal monazite ranges in size from 220 to 450 µm, and may constitute up to 0.01 vol.% of the sandstone. It is locally embedded in clay matrix, is intergrown with pyrite, and coats quartz overgrowths around detrital quartz (Fig. 6b). Minor galena (<0.1 vol.%) is present in between anatase grains (Fig. 6c) but also in anhedral hydrothermal monazite grains in which U decay may have contributed Pb for galena precipitation (Fig. 6b). Xenotime outgrowths on zircon were observed

locally (Fig. 6a). Fluorapatite, identified by SEM-EDX analyses, is typically in the range of 50 to 450 µm and constitutes about 0.02 vol.% where it coats detrital quartz and is often included in quartz overgrowths (Fig. 6d).

The Lower Sandstone orebody lacks this peculiar P-REE-Ti mineral association. Only scarce fluorapatite was observed. The Lower Sandstone orebody is the only paleoaquifer characterized by extensive Ba-bearing K-feldspar overgrowth/cement around detrital K-feldspar grains (Lucks, 2004; this study). Optical cathodoluminescence images show a systematic yellowish tint of the Ba-bearing overgrowths around the detrital K-feldspar grains, which are characterized by different tints of cathodoluminescence (e.g., light blue, pink) indicative of a heterogeneous provenance (Fig. 5f).

The sandstone orebody at Vassbo shares most of the characteristics of the Lower Sandstone orebody at Laisvall. Exceptions include the occurrence of fluorapatite, which can constitute up to 0.5 vol.% in some samples, and locally hydrothermal monazite, ranging in size from 110 to 140 µm (<0.01 vol.%), similar to that observed in the Upper sandstone orebody at Laisvall.

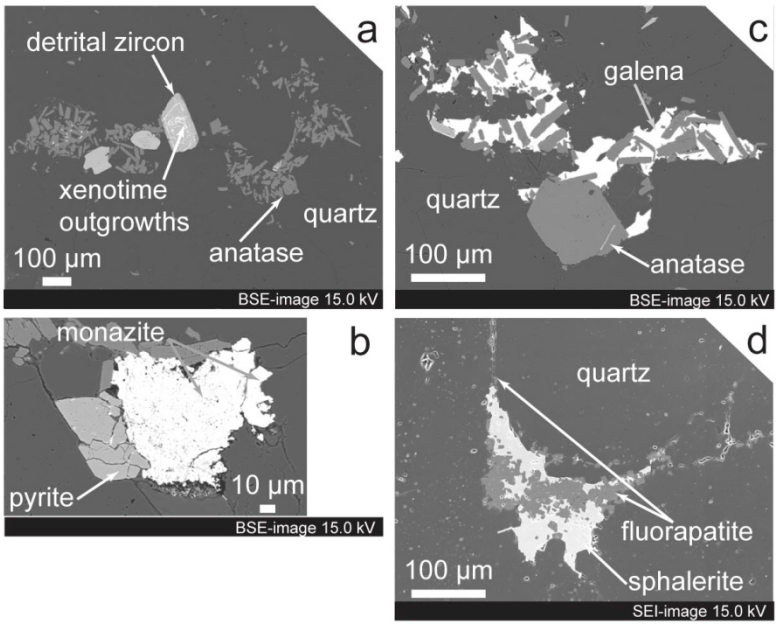

Fig. 6 a.Tightly quartz-cemented Upper Sandstone at Laisvall with authigenic anatase coating detrital quartz, zircon and monazite. Presence of xenotime outgrowths on detrital zircons (back-scattered electron mode BSE, scanning electron microprobe image). b. Authigenic monazite associated with diagenetic pyrite. The largest monazite grain has multiple nano-scale galena inclusions that are probably related to U-decay in monazite. The smallest monazite grain does not show any inclusions (BSE-image). c. Authigenic anatase coating quartz cemented by galena (BSE-image). d. Authigenic fluorapatite coating detrital quartz and included in quartz overgrowths. A second generation of aggregates of euhedral to subhedral fluorapatite, co-genetic with sphalerite, has been identified (secondary electron mode SEI, scanning electron microprobe image).

By using QEMSCAN mapping data (Appendix 1), mineral phases were classified into two groups: (i) detrital phases (e.g., quartz, K-feldspar, zircon, mica), quartz ± K-feldspar cements, framboidal and diagenetic pyrite; and (ii) calcite, barite ± fluorite and Pb-Zn sulfides. For each group, the total sum of pixels occupied by each mineral phase was calculated and divided by the total amount of pixels in the image. In this manner, an estimate for the fraction of porosity occupied by calcite and barite cements was made. These cements protected sandstone from quartz cementation and, by contrast to quartz,

were prone to dissolution and replacement at a later stage by sulfides. QEMSCAN mapping show that this fraction may amount to 29 vol.% (Fig. 4a). By contrast, in sandstone dominated by quartz cement (Fig. 4b), the porosity occupied by Pb-Zn sulfides ± calcite ± barite ± fluorite cements is only about 8 vol.%.

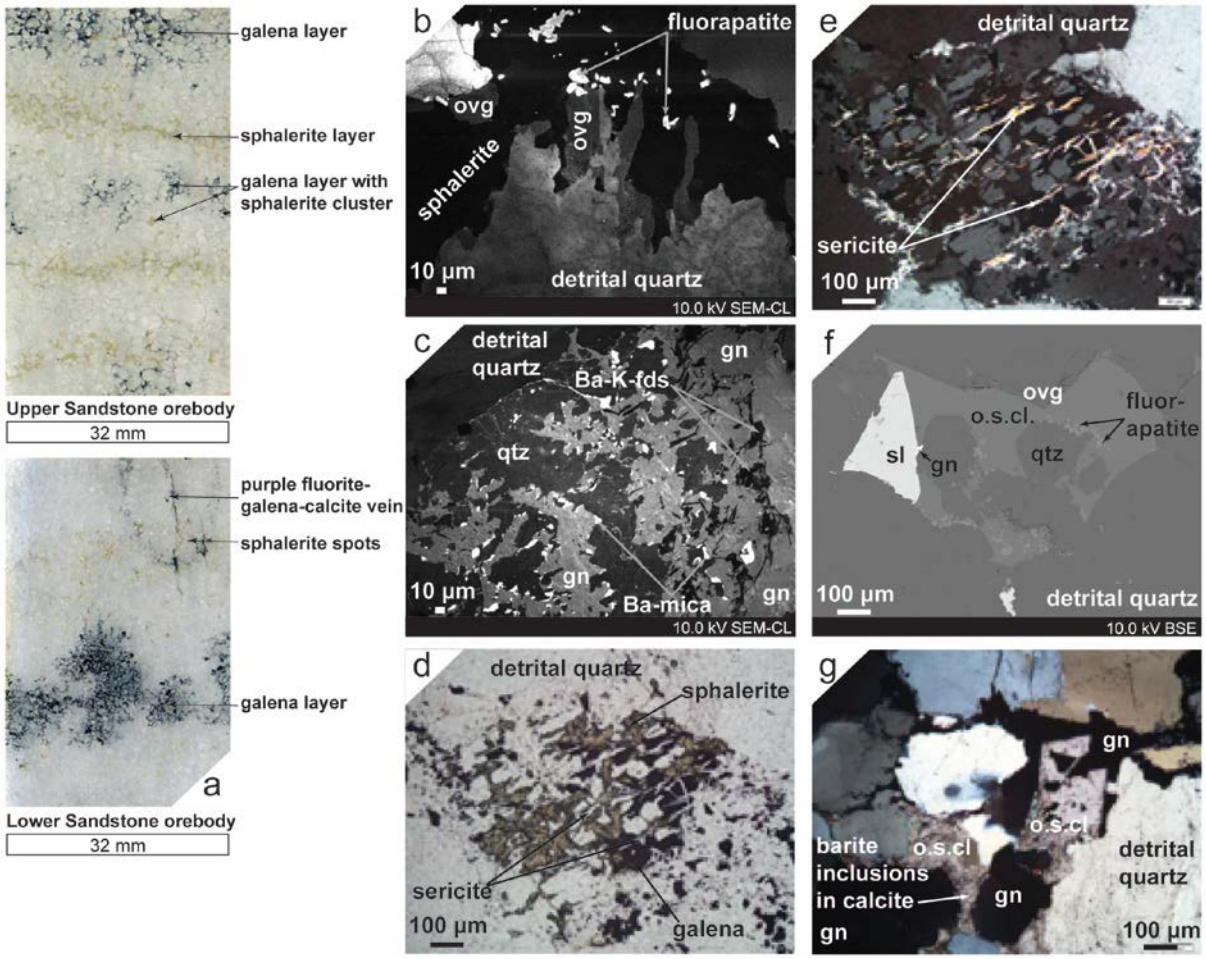

Fig. 7 a. Representative thin sections of Pb-Zn mineralization in the Upper Sandstone and Lower Sandstone orebodies at Laisvall. The Upper Sandstone orebody typically shows alternating bands of galena and sphalerite while the Lower Sandstone orebody is characterized by galena and sphalerite clusters and, only locally, galena bands. b. Scanning electron microprobe image in cathodoluminescence mode (SEM-CL) of sphalerite ± fluorapatite mineralization interstitial to dissolved detrital quartz with diagenetic overgrowths (Upper Sandstone orebody, Laisvall). c. SEM-CL image of galena ± Ba-K-feldspar ± Ba-mica mineralization between dissolved detrital quartz with diagenetic overgrowths (Lower Sandstone orebody, Laisvall). d. Details of sphalerite-galena mineralization intergrown with sericite and ore-stage quartz in the Lower Sandstone orebody, Laisvall (transmitted light microscopy). e. Same field of observation as Fig. 7d (transmitted light microscopy, crossed nicols). f. Back-scattered electron microprobe image (BSE) of ore-stage calcite (o.s.cl.) and sphalerite ± galena after quartz overgrowth and fluorapatite precipitation (Upper Sandstone orebody, Laisvall). g. Galena mineralization associated with anhedral to subhedral ore-stage calcite after reductive dissolution of barite in the Upper Sandstone orebody, Laisvall (transmitted light microscopy, crossed nicols).

Zn-Pb sulfide ore stage

Pb and Zn sulfides are interstitial to detrital quartz grains and are referred to as disseminated mineralization hereafter. Thin sections of representative ore samples from the Upper Sandstone and Lower Sandstone orebodies at Laisvall are shown in Fig. 7a. The Upper Sandstone orebody is characterized by alternating layers of galena and yellow-orange sphalerite with local clusters of

sphalerite or galena. Galena in the Lower Sandstone orebody typically forms large clusters (up to several millimeters across) which in places form continuous layers roughly parallel to bedding. Honey to light beige sphalerite also occurs as clusters. Mineralization in the sandstone orebody at Vassbo is similar to that in the Lower Sandstone orebody at Laisvall. In both the Laisvall and Vassbo orebodies, the contacts between quartz and Pb-Zn sulfides are irregular. Lead-zinc sulfides are coeval with and/or post-date local quartz dissolution (Figs. 7b and 7c). Both detrital quartz and diagenetic quartz overgrowths were affected by this episode of dissolution (Fig. 7b).

In detail, galena and sphalerite show complex intergrowth with a repetition of episodes of precipitation and replacement (Fig. 3). Sphalerite, essentially in the Upper Sandstone orebody at Laisvall but also at Vassbo, is typically intergrown with euhedral to subhedral, 10 to 30 µm-large fluorapatite crystals (Figs. 6d and 7b). Galena is frequently intergrown with <20 µm-long Ba-K-feldspar and Ba-mica in the Lower Sandstone orebody at Laisvall and in the sandstone orebody at Vassbo (Fig. 7c). Furthermore, sericite shards are commonly intergrown with Pb-Zn sulfides (Figs. 7d and 7e). Chalcopyrite (<< 1 vol.%) is rare.

Ore-stage calcite is not abundant in the orebodies at Laisvall and Vassbo. It was mainly found, in small amounts, in the Upper Sandstone orebody and in the sandstone orebody at Vassbo (Figs. 7f and g) but was not identified in the Lower Sandstone orebody. Ore-stage calcite grains are less than 100 µm and fill in the porosity left between quartz and fluorapatite. Subhedral ore-stage calcite (<100 µm) intergrown with galena is common where galena replaced barite cement in the Upper Sandstone orebody (Fig. 7g).

Solid bitumen in the cementing phases

Locally, in the Lower Sandstone orebody at Laisvall, pre-mineralization barite ± calcite ± fluorite cement contains abundant black solid aggregates, essentially as inclusions in barite. They are mostly present in barren parts or in spots where Pb-Zn sulfides precipitated after dissolution of both barite and quartz. These black solid inclusions were identified as solid bitumen by SEM-BSE images and SEM-EDX analysis. Raman spectrometry of these inclusions shows main peaks at 1324–1327 cm^{-1} and 1607 cm^{-1} and spectra similar to those obtained for solid bitumen from the San Vicente Zn-Pb MVT deposit, Peru (Spangenberg and Macko 1998). Solid bitumen in the Upper Sandstone orebody is often intergrown with sphalerite (Fig. 8a), in particular where sphalerite forms relatively continuous layers (Fig. 7a). The characteristic Raman peak of CH_4 at 2913 cm^{-1} was recognized in black fluid inclusions in this sphalerite species. These observations are in line with the results of Rickard et al. (1975), suggesting that the mineralizing fluids contained "petroleum-like compounds", and the optically-recognized hydrocarbons in fluid inclusions (Lindblom 1986). The section below on the molecular composition of bitumens constrains the type and origin of these "petroleum-like compounds".

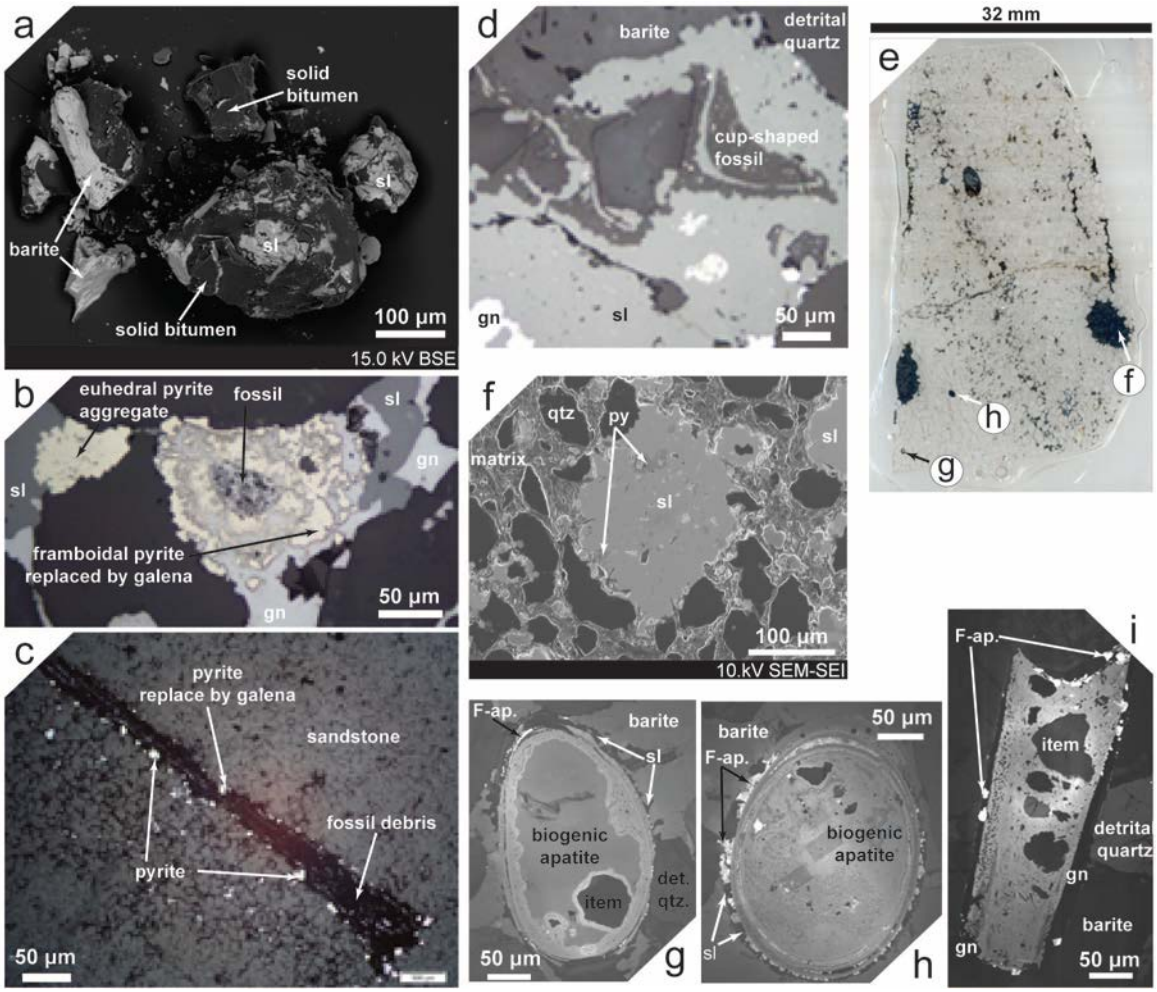

Fig. 8 a. Crystal fragments showing solid bitumen intergrowth with sphalerite (sl) and solid bitumen inclusions in barite (back-scattered electron microprobe image, BSE). b. Reflected light microscopy image showing the association of fossil with a shell of framboidal pyrite replaced by galena (gn) and sphalerite. Diagenetic pyrite aggregates are replaced by sphalerite. c. Irregular framboidal pyrite replaced by galena and/or sphalerite in fossil lamellae or tubes (reflected light microscopy). d. Cup-shaped fossil debris where framboidal pyrite was replaced by sphalerite ± galena. e. Scan of representative thin section of the barite-calcite-galena-sphalerite cemented sandstone orebody at Vassbo. Black pebbles of several millimeters and several dark-green to black ovoid pellets (<1–2 mm) are disseminated in the sandstone. f. Detail of one of the black pebbles that are composed of quartz fragments and 100–200 µm sulfide aggregates in clay-phyllosilicate matrix (SEM-secondary electron microscopy, SEM-SEI). g, h. SEM-CL images of dark-green to black ovoid fecal pellets made of biogenic apatite and various occluded items. Sphalerite precipitated at the interface with these fecal pellets after reductive dissolution of barite cement. i. Angular porous fragment of biogenic apatite with inclusions of crystal fragments. This fragment has a reaction rim of galena and fluorapatite at the interface with barite cement (SEM-CL image).

Organic debris in the sandstone orebodies at Vassbo and Laisvall

In the sandstone orebody at Vassbo, in particular where microfossils and other organic debris are abundant, early diagenetic framboidal pyrite is frequently replaced by Pb-Zn sulfides. Typically, microfossils (< 50 µm) are occluded in a shell of pyrite replaced by galena and/or sphalerite (Fig. 8b). Framboidal pyrite replaced by galena and/or sphalerite is also found in fossil lamellae or tubes (Fig. 8c) and cup-shaped fossil debris (Fig. 8d), which bear resemblance with pyritized organic clots identified as algal fragments in Cambrian black-shale-hosted polymetallic Ni-Mo deposits in South China (Cao et al. 2013).

Figure 8e shows barite-calcite-galena-sphalerite cemented sandstone from the sandstone orebody at Vassbo, with black pebbles several millimeters across included in sandstone (Figs. 8e and 8f). These black pebbles are composed of quartz fragments and 100 to 200 µm large sulfide aggregates embedded in clay-phyllosilicate matrix. SEM-secondary electron microscopy (SEM-SEI) and SEM-CL images reveal that pre-existing pyrite aggregates were replaced by sphalerite (Fig. 8f).

In addition, dark-green to black ovoid pellets (<1 to 2 mm) are disseminated in the sandstone at Vassbo (Figs. 8e, 8g and 8h). These pellets are made of apatite and various occluded components (mostly quartz fragments). By analogy and comparison with pellets described elsewhere, including along the Precambrian–Cambrian boundary interval (Brasier, 1992), in the lower Cambrian Xiaoton section and in the lower Cambrian part of the Niutitang Formation in South China (Kribek et al. 2007; Cremonese et al. 2013), we propose that these features are fecal pellets made of biogenic apatite. Similar phosphatized fecal pellets are reported from various deposits in South China in formations contemporaneous with the lower Cambrian Vassbo Formation (Shields-Zhou and Zhu 2013; Shen et al. 2014). Examples of such fecal pellets commonly found in more recent analogs, e.g., Cretaceous Negev phosphorites, Israel (Soudry and Champetier 1983), and Paleocene to Eocene phosphorite sedimentary deposit at Ras-Draâ, Tunisia (Ben Hassen et al. 2010), are remarkably similar to the pellets identified in sandstone at Vassbo. Sphalerite precipitated with fluorapatite onto these fecal pellets after dissolution of the surrounding barite cement (Figs. 8g and 8h).

At Laisvall, framboidal pyrite and organic debris are less abundant. However, angular fragments made of biogenic apatite with a porous texture and including various types of debris were identified (Fig. 8i). Similar reaction rims made of galena and fluorapatite are identified at the contact between fossils and barite cement.

Sulfur isotope composition of sulfides and barite

The range and distribution of $\delta^{34}S$ values of the analyzed sulfide and sulfate minerals in the orebodies at Laisvall and Vassbo are graphically presented in Fig. 9 and summarized statistically in Table 1. The raw data produced in the current work are given in Appendix 2. These data were combined with previous data from Laisvall (cf. Rickard et al. 1979; Rickard et al. 1981) and Vassbo (cf. Wallin 1982; Broman 1983). Several data sets stand out on the basis of petrographic and stratigraphic criteria.

The $\delta^{34}S$ values of sphalerite and galena from disseminated mineralization at Laisvall and Vassbo are all positive, ranging between 14.2 and 34.1‰, and 11.5 and 29.2‰, respectively. The lighter values for sphalerite (<21.4‰) and galena (<17.5‰) are systematically found at Vassbo. By contrast to Pb-Zn sulfides at Laisvall, the distribution of sphalerite $\delta^{34}S$ values at Vassbo is bimodal; one mode at 19.5 ± 2.1‰ (n = 10), and the other at 32.9 ± 1.2‰ (n = 2).

At Laisvall, the $\delta^{34}S$ values for sphalerite in the Upper and Lower Sandstones fall in a similar range (21.4 to 33.8‰; 24.1 to 31.5‰, respectively) with average values of 29.2 ± 2.5‰ (1 standard deviation, n = 22) and 28.6 ± 2.1‰ (n = 18) and, respectively. The $\delta^{34}S$ values for galena in the Upper

and Lower Sandstones (18.3 to 28.8‰; 17.5 to 29.2‰, respectively) are also remarkably similar with average values of 24.2 ± 2.7‰ (n = 33) and 23.7 ± 3.4‰ (n = 40), respectively.

Sphalerite in the Upper Sandstone orebody in the feeder fault area of the Central Malm at Laisvall (cf. Saintilan et al., 2015) has a value of 2.3‰. Galena in steeply-dipping veinlets in the Upper and Lower Sandstones has also positive values, overlapping with those from disseminated galena mineralization.

At Laisvall, barite in the Upper Sandstone orebody has values between 14.8 and 32.7‰ (21.8 ± 5.9‰, n = 8) while barite in the Lower Sandstone samples averages 5‰ lighter (15.1 ± 0.8‰, n = 2). Barite in the sandstone orebody at Vassbo has similar δ^{34}S values to those at Laisvall between 16.2 and 23.1‰.

Euhedral diagenetic pyrite in the Upper and Lower Sandstones at Laisvall has δ^{34}S values between 21.0 and 32.5‰ (26.0‰, n = 20). The values of euhedral to subhedral diagenetic pyrite at Vassbo fall between 9.3 and 17.7‰ (15.3 ± 2.5‰, n = 10) with some higher values at 24.4 and 28.7‰ (26.5 ± 2.1‰, n = 2).

Framboidal pyrite of the Grammajukku Formation has a δ^{34}S value of –10.1‰. At the contact with the overlying shale of the Grammajukku Formation (Fig. 2a), one pyrite in the Upper Sandstone orebody at Laisvall was found with δ^{34}S value of –6.4‰. At Vassbo, a framboidal pyrite sample has a δ^{34}S value of –8.0 ‰ whilst δ^{34}S values for pyrite in the phosphorite conglomerate above the sandstone orebody (Fig. 2b) fall between –13.1 and 7.5‰.

The δ^{34}S values for pyrite in organic-rich shale of the Alum Shale Formation are between 6.8 and 7.6‰ at Vassbo. These values are lower than the values for pyrite in the Alum Shale Formation at Laisvall (14.5 to 16.0‰; Rickard et al. 1979). The difference in the sulfur isotope composition of pyrite between the two locations of Alum Shale Formation is significant and commented on below.

Table 1. Sulfur isotope data of sulfides and sulfates from the orebodies at the Laisvall and Vassbo deposits.

Mineral	δ^{34}S (‰, VCDT)
	Range (average ± 1 standard deviation, number of samples[a] = x)
Upper Sandstone orebody, Laisvall	
Sphalerite[b]	21.4–33.8 (29.2 ± 2.5, 22)
Galena	18.3–28.8 (24.5 ± 2.7, 33)
Galena in vein	17.8–28.4 (23.5 ± 5.1, 4)
Pyrite (non-framboidal)	21.0–32.5 (26.0 ± 5.9, 13)
Barite	14.2–32.7 (21.8 ± 5.9, 8)
Lower Sandstone orebody, Laisvall	
Sphalerite	24.1–31.5 (28.6 ± 2.1, 18)
Galena	17.5–29.2 (23.7 ± 3.4, 40)
Galena in vein	22.7–26.1 (24.6 ± 1.3, 5)
Pyrite (non-framboidal)	21.7–30.6 (25.4 ± 2.6, 7)
Barite	14.0–15.7 (15.1 ± 0.8, 2)
Quartz sandstone orebody, Vassbo	
Sphalerite	14.2–21.7 (19.5 ± 2.2, 10) and 31.6–34.1 (32.9 ± 1.2, 2)
Galena	11.5–26.3 (19.2 ± 3.8, 18)
Pyrite (non-framboidal)	9.3–17.7 (15.3 ± 2.5, 11) and 24.4–28.7 (26.5 ± 2.1, 2)
Barite	16.2–23.1 (20.8 ± 2.2, 6)

a: this study; Rickard et al., 1979; Rickard et al., 1981; Wallin, 1982

b: except sphalerite in the feeder fault area of the Central Malm (n=1) with sulphur isotope composition of 2.3‰

Strontium isotope composition of barite and phosphorite

Barite in the Upper Sandstone and Lower Sandstone orebodies at Laisvall has $^{87}Sr/^{86}Sr$ ratios of 0.718791 ± 14 and 0.722349 ± 14, respectively (Table 2). The phosphorite pellet aliquot from the phosphorite conglomerate has a $^{87}Sr/^{86}Sr$ ratio of 0.721016 ± 14.

Total organic carbon content, C and N isotope composition of organic matter in shale at Laisvall

The dark grey and black shale samples of the Alum Shale Formation have TOC and TON contents from 0.33 to 3.03 wt.% (average value of 1.27 ± 0.94 wt.%, n = 12), and 0.02 to 0.08 wt.% (0.06 ± 0.02 wt.%, n = 8), respectively (Table 3). The $\delta^{13}C_{org}$ values vary from –32.5 to –29.5‰ (–31.2 ± 1.4‰, n = 12); the $\delta^{15}N_{org}$ values from 1.5 to 3.3‰ (2.3 ± 0.7‰, n = 8).

The green and grey shale samples of the Grammajukku Formation have TOC and TON contents of 0.12 to 0.20 wt.% (0.16 ± 0.02 wt.%, n = 8), and 0.03 to 0.07 wt.% (0.05 ± 0.01 wt.%, n = 12), respectively (Table 3). The $\delta^{13}C_{org}$ values vary from –32.3‰ to –29.2‰ (–30.4 ± 1.0‰, n = 8); the $\delta^{15}N_{org}$ values from 2.1 to 3.3‰ (2.8 ± 0.4‰, n = 12).

The two types of shale formation have similar $\delta^{13}C_{org}$ and $\delta^{15}N_{org}$ values and TON contents despite the much lower TOC contents of the shales in the Grammajukku Formation in comparison to those of the shales in the overlying Alum Shale Formation.

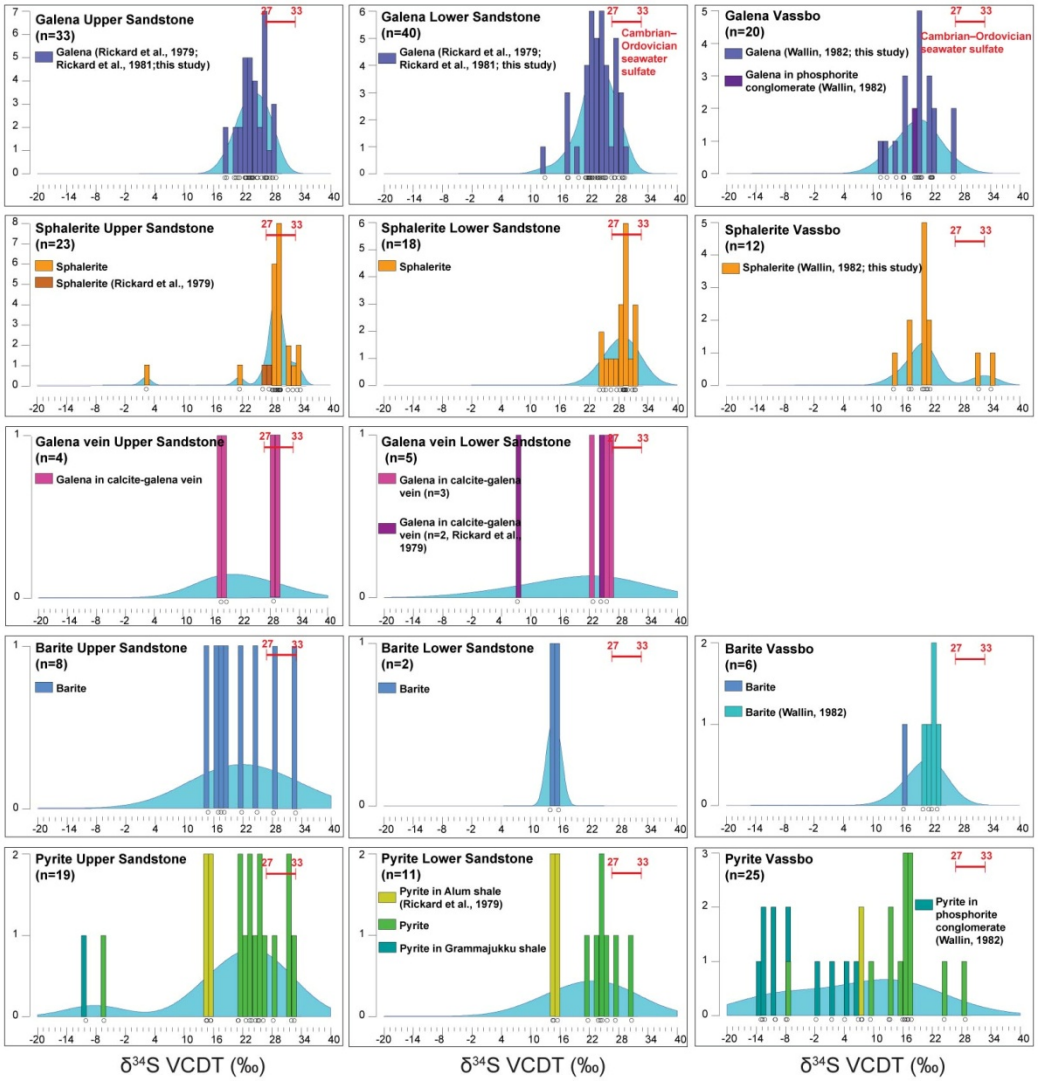

Fig. 9 Frequency distribution of $\delta^{34}S$ values for galena, sphalerite, galena in vein, barite and pyrite in the Upper Sandstone and Lower Sandstone orebodies at Laisvall. Frequency distribution of $\delta^{34}S$ values for galena, sphalerite, barite and pyrite in the sandstone orebody at Vassbo.

Table 2. Sr isotope data for phosphorite pellet in the conglomerate above the Upper Sandstone and barite cement in the Upper and Lower Sandstones (Laisberg Formation, Laisvall)

Sample	Stratigraphy at Laisvall	$^{87}Sr/^{86}Sr$	$\pm 2\sigma$ ($x10^{-6}$)
11LAI16-1	Phosphorite pellet in phosphorite polymict conglomerate	0.721016	14
12LAI73	Barite cement in Upper Sandstone ore horizon	0.718791	14
12LAI64	Barite cement in Lower Sandsone ore horizon	0.722349	14

Table 3. Total organic carbon content (TOC wt.% C), carbon isotope data, total nitrogen content (TON wt.% N), and nitrogen isotope data of organic matter in shale samples from the Alum Shale and Grammajukku Formations in the stratigraphy at Laisvall

Samples		**TOC (wt. % C)**	**$\delta^{13}C_{org}$ (‰ VPDB)**	**TON (wt. % N)**	**$\delta^{15}N_{org}$ (‰ AIR–N_2)**
		range (average ± 1 standard deviation, n = x)	range (average ± 1 standard deviation, n = x)	range (average ± 1 standard deviation, n = x)	range (average ± 1 standard deviation, n = x)
ASF 11	Black shale above limestone horizon, Alum Shale Formation	2.65–3.03 (2.80±0.17, 3)	–32.5 to –32.0 (–32.3±0.2, 3)	0.08	2.0–2.1 (2.0±0.1, 2)
ASF 9	Dark grey shale, Alum Shale Formation	1.14–1.35 (1.24±0.09, 3)	–33.0 to –32.8 (–32.9±0.1, 3)	0.08	1.5–1.6 (1.5±0.1, 2)
ASF 10	Dark grey shale, Alum Shale Formation	0.55–0.84 (0.66±0.13, 3)	–29.8 to –29.5 (–29.6±0.1, 3)	0.05	2.2 (2.2±0.0, 2)
ASF 4-0	Dark grey shale, Alum Shale Formation	0.33–0.41 (0.38±0.03, 3)	–30.8 to –29.5 (–30.1±0.5, 3)	0.02–0.03	3.3 (3.3±0.0, 2)
		1.27±0.94 (n = 12)	–31.2±1.4 (n = 12)	0.06±0.02 (n = 8)	2.3±0.7 (n = 8)
ASF 1	Green–grey shale, Grammajukku Formation	0.17 (1)	–32.3 (1)	0.06	2.7 (2.7±0.0, 2)
ASF 7	Grey shale, Grammajukku Formation	0.14–0.21 (0.17±0.03, 2)	–31.5 to –29.5 (–30.5±1.0, 2)	0.03	3.0–3.2 (3.1±0.1, 2)
ASF 6	Grey shale, Grammajukku Formation	0.18–0.20 (0.19±0.01, 2)	–30.3 to –30.0 (–30.1±0.1, 2)	0.04	2.9–3.1 (3.0±0.1, 2)
ASF 8	Grey shale, Grammajukku Formation	0.12 (1)	–30.1 (1)	0.07	2.4–2.6 (2.5±0.1, 2)
ASF 2	Green shale, Grammajukku Formation	0.17 (1)	–29.2 (1)	0.03	2.1–2.3 (2.2±0.1, 2)
ASF 3	Green shale, Grammajukku Formation	0.14 (1)	–30 (1)	0.04	3.3–3.4 (3.3±0.1, 2)
		0.16±0.02 (n = 8)	–30.4±1.0 (n = 8)	0.05±0.01 (n = 12)	2.8±0.4 (n = 12)

Table 4. Distribution of hydrocarbons and selected biomarker parameters in organic-rich shale samples of the Alum Shale Formation, mineralized samples of the Upper Sandstone and Lower Sandstone orebodies at Laisvall, and a barren Lower Sandstone sample from an outcrop located 5 km north of the Laisvall mine. CPI: carbon preference index for n-alkanes calculated as the sum of odd carbon number to the sum of even carbon number over the total carbon number range; Pr: pristane; Ph: phytane.

Samples and lithology	*n*-alkanes (maxima)	CPI	Pr/Ph	Pr/n-C_{17}	Ph/n-C_{18}
Organic-rich shale (1.08 wt.% TOC), Alum Shale Formation (ASF4-1)	C_{16}-C_{32} (C_{19}-C_{20})	1.04	0.39	0.62	0.65
Organic-rich shale (1.08 wt.% TOC), Alum Shale Formation (ASF4-2)	C_{16}-C_{32} (C_{19}-C_{20})	0.95	0.51	0.62	0.60
Sphalerite-galena mineralized Upper Sandstone orebody (LAI14)	C_{16}-C_{28} (C_{20}, C_{21}, C_{22}, C_{23})	0.95	0.38	0.70	0.55
Galena±sphalerite mineralized Lower Sandstone orebody (LAI33)	C_{17}-C_{30} (C_{22}-C_{23})	0.93	0.44	0.71	0.62
Barren Lower Sandstone (LAI90)	C_{18}-C_{29} (C_{20})	0.55	0.05	1.00	0.52

Molecular composition of bitumens

Representative gas chromatograms (GC) of the saturated hydrocarbon (HC) fraction from the organic-rich (TOC 1.08 wt.%) shale samples ASF4-1 and ASF4-2, the mineralized Upper Sandstone and Lower Sandstone samples, and the barren Lower Sandstone sample are shown in Figure 10. The dominant resolvable compounds in the GC traces of the saturated HC are *n*-alkanes in the C_{15}–C_{32} range with maxima between C_{19} and C_{23}, pristane (Pr) and phytane (Ph). Bell-shaped features corresponding to high amounts of unresolved complex mixture (UCM) of hydrocarbons eluting between C_{17} and C_{28} are present and characteristic of the GC traces of the organic-rich shale and the mineralized sandstone samples (Figs. 10a, 10b and 10c). The distribution of *n*-alkanes does not show any odd over even C-predominance (CPI = 0.93–1.04; Table 4), except for the barren sandstone sample (Fig. 10d) characterized by a dominance of even C homologues (CPI = 0.55).

The distribution of hopanes (m/z 191) and steranes (m/z 217) in the organic-rich shale and mineralized sandstone samples are remarkably similar (Fig. 11). Tricyclic triterpanes in the range C_{25}–C_{29} and hopanes in the range C_{27}–C_{35} were identified in the m/z 191 mass chromatograms of all samples. Steranes in the C_{27}–C_{29} range were detected in the m/z 217 mass chromatograms of the analyzed samples.

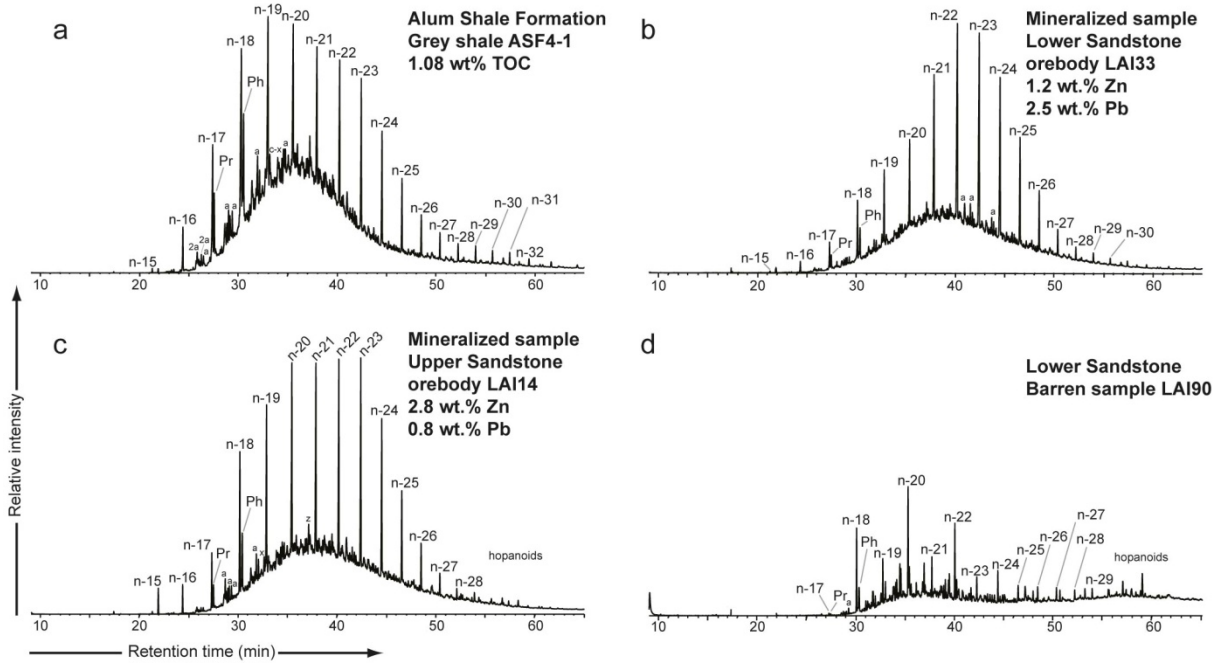

Fig. 10 Total ion chromatograms (TIC), obtained by gas chromatography-mass spectrometry (GC-MS) of the saturated hydrocarbon fraction of organic-solvent extractable bitumen, show dominance of normal alkanes (n-x, x = number of carbon atoms) in mineralized and barren samples at Laisvall. a. Organic-rich shale in the Alum Shale Formation, b. Lower Sandstone, c. Upper Sandstone, d. Barren Lower Sandstone. The branched alkanes pristane (2, 6, 10, 14 tetramethylpentadecane) and phytane (2, 6, 10, 14 tetramethylhexadecane) from the group of regular isoprenoid hydrocarbons are also present. Cyclic alkanes forming rings of six carbon atoms (cyclohexane) were detected in some samples. Molecular ratios such as pristane/phytane and carbon preference index (CPI) were calculated from the area below the peaks. Abbreviations: x= C number; C_x = *n*-alkanes with x C number; Pr = Pristane; Ph = Phytane; a = 2 and 3 methylalkanes, 2a = diethyl- or dimethylalkanes; c-x: cyclohexane.

The difference between the barren and mineralized samples (Fig. 10; Table 4) can be summarized as follows: (i) the presence of a UCM is characteristic of the GCs of the mineralized sandstone samples that share this feature with the Alum shale samples; (ii) the maxima in the *n*-alkanes distribution are in the $C_{22–23}$ range in the mineralized samples and at C_{20} in the barren one; (iii) the Ph/*n*-C_{18} ratios are higher in the mineralized samples; and (iv) low molecular weight hydrocarbons with carbon number lower than C_{22}, which are commonly considered as marine algal and/or bacterial derivatives (cf. Gelpi et al. 1970; Spangenberg and Herlec 2006), are common to and characteristic of the mineralized sandstone and Alum shale samples.

These results match the outcome of the study that identified the kerogen structure of the Alum Shale Formation as primarily consisting of algal organic matter (Bharati et al. 1991). More importantly, the hydrocarbon distributions and biomarkers point to a common algal and bacterial source of organic matter for the derivatives found in the Alum shale and the mineralized sandstone samples.

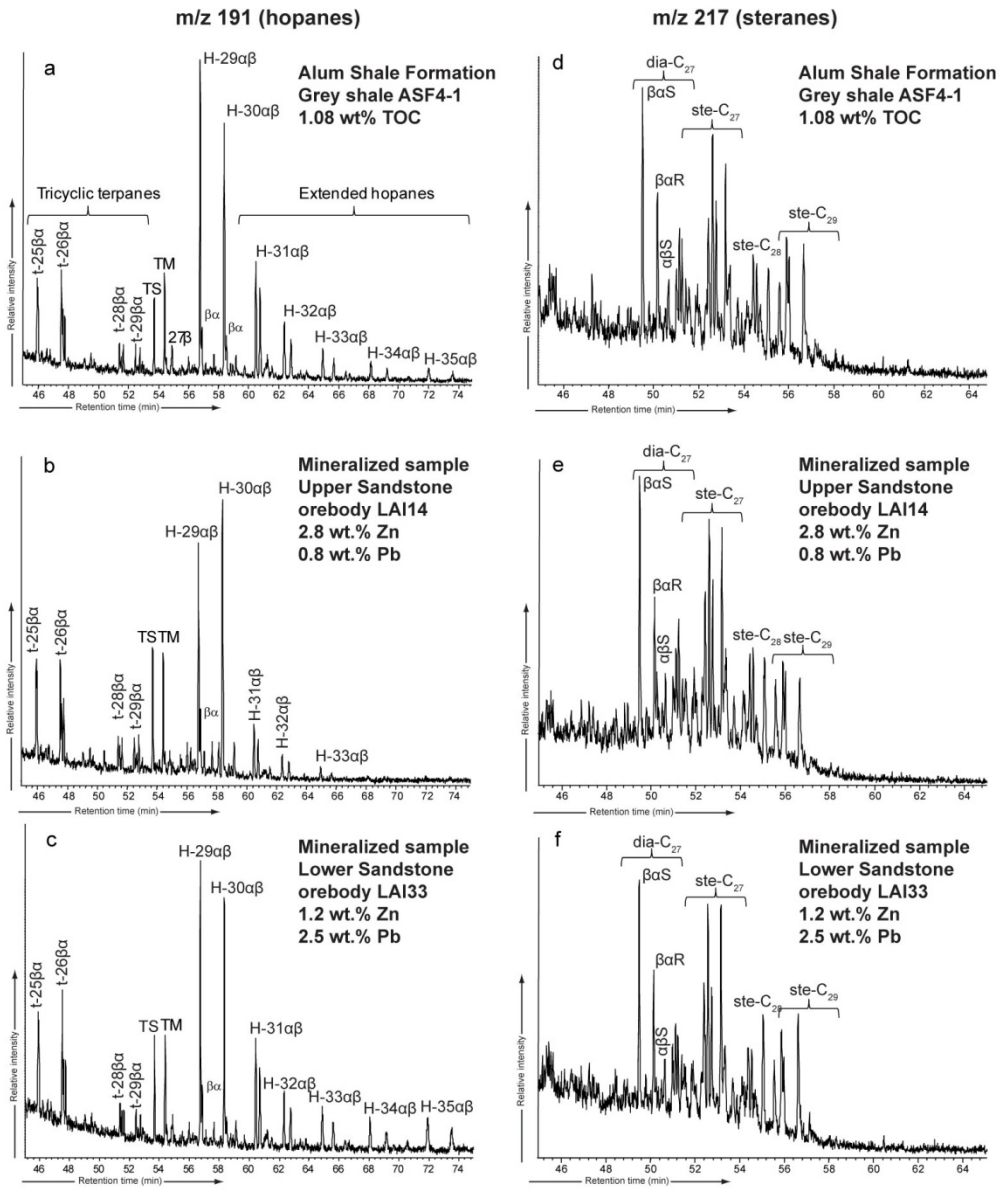

Fig. 11 Mass chromatograms showing the distribution of hopanes (m/z 191) and steranes (m/z 217) in the saturated hydrocarbon fraction of organic-solvent extractable bitumen obtained by gas chromatography-mass spectrometry (GC-MS) in the following samples at Laisvall: a, d. Organic-rich shale in the Alum Shale Formation, b, e. Upper Sandstone, c, f. Lower Sandstone.

Discussion

Diagenesis in sandstone

New insights into the paleoenvironment of deposition of the Alum Shale Formation

The low $\delta^{13}C_{org}$ values (average values of –31.2‰ and –30.4, respectively) in the middle Cambrian to Lower Ordovician Alum Shale and lower Cambrian Grammajukku Formations suggest an isotopically light carbon source with consumption of ^{13}C depleted inorganic carbon (DIC) derived from oxidation of dissolved organic carbon (DOC) compounds. In addition, the ranges of $\delta^{15}N_{org}$ values and nitrogen contents in the Alum Shale Formation (1.5 to 3.3‰ and 0.02 to 0.08 wt.%, respectively) are in accordance with N_2-fixation being the prevalent biochemical process over normal

marine production during shale deposition. This process was identified as dominating the N-cycle in stratified early Cambrian oceans with oxic surface waters and anaerobic conditions in the bottom waters (Beaumont and Robert 1999; Cremonese et al. 2013; Spangenberg et al. 2014; Ader et al. 2014).

The Alum Shale Formation was deposited in a shallow sea following deposition in lower Cambrian time of a transgressive siliciclastic sequence comprising subtidal shale, phosphorite lag and a fluvial-beach-tidal sandstone complex (Willdén 1980; Thickpenny 1984). The stratigraphic sequence bears similarities with the Precambrian Baraga Group, Michigan, USA (Nelson et al. 2010; Peir Pufahl, pers.comm. 2014), and suggests continuous continental input of nutrients (N, P, trace elements) associated with increased weathering. Our new biogeochemical data suggest that the middle Cambrian to Lower Ordovician epicontinental sea, in which the Alum Shale Formation was deposited, may have been characterized by oxic surface waters and anaerobic conditions in the bottom waters. Deposition of pyrite- and organic-rich ^{13}C-depleted carbonaceous shales of the Alum Shale Formation would illustrate rapid organic C burial with development of an anoxic/euxinic sediment-water interface (e.g., Spangenberg et al. 2014). The higher $\delta^{34}S$ values in pyrite in the Alum Shale Formation immediately above sandstone at Laisvall (14.5 to 16‰) compared to those at Vassbo (6.8 to 7.6‰) might reflect established euxinic conditions and transient increase in the amount of buried organic carbon (cf. Gill et al. 2010) at Laisvall. Strongly redox-stratified and eutrophic basins of lower Cambrian age were also described in the area of Lake Mjøsa in southern Norway (e.g., Vidal and Nystuen 1990).

Burial diagenesis in sandstone and P-REE-Ti mineral association

The present work has identified significant amounts of diagenetic anatase, monazite, fluorapatite and, to a lesser extent, xenotime in the ore-bearing sandstone units, in particular the Upper Sandstone at Laisvall. These minerals show similar concentrations (<0.05 vol%) as early diagenetic aluminophosphates and xenotime reported by Rasmussen (1996) in Australian marine sandstones of Archean to Cretaceous ages, but, at Laisvall, they occur as significantly larger crystals (50 to 450 µm at Laisvall vs. <0.1 to 10 µm in Australian examples). The depositional environment of the Alum Shale Formation during middle Cambrian to Lower Ordovician time described above can explain this authigenic P-REE-Ti mineral association formed beneath the sediment-water interface in several parts of the Upper Sandstone.

Similar P-REE-bearing mineral associations are common in black shale and are related to abiogenic processes (e.g., Upper Devonian black shale in Yukon, Oberger et al. 2003; Ordovician black shale in England, Lev et al. 1998). In accordance with the work of Rasmussen (1996) and Nelson et al. (2010), the following sequence of events can be proposed for the Upper Sandstone at Laisvall (Fig. 12). In the oxic zone of sediments (Fig. 12a), decomposition of organic matter released phosphorous that was adsorbed along with REEs onto newly-formed Fe-(oxyhydr)oxides. At the same

time, anatase precipitated and enclosed detrital quartz, zircon and monazite. In the anoxic zone (Figs. 12b and 12c), Fe-(oxyhydr)oxides were no longer stable. Iron was then fixed in pyrite formed from hydrogen sulfide produced during decomposition of organic matter (e.g., pyrite with $\delta^{34}S$ value of –6.4‰ in the Upper Sandstone). REEs and P released from Fe-(oxyhydr)oxides and clay particles precipitated as authigenic monazite associated with pyrite (Fig. 6b) while fluorapatite precipitated from fluorine in connate seawater. With continuous burial, xenotime outgrowths may have formed on detrital zircon (e.g., Fig.6a). A similar mineral association was described at the Magellan MVT Pb deposit in the Paleoproterozoic Earaheedy Basin in Western Australia (Muhling et al. 2012) where authigenic monazite grains were successfully dated by SHRIMP and gave a lower age limit for MVT mineralization. Monazite in the Upper Sandstone orebody at Laisvall could not be dated, since the grains were too small to be separated and most grains contained micrometer-size galena that would have complicated interpretation of U-Pb analyses (Fig. 6b).

In the Lower Sandstone at Laisvall, Ba-bearing K-feldspar overgrowths around K-feldspar detrital grains and the absence of barite attest to the presence of Ba-bearing and sulfate-poor hydrothermal fluids. In this unit and in the sandstone at Vassbo, precipitation of fluorapatite onto K-feldspar grains and as a coating to detrital quartz, as well as the stability of fossil phosphate fragments (Figs. 8g, 8h, 6d) suggest relatively alkaline pH conditions (Ben Hassen et al. 2010). The coeval precipitation of framboidal pyrite is consistent with anoxic conditions.

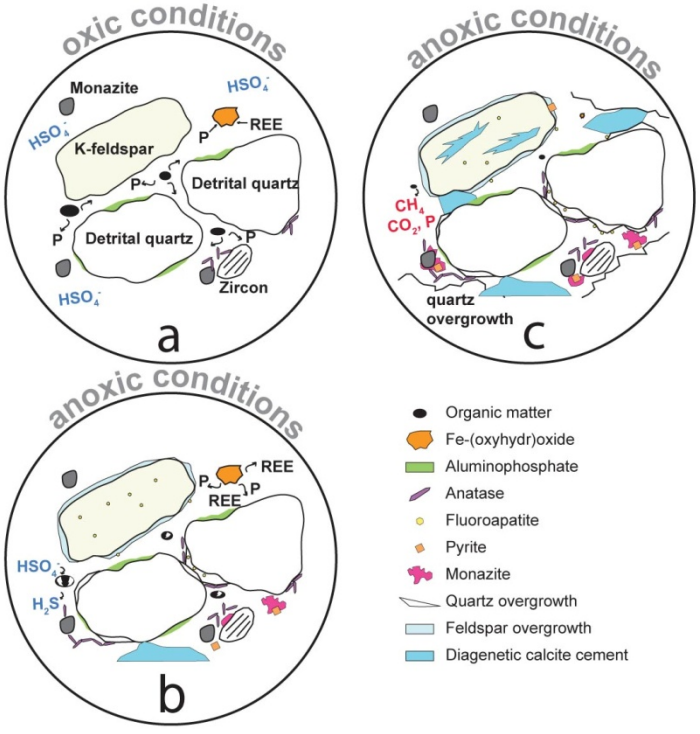

Fig. 12 Schematic diagrams showing the main mineralogical precipitation reactions of burial diagenesis operating in oxic conditions or anoxic conditions in the Upper Sandstone during deposition of the middle Cambrian to Lower Ordovician Alum Shale Formation.

Calcite and barite cementation and establishment of the porosity for subsequent Pb-Zn mineralization

The occurrence, in places, of manganiferous calcite is typical of pre-compaction calcite cement in a sandstone reservoir (e.g., pre-compaction calcite cement in the Albert Formation reservoir sandstone, New Brunswick, Canada; Chowdhury and Noble 1996). Extensive calcite cementation was accompanied by pyrite precipitation in all studied sandstone aquifers (Fig. 3).

Serrated and etched edges of calcite cement are evidence of its local dissolution at the onset of or during barite precipitation at slightly more acidic pH. Partial dissolution of K-feldspar in the Lower Sandstone at Laisvall and the sandstone at Vassbo produced additional porosity during calcite and barite precipitation (cf. Fig. 4a).

Precipitation of calcite and barite cements, in contrast to quartz cementation, may leave a certain intercrystalline porosity in sandstone paleoaquifers and enable fluid movement by capillarity (Surdam and Yin 1993). In addition, subsequent partial dissolution of calcite and barite provides a potential for permeability necessary for mineralization at a later stage (Fig. 4, 5c). Surdam and Yin (1993) described the importance of carbonate cement that ensures the preservation of intergranular volume of porosity and, in part, original porosity (Figs. 4). At Laisvall and Vassbo, available porosity for epigenetic mineralization was about 29 vol.% in sandstone paleoaquifers where calcite and barite cements, locally replaced subsequently by Pb-Zn sulfides, were widespread (Fig. 4a). By contrast, porosity at the onset of the pre-Pb-Zn sulfide stage was as low as 8 vol.% in sandstone dominated by quartz cement and lacking calcite and barite cements (Fig. 4b).

Bulk C and O isotope data for calcite are available at Vassbo (cf. Wallin 1982; Broman 1983) and Laisvall (cf. Rickard et al. 1979). However, these analyses were not constrained petrographically. A discussion on the two processes that might explain the C isotopic composition (δ^{13}C values < –8‰) of calcite cements at Laisvall and Vassbo is presented in the section below dealing with the sources of hydrogen sulfide for Pb-Zn mineralization.

The recalculated δ^{18}O values (–22 to –14‰, Fig. 13, cf. data in Rickard et al. 1979; Wallin 1982; Broman 1983) of calcite cements at Laisvall and Vassbo are extremely ^{18}O-depleted compared with the O isotope values of –10 to –7‰ reported for Cambrian to Ordovician seawater and carbonate rocks (cf. Veizer et al. 1999; Veizer 2004; Ishikawa et al. 2008; Prokoph et al. 2008). Menotti (2006) interpreted "anomalous" and relatively depleted δ^{18}O values (–14 to –10‰) of carbonate rocks of the Taconic passive margin of Laurentia (upper Cambrian), New York, USA as illustrating an overprint on the primary oxygen signal by ^{18}O-depleted water during diagenesis. Porous and permeable calcite-cemented sandstone at Laisvall and Vassbo were prone to exchange with diagenetic fluids and crystallization of ^{18}O-depleted calcite.

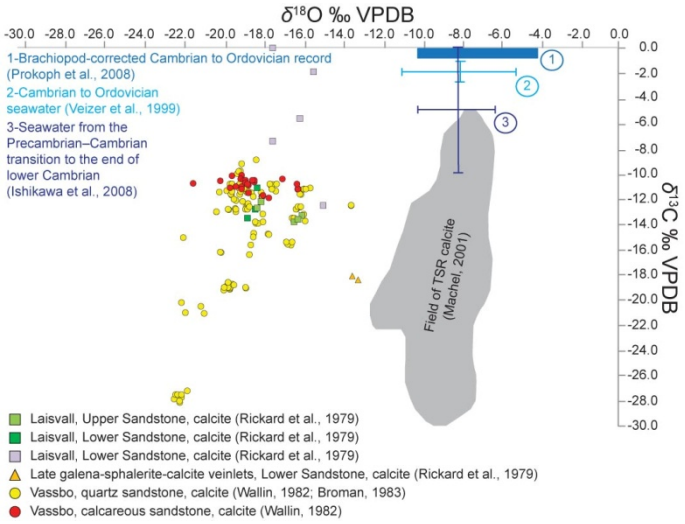

Fig. 13 δ^{13}C VPDB vs. δ^{18}O VPDB plot of calcite from the orebodies at Laisvall and Vassbo. Data compiled from the published literature for the Laisvall deposit (Rickard et al., 1979) and the Vassbo deposit (Wallin, 1982; Broman, 1983). Oxygen isotope data VSMOW were converted to VPDB. The empirical fields of TSR-produced calcite (Machel, 2001), brachiopod-corrected Cambrian to Ordovician record (Prokoph et al., 2008), Cambrian to Ordovician seawater (Veizer et al., 1999), and seawater from the Precambrian–Cambrian transition to the end of the lower Cambrian (Ishikawa et al., 2008) are shown for reference.

Hydrocarbon origin and migration

The pronounced differences in gas chromatograms of the mineralized and barren sandstone samples indicate that hydrocarbons involved in the mineralizing processes were not derived from scarce kerogen indigenous to the sandstone (Figs. 10 and 11). The similarity of the hydrocarbon distributions (Figs. 10 and 11) of the organic-rich shale (Alum Shale Formation) and the mineralized sandstone samples, the common algal and bacterial source of organic matter for the derivatives found in these samples, and the lack of other potential hydrocarbon source rock in the stratigraphy in the region suggest that the Alum Shale Formation was the source of hydrocarbons and other organic compounds (e.g., organic acid anions) that migrated into sandstone and were involved in the mineralizing processes for Pb-Zn mineralization at Laisvall.

Hydrocarbon generation necessitates that carbonaceous shales from the Alum Shale Formation were buried and heated sufficiently (> 60°C) to enter into the oil window. In addition, following hydrocarbon generation in the source rock, favorable settings are needed for hydrocarbons to migrate downward and laterally into Ediacaran to Cambrian sandstone. We propose that hydrocarbons were generated by carbonaceous shales in the Alum Shale Formation buried in the early Caledonian foreland basin to the northwest of the continental passive margin of Baltica and the locations of the Laisvall and Vassbo deposits (Fig. 14; Saintilan et al. *in press*). Hydrocarbon migration (downward and laterally) was possible given that the Alum Shale Formation was in close contact with underlying sandstone (e.g., a setting similar to that in the stratigraphy at Vassbo, cf. Fig. 2b). The presence of an additional shale aquitard between the Alum Shale Formation and underlying sandstone (e.g., the Grammajukku Formation) is a local feature characteristic of the stratigraphy at Laisvall (Fig. 2a). It is

suggested that hydrocarbon, which had entered sandstone in the foredeep, could migrate cratonward and eventually accumulate to favorable locations/traps to the southeast (Figs. 14a, 14b, 14c).

At 467 ± 5 Ma (Middle Ordovician), i.e., the proposed age for sphalerite mineralization at Laisvall, favorable settings may have conditioned accumulation of hydrocarbons in trap sites located ~20 km southeast of the forebulge and the edge of the early Caledonian foreland basin, and corresponding to the present-day location of the Laisvall deposit (Fig. 14b and 14c; Saintilan et al. *in press*).

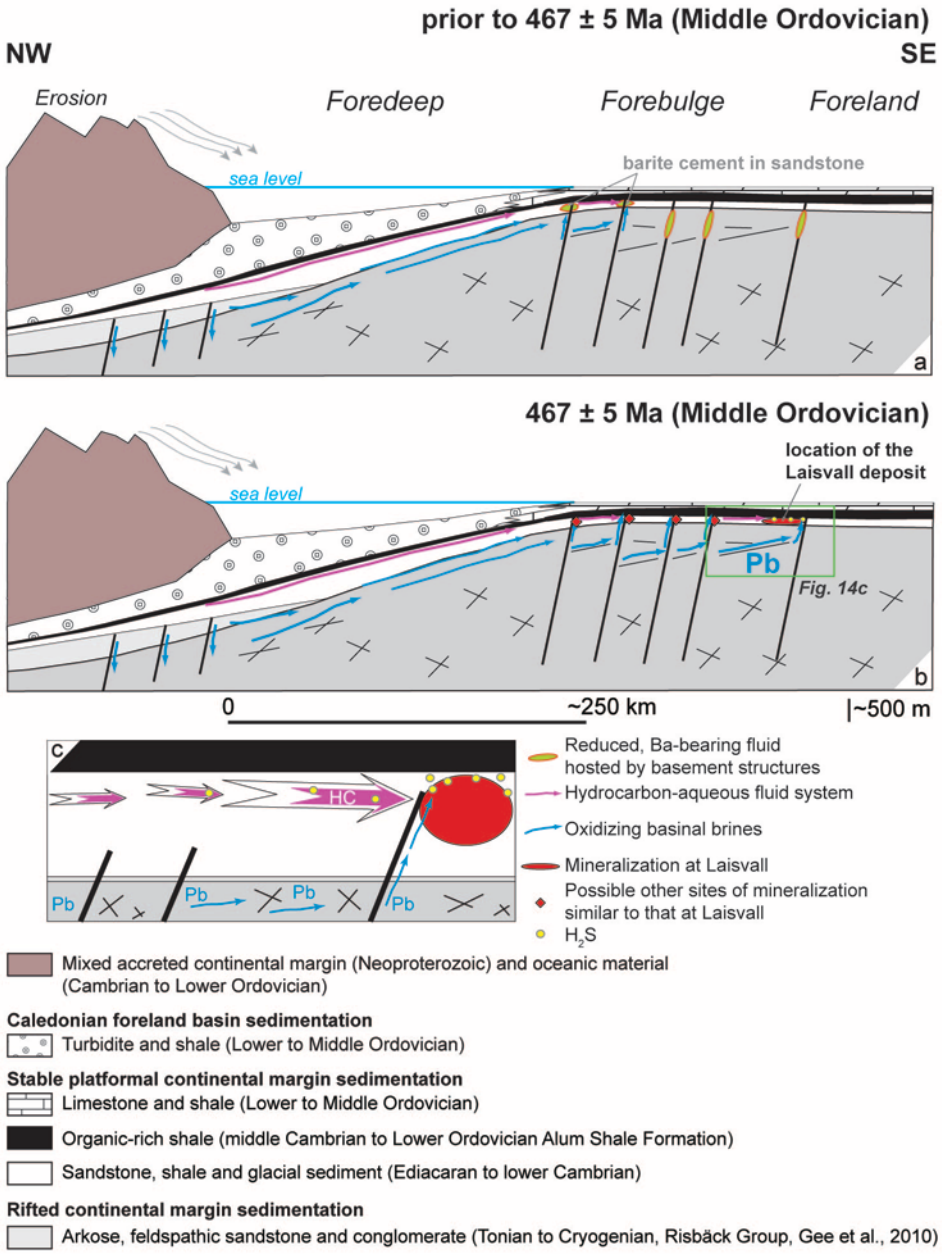

Fig. 14 (previous page) Genetic model for the Laisvall deposit in connection with the development of a foreland basin during early Caledonian orogenic activity (upper Cambrian to Middle Ordovician) a. Paleotectonic situation prior to the proposed mineralization age for the Laisvall deposit at 467 ± 5 Ma in Middle Ordovician time. b. Paleotectonic situation at the proposed mineralization age for the Laisvall deposit in Middle Ordovician time. NW–SE paleocross-section showing the location of the present-day Laisvall deposit ~20 km SE of the edge of the basin and its forebulge (after Greiling and Garfunkel, 2007; Saintilan et al., *in press*). Reactivation of basement structures which affected Ediacaran to Cambrian sandstone in the Phanerozoic (e.g., faults in the basement at Laisvall) occurred close to the forebulge (Saintilan et al., 2015, *in press*). Organic-rich shales of the Alum Shale Formation produced hydrocarbon as these were buried and heated in the foredeep beneath syn-orogenic and pre-orogenic sediments and the accretionary load (Saintilan et al., *in press*, this study). Hydrocarbon migration occurred from organic-rich shales into Ediacaran to Cambrian sandstones, then cratonward in sandstone, and finally accumulated in favorable traps (e.g., at the Laisvall deposit). It is possible that similar trap sites favorable for mineralization existed to the west of the site of mineralization at Laisvall. If deposits were formed at these sites locating resurgence of metal-bearing brines and favorable hydrocarbon accumulation, these deposits might be present today either beneath the Caledonian thrust nappes in autochthonous sandstone, or included in the lowermost allochthonous units inside the Caledonian orogen. **c**. Close-up of the mineralizing process at Laisvall.

Pb-Zn mineralization

Pre-sulfide stage barite precipitation

The sulfur isotopic composition of barite in the Lower Sandstone and Upper Sandstone orebodies at Laisvall (range 14–32.7‰, Figs. 9) suggests that sulfate in barite was derived from: (i) Cambrian to Ordovician seawater (range 27–33‰; Claypool et al. 1980) present or migrating in permeable sandstone paleoaquifers, which was locally diluted by (ii) formation waters with sulfate derived from the oxidation of pyrite in organic-rich shale in the overlying Alum Shale Formation (range 14.5–16.0‰; Rickard et al., 1979). Sulfur isotope fractionation during precipitation of sulfate minerals from dissolved sulfate is small (< 0.5 ‰; Ohmoto and Rye 1979). However, the obtained $^{87}Sr/^{86}Sr$ ratios of barite in the Upper Sandstone and Lower Sandstone orebodies (0.718791 ± 14 and 0.722349 ± 14, respectively) are much higher than the $^{87}Sr/^{86}Sr$ ratios of Cambrian to Ordovician seawater (e.g., around 0.709; Veizer et al. 1999). These ratios are also higher than the initial $^{87}Sr/^{86}Sr$ ratio for sphalerite (0.7159000 ± 60) obtained during Rb-Sr geochemistry work (Saintilan et al. *in press*).

The $^{40}Ar/^{36}Ar$ ratios (range 4000–6500) and high concentrations of $^{40}Ar^*$ in fluid inclusions preserved in barite at Laisvall suggest that these fluids had a long pre-mineralization crustal residence time (in the order of 100 Ma; Kendrick et al. 2005). These data are compatible with the highly radiogenic $^{87}Sr/^{86}Sr$ ratios in barite at Laisvall. In addition, fluid inclusions in barite have salinities of 18 ± 8 wt. % NaCl eq. and Br/Cl ratios of c. 3 to 5 x 10^{-3} (data from barite at Laisvall and Osen, cf. Kendrick et al. 2005).

It is proposed that crustal, saline, Ba-bearing and sulfate-poor fluids in equilibrium with Paleoproterozoic basement rocks resided in structures in the basement. Upon cratonward migration of oxidizing, metal-bearing basinal brines derived from the early Caledonian foreland basin during the Middle Ordovician (see detailed description of these brines in the next section), the Ba-bearing fluids at Laisvall were forced and expelled upward from their host structures into the overlying sandstone along reactivated steeply dipping faults in the basement (Saintilan et al. 2015; Fig. 14a). Upon

termination of the flow of oxidizing basinal brines cratonward, hydrodynamics was progressively restored to equilibrium and the plumbing system returned to a situation of fluids in equilibrium with basement rocks. This hypothesis is supported by field evidence of calcite-fluorite ± pyrite veins hosted by fractures in the basement of the Laisvall deposit in the proximity of the main feeder faults. Saintilan (2015) suggested that these basement veins formed during large-scale fluid flow from reduced and basement-interacted hydrothermal fluids that were in equilibrium with basement rocks.

Barite precipitated upon mixing of the reduced, neutral, Ba-bearing fluids with the above-described sulfate pool present in Ediacaran to Cambrian sandstone. The unusually high I/Cl values (60–1600 x 10^{-6}) in fluid inclusions in barite at Laisvall (Kendrick et al. 2005) suggest that fluids involved in the pool of sulfate in Ediacaran to Cambrian sandstones must have interacted with I-rich organic matter in organic-rich sedimentary rock in the subsurface. It is possible that formation waters, which diluted connate Cambrian to Ordovician seawater in Ediacaran to Cambrian sandstone, interacted with I-rich organic matter and oxidized pyrite from the carbonaceous shale of the Alum Shale Formation during migration in the subsurface.

The similarity of the sulfur isotope composition of barite and the noble gas and halogen compositions of fluid inclusions in barite at Osen, Vassbo and Laisvall (Fig. 9 and Kendrick et al. 2005) suggests a homogeneous fluid-flow model for basement-hosted Ba-bearing fluids at a regional scale. Pre-Pb-Zn sulfide stage barite cementation is a key feature common to several sandstone-hosted Pb-Zn deposits along the erosional front of the Caledonian orogen (e.g., Osen, Vassbo, Laisvall).

Sources of metal-bearing brines and their resurgence in sandstone

The results of microthermometry, noble gas and halogen analyses in fluid inclusions in sphalerite and galena at Laisvall and Vassbo (Lindblom 1986; Kendrick et al. 2005) suggest that saline (c. 24 wt% NaCl eq., Br/Cl of c. 8 x 10^{-3} much greater than seawater), crustal fluids involved in mineralizing processes had interacted with basement rocks ($^{40}Ar/^{36}Ar$ ratios of c. 500 to 1800; low to moderate $^{40}Ar^*$ concentrations). The initial $^{87}Sr/^{86}Sr$ ratio for sphalerite (0.7159000 ± 60) obtained during Rb-Sr geochemistry work (Saintilan et al. *in press*) may be close to the $^{87}Sr/^{86}Sr$ ratio for these evolved basement-interacted fluids.

These geochemical data, combined with the geodynamic setting proposed for the timing of mineralization at Laisvall as a response to early Caledonian orogenic activity, are compatible with these fluids being basinal brines that resided in and interacted with pre-Ediacaran, rift-related feldspathic sandstones and arkoses containing detritus from the Baltica continent (Risbäck Group, cf. Gee et al. 2010), which were preserved in the deeper part of the early Caledonian foreland basin (Fig. 14a, 14b; Saintilan et al. *in press*).

Basinal brines flowed cratonward along the lower units of the basin, along the unconformity between Ediacaran to Cambrian sediments and the crystalline basement, and along fractures, including gently dipping sheet joints, in the upper part of the basement. The evolved basinal brines had

temperatures around 120° to 180°C at the mineralization site (cf. fluid inclusion data in sphalerite in Lindblom, 1986) and, consequently, probably had higher temperatures when they migrated through the Baltica basement. For this reason, these oxidizing and saline fluids had the potential for transporting metals (Lindblom 1986; Kendrick et al. 2005). Lead radiogenic isotope data indicate that metals were essentially derived from basement rocks and their erosional products (Rickard et al. 1981; Johansson and Rickard 1984; Romer 1992, Saintilan 2015). At Laisvall, these evolved metal-bearing brines resurged towards the Middle Ordovician along reactivated steeply dipping faults in the basement that also affected the Ediacaran to Cambrian sandstones (Fig. 14b, 14c; Saintilan et al. 2015; *in press*).

Sources of hydrogen sulfide

The relatively small range of heavy $\delta^{34}S$ values (average 24–29‰) for Pb-Zn sulfides (Fig. 15) suggests that most H_2S in the mineralizing fluid was produced during thermochemical sulfate reduction (TSR, cf. Krouse et al. 1988; Machel 2001; Anderson 2008) of mainly Cambrian to Ordovician seawater sulfate with oxidation of organic compounds (e.g., hydrocarbons). Fractionation between TSR-produced H_2S and H_2S fixed in sphalerite is negligible (cf. Ohmoto and Rye 1979). A schematic net mass balance of the TSR reaction was proposed by Machel (1987, 2001): hydrocarbons + HSO_4^{2-} → altered hydrocarbons + solid bitumen + $H_2S(HS^-)$ + $HCO_3^-(CO_2)$ (+ H_2O). The products of this reaction are discussed here (e.g., H_2S, $HCO_3^-(CO_2)$) and in the later text (e.g., altered hydrocarbons, solid bitumen).

The heaviest sulfur isotope composition corresponds petrographically to sphalerite (range 29–33‰) and galena (range 22–29‰) located in the pores between quartz grains and is interpreted as the product of thermochemical reduction of aqueous sulfate with a composition of Cambrian to Ordovician seawater (27 to 33 ‰; Claypool et al. 1980). The rest of the spectrum of sulfur sphalerite isotope values corresponds to sphalerite formed by thermochemical reductive dissolution of barite (described in detail below) which has sulfate values between 14 and 33‰ (Table 1). Hydrogen sulfide produced by TSR was subordinately consumed by minor pyrite showing $\delta^{34}S$ signatures between 30.5 and 32.5‰ (Fig. 9, Table 1), prior to extensive consumption of TSR-produced hydrogen sulfide by galena and sphalerite.

Textural and geochemical evidence (Figs. 8 and 9) indicates that a subordinate source of hydrogen sulfide for Pb-Zn sulfide precipitation with sulfur isotope compositions of 21–27‰ at Laisvall and 12–18‰ at Vassbo was the replacement, at an early stage, of diagenetic pyrite ± framboidal pyrite (Fig. 15).

A third subordinate and localized source of hydrogen sulfide was identified at Laisvall in the feeder fault zone area (e.g., Fig. 16) of the Central Malm (Saintilan et al. 2015) where sphalerite has sulfur isotope compositions around 2‰ (Figs. 15) that may be explained by reduced sulfur derived from sulfide (e.g., pyrite) in crystalline basement rocks.

Sulfide types with specific isotope compositions estimated petrographically and using evidence from QEMSCAN image analysis suggest that TSR was the main source of hydrogen sulfide at Laisvall (~90 vol %) and Vassbo (~70 vol %) whereas pyrite replacement amounted to ~10 vol % at Laisvall and ~30 vol% at Vassbo. It is proposed that TSR is a key control in the generation of a Laisvall-type deposit to an economic level.

The oxidation of organic compounds (e.g., hydrocarbons) during TSR produces ^{13}C-depleted dissolved inorganic carbon which may precipitate calcite of low δ^{13}C values (TSR-calcite; cf. Machel 1987, 2001). Previous stable C and O isotope studies at Vassbo (cf. Wallin 1982; Broman 1983) reported data for calcite in the sandstone orebody and the underlying essentially barren calcareous sandstone (Fig. 2b). Although these analyses were not constrained petrographically, the following three calcite groups could be distinguished on the basis of their C isotope composition (Fig. 13): (1) –15 to –8‰, (2) –22 to – 18‰, and (3) –30 to –28‰. Group 1 is common to both the sandstone orebody and the barren calcareous sandstone and thus might correspond to diagenetic calcite cement common to these horizons. A preferred hypothesis is that the C isotopic composition of group 1 calcite is related to dissolved inorganic carbon resulting from the oxidation of organic compounds during genesis. On the other hand, the occurrence of strongly ^{13}C-depleted calcite (groups 2 and 3) in the sole sandstone orebody at Vassbo may correspond to subhedral TSR-calcite which was identified and constrained petrographically in the current study. By contrast, the orebodies at Laisvall are characterized by a paucity of ore-stage calcite, which is very fine-grained and intimately intergrown with Pb-Zn sulfides (Figs. 7f and g). No C isotope data are available for this calcite.

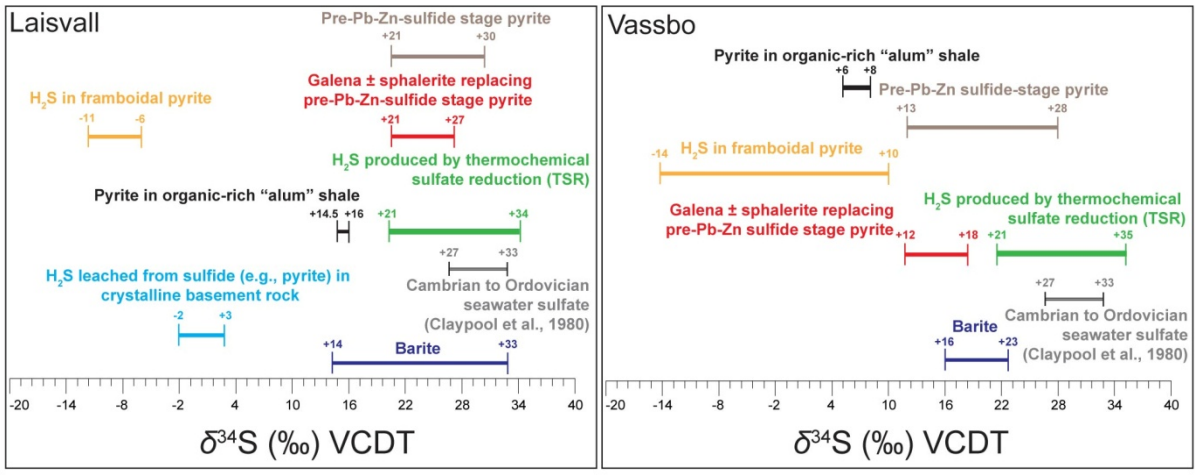

Fig. 15 Comparison of the ranges of sulfur isotope composition in sulfides and barite at Laisvall and Vassbo with the compositions of possible sources of reduced sulfur. See text for further details.

Formation of solid bitumen, timing of TSR and TSR reaction zones

Two types of solid bitumen occur in the orebodies at Laisvall: (i) solid bitumen intergrown with sphalerite in the Upper Sandstone orebody; and (ii) solid bitumen inclusions in barite cement and, in a few places, in fluorite or calcite cements in the Lower Sandstone orebody. The timing of TSR (mainly

before and to some extent during Pb-Zn mineralization), and the size and location of TSR reaction zones can be estimated from these petrographic observations.

Timing of TSR

Efficient TSR requires temperatures of at least 100° to 140°C (Machel 1987; Heydari and Moore 1989; Goldhaber and Orr 1995; Worden et al. 1995; Simpson et al. 1996; Machel 2001, Anderson 2008) and pH of 4 to 8. Temperatures of 120° to 180°C during mineralization have been proposed on the basis of fluid inclusion studies in sphalerite at Laisvall (Lindblom, 1986) whereas evidence for slightly acidic conditions during mineralization are given by the presence of sericite in sphalerite and galena (Figs. 7d, e) and the paucity of ore-stage calcite.

Intimate intergrowth of solid bitumen with sphalerite in the Upper Sandstone orebody (Fig. 8a) suggests that this bitumen formed during the main stage of Pb-Zn mineralization. Given that the main source of hydrogen sulfide at Laisvall was produced during TSR, this bitumen is interpreted as a by-product of TSR. Hence, this petrographic evidence would imply that TSR may have occurred in part during and not only before Pb-Zn mineralization. This scenario is compatible with the experimental results by Thom and Anderson (2008) suggesting that TSR may occur during mineralization in MVT deposits.

It is critical to understand the timing of hydrocarbon migration into the sandstones at the mineralization site, and the relative time span needed for TSR to produce H_2S for the precipitation of Pb-Zn sulfides. Information is provided by the presence of solid bitumen inclusions in pre-Pb-Zn sulfide stage barite cement and more rarely in earlier calcite cement. It is possible that hydrocarbon flowed in the sandstone paleoaquifers prior to and during barite precipitation (Fig. 3; Fig. 16 situation L1). At Laisvall, it is proposed that the change of the main cement from calcite to barite is coeval with hydrocarbon migration in sandstone. With continuous flow of aqueous fluids in the bottom parts of paleoquifers (e.g., the bottom part of the Lower Sandstone paleoaquifer at Laisvall, Fig. 16 situation L2), hydrocarbons were altered and solid bitumen formed and was included in barite ± fluorite (Fig. 16 situation L3). Simultaneously, in the higher parts of the sandstone paleoaquifers, TSR reaction zones between hydrocarbons and aqueous sulfate were preserved and H_2S could form and accumulate (Fig. 16 situations U1 and U2) while barite precipitated in the lower parts. This interpretation is supported by the morphology of the orebodies at Laisvall and Vassbo, where mineralization is most abundant towards the roof of the sandstone paleoaquifers, reflecting paleo-supply of H_2S for sulfide precipitation (Fig. 14c, 16; Saintilan et al. 2015).

TSR reaction zones

Machel (2001) stressed the necessity of the physical contact between hydrocarbon and aqueous sulfate for TSR to occur, given the fact that the sulfate does not react by TSR in the solid state. Reduced sulfur could have been generated at Laisvall and Vassbo at the site of mineralization or west

of it and subsequently transported to the mineralization site (Fig. 14c). TSR may have taken place before sulfide mineralization at the Laisvall ore site, where parts of the pores in the sandstone reservoirs (e.g., the Upper Sandstone orebody and several parts of the Lower Sandstone orebody) remained distinctly hydrocarbon-filled and underlain by parts with water-filled pores (Fig. 16 situations U1 to U3). In this situation, TSR is confined to a hydrocarbon-water interface. TSR may then occur throughout the entire hydrocarbon-containing part of the reservoir, if the irreducible water saturation (i.e., the fraction of the pore space occupied by water when hydrocarbon content is at maximum) is high (cf. Machel 2001). Such ideal conditions may have prevailed in the Upper Sandstone and locally in the Lower Sandstone orebodies, where continuous, horizontal and alternating layers of galena and sphalerite are observed (Figs. 7a and 16 situation U3). Upward migration, fluctuation of the hydrocarbon-water interface, and formation of H_2S along this interface may explain the layering of the ore.

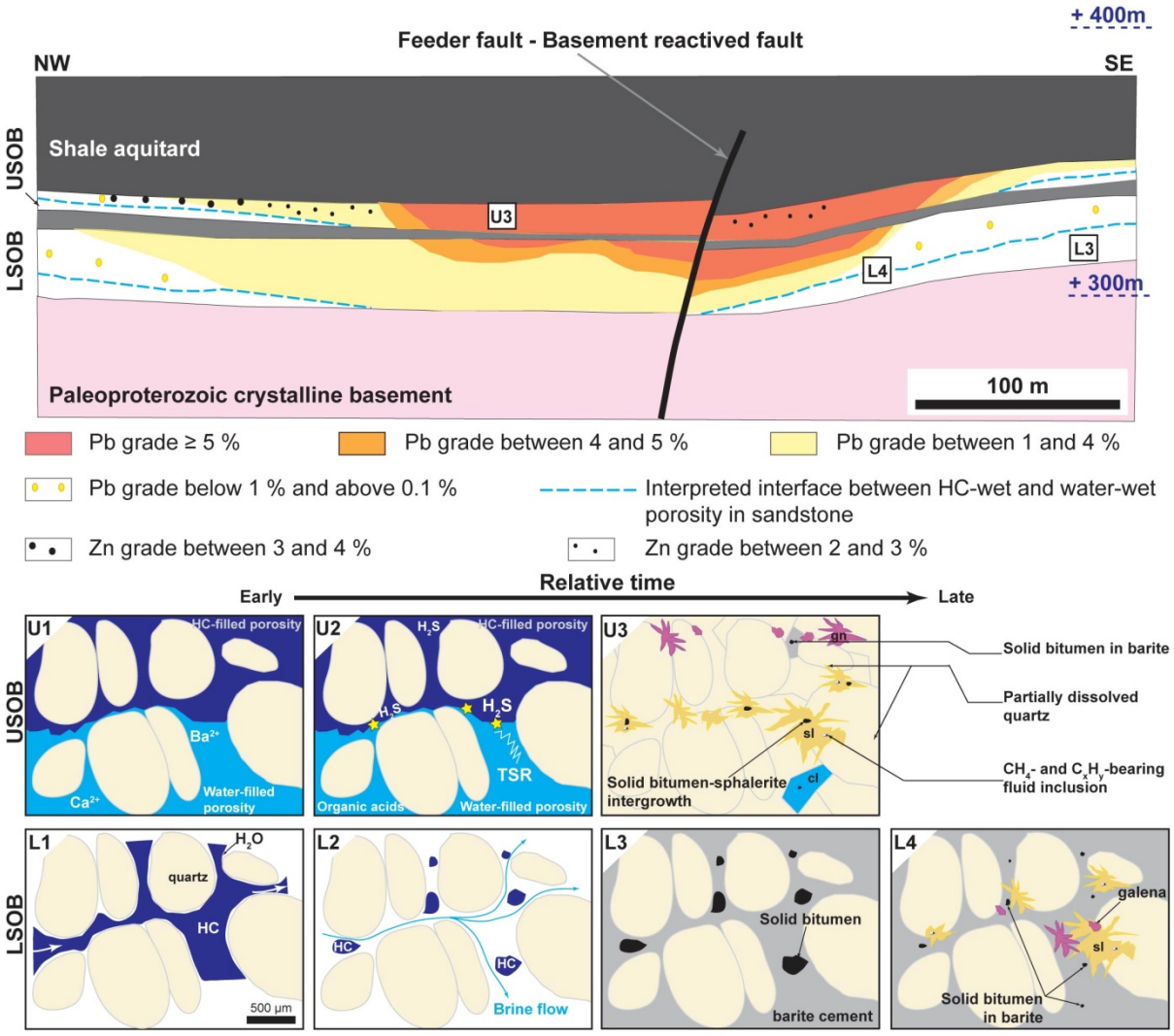

Fig. 16 (previous page) NW–SE cross-section across the Nadok feeder fault system (between c. 300 and 400 m above sea level) showing the Pb-Zn grade distribution in the Upper Sandstone and Lower Sandstone orebodies (USOB and LSOB) separated by the relatively impermeable Middle Sandstone (modified after Saintilan et al., 2015). Situations L1, L2, U1 and U2 illustrate processes before and leading to mineralization. Situations L3, L4 and U3 correspond to mineralized and barren parts as observed today in macroscopic and microscopic samples. The locations L3, L4 and U3 are shown on the section. Styles of porosity-filling in the water-hydrocarbon system in the paleoaquifers at Laisvall and Vassbo, as deduced from textural evidence, occurrence of solid organic matter, and sulfur isotope composition of barite and Pb-Zn sulfides. Hydrocarbon (HC) can be oil or gas. L1: Parts of sandstone paleoaquifers were HC-wet following exogenous hydrocarbon migration. L2: Flow of aqueous fluids altered hydrocarbons, isolated hydrocarbon droplets and gave rise to the formation of solid bitumen. L3: Prior to or as thermochemical sulfate reduction proceeded and produced H_2S, barite cement precipitated and enclosed solid bitumen. L4: Pb-Zn sulfides precipitated from H_2S produced during reductive dissolution of barite by organic acids. Some quartz dissolution coeval with barite dissolution accommodated secondary porosity for Pb-Zn sulfide precipitation (see also Fig. 17 and text for explanation). U1: Parts of the paleoaquifers showed porosity stratification with an HC-wet part underlain by a water-wet part. U2: TSR occurred at the interface between the HC-filled porosity and the water-filled porosity and H_2S was produced (after Machel, 2001; Andersson, 2008). U3: Upward migration, fluctuation of the hydrocarbon-water interface, and formation of H_2S along this interface may explain the alternating layers of galena and sphalerite.

Reductive dissolution of barite and timing and origin of quartz dissolution

Barite cement in the Lower Sandstone orebody at Laisvall and the sandstone orebody at Vassbo was dissolved locally together with quartz and replaced by sphalerite and galena. Given the necessity to have aqueous sulfate for TSR to take place (Machel 2001), this means that sulfate through barite dissolution was placed again into solution and reduced in situ via TSR (Fig. 16 situation L4).

Solubility of barite is favored by increasing salinity and decreasing temperature between 200°C and 100°C (Rimstidt 1977; Hanor 2000). In addition, organic acids can increase reservoir porosity by dissolving minerals (via cation-organic acid anion complexation) or by increasing their dissolution rates (Knauss et al. 1997; Surdam et al. 1984; Greenwood et al. 2013). Chemical thermodynamic speciation modeling suggests that organic acids influence significantly the solubility of alkaline earths (e.g., Ba^{2+}; Knauss et al. 1997 in Greenwood et al. 2013), and chemical dissolvers based on the aminoacetate group are well known as strong chelating agents for barium ions that are used in the petroleum industry and in environmental remediation. Organic acids are common by-products of the TSR reaction (Machel 2001). These organic acids are also present and highly soluble in low-salinity subsurface formation waters (Hanor, 1996). Hence, it is probable that organic acids were present in sandstone before and during mineralization. Thus, we propose that dissolution of barite by organic acids could place barium and sulfate in solution at Laisvall and Vassbo. Sulfate could be reduced via TSR in the areas of barite ± quartz dissolution and more Pb-Zn sulfides precipitated. Similar reductive dissolution of barite was reported for stage 3 of sphalerite mineralization at the shale-hosted Zn-Pb-Ag Red Dog deposit, Alaska, USA (cf. Kelley et al. 2004).

Two complementary processes (one organic and one inorganic) can be advocated to explain the quartz dissolution features mentioned above. Quartz dissolution, which locally created secondary porosity for mineralization (Fig. 17), is common in areas of reductive barite dissolution and/or in spaces where sulfides are intergrown with sericite (Figs. 3, 7b, 7c, 16). Bennett (1991) showed that organic acid-rich aqueous systems can lower the activation energy of quartz dissolution by 20 % at

neutral pH and temperature as low as 25 to 70°C. Dissolution of quartz and its solubility might have been increased by organic acids either present in formation waters or as by-products of the TSR reaction.

Cations such as Ba^{2+}, K^{+} and to a lesser extent Ca^{2+} are known for their thermodynamic property named «frequency of solvent exchange» (K_{ex}) that lowers the activation energy for quartz dissolution (Dove and Nix 1997; Dove 1999). According to these authors, these cations favor quartz dissolution by enabling the protonation of Si–O bridging structures due to their tendency of high exchange rate at the quartz–solution interface. Barium cations could be placed in solution via reductive dissolution of barite at the time of Pb-Zn sulfide precipitation, while potassium and calcium cations were already in solution due to K-feldspar dissolution during diagenesis and calcite replacement by barite, respectively.

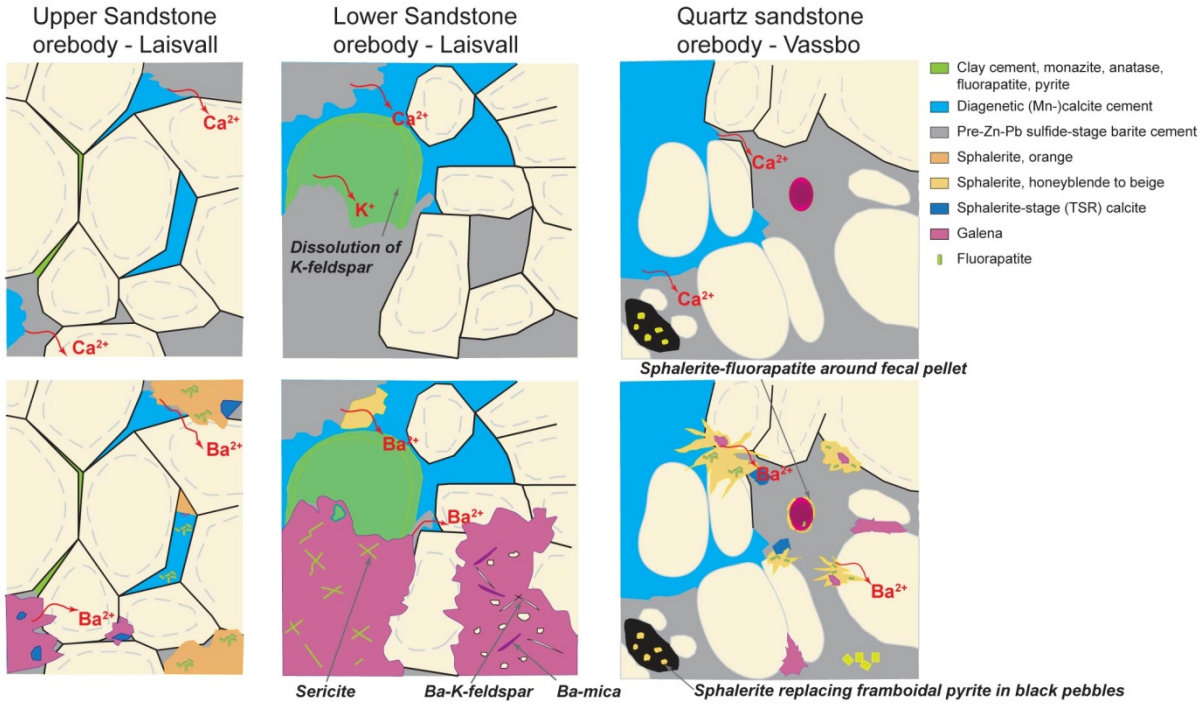

Fig. 17 Creation of secondary porosity for Pb-Zn sulfide precipitation by quartz (detrital quartz and overgrowth) dissolution due to the thermodynamic property of Ba^{2+}, K^{+}, and Ca^{2+} cations known as "frequency of solvent exchange" and the action of organic acids in the Upper Sandstone and Lower Sandstone orebodies at Laisvall, and the sandstone orebody at Vassbo.

Conclusions

Recent findings on the control of reactivated, Proterozoic basement structures on the location and genesis of the sandstone-hosted Laisvall and Vassbo deposits in Sweden (Saintilan et al. 2015) and the establishment of a Rb-Sr age of 467 ± 5 Ma for the mineralization at Laisvall (Saintilan et al. *in press*) have provided a basis for a better understanding of the processes of Pb-Zn mineralization at these deposits. A geodynamic setting in which the Laisvall deposit was in proximity of the forebulge to a foreland basin, developed in connection with early Caledonian continent-arc collision, has been

proposed (Saintilan et al., *in press*). The current study has added the following elements to refine the two-fluid mixing model presented by Rickard et al. (1975; 1979), Lindblom (1986) and Kendrick et al. (2005) for Pb-Zn mineralization at Laisvall and, by consequence, Vassbo, involving the mixing of metal-bearing basinal brines with a pool of H_2S in sandstone.

- The study of the diagenetic cements preceding mineralization in sandstone has shown that precipitation of pre-Pb-Zn sulfide stage calcite and barite protected sandstone from quartz cementation. The available porosity for epigenetic mineralization, including that produced by subsequent partial dissolution of calcite and barite cement, was almost four times higher in calcite- and barite-cemented sandstone paleoaquifers (29 %) than in those mainly cemented by quartz (8 %).
- A peculiar P-REE-Ti authigenic mineral association comprising monazite, fluorapatite and anatase in the Upper Sandstone at Laisvall reflects diagenetic processes and anoxic conditions in sandstone influenced by the euxinic character of the overlying and regionally extensive Alum Shale Formation. The latter was deposited in a redox-stratified, epicontinental sea in the middle Cambrian to Lower Ordovician.
- Barite and calcite precipitating before the Pb-Zn sulfide stage is a key feature of all Laisvall-type deposits (e.g., Laisvall, Vassbo, Osen). Barite precipitated and cemented sandstone through the mixing of: (i) basement-interacted (high radiogenic Sr ratios of 0.718–0.722 and other geochemical indicators published previously; cf. Kendrick et al. 2005), Ba-bearing, neutral, and relatively reduced fluids; with (ii) a sulfate pool ($\delta^{34}S$ values = 14–33‰) in sandstone comprising Cambrian to Ordovician seawater diluted by subsurface formation waters.
- Evolved metal-bearing brines resurged during the Middle Ordovician from the crystalline basement along reactivated, steeply dipping faults in the basement that also affected the Ediacaran to Cambrian sandstones at Laisvall. These brines were contained in pre-Ediacaran, rift-related feldspathic sandstones and arkoses (Risbäck Group) containing detritus from the Baltica continent, which were preserved in the deeper part of the early Caledonian foreland basin. As a response to the early Caledonian orogenic activity, basinal brines flowed cratonward along the lower units of the basin, along the unconformity between Ediacaran to Cambrian sediments and the crystalline basement, and along fractures, including gently dipping sheet joints, in the upper part of the basement. These hot (> 120° to 180°C), basement-interacted (initial Sr ratio in sphalerite of 0.7159, $^{40}Ar/^{36}Ar$ ratios of c. 500 to 1800; low to moderate $^{40}Ar^*$ concentrations), oxidizing, slightly acidic and saline brines (c. 24 wt.% NaCl eq., Br/Cl of c. 8 x 10^{-3} much greater than seawater; Lindblom, 1986; Kendrick et al., 2005; this study) had the potential for transporting metals that were derived from basement rocks and their erosional products (Rickard et al. 1981; Johansson and Rickard 1984; Romer 1992, Saintilan 2015).
- Dissolution of calcite cement, the presence of sericite in Pb-Zn mineralization, and the lack of significant calcite precipitation during mineralization confirm that brines were slightly acidic during the Pb-Zn sulfide stage.

- The change from barite-calcite cementation to Pb-Zn sulfide precipitation in sandstone illustrates a major change in the plumbing system at Laisvall. It is proposed that the reactivated basement structures (cf. Saintilan et al. 2015) at Laisvall were first used by the Ba-bearing, reduced and neutral fluids described above. These fluids were in equilibrium with basement rocks and had a long pre-mineralization residence time in the basement. As a result of the early Caledonian orogenic activity, fluids migrated cratonward and Ba-bearing fluids were firstly expelled from their host structures into overlying sandstone by using basement structures. Subsequently, slightly acidic metal-bearing brines migrated through the same plumbing system. The early Caledonian arc-continent collision can account for the necessary flow to prevent these brines from equilibrating with the basement rocks. Recognition of barite cements in sandstone outcrop or drillcore may be used as an exploration vector, since it could be spatially associated with fertile structures in the basement.
- The Pb-Zn sulfide stage was locally accompanied by minor quartz dissolution. It is spatially associated with clusters of sphalerite-galena or with zones of barite dissolution. Quartz dissolution is interpreted to be triggered by organic acids and reactive cations (e.g., Ba^{2+} and K^{+}).
- The gas chromatograms of saturated hydrocarbons obtained in the present study indicate that exogenous hydrocarbons migrated from source rocks in the middle Cambrian to Lower Ordovician Alum Shale Formation into sandstone where they accumulated in favorable traps. Hydrocarbon generation occurred in organic-rich Alum shales that were buried and heated into the oil window in the foredeep of the early Caledonian foreland basin. Downward and lateral hydrocarbon migration was possible given that the Alum Shale Formation was in close contact with underlying Ediacaran to Cambrian sandstone. The presence of solid bitumen inclusions in barite suggest that hydrocarbon migration had already started prior to or during barite-calcite cementation of the sandstone units.
- At the proposed age for sphalerite mineralization at Laisvall (467 ± 5 Ma, Middle Ordovician), hydrocarbons could have accumulated in traps at the present-day location of the Laisvall deposit, ~20 km southeast of the forebulge.
- The morphology of the orebodies at Laisvall and Vassbo with the most abundant mineralization towards to the roof of the sandstone paleoaquifers reflects the supply of H_2S in traps of accumulated hydrocarbon. Indeed, the main source of hydrogen sulfide at Laisvall (average $\delta^{34}S$ = 24–29‰) was produced in sandstone during thermochemical sulfate reduction (TSR) and oxidation of exogenous hydrocarbons. The source of aqueous sulfate in sandstone was Cambrian to Ordovician seawater (27–33‰) diluted by subsurface formation waters which had oxidized pyrite in organic-rich shale of the Alum Shale Formation (14.5–16‰). A subordinate source of hydrogen sulfide for Pb-Zn sulfide (21–27‰ at Laisvall and 12–18‰ at Vassbo) was the replacement, at an early stage, of diagenetic pyrite and framboidal pyrite. A third localized source of hydrogen sulfide was identified at Laisvall in the feeder fault zone area of the Central Malm faults, where reduced sulfur fixed in sphalerite (2‰) was derived from sulfide (e.g., pyrite) in crystalline basement rocks. Finally, sulfate derived from

barite dissolution also underwent TSR and accounted for part of H_2S used for sphalerite ± galena precipitating in the new porosity ($\delta^{34}S$ values of 14–33‰).

- Continuous and horizontal layers of sulfides roughly parallel to bedding suggest that TSR took place at the hydrocarbon-water interface between distinctly hydrocarbon-filled and underlying water-filled parts of the porosity of the sandstone reservoirs. Upward migration, fluctuation of the hydrocarbon-water interface and formation of H_2S along this interface may explain the alternating layers of galena and sphalerite.
- The occurrence of solid bitumen intimately intergrown with sphalerite suggests that a subordinate amount of H_2S was produced by TSR during Pb-Zn mineralization, as suggested by Thom and Anderson (2008) based on experimental result on the kinetics of TSR. However, the bulk of H_2S is inferred to have been produced by TSR prior to Pb-Zn mineralization.

The proposed genetic model may be applied to explore for additional deposits in Sweden and Norway in autochthonous rocks along the erosional front or beneath the Caledonian orogen. Three key exploration tools are: (i) the identification of reactivated basement structures; (ii) recognition and, petrographic and geochemical characterization of pre-Pb-Zn sulfide stage barite cement; (iii) the identification of the TSR process supplying H_2S for Pb-Zn sulfide precipitation.

Acknowledgements

This research has been financially supported by Boliden AB (Sweden) and the Swiss National Science Foundation (SNF, Switzerland, FN 146 353). The Geological Survey of Sweden (SGU) provided financial and logistic support for much of the fieldwork in Sweden and for the participation of Michael B. Stephens. The staff members at SGU in Malå are thanked for their help at the national core archive. The authors are grateful to Boliden AB including Hans Årebäck (former exploration manager) and Rodney L. Allen (Manager Geology Research and Development) for financial and logistical support for the work carried out in Boliden and also for stimulating discussions. The staff working at the core archive in Boliden is acknowledged for supplying drill cores. Ulf Sandström, field technician in Boliden, is thanked for his help managing the device during extraction of samples from outcrops in the Laisvall mine area. Dr. Thierry Adatte (University of Lausanne, Switzerland) is thanked for carrying out Rock-Eval and total organic carbon analyses of the shale samples.

References

Ader M, Sansjofre P, Halverson GP, Busigny V, Trindade RIF, Kunzmann M, Nogueira ACR (2014) Ocean redox structure across the Late Neoproterozoic Oxygenation Event: A nitrogen isotope perspective. Earth Planet Sc Lett 396:1-13

Anderson GM (2008) The mixing hypothesis and the origin of Mississippi Valley-type ore deposits. Econ Geol 103:1683-1690

Beaumont V, Robert F (1999) Nitrogen isotope ratios of kerogns in Precambrian cherts: record of the evolution of atmosphere chemistry? Prec Res 96:63-82.

Ben Hassen A, Trichet J, Disnar J-R, Belayouni H (2010) Pétrographie et géochimie comparées des pellets phosphatés et de leur gangue dans le gisement phosphaté de Ras-Draâ (Tunisie). Implications sur la genèse des pellets phosphatés. Swiss Journal of Geoscience 103:457-473

Bennett PC (1991) Quartz dissolution in organic-rich aqueous systems. Geochim Cosmochim Acta 55:1781-1797

Bergman S, Stephens MB, Andersson J, Kathol B, Bergman T (2012) Geological map of Sweden: Geological Survey of Sweden, scale 1:1 000 000, 1 sheet

Bharati S, Patience RL, Larter SR, Standen G, Poplett IJF (1995) Elucidation of the Alum Shale kerogen structure using a multi–disciplinary approach. Org Geochem 23:1043–1058

Bjørlykke A, Sangster DF (1981) An overview of sandstone lead deposits and their relation to red-bed copper and carbonate-hosted lead-zinc deposits. Econ Geol 75th Anniversary Volume:179-213

Bradley DC, Leach DL (2003) Tectonic controls of Mississippi Valley-type lead-zinc mineralization in orogenic forelands. Miner Deposita 38:652-667

Brasier MD (1992) Nutrient-enriched waters and the early skeletal fossil record. Journal of the Geological Society, London 49:621-629

Broman C (1983) Fluid inclusion thermometry in sphalerite from the Vassbo lead-zinc deposit, Sweden. Stockholm University, Ore Research Group, Annual Report, pp103-116

Cao J, Hu K, Zhou J, Shi C, Bian L,Yao S (2013) Organic clots and their differential accumulation of Ni and Mo within early Cambrian black-shale-hosted polymetallic Ni-Mo deposits, Zunyi, South China. J Asian Earth Sci 62:531-536

Christofferson HC, Wallin B, Selkman S, Rickard DT (1979) Mineralization controls in the sandstone lead-zinc deposit at Vassbo, Sweden. Econ Geol 74:1239-1249

Chowdhury AH, Noble JPA (1996) Origin, distribution and significance of carbonate cements in the Albert Formation reservoir sandstones, New Brunswick, Canada. Marine and Petroleum Geology 13:837-846

Claypool GE, Holser WT, Kaplan IR, Sakai H, Zak I (1980) The age curves of sulfur and oxygen isotopes in marine sulfate and their mutual interpretation. Chem Geol 28:199-260

Cremonese, L, Shields-Zhou G, Struck U, Ling H-F, Och L, Chen X, Li D (2013) Marine biogeochemical cycling during the early Cambrian constrained by nitrogen and organic carbon isotope study of the Xiaotan section, South China. Prec Res 225:148-165

Dallmeyer RD and Gee DG (1986) $^{40}Ar/^{39}Ar$ mineral dates from retrogressed eclogites within the Baltoscandian miogeocline: Implications for a polyphase Caledonian orogenic evolution: Geologic Society of America Bulletin 97:26-34.

Dove PM (1999) The dissolution kinetics of quartz in aqueous mixed cation solutions. Geochim Cosmochim Acta 63:3715-3727

Dove PM, Nix CJ (1997) The influence of the alkaline earth cations, magnesium, calcium, and barium on the dissolution kinetics of quartz. Geochim Cosmochim Acta 61:3329-3340

Gee DG (1972) The regional geologic context of the Tåsjö uranium project, Caledonian front, Central Sweden. Geologic Survey of Sweden, Årsbok 66 2, Ser C, 671, 37 p.

Gee DG (1975) A tectonic model for the central part of the Scandinavian Caledonides. Am J Sc 275A:468–515

Gee DG, Fossen H, Henriksen N, Higgins AK (2008) From the early Paleozoic platforms of Baltica and Laurentia to the Caledonide orogen of Scandinavia and Greenland. Episodes 31:1-8

Gee DG, Juhlin C, Pascal C, Robinson P (2010) Collisional orogeny in the Scandinavian Caledonides (COSC). Journal of the Geologic Survey of Sweden (GFF) 132:29-44

Gee DG, Ladenberger A, Dahlqvist P, Majka J, Be'eri-Shlevin Y, Frei D, Thomsen T (2013) The Baltoscandian margin detrital zircon signatures of the central Scandes. In: Corfu F, Gasser D, Chew DM (eds) New Perspectives on the Caledonides of Scandinavia and Related Areas. London, Geologic Society Special Publication 390:131-155

Gelpi E, Schneider H, Mann J, Oro J (1970) Hydrocarbons of geochemical significance in microscopic algae. Phytochemistry 9:603–612.

Gerdemann PE, Meyers HE (1972) Relationships of carbonate facies patterns to ore distribution and to ore genesis in the Southeast Missouri lead district. Econ Geol 67:426-433

Gill BC, Lyons TW, Young SA, Kump LR, Knoll AH, Saltzman MR (2010) Geochemical evidence for widespread euxinia in the Later Cambrian ocean. Nature 469:80-83

Goldhaber MB, Orr WL (1995) Kinetic controls on thermochemical sulfate reduction as a source of sedimentary H_2S. In: Vairavamurthy MA, Schoonen MAA (eds) Geochemical transformations of sedimentary sulfur. ACS Symposium Series 612, pp 412-425

Greenwood PF, Brocks JJ, Grice K, Schwark L, Jaraula CMB, Dick JM, Evans KA (2013) Organic geochemistry and mineralogy. I. Characterization of organic matter associated with metal deposits. Ore Geology Reviews 50:1–27

Gregg JM (1985) Regional epigenetic dolomitization in the Bonneterre Dolomite (Cambrian), southeastern Missouri. Geology 13:503-506

Gromet LP, Sjöström H, Bergman S, Claesson S, Essex RM, Andreasson PG and Albrecht L (1996) Contrasts in ages of metamorphism in the Seve Nappes: U-Pb results from the central and northern Swedish Caledonides: Journal of the Geologic Survey of Sweden (GFF) 118:36-38

Hanor JS (1996) Controls on the solubilization of lead and zinc in basinal brines. Society of Economic Geologists Special Publication 4:483-500

Hanor JS (2000) Barite-celestite geochemistry and environments of formation. Reviews in Mineralogy and Geochemistry 40:193-275

Heijlen W, Muchez P, Banks DA, Schneider J, Kucha H, Keppens E (2003) Carbonate-hosted Zn-Pb deposits in Upper Silesia, Poland: Origin and evolution of mineralizing fluids and constraints on genetic models. Econ Geol 98:911-932

Heydari E, Moore CH (1989) Burial diagenesis and thermochemical sulfate reduction, Smackover Formation, southeastern Mississippi Salt Basin. Geology 12:1080-1084

Ishikawa T, Ueno Y, Komiya T, Sawaki Y, Han J, Shu D, Li Y, Maruyama S, Yoshida N (2008) Carbon isotope chemostratigraphy of a Precambrian/Cambrian boundary section in the Three Gorge area, South China: Prominent global-scale isotope excursions just before the Cambrian Explosion. Gondwana Research 14:193-208

Israelson C, Halliday AN, Buchardt B (1996) U-Pb dating of calcite concretions from Cambrian black shales and the Phanerozoic time scale. Earth Planet Sc Lett 141:153-159

Johansson Å, Rickard DT (1984) Isotope composition of Phanerozoic ore leads from the Swedish Segment of the Fennoscandian Shield. Miner Deposita 19:249-255

Jones HD, Kesler SE, Furman FC, Kyle JR (1996) Sulfur isotope geochemistry of Southern Appalachian Mississippi Valley-type deposits. Econ Geol 91:355-367

Kelley KD, Leach DL, Johnson CA, Clark JL, Fayek M, Slack JF, Anderson VM, Ayuso RA, Ridley WI (2004) Textural, compositional, and sulfur isotope variations of sulfide minerals in the Red Dog Zn-Pb-Ag deposits, Brooks Range, Alaska: Implications for ore formation. Econ Geol 99:1509-1532

Kendrick MA, Burgess R, Harrison D, Bjørlykke A (2005) Noble gas and halogen evidence for the origin of Scandinavian sandstone-hosted Pb-Zn deposits. Geochim Cosmochim Acta 69:109-129

Kesler SE, Jones HD, Furman FC, Sassen R, Anderson WH, Kyle JR (1994) Role of crude oil in the genesis of Mississippi Valley-type deposits: Evidence from the Cincinnati arch. Geology 22:609-612

Knauss KG, Copenhaver SA, Braun RL, Burnham AK (1997) Hydrous pyrolysis of New Albany and Phosphoria Shales: production kinetics of carboxylic acids and light hydrocarbons and interactions between the inorganic and organic chemical systems. Org Geochem 27:477–496

Kribek B, Sykorova I, Pasava J, Machovic V (2007) Organic geochemistry and petrology of barren and Mo-Ni-PGE mineralized marine black shales of the Lower Cambrian Niutitang Formation (South China). Coal Geology 72:240-256

Krouse HR, Viau CA, Eliuk LS, Ueda A, Halas S (1988) Chemical and isotopic evidence of thermochemical sulfate reduction by light hydrocarbon gases in deep carbonate reservoirs. Nature 333:415-419

Kullerud K, Stephens MB, Zachrisson E (1990) Pillow lavas as protoliths for eclogites: evidence from a late Precambrian–Cambrian continental margin, Seve Nappes, Scandinavian Caledonides: Contributions to Mineralogy and Petrology 99:344-351

Leach DL, Bradley D, Lewchuk MT, Symons DTA, de Marsily G, Brannon J (2001) Mississippi Valley-type lead-zinc deposits through geological time: Implications from recent age-dating research. Miner Deposita 36:711-740.

Leach DL, Sangster DF, Kelley KD, Large RR, Garven G, Allen CR, Gutzmer J, Walters S (2005) Sediment-hosted Pb-Zn deposits: A global perspective. Economic Geology 100th Anniversary Volume:561–607

Leach DL, Taylor RD, Fey DL, Diehl SF, Saltus RW (2010) A deposit model for Mississippi Valley-type lead-zinc ores. Scientific Investigations Report 2010-5070-A, US Geological Survey, pp 52

Lev SM, McLennan SM, Hanson GN (1998) Mineralogic controls on REE mobility during black-shale diagenesis. Journal of Sedimentary Research 69:1071-1082

Lindblom S (1986) Textural and fluid inclusion evidence for ore deposition in the Pb-Zn deposit at Laisvall, Sweden. Econ Geol 81:46-64

Ljungner E (1950) Urbergsytans form vid Fjällranden. Journal of the Geological Survey of Sweden (GFF) Bd 72:H 3 (in Swedish)

Lucks TJ (2004) Controls on the ore distribution of the Laisvall deposit, Sweden. Unpublished Doctoral Thesis University of Cardiff, Cardiff, UK

Lyle JR (1977) Petrography and carbonate diagenesis of the Bonneterre Formation in the Viburnum Trend area, Southeast Missouri. Econ Geol 72:420-434

Machel HG (1987) Some aspects of diagenetic sulfate-hydrocarbon redox-reactions. In: Marshall JD (ed) Diagenesis of sedimentary sequences. Geol Soc Spec Publ 36:15-28

Machel HG (2001) Bacterial and thermochemical sulfate reduction in diagenetic settings–old and new insights. Sedim Geol140:143–175

Menotti TA (2006) Lower Paleozoic oxygen isotope values from carbonate rocks: Primary or diagenetic? Senior thesis in Geosciences, Bachelor of Science, Pennsylvania State University, Pennsylvania, USA, pp 43

Muhling JR, Fletcher IR, Rasmussen B (2012) Dating fluid flow and Mississippi Valley-type base-metal mineralization in the Paleoproterozoic Earaheedy Basin, Western Australia. Prec Res 212-213:75-90

Nelson GJ, Pufahl PK, Hiatt EE (2010) Paleoceanographic constraints on Precambrian phosphorite accumulation, Baraga Group, Michigan, USA. Sedim Geol 226:9-21

Nielsen AT, Schovsbo NH (2011) The Lower Cambrian of Scandinavia: Depositional environment, sequence stratigraphy and paleogeography. Earth-Science Reviews 107:207-310

Oberger B, Gallien J-P, Pinti DL, Fialin M, Daudin L, Gröcke DR, Pasava J (2005) Nitrogen and carbon partitioning in diagenetic and hydrothermal minerals from Paleozoic black shales (Selwyn Basin, Yukon Territories, Canada). Chem Geol 218:249-264

Oberger B, Pasava J, Gallien J-P, Daudin L, Pinti DL (2003) Biogenic and abiogenic hydrothermal sulfides: controls of rare metal distribution in black shales (Yukon Territories, Canada). Journal of Geochemical Exploration 78-79:559-563

Ohmoto H, Rye RO (1979) Isotopes of sulfur and carbon. In: Barnes HL (ed) Geochemistry of Hydrothermal Ore Deposits, Wiley, New York, pp 509-567

Pirrie D, Butcher AR, Power MR, Gottlieb P, Miller GL (2004) Rapid Quantitative Mineral and Phase Analysis Using Automated Scanning Electron Microscopy (QEMSCAN); Potential Applications in Forensic Geoscience. Geological Society, London, Special Publication 232:123-136.

Prokoph A, Shields GA, Veizer J (2008) Compilation and time-series analysis of a marine carbonate $\delta^{18}O$, $\delta^{13}C$, $^{87}Sr/^{86}Sr$ and $\delta^{34}S$ database through Earth history. Earth-Science Reviews 87:113-133

Rasmussen B (1996) Early diagenetic REE-phosphate minerals (florencite, gorceixite, crandallite, and xenotime) in marine sandstones: a major sink for oceanic phosphorous. Am J Sc 296:601-632

Rickard DT (1983) Precipitation and mixing mechanisms in Laisvall-type sandstone Pb-Zn deposits. In: Kirsvarsanyi G, Hagni R, Pratt W and Koening JW (eds) Proceedings of the International Conference on Mississippi Valley Type Lead-Zinc Deposits. Rolla, Missouri, 1983

Rickard DT, Willdén M, Mårde Y, Ryhage R (1975) Hydrocarbons associated with Pb–Zn ores at Laisvall, Sweden. Nature 255:131–133

Rickard DT, Willdén MY, Marinder NE, Donnelly TH (1979) Studies on the genesis of the Laisvall sandstone lead-zinc deposit, Sweden. Econ Geol 74:1255-1285

Rickard DT, Coleman M, Swainbank I (1981) Lead and sulfur isotopic compositions of galena from the Laisvall sandstone Pb-Zn deposit, Sweden. Econ Geol 76:2042-2046

Rimstidt JD (1977) Gangue mineral transport and deposition. In: Barnes HL (ed) Geochemistry of hydrothermal ore deposits-third edition: New York, John Wiley, pp. 487–515

Roberts D, Gee DG (1985) An introduction to the structure of the Scandinavian Caledonides. In: Gee DG, Sturt BA (eds) The Caledonide Orogen–Scandinavia and related areas, Wiley, Chichester, pp. 55–68

Roberts D, Siedlecka A (2002) Timanian orogenic deformation along the northeastern margin of Baltica, Northwest Russia and Northeast Norway, and Avalonian–Cadomian connections: Tectonophysics 352:169-184.

Romer R (1992) Sandstone-hosted lead-zinc mineral deposits and their relation to the tectonic mobilization of the Baltic Shield during the Caledonian orogeny, a reinterpretation: Miner Petro 47:67-85.

Root D, Corfu F (2012) U-Pb geochronology of two discrete Ordovician high-pressure metamorphic events in the Seve Nappe Complex, Scandinavian Caledonides: Contribution to Mineralogy and Petrology 163:769-788

Rowan EL (1986) Cathodoluminescent zonation in hydrothermal dolomite cements: Relationship to Mississippi Valley-type Pb-Zn mineralization in southern Missouri and northern Arkansas. In: Hagni RD (ed) Process mineralogy VI, Warrendale, Pennsylvania, Metallurgical Society, pp. 69-87

Saintilan NJ (2015) Key controls, age, source of metals and role of hydrocarbons on the origin of Laisvall-type Pb-Zn deposits and their relationship to calcite-fluorite-Zn±Pb sulfide vein-type mineralization in Baltica basement (Sweden). PhD thesis, University of Geneva, Geneva, Switzerland.

Saintilan NJ, Stephens MB, Lundstam E, Fontboté L (2015) Control of reactivated basement structures on sandstone-hosted Pb-Zn deposits along the Caledonian Front, Sweden: Evidence from airborne magnetic field data, structural analysis and ore grade modeling. Econ Geol110:91-117.

Saintilan NJ, Schneider J, Stephens MB, Chiaradia M, Kouzmanov K, Wälle M, Fontboté L (*in press*) A Middle Ordovician age for the Laisvall sandstone-hosted Pb-Zn deposit, Sweden: A response to early Caledonian orogenic activity. Econ Geol

Santallier DS (1988) Mineralogy and crystallization of the Seve eclogites in the Vuoggatjålme area, Swedish Caledonides of Norrbotten: Journal of the Geologic Society of Sweden (GFF) 110:89-98

Shen C, Pratt BR, Zhang X-G (2014) Phosphatized coprolites from the middle Cambrian (Stage 5) Duyun fauna of China. Palaeogeography, Palaeoclimatology, Palaeoecology 410:104-112.

Shields-Zhou G, Zhu M (2013) Biogeochemical changes across the Ediacaran–Cambrian transition in South China. Prec Res 225:1-6

Simpson G, Yang C, Hutcheon I (1996) Thermochemical sulfate reduction: a local process that does not generate thermal anomalies. In: Ross GM (ed) Alberta Basement Transect Workshop, Lithoprobe Report 51, pp 241-245

Skiöld T (1988) Implications of new U-Pb zircon chronology to early Proterozoic crustal accretion in northern Sweden. Prec Res 38:147-164

Söderlund U, Isachsen C, Bylund G, Heaman L, Patchett PJ, Vervoort JD, Andersson UB (2005) U-Pb baddeleyite ages and Hf, Nd isotope chemistry constraining repeated mafic magmatism in the Fennoscandian Shield from 1.6 to 0.9 Ga. Contributions to Mineralogy and Petrology 150:174-194

Soudry D, Champetier Y (1983) Microbial processes in the Negev phosphorites (southern Israel). Sedimentology 30:411-423.

Spangenberg JE, Sharp Z, Fontboté L (1995) Apparent stable isotope heterogeneities in gangue carbonates of the Mississippi Valley-type Zn-Pb deposit of San Vicente, central Peru. Miner Deposita 30:67-74.

Spangenberg JE, Fontboté L, Sharp Z, Hunziker J (1996) Carbon and oxygen isotope study of hydrothermal carbonates in the Zn-Pb deposits of San Vicente, central Peru: a quantitative modeling on mixing processes and CO_2 degassing. Chem Geol 133:289-315

Spangenberg JE, Macko SA (1998) Organic geochemistry of the San Vicente Zn-Pb district, eastern Pucará Basin, Peru. Chem Geol 146:1-23

Spangenberg JE, Herlec U (2006) Hydrocarbon biomarkers in the Topla-Mežica Zn-Pb deposits, Northern Karavanke/Drau Range, Slovenia: Paleoenvironment at the site of ore formation. Econ Geol 101:997-1021

Spangenberg JE, Bagnoud–Velásquez M, Boggiani PC, Gaucher C (2014) Redox variations and bioproductivity in the Ediacaran: Evidence from inorganic and organic geochemistry of the Corumbá Group, Brazil. Gondwana Research 26:1186-1207.

Stephens MB (1988) The Scandinavian Caledonides: a complexity of collisions: Geology Today 4:20-26

Sturt BA (1978) The Norwegian Caledonides. Geological Survey of Canada Paper 78:13-16

Surdam RC, Boese SW, Crossey LJ (1984) The chemistry of secondary porosity. In: McDonald DA, Surdam RC (eds) Clastic diagenesis, American Association of Petroleum Geologists Memoir 37, pp 127-149

Surdam RC, Yin P (1993) Organic acids and carbonate stability, the key to predicting positive porosity anomalies. In: Pittman ED, Lewan MD (eds) Organic acids in Geological Processes, Springer-Verlag, Berlin-Heidelberg-New York, pp 399-448

Thickpenny A (1984) The sedimentology of the Swedish alum shales. In: Stow DAV, Piper DJW (eds) Fine-grained sediments, Geological Society Special Publications 15, London, pp. 511–525

Thom J, Anderson GM (2008) The role of thermochemical sulfate reduction in the origin of Mississippi Valley-type deposits. I. Experimental results. Geofluids 8:16-26

Veizer J (2004) Isotope data, Phanerozoic database, $\delta^{18}O$ update-2004: http://www.science.uottawa.ca/geology/isotope_data

Veizer J, Ala D, Azmy K, Bruckschen P, Buhl D, Bruhn F, Carden GAF, Diener A, Ebneth S, Godderis Y, Jasper T, Korte C, Pawellek F, Podlaha OG, Strauss H (1999) $^{87}Sr/^{86}Sr$, $\delta^{13}C$ and $\delta^{18}O$ evolution of Phanerozoic seawater. Chem Geol161:59-88

Vidal G, Nystuen JP (1990) Lower Cambrian acritarchs and the Proterozoic–Cambrian boundary in southern Norway. Norsk Geologisk Tidsskrift 70:191–222

Voss RL, Hagni RD (1985) The application of cathodoluminescence microscopy to the study of sparry dolomite from the Viburnum Trend, Southeast Missouri. In: Hausen DM, Kopp OC (eds) Mineralogy; applications to the mineral industry: Proceedings of the Paul F. Kerr Memorial Symposium, pp. 51-68.

Wallin B (1982) Sedimentology of the Lower Cambrian sequence at Vassbo, Sweden. PhD thesis Acta Universitatis Stockholmiensis, Stockholm, Sweden

Willdén MY (1980) Paleoenvironment of the autochthonous sedimentary rocks sequence at Laisvall, Swedish Caledonides. PhD thesis Stockholms Universitets Geologiska Institutionen, Stockholm, Sweden

Worden RH, Smalley PC, Oxtoby NH (1995) Gas souring by thermochemical sulfate reduction at 140°C. Am Assoc Pet Geol Bull 79:854-863

Xue C, Zeng R, Liu S, Chi G, Qing H, Chen Y, Yang J, Wang D (2007) Geologic, fluid inclusion and isotopic characteristics of the Jinding Zn–Pb deposit, western Yunnan, South China: A review. Ore Geology Reviews 31:337-359

Polyphase Vein-Type Mineralization in the Fennoscandian Shield at Åkerlandet, Järvsand and Laisvall along the Erosional Front of the Caledonian Orogen, Sweden

Nicolas J. Saintilan[1], Jens Schneider[2], Massimo Chiaradia[1], Richard Spikings[1], Jorge E. Spangenberg[3], Alexey Ulianov[4], Michael B. Stephens[5,6], Lluís Fontboté[1]

[1]*Department of Earth and Environmental Sciences, University of Geneva, Rue des Maraîchers 13, 1205 Geneva, Switzerland*

[2]*Department of Mineralogy, Technische Universität Bergakademie Freiberg, Brennhausgasse 14, 09596 Freiberg, Germany*

[3]*Institute of Earth Surface Dynamics, University of Lausanne, Building Geopolis, 1015 Lausanne, Switzerland*

[4]*Institute of Earth Sciences, University of Lausanne, Building Geopolis, 1015 Lausanne, Switzerland*

[5]*Geological Survey of Sweden (SGU), Box 670 SE-751 28 Uppsala, Sweden*

[6]*Department of Civil, Environmental and Natural Resources Engineering, Division of Geosciences, Luleå University of Technology, SE-971 87 Luleå, Sweden*

Corresponding author:

Nicolas J. Saintilan

nicolas.saintilan@unige.ch

Tel: +41 22 379 66 97

Fax: +41 22 379 32 10

Keywords calcite-fluorite, vein, Paleoproterozoic, Fennoscandian Shield, adularia, sphalerite, transtensional, reactivation, Sveconorwegian, Caledonian

Abstract

Three calcite-fluorite-sulfide vein deposits and occurrences in crystalline basement rocks (continent Baltica) of the Fennoscandian Shield were studied at Åkerlandet, Järvsand and Laisvall, Sweden. The Åkerlandet and Järvsand occurrences are located along the current erosional front of the Caledonian orogen. Similar mineralization in form of veinlets is found at Laisvall in the granitic basement beneath unconformable Ediacaran to Cambrian siliciclastic cover rocks that are in turn overlain by Caledonian thrust nappes. The sandstone-hosted Mississippi Valley-type Laisvall Pb-Zn deposit (mined until 2001) occurs in this autochthonous sedimentary sequence.

At the three studied vein systems, fractures striking NNW–SSE and NNE–SSW to NE–SW were filled in by calcite, fluorite ± pyrite ± galena. At Laisvall, such basement-hosted veins have the same orientation as cover-hosted faults interpreted as feeders to the sandstone-hosted Pb-Zn deposits. At Järvsand, structural analysis showed that these veins formed along NNE–SSW R-shears to a main N–S shear fault zone with dextral component of movement as a response to NW–SE bulk horizontal extension.

At Åkerlandet, at least two mineral generations preceded the precipitation of fluorite and calcite. Fractures composing a sinistral N–S shear zone in transtension with NW–SE R-Riedel shears formed or re-opened in late Sveconorwegian time (^{40}Ar-^{39}Ar thermochronology on adularia delivers a preliminary age between 950 and 980 Ma) as a result of bulk horizontal ENE–WSW extension. Adularia-quartz precipitated in open space from slightly acidic, low-temperature fluids prior to sphalerite ± galena mineralization for which available Rb-Sr isotope geochemistry data on sphalerite are consistent either with an age of 544 ± 4 Ma (late Ediacaran) or of 468 ± 5 Ma (Middle Ordovician). Zn ± Pb sulfides were formed by saline, relatively oxidizing, low-temperature (110° to 160°C) and slightly acidic hydrothermal fluids transporting metals and deriving H_2S (δ^{34}S values of –3.1 to 0.1‰) from the leaching of minor sulfides in basement rocks that were sericitized in places.

Precipitation of fluorite and calcite in basement fractures at Åkerlandet and Laisvall resulted from the mixing of (i) evolved, basement-interacted (calcite and fluorite with ^{87}Sr/^{86}Sr ratios of 0.717–0.732), near neutral, metal-poor and relatively reduced (negative Eu anomaly recorded in calcite, log f_{O2} = around –55) fluids with (ii) organic matter-interacted, H_2S-bearing fluids likely derived from sedimentary cover rocks including the middle Cambrian to Lower Ordovician Alum Shale Formation (as suggested by petrographic evidence of bitumen and S, C, O isotope data).

At Laisvall, our data suggest that the same basement structures were used at a previous stage in Middle Ordovician time (467 ± 5 Ma) as plumbing system by oxidizing, slightly acidic, metal-bearing brines involved in Pb-Zn mineralization in the overlying sandstone.

The new results are consistent with polyphase brittle deformation and fracture opening recording c. 500 Ma of hydrothermal activity in this part of the Fennoscandian Shield, i.e., a pattern similar to the basement-hosted fracture system at Forsmark in southern Sweden where multi-disciplinary studies highlighted more than 1700 Ma of hydrothermal activity.

Introduction

Mineralized vein deposits and occurrences (Fig. 1), commonly referred to as "calcite-galena veins" in the literature, occur along the coastline of the Barents Sea and Baltic Sea in Norway, Sweden, Finland, and the Russian Federation (e.g., Moorbath and Vokes, 1963; Wickman et al., 1963; Grip, 1967, 1973; Gee, 1972; Johansson and Rickard, 1984; Lindahl and Bjørlykke, 1988; Sundblad, 1990). Mineralization is observed along fractures in Paleoproterozoic and Archean crystalline rocks of the Fennoscandian Shield (Koistinen et al., 2001) comprising the Ediacaran to Silurian continent Baltica.

Similar vein deposits are reported along the eastern erosional front of the Caledonian orogen in Sweden and Norway. These include the calcite-fluorite-Zn ± Pb sulfide vein deposit and occurrence at Åkerlandet and Järvsand (Johansson, 1983a, 1983b, 1984) as well as similar deposits in the Storuman vein district (Billström et al., 2012), all hosted by Paleoproterozoic crystalline or metasedimentary rocks belonging to continent Baltica (Fig. 1). Sulfides, calcite and fluorite in all these vein deposits have been assumed in previous works to be co-genetic and related to a single hydrothermal event.

Owing to the proximity of these basement-hosted vein deposits with the erosional front of the Caledonian orogen and the mineralogical similarities (calcite, fluorite, Pb-Zn sulfides) shared with Laisvall-type Pb-Zn deposits hosted in Ediacaran to Cambrian sandstone currently located at this erosional front (e.g., Laisvall, Vassbo; Grip, 1967, 1973; Rickard et a., 1979; Christofferson et al., 1979; Saintilan et al., 2015, *in press*), a genetic link between these two types of deposit was investigated in several studies (e.g., Wickman et al., 1963; Grip, 1967; Johansson and Rickard, 1984). In particular, Johansson and Rickard (1984) stated that certain vein deposits represent feeder traces of metal-bearing fluids in the crystalline basement for Laisvall-type mineralization.

Benefiting from access to legacy data and exploration reports from the 1930's to 2000's from Boliden AB Sweden, Saintilan et al. (2015) re-discovered calcite-fluorite-pyrite ± chalcopyrite veinlets in the crystalline Paleoproterozoic basement beneath the Laisvall Pb-Zn deposit (Fig. 1). These veinlets had been reported during exploration drilling in 1951 (Claesson, 1951 Boliden AB internal reports, unpub.) but had never been studied.

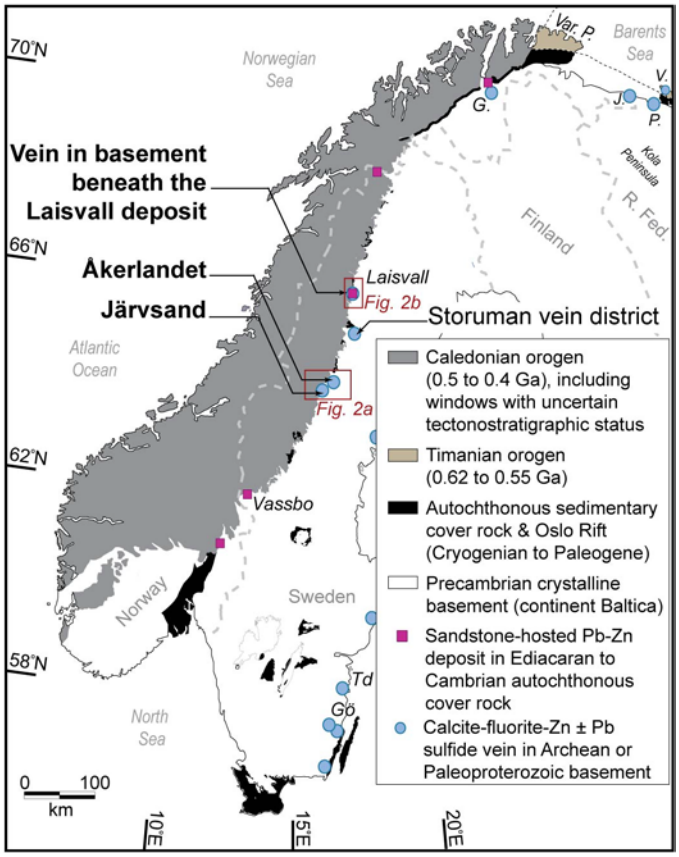

Fig. 1 Simplified geologic map of Scandinavia (modified after Roberts and Siedlecka, 2002; Gee et al., 2008 and Bergman et al., 2012). The locations of calcite-fluorite-Zn ± Pb sulfide vein-type mineralization in the Åkerlandet and Storuman areas hosted by Paleoproterozoic crystalline basement rocks along the erosional front of the Caledonian orogen, northern Sweden, are shown. The locations of similar vein-type mineralization in Paleoproterozoic basement rocks in northern Norway (e.g. G.: Gurrogaissa), in Archean basement rocks in northern Norway and Russia (e.g. J.: Jakobselv, P.: Peuravuono), in rocks of the Timanian orogen in Russia (e.g. V.: Vaitolahti) and in Paleoproterozoic rocks in southern Sweden (e.g. Td: Tindered, Gö: Götemar) are also presented (after Gee, 1972; Sundblad, 1990; Alm et al., 2005). In addition, the locations of Pb-Zn deposits hosted by Ediacaran to Cambrian sandstone in siliciclastic sedimentary cover rock to the crystalline basement along the erosional front of the Caledonian orogen are shown (after Zachrisson, 1980; Stephens, 1986). Abbreviations: R. Fed.: Russian Federation; Var. P.: Varanger Peninsula.

The current work focuses on these Åkerlandet, Järvsand and Laisvall basement vein deposits and occurrences. It has been designed to (1) present the first study of the structural setting of vein-type mineralization at Åkerlandet and Järvsand; (2) provide paragenetic sequences, and descriptions of previously unrecognized minerals and host rock alteration at the three vein occurrences; (3) make an attempt to date these mineralogical components (^{40}Ar-^{39}Ar thermochronology on adularia at Åkerlandet; Sm-Nd geochronology on calcite and fluorite at Åkerlandet and Laisvall); (4) carry out radiogenic and stable isotope geochemistry work (Sr, Sm, Nd, S, C and O) on calcite, fluorite and sulfides to provide information on the composition and redox properties of the fluid(s) that formed these veins. Owing to the limited outcropping conditions in these veins, constraints based on points (3) and (4) remain limited. The findings of points 1 to 4 should test the conclusions drawn by Johansson and Rickard (1984) regarding a genetic link between basement-hosted vein-type mineralization and Laisvall-type deposits. In addition, the current study ambitions to determine whether basement-hosted

vein deposits reflect a single phase or polyphase hydrothermal activity and reactivation of structures in the Fennoscandian Shield.

On the basis of airborne magnetic data, structural analysis, geologic modeling in 3D space and Rb-Sr geochronology of sphalerite, two recent studies at Laisvall (Fig. 1) showed that reactivation of Paleoproterozoic structures in the crystalline Baltica basement occurred during deposition of Ediacaran to Cambrian sandstone while metal-bearing brines resurged through these same structures during strata-bound Pb-Zn mineralization in sandstone in Middle Ordovician time (467 ± 5 Ma), as a response to early Caledonian orogenic activity (Saintilan et al., 2015, *in press*). In addition, Billström et al. (2012) reported a late Ediacaran Rb-Sr age of 531 ± 6 Ma for sphalerite mineralization in basement-hosted vein deposits in the Storuman district. Saintilan et al. (*in press*) presented two hypotheses, both geologically meaningful, for the timing of sphalerite mineralization at Åkerlandet using Rb-Sr sphalerite geochronology at 544 ± 4 Ma, similar to data from the Storuman district, or at 468 ± 5 Ma, similar to the timing of strata-bound Pb-Zn mineralization at Laisvall.

This array of evidence, combined with the findings of polyphase brittle deformation and at least three mineral generations recording more than 1700 Ma of hydrothermal activity in the Fennoscandian Shield at, for example, Forsmark in southern Sweden (Sandström et al., 2009; Saintot et al., 2011; Stephens et al., 2015), suggests a long history of activation or re-activation of brittle structures over the entire shield.

Geologic setting

Baltica basement, sedimentary cover rocks, and Timanian and Caledonian orogens

In the northern and central parts of Sweden (Fig. 1), the crystalline Baltica basement is dominated by Paleoproterozoic and Archean rocks affected by a 2.0 to 1.8 Ga orogenic system (Svecokarelian orogen; Koistinen et al., 2001). Late Paleoproterozoic to early Neoproterozoic (1.7 to 0.9 Ga), generally better-preserved magmatic and sedimentary rocks, are a subordinate component.

The Baltica continent formed after rifting and subsequent opening of the Iapetus Ocean around 610 Ma (Gee, 1975; Svenningsen, 2001) and was subsequently overlain by a thin platformal cover of Ediacaran to Silurian sedimentary rocks initiated on its western continental margin (present-day coordinates; Fig. 1). Along the north-eastern continental margin of Baltica (present-day coordinates; Fig. 1), sedimentation onto Archean and Paleoproterozoic crystalline basement rocks commenced in the early Cryogenian and continued in the Ediacaran (Roberts and Siedlecka, 2002). Sedimentation occurred in an elongate basin controlled by important NW–SE faults along pre-existing, deep-seated anisotropies in the basement (Roberts and Siedlecka, 2002). These sedimentary rocks are tectonically juxtaposed to the north against folded and metamorphosed rocks belonging to the 0.62 to 0.55 Ga Timanian orogen (Roberts and Siedlecka, 2002; Pease et al., 2008; Fig. 1).

In the western part of Scandinavia, the Baltica basement and sedimentary cover rocks as well as the Timanian orogen are overlain by thrust sheets belonging to the 0.5 to 0.4 Ga Caledonian orogen

(Gee, 1975; Roberts and Gee 1985; Fig. 1), which resulted from a polyphase tectonic evolution (Gee, 1972; Sturt, 1978; Dallmeyer and Gee, 1986). A foreland basin developed during the Lower to Middle Ordovician as a response to the early collision of the western margin to Baltica with an outboard island arc, the collision producing a mountain belt comprising mixed accreted Neoproterozoic rocks from the western continental margin to Baltica and oceanic material. The rocks derived from this continental margin, preserved northwest of Laisvall in the allochthonous units referred to as the Seve Nappe Complex, contain eclogites that were exhumed to higher crustal levels at c. 490 to 460 Ma (Dallmeyer and Gee, 1986; Santallier, 1988; Stephens, 1988; Kullerud et al., 1990; Gromet et al., 1996; Greiling and Garfunkel, 2007; Root and Corfu, 2012). The early continent-arc collision and foreland basin development preceded the closure of the Iapetus Ocean and terminal continent-continent (Baltica-Laurentia) collision, which probably began at c. 450 Ma, during the latest part of the Ordovician, and continued through the Silurian into Devonian time with emplacement of the Caledonian thrust nappes (Gee, 1975; Stephens, 1988; Gee et al., 2010; Root and Corfu, 2012).

Calcite-fluorite-Zn ± Pb sulfide vein deposits along the erosional front of the Caledonian orogen

Moorbath and Vokes (1963), Wickman et al. (1963), Grip (1967, 1973), Gee (1972), Johansson and Rickard (1984), Lindahl and Bjørlykke (1988) and Sundblad (1990) reported several "calcite-galena vein" deposits in the Paleoproterozoic and Archean basement of Baltica. Several of these vein deposits and occurrences occur 10 to 35 km east of the erosional front of the Caledonian orogen in Sweden and Norway (Fig. 1). In addition, quartz-calcite-barite-galena-sphalerite or calcite-galena veins (Sundblad, 1990) are found along the shoreline of the Kola Peninsula in Norway and Russia (Fig. 1). In all cases, lead isotope studies suggest that Pb in galena was derived from local Precambrian basement rocks (Johansson, 1983a; Johansson and Rickard, 1984; Lindhal and Bjørlykke, 1988; Sundblad, 1990; Romer and Wright, 1993; Billström et al., 2012).

Along the current erosional front of the Caledonian orogen, in the central part of Sweden, the calcite-fluorite-Zn ± Pb sulfide vein deposits and occurrences at Åkerlandet and Järvsand in the Åkerlandet district studied in this work (Figs. 1) are hosted by migmatitic paragneiss with leucogranite (1.9 Ga) and coarsely porphyritic granite (1.8 Ga), respectively (Fig. 2a). Similar vein deposits hosted by metasedimentary rocks (1.9 Ga) intruded by the same 1.8 Ga granite occur in the Storuman district 75 km north of Åkerlandet (Fig. 1). Microthermometry studies of single fluid inclusions in calcite, fluorite and sphalerite suggested that the vein deposits in both districts formed from hot (160–200°C) saline hydrothermal fluids (Johansson, 1983b, 1984; Billström et al., 2012), possibly involving locally mixing with cooler (< 70°C) less saline fluid (cf., Billström et al., 2012).

Basement-hosted calcite-fluorite-pyrite ± chalcopyrite veinlets were reported ~200 km north of the Storuman vein district, beneath the strata-bound Pb-Zn deposit hosted by Ediacaran to Cambrian sandstone at Laisvall (Saintilan et al., 2015; Fig. 1). Vein-type mineralization is hosted by Paleoproterozoic (1.8 Ga) granite (Skiöld, 1988; Saintilan et al., 2015). The veinlets are situated ~350

m underneath sedimentary cover rocks, including Ediacaran to Cambrian sandstone (Laisberg Formation) overlain by Cambrian shale and siltstone (Grammajukku Formation), Cambrian to Lower Ordovician carbonaceous shale (Alum Shale Formation), and, at a higher structural level, the Caledonian thrust nappes (Fig. 2b). These basement-hosted veinlets at Laisvall, studied in the present work, are located close to the southern segments of two faults in the sandstone (Fig. 2b), which formed by reactivation of structures in the Paleoproterozoic basement (Saintilan et al., 2015). These authors and a complementary geochronological study (Saintilan et al., *in press*) proposed that at least one of these faults, the Nadok fault (Fig. 2b), was active during mineralization in sandstone during Middle Ordovician time, forming a channel way for metal-bearing brines, which migrated through and leached metals from permeable basement rocks.

Lilljequist (1965, 1973) conducted a systematic survey of faults and joints in the Paleoproterozoic basement in the Laisvall area and in the mine. The basement is strongly fractured and joint planes are often covered in epidote, chlorite and iron oxides. Joints filled with fluorite-calcite-pyrite ± chalcopyrite have been observed more rarely. Three main join sets were recognized: (1) NNW–SSE to NW–SE joints, dipping moderately to SW with slickenlines suggesting thrust movement from SW. No differential movement can be seen. Both calcite and fluorite coat these joints; (2) NNW–SSE joints, steeply dipping to NE and coated with both calcite and fluorite; (3) NNE–SSW to NE–SW joints, subvertical, calcite coating. Barren subvertical N–S fractures are also abundant.

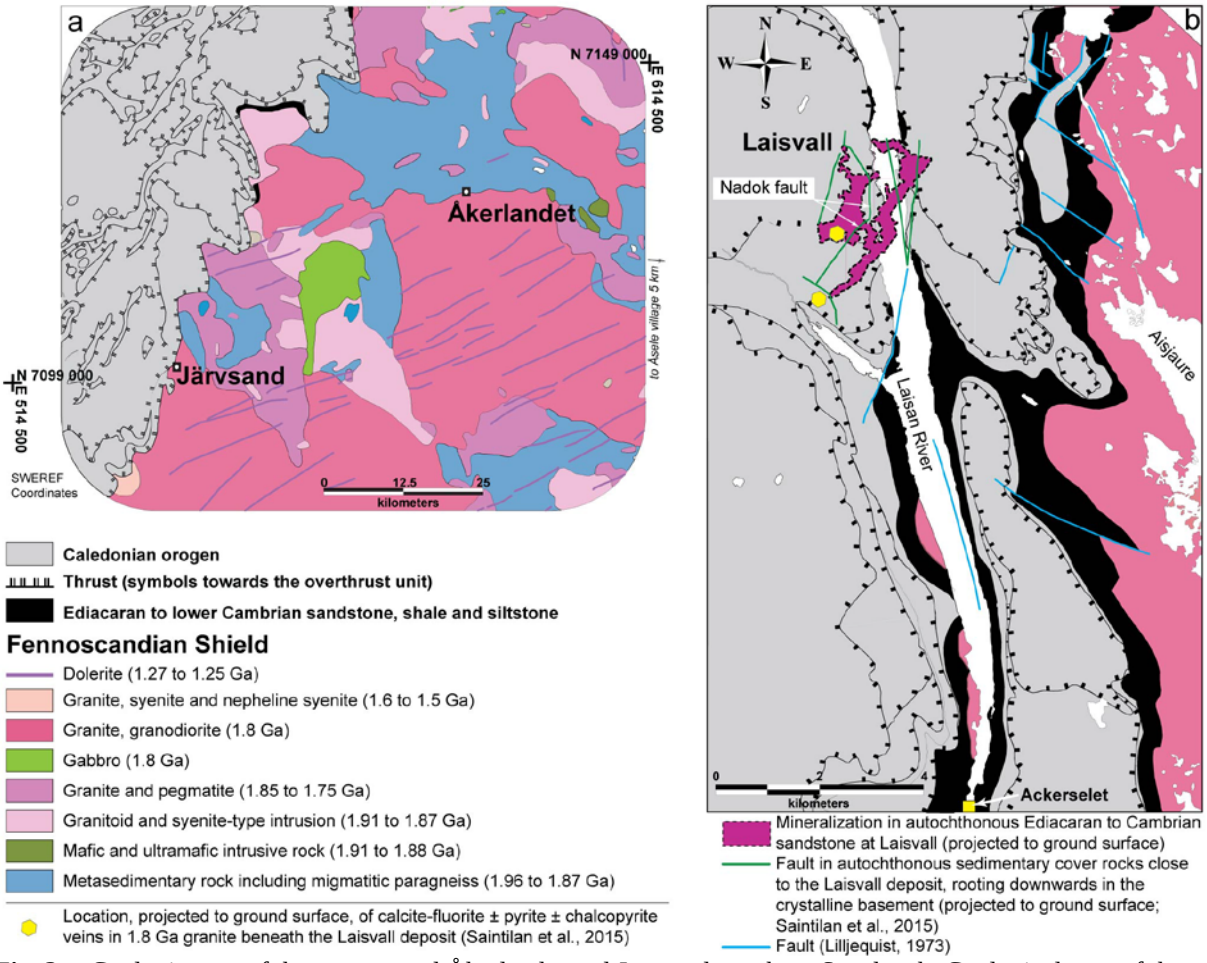

Fig. 2 a. Geologic map of the area around Åkerlandet and Järvsand, northern Sweden. b. Geological map of the Laisvall area (modified after Lilljequist, 1973 and Bergman et al., 2012). The projections to ground surface of the Laisvall orebodies and the two veinlet occurrences in Paleoproterozoic basement beneath the Laisvall deposit are also shown.

Field methodology and analytical procedures

Structural mapping

Standard methodology was used at the Åkerlandet and Järvsand deposits to acquire brittle structural data from the rocks inside and hosting the veins. Strike and dip information, using right-hand rule systematics, were recorded for all fractures longer than 1 m, which, at Åkerlandet, were locally close enough to define a fracture cleavage in the host migmatitic paragneiss. Information on slickenlines with pitch was recorded in the corresponding plane if available. The data have been visualized and contoured using the software Stereonet 9 (Allmendinger et al., 2013; Cardozo and Allmendinger, 2013). Emphasis was placed on the identification of kinematic indicators in order to constrain shear sense. Minerals filling fractures (e.g., calcite, fluorite, sphalerite, and galena) were also systematically recorded as well as the presence or absence of alteration in the host rock along the fracture walls. Geologic maps were drawn in the field and structural readings were directly reported on maps after measurement. At Åkerlandet, three cross-sections were also drawn through the deposit; two on the southern and northern walls of the quarry and a third one on outcrops about 20 m south of the quarry.

The retrieved borehole material containing veinlets in the basement at Laisvall was not oriented. For this reason, no structural analysis could be performed at this deposit.

Sample petrography and sample preparation for geochemical studies

At Åkerlandet, the intensely mineralized, sphalerite-rich, calcite-fluorite-sulfide vein was sampled (n = 6) from an adit in a previously operated small-scale quarry within the main mineralized volume. Following petrographic work, three samples (AKE01, AKE04, and AKE06) were selected for geochemical work. At Järvsand, a vein sample was collected from one accessible, narrow (30 cm) and 40 cm-deep mineralized vein that was exposed along the shore of the Lake Järvsjö at low-stand water level. At Laisvall, calcite-fluorite veinlets were mentioned in the core logs of two boreholes LAI 1031 and LAI 1088 (Boliden AB internal exploration reports, 1951, unpub.) that had reached into the crystalline basement beneath the Laisvall deposit (Fig. 2b; Lilljequist, 1973). These boreholes were retrieved at the core archive of the Geological Survey of Sweden in Malå and sampled.

Thin sections through the veins and their host rocks were produced for each sample. They were studied using transmitted and reflected light microscopy, and a Cl8200 MK5-optical cathodoluminescence microscope with a cold cathode that was mounted on a petrographic microscope. The beam conditions were set at 15 kV and 50–60 mA with an unfocused beam of approximately 1 cm in an observation chamber with a residual pressure of 80 mTorr. The relationships between luminescent minerals (e.g. calcite, fluorite), silicates and sulfides were described on non-coated samples. Some fragments of quartz coated with undefined black material from the Åkerlandet vein deposit were mounted on a stub, coated with gold, and this material was investigated using a scanning-electron microscope (SEM) in back-scattered electron (BSE) mode.

After petrographic investigations, all vein samples were isolated from their host rocks by sawing, crushed using a hydraulic press and sieved. The following size fractions were kept: i) 500–315 µm; ii) 315–125 µm. The 315–125 µm size fractions from the Åkerlandet samples were used to obtain 5–6 mg adularia aliquots for ^{40}Ar-^{39}Ar geochronology. A two-fold heavy liquid separation using sodium polytungstate (SPT) was performed. Heavy minerals (sphalerite, galena, calcite and fluorite) were separated from adularia and quartz using SPT with adjusted density (ρ) at 2.68. The light fraction containing adularia (specific gravity, ρ = 2.55-2.63 g/cm^3) was further treated using diluted SPT (ρ=2.65) in order to isolate adularia from quartz and some remaining calcite. Adularia aliquots (n = 3) were obtained by handpicking under a binocular microscope. Fluid inclusions in adularia were not identified during petrographic study.

Clean calcite and both green and purple fluorite aliquots (c. 200 mg) were handpicked by eye from the 500–315 and 315–125 µm size fractions from the Laisvall veinlet samples, while green fluorite and calcite aliquots were handpicked under a binocular microscope from the heavy mineral separate of sample AKE01. Calcite aliquots were rinsed in deionized water (>18MΩ resistance; DI) and dried, while the fluorite aliquots were rinsed in DI and 0.2 M HCl to remove any calcite dust, and

dried. These aliquots were powdered and fractions of fluorite (20–40 mg) and calcite (100–200 mg) were weighed in screw-top Teflon vials and used for Sr, Sm, and Nd radiogenic isotope studies. In addition, tin capsules containing 100–250 µg of each powdered calcite aliquot from Laisvall and Åkerlandet were prepared for C and O isotope analyses.

Sulfide (galena and sphalerite or pyrite) aliquots from the heavy mineral fraction of the Åkerlandet and Laisvall vein samples were handpicked under a binocular microscope for S isotope studies. Euhedral galena crystals were collected directly on macroscopic samples from the Järvsand deposit. All aliquots (n = 4 and duplicates) were subsequently powdered using an agate mortar and pestle.

Adularia mineral chemistry and ^{40}Ar-^{39}Ar geochronology

The quality of the three adularia separates was verified by single crystal analysis by Raman spectrometry at the University of Geneva, Switzerland using a LABRAM confocal Raman microspectrometer with a 532.8-nm He-Ne laser coupled to a B40 Olympus microscope with a 50× objective. The textural zoning of adularia in the three thin sections from the Åkerlandet vein samples was investigated by SEM-BSE. Major (K, Na, Ca, Al, and Si) and trace (Ba) elements in adularia were quantified by electron microprobe analysis (EMPA, JEOL 8200 electron Superprobe) at the University of Lausanne, Switzerland. For standardization and calibration, miscellaneous native silicate phases were used (Table 1) while an acceleration voltage of 15 kV and a beam current of 15 nA were used for all analyses. The spatial resolution of the electron microprobe was adjusted to 2 µm. Raw data for feldspar analyses were reduced with the ZAF matrix correction by Armstrong (1984). Several line segments were analyzed to detect intra-grain variability examined by BSE imaging. Detection limits are in the range of 100-200 ppm except for Ba (~250 ppm). Data for Si, K, Na, Ca, Al, and Ba are reported as atomic proportions and oxides wt.%, and the K/Ca was calculated where Ca was above detection limit and quantified.

Table 1. Settings and reference crystal material used for adularia microprobe analysis.

Adularia *15 kV, 15 nA, 2 µm*				
			Measurement time (s)	
Element	**Crystal**	**Reference Material**	**Peak**	**Background**
K	PETH	Orthoclase	10	5
Na	TAP	Albite	20	10
Ca	PETJ	Wollastonite	20	10
Al	TAP	Orthoclase	30	15
Si	TAP	Wollastonite	20	10
Ba	PETJ	Benitoite	30	15

The adularia aliquots were rinsed in deionized water in an ultrasonic bath, packed in copper foil, and irradiated in the CLICIT facility of the TRIGA reactor at Oregon State University, USA, for

30 hours. $^{40}Ar/^{39}Ar$ thermochronology analyses and data reduction were carried out at the University of Geneva, Switzerland, following the procedure described in Villagomez and Spikings (2013). The aliquots were heated with a 55W IR-CO_2 laser for 30 seconds, with 5 minutes cleaning with a ST101 and AP10 getter in a stainless steel extraction line. Data were collected with an Argus mass spectrometer equipped with four high-gain (10^{12} Ω) Faraday detectors (^{36}Ar, ^{37}Ar, ^{38}Ar, ^{39}Ar), and a single 10^{11} Ω Faraday detector (^{40}Ar), and corrected for blanks, interfering nucleogenic reactions and decay of ^{37}Ar and ^{39}Ar. The three samples have a J value of J = 0.0078070 ± 0.0000125. A mass discrimination correction of 0.983 ± 0.051 a.m.u. was determined by online measurement of air and was applied to the data.

Radiogenic isotope geochemistry (Sr, Sm and Nd)

Calcite aliquots were dissolved in 0.5 M HCl whereas fluorite aliquots were dissolved in Aqua Regia on a hot plate at 150°C. All calcite and fluorite aliquots were spiked using a $^{149}Sm/^{150}Nd$ spike prepared at ETH Zürich, Switzerland. All Teflon ware that came in contact with samples was cleaned by acid and all chemical procedures were carried out in HEPA-filtered clean air stations. A "Sandwich" separation protocol was used for Sr and REE using EICHROM Sr Resin®, Pre Filter Resin® and TRU Resin®. 50 µl Teflon columns were connected onto TRU Resin columns and the dissolved aliquots were added in 300 µl HNO_3 2M. Rinsing was carried out by adding 250 µl HNO_3 2M. Sr Resin columns were disconnected from TRU Resin columns and put back on a separate rack. The Sr Resin columns were rinsed twice with 200 µl HNO_3 2M and Sr elution was then collected by adding 1000 µl H_2O. Two drops of H_3PO_4 were added into Sr beakers that were dried on a hot plate. TRU Resin columns were rinsed twice with 200 µl HNO_3 2M and REE elution was obtained by firstly adding 300 µl H_2O and then 1000 µl H_2O. Nd and Sm were further purified from REE elution using 1ml Teflon columns EICHROM Ln Resin® (50-100µm). Sampling was carried out in 1.8 ml HNO_3 0.05 M. Rinsing was completed three times using 250 µl HCl 0.25 M and Ce elution was collected using 5 ml HCl 0.25 M. Nd elution was then obtained by using 6 ml HCl 0.25 M and two drops of H_3PO_4 were added into the Nd beakers that were dried on a hot plate. Rinsing was carried out with 2 ml HCl 0.5M and Sm elution was collected with 2.5 ml HCl 0.5M. Two drops of H_3PO_4 were also added into the Sm beakers that were put on a hot plate.

Sm and Nd separates were loaded on Re double filaments with 1M HNO_3. Isotopic measurements of the Sm and Nd cuts (Sm concentrations, Nd concentrations, and $^{147}Sm/^{144}Nd$, $^{143}Nd/^{144}Nd$ ratios) were performed on Thermo Fisher TRITON thermal ionization mass spectrometer (TIMS) at the University of Geneva, Switzerland. External reproducibility of the JNdi-1 standard ($^{143}Nd/^{144}Nd$ = 0.512115; Tanaka et al., 2000) is < 5 ppm. The Sr separates were re-dissolved in 5 ml of ~2% HNO_3 solutions and ratios were measured using a Thermo Neptune PLUS Multi-Collector ICP-MS in static mode at the University of Geneva, Switzerland. The $^{88}Sr/^{86}Sr$ (8.375209) ratio was used to monitor internal fractionation during the run. Interferences at masses 84 (^{84}Kr), 86 (^{86}Kr) and

87 (^{87}Rb) were also corrected in-run by monitoring ^{83}Kr and ^{85}Rb. The SRM987 standard was used to check external reproducibility, which on the long-term (more than 100 measurements during one year) was ±10 ppm. The internally corrected $^{87}Sr/^{86}Sr$ values were further corrected for external fractionation (due to a systematic difference between measured and a nominal standard ratio of the SRM987 of $^{87}Sr/^{86}Sr$ = 0.710248) by a value of -0.039‰ per a.m.u. A $^{87}Sr/^{86}Sr$ ratio of 0.721269 ± $8x10^{-6}$ is reported as 0.721269 ± 8.

Calcite and fluorite mineral chemistry using LA-ICPMS

The rare earth elements (REE) pattern of calcite and fluorite can yield valuable information on the paleoenvironment during mineral precipitation and the origin of the hydrothermal fluids. An effort was made to locate analytical spots in crystal domains devoid of fluid inclusions. *In situ* trace and rare earth element analyses of calcite and fluorite species from the Åkerlandet vein deposit (n = 8 for calcite, n = 32 for green fluorite) and the Laisvall basement veinlets (n = 26 for calcite, n = 32 for green fluorite, n = 23 for purple fluorite) were performed by LA-ICPMS at the Institute of Earth Sciences, University of Lausanne, Switzerland, using a sector-filed Element XR ICP mass spectrometer interfaced to an UP-193FX 193 nm excimer ablation system. Helium was used as a carrier gas. The on-sample laser beam fluence was set at 5 J/cm^2 at a repetition rate of 10Hz. The spectrometer was operated at low resolution and was optimized for a maximum sensitivity at ThO^+/Th^+ and Ba^{2+}/Ba^+ ratios of 0.07 and 2.9 %, respectively. Isotopes analyzed were ^{25}Mg, ^{42}Ca, ^{43}Ca, ^{55}Mn, ^{57}Fe, ^{85}Rb, ^{88}Sr, ^{89}Y, ^{139}La, ^{140}Ce, ^{141}Pr, ^{143}Nd, ^{147}Sm, ^{151}Eu, ^{157}Gd, ^{159}Tb, ^{163}Dy, ^{165}Ho, ^{166}Er, ^{169}Tm, ^{172}Yb, and ^{175}Lu. Four 10 ms readings were acquired for each of the isotopes within a scan window of 10% of the peak size, resulting in a total dwell time of 40 s per isotope. The NIST 612 soda-lime-silica glass doped with trace elements was used to calibrate the instrument mass fractionation. Concentration values in this standard were taken from Pearce et al. (1997). ^{42}Ca served for internal standardization. Its abundances in the analyzed grains were set stoichiometrically. Mg and Mn, and Rb and Sr were used to monitor the presence of calcite inclusions and K-feldspars host rock xenoliths in fluorite, respectively. Iron was used to monitor the presence of pyrite in calcite and fluorite. The distribution of rare earth elements and ytrrium (REY) is described by their REY_{PAAS} patterns (PAAS: normalized to post-Archean Australian shale after McLennan, 1989). Light rare earth elements (LREE) are La, Ce, Pr, Nd, and Sm. Transition rare earth elements (MREE) are Eu and Gd while heavy rare earth elements (HREE) are Tb, Dy, Ho, Er, Tm, Yb and Lu.

Stable isotope geochemistry (S, C and O)

The sulfide aliquots were analyzed for the stable sulfur isotope composition (δ^{34}S) by elemental analysis and isotope ratio mass spectrometry (EA-IRMS) at the University of Lausanne, Switzerland. The EA-IRMS analyses were carried out using a Carlo Erba 1108 elemental analyzer connected to a Thermo Fisher Delta V stable isotope ratio mass spectrometer that was operated in the continuous He

flow mode. The stable isotope composition of sulfur is reported in the delta (δ) notation as the per mil (‰) deviation of the isotope ratio ($^{34}S/^{32}S$) relative to the VCDT standard. The precision of the EA-IRMS analyses, evaluated by replicate measurements of laboratory standards (barite, sphalerite, and pyrite) and international reference materials (sphalerite, silver sulfide) is better than ±0.3‰ (1σ).

Carbon and oxygen isotope compositions ($\delta^{13}C$ and $\delta^{18}O$) of the calcite aliquots were determined at the University of Lausanne, Switzerland by using a Thermo Fisher Scientific carbonate-preparation device and Gas Bench II connected to a Delta Plus XL isotope ratio mass spectrometer that was operated in the continuous He flow mode. The CO_2 was extracted from calcite with 100% phosphoric acid at 70 °C for calcite. The stable C and O isotope ratios are reported in the delta (δ) notation as the per mil (‰) deviation relative to the Vienna Pee Dee belemnite (VPDB) standard for carbon and Vienna Standard Mean Ocean Water (VSMOW) for oxygen. Both the raw $\delta^{18}O$ VSMOW values and these converted VPDB are reported. The analytical reproducibility estimated from replicate analyses of the laboratory standard (Carrara marble, $\delta^{13}C$ = 1.95‰ and $\delta^{18}O$ = 29.16‰) was ±0.05 ‰ for $\delta^{13}C$ and ± 0.09 ‰ for $\delta^{18}O$ (1σ).

Results

Structural mapping and data analysis

Åkerlandet

The structural data set for Åkerlandet is presented in Appendix 1. Mineralization occurs along the western margin of a fault zone that strikes approximately N–S, cross-cutting migmatitic paragneiss and leucogranite (Fig. 3). This fault zone mainly outcrops on the ground surface within a small-scale quarry, which is partially flooded, and along two W–E profiles in the quarry; it is also exposed along a third W–E profile approximately 20 m to the south of the quarry. The zone is 5–6 m wide in the quarry area (e.g. profiles 1 and 2) but reduces to 2–3 m to the south (e.g., profile 3).

The fault zone is characterized by predominantly steeply dipping fractures without any observed mineral filling and two main sets of mineralized fractures occurring as veins: (1) Steeply dipping NNW–SSE to NNE–SSW fractures with calcite, sphalerite and minor galena. (2) Steeply dipping NW–SE fractures with only calcite. The angle between these two sets of fractures varies between 27° and 47°. The sulfide-bearing fractures occur along what is inferred to be the main fault; slickenlines (e.g., profile 1) indicate an oblique sense of displacement with a sinistral strike-slip and an east-side-up sense of shear. The fractures mineralized solely by calcite are inferred to be secondary R-shears with respect to the main fault along which the sulfide mineralization took place.

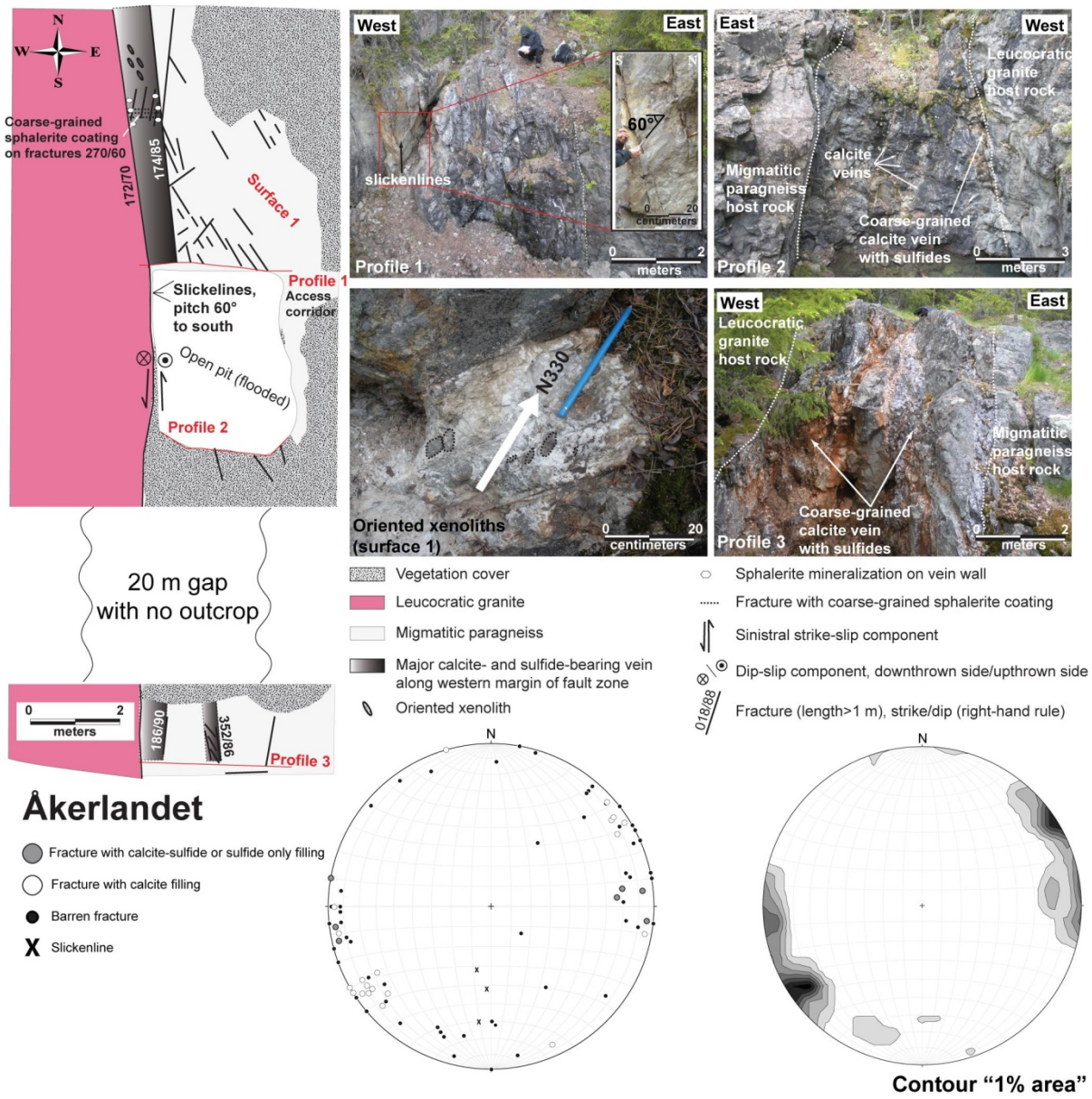

Fig. 3 Geologic and structural map of the Åkerlandet vein deposit. The locations of Profiles 1, 2 and 3 and Surface 1, where the photographs were taken, are shown on the ground surface map. Structural data are presented in the lower hemisphere equal-area stereographic projections.

Järvsand

The structural data set for Järvsand are provided in Appendix 1. The galena occurrence is situated along a fault zone with a high density of fractures exposed for ~100 m along the western shore of Lake Flåsjön (Fig. 4). The mineralized calcite-galena veins occur on the eastern side of a sandy beach and continue underneath the lake towards the north-east (Fig. 4).

In the studied area, the shore area is characterized by six sets of veins and fractures that are all steeply dipping: (i) Veins with calcite-galena fillings striking NNE–SSW; (ii) fractures with NNW–SSE or NW–SE strike and dextral strike-slip displacement; (iii) fractures with sinistral strike-slip displacement striking N–S or NW–SE; (iv) fractures with south-side-down displacement oriented NW–SE; (v) fractures with strike in the NE–SW quadrant that are displaced along younger fractures

with variable orientation that are clearly minor faults; (vi) fractures with variable orientation without any kinematics that form the majority of the fractures. Different senses of movement along fractures with similar orientation (NW–SE) are recognized.

Brown-grey streaks of oxidized pyrite highlight sigmoidal structures in the calcite-galena veins (inset in Fig. 4). Most of these structures highlighted by oxidized pyrite are oriented ~N–S to ~NNE–SSW, with dextral strike-slip component of movement and seem to have displaced other structures oriented NNW–SSE. This interpretation of the kinematics is supported by the dextral strike-slip displacement of a pegmatitic dyke in the 1.8 Ga granite across the calcite-galena vein closest to the shoreline.

In the northern part of the mapped area (not shown on Fig. 4), steep fractures with NNE–SSW orientation occur as R-shears in connection with longer, steep fractures with N–S to NNW–SSE strike, implying dextral movement along both these sets. For this reason, the steep calcite-galena veins with NNE–SSW orientation in the southern mapped area (Fig. 4) are also interpreted as R-shears to the main fault orientation in a N–S to NNW–SSE direction.

Vein mineralogy and host-rock alteration

Åkerlandet

The paragenetic sequence established for the Åkerlandet vein deposit is given in Fig. 5.The edges of veins are sharp. Sericitization of plagioclase and K-feldspar in the host rock occurs in spots up to at least 5 cm from the edges of the mineralized veins. The 0.2 to 1.0 m wide veins are zoned inwards from the edges to the core with the following three components (Figs. 5 and 6a):

(1) The vein starts over 1 to 2 cm by microcrystalline rhombic adularia and quartz with scarce, very fine-grained sphalerite, anhedral fluorite and calcite filling voids (Fig. 6a). The groundmass of adularia and quartz appears dusty. This part of the vein might represent an alteration of the host rock. This section is followed by some coarser-grained euhedral adularia and quartz crystals (c. 300–500 μm) in a groundmass of microcrystalline rhombic adularia and quartz. Anhedral sphalerite fills in void spaces in the adularia-quartz groundmass. Minor anhedral fluorite and calcite are also present filling spaces between crystals of adularia and quartz.

(2) Between components 1 and 3, the veins shows over ~500 μm coarse-grained euhedral adularia intergrown with euhedral quartz and sphalerite crystals. Large sphalerite crystals appear to have grown onto euhedral adularia towards the core of veins. In addition, organic compounds lining and coating quartz cemented by large calcite crystals were identified by SEM-EDX analysis. The organic compounds contain large amounts of apatite and submicron-scale Ag-As-Co-Ni-bearing iron sulfide, most probably pyrite (Figs. 6b and 6c).

(3) The core of the veins is filled with abundant calcite which precipitated after euhedral fluorite with growth bands (Figs. 6a and 6d). Subhedral microquartz rims fluorite crystals in saw-like pattern. A first dark-orange-luminescent calcite I generation underwent dissolution prior to

precipitation of light-orange-luminescent calcite II (Figs. 6a and 6d). Fluorite and calcite cement brecciated clasts made of sphalerite ± galena (component 2) which had grown on microcrystalline adularia and quartz groundmass from component (1).

Adularia is mostly very fine-grained (<0.2 mm) in component 1 while euhedral coarse-grained adularia is the dominant type of adularia in component 2. Onto weathered surfaces adularia is altered to illite and kaolinite. The mineralization styles at Åkerlandet provide evidence for open-space filling mineralization occurring along newly opened or re-opened fractures with or without brecciation of the previous stages of mineral precipitation.

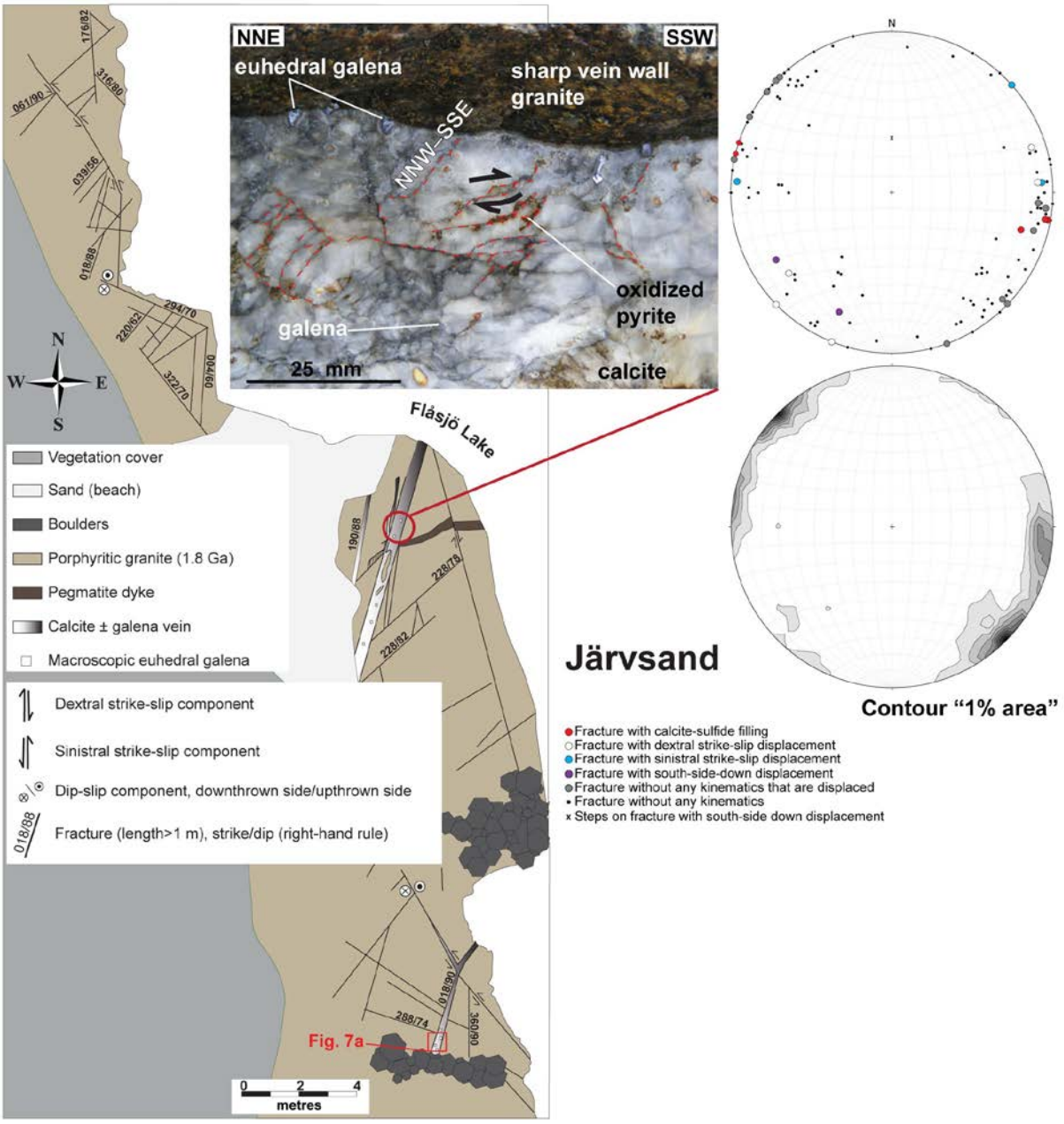

Fig. 4 Geologic and structural map of the Järvsand vein occurrence. Inset shows a typical calcite-galena vein at this site. The location where the macrophotograph presented in Fig. 7a was taken is shown. Structural data are presented in the lower hemisphere equal-area stereographic projections.

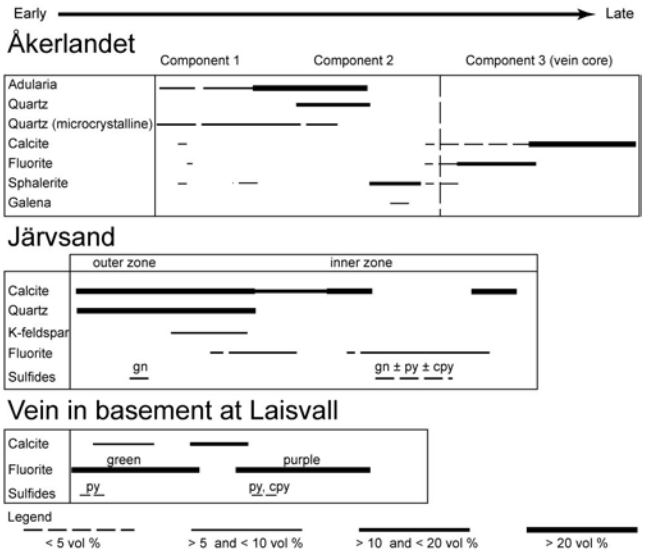

Fig. 5 Paragenetic sequences of the basement vein mineralization at Åkerlandet, Järvsand and Laisvall.

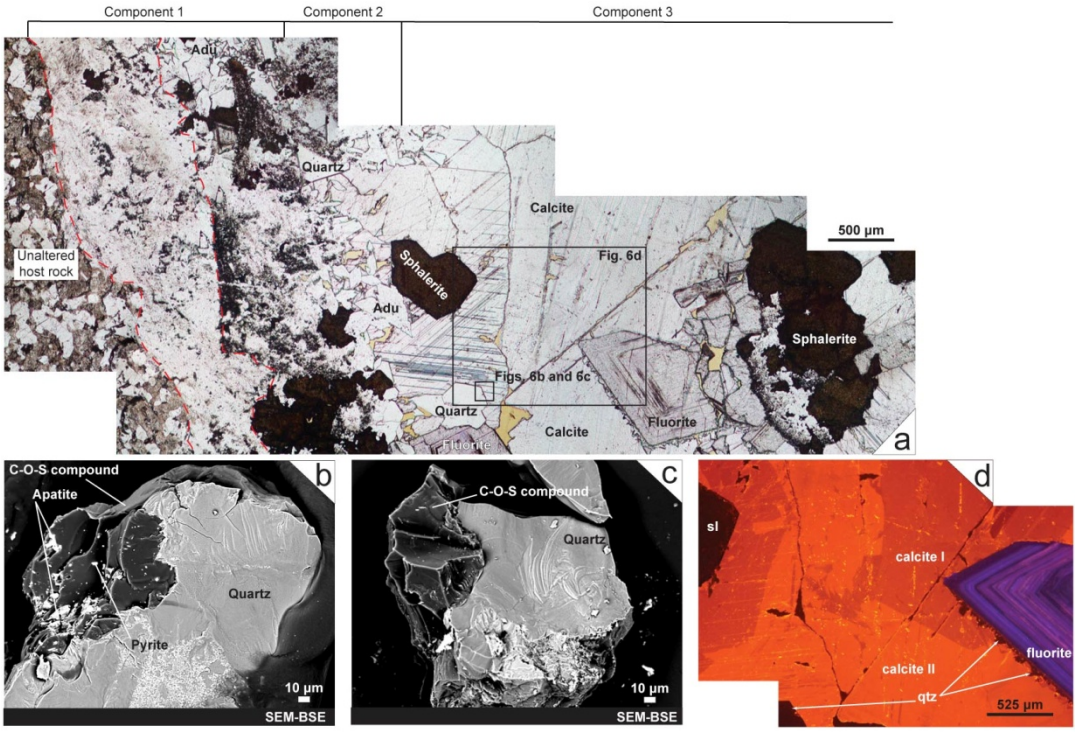

Fig. 6 a. Photomicrograph panorama through the Åkerlandet mineralization from the host rock edge to the vein core. b. Scanning-electron microprobe image, back-scattered electron mode (SEM-BSE) of solid organic matter containing apatite and pyrite lining hydrothermal quartz. c. SEM-BSE image of solid organic matter lining hydrothermal quartz. d. Optical cathodoluminescence image of oscillatory-zoned fluorite and calcite I and II.

Järvsand

The Järvsand occurrence is characterized by 0.2 to 0.7 m wide calcite veins, which have sharp walls and no macroscopically visible alteration in the porphyritic, 1.8 Ga granite host rock. The veins are symmetrical with respect to their NNE–SSW central axis with a zoning composed of outer and inner components (Fig. 7a).

The outer part of the veins is granular in outcrop and microscopic observations show it is composed of euhedral quartz and euhedral to subhedral calcite, cemented by anhedral K-feldspar and

scarce anhedral fluorite (Figs. 7a, 7b, and 7c). Galena is included in quartz or is interstitial to quartz and calcite together with accessory pyrite.

The inner part of the veins is characterized by massive, coarse-grained calcite and fluorite with fine-grained galena and pyrite (Figs. 7a, 7d, 7e). Some euhedral galena cubes are weathered positively with respect to the bulk calcite mineralization (Fig. 5a). These galena cubes have accessory chalcopyrite and both sulfides replaced pyrite. Along the central vein axis, there are aligned fragments of the outer zone component (Fig. 7a). These observations suggest that the fracture was reopened with formation of the inner zone component after the development of the outer part of the veins. The sigmoidal features highlighted by oxidized pyrite described above are seen locally in this inner part of the vein.

We conclude that two separate hydrothermal phases of open-space filling mineralization occurred at Järvsand (Fig. 5): (1) An earlier phase that formed the outer parts comprising hydrothermal quartz, calcite, K-feldspar ± fluorite ± pyrite ± galena-chalcopyrite; and (2) a later phase related to reopening of the fracture that formed the inner part containing calcite-fluorite ± galena-pyrite and broken fragments of the outer zone aligned in the strike direction of the veins.

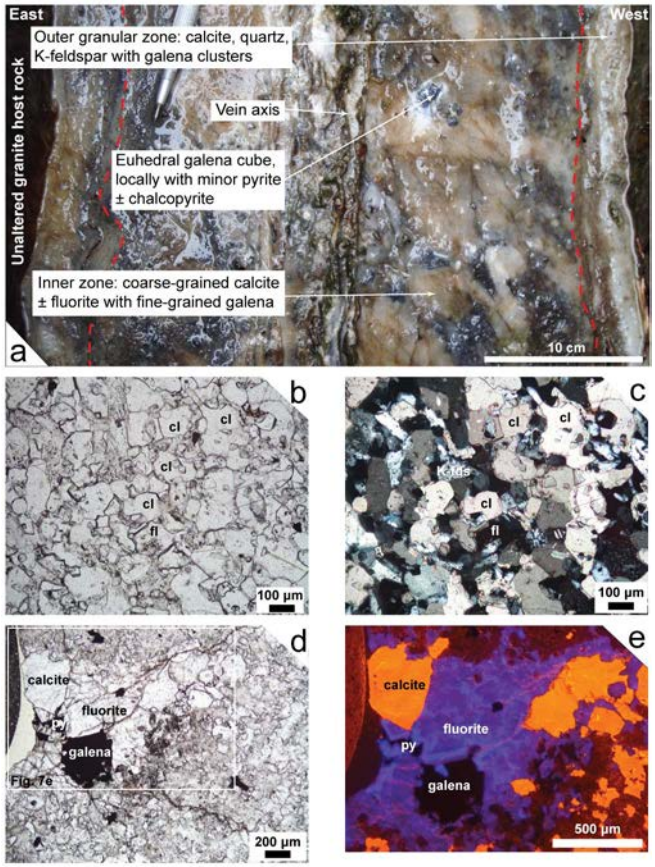

Fig. 7 a. Oriented macrophotograph of a calcite-galena vein, symmetrical along its N–S axis, at Järvsand. b and c. Microphotographs (transmitted light and crossed nicols transmitted light, respectively) of the outer zone described in Fig. 7a. d and e. Microphotographs (crossed nicols transmitted light and optical cathodoluminescence, respectively) of the inner zone described in Fig. 7a.

Laisvall basement veinlets

The veinlets consist of calcite and fluorite with minor pyrite ± chalcopyrite (Fig. 8). They are characterized by sharp vein walls. The host rock granite underwent weak and unevenly distributed alteration with formation of calcite (mainly on plagioclase), chlorite (mainly on hornblende), and minor sericite (mainly on K-feldspar). This alteration, typical for low-temperature slightly acidic fluids, enters into the granite in the range of 5 to maximum 10 cm from the veins.

The outer part of the veinlets consists of coarse-grained, green fluorite with coarse-grained anhedral calcite filling interstices, whereas the central part contains large grains of anhedral coarse-grained calcite separated by purple fluorite cementing brecciated calcite and, subordinate, granite host rock fragments (Fig. 8). Scarce euhedral pyrite and accessory chalcopyrite inclusions are found in calcite and fluorite (Figs. 5 and 8). The petrographic evidence suggests that the bulk calcite precipitation occurred during and after the growth of green fluorite (Fig. 5). Calcite was subsequently brecciated and cemented by purple fluorite during the second stage of open-space fluorite precipitation which occurred during a re-opening of the fracture system.

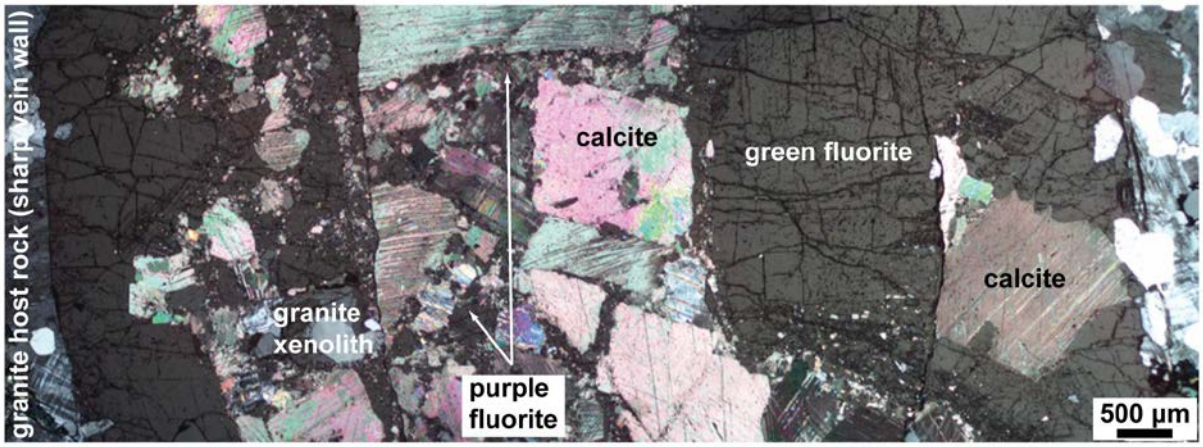

Fig. 8 Photomicrophotograh panorama of the basement veinlet mineralization at Laisvall (crossed nicols transmitted light).

Adularia mineral chemistry and ^{40}Ar-^{39}Ar thermochronology

Optical microscopy investigations showed that coarse-grained adularia from component 2 does not have any readily recognizable internal zoning and growth generations. However, SEM-BSE images (Fig. 9a) reveal complicated adularia crystals with various textural domains identified in different shades of grey. The Si, K, Na, Al, Ca and Ba electron microprobe analyses in adularia are provided in Appendix 2 and summarized statistically in Table 2. Si, K, Na and Al values are rather homogeneous whereas Ca and Ba values show greater variation (Table 2). The K/Ca ratios also vary significantly (Table 2). These findings are of importance for the validation and interpretation of the results of ^{40}Ar-^{39}Ar thermochronology.

Results from ^{40}Ar-^{39}Ar step-heating of adularia aliquot AKE04 are shown in an age spectrum plot (Fig. 9b) and the data are summarized in Table 3. Individual, contiguous heating steps do not

define a plateau, and overall the age spectra is disturbed. The gas released at high temperatures was derived from regions within the adularia with K/Ca ratios above 3.2, and represents 38.1 % of the total ^{39}Ar released, yielding individual step ages that range between 900 and 1050 Ma. Gas released at lower temperatures is derived from regions within the adularia with K/Ca ratios between 1.5 and 3.2 (61.9 % of the total ^{39}Ar released), with steps ages ranging between 650 and 900 Ma. This topology is not characteristic of excess ^{40}Ar, and juxtaposed older and younger dates within the high-temperature range can be explained by ^{39}Ar recoil. The other two aliquots (AKE01 and AKE06) yielded uninterpretable data (Appendix 3).

Despite the disturbed nature of the age spectrum, the overall topology for aliquot AKE04 may be compatible with partial thermal resetting of adularia, leading to 40Ar loss and a mixing trend between two hydrothermal events. We suggest that the four step ages between 900 and 1050 Ma (high-temperature steps; Fig. 9b) may approximate the time of crystallization of adularia. The presence of regions within the adularia crystals (Fig. 9a) with variable composition (e.g., Ca, Ba ± K) may account for ^{39}Ar recoil, implying that regions with high K content yield ages (e.g., c. 1007 Ma) that are older than the actual age, whereas regions with low K content yield younger ages (e.g., c. 925 Ma). High-temperature steps with ages of 950 and 980 Ma may be the most accurate estimates of the crystallization age of the adularia.

Table 2. Minimum, maximum, average and standard deviation values for major and trace elements analyzed in adularia. The K/Ca ratio was quantified for 171 analyses where Ca could be quantified.

	Si	**K**	**Na**	**Ca**	**Al**	**Ba**	**K/Ca**
n=275	**wt.%**	**wt.%**	**wt.%**	**wt.%**	**wt.%**	**wt.%**	
Minimum	61.14	14.92	0.04	0.01	17.89	0.07	49
Maximum	65.79	16.21	0.17	0.33	18.83	0.72	1460
Average	64.37	15.93	0.10	0.05	18.39	0.30	630
Standard deviation	0.69	0.14	0.02	0.04	0.16	0.12	382

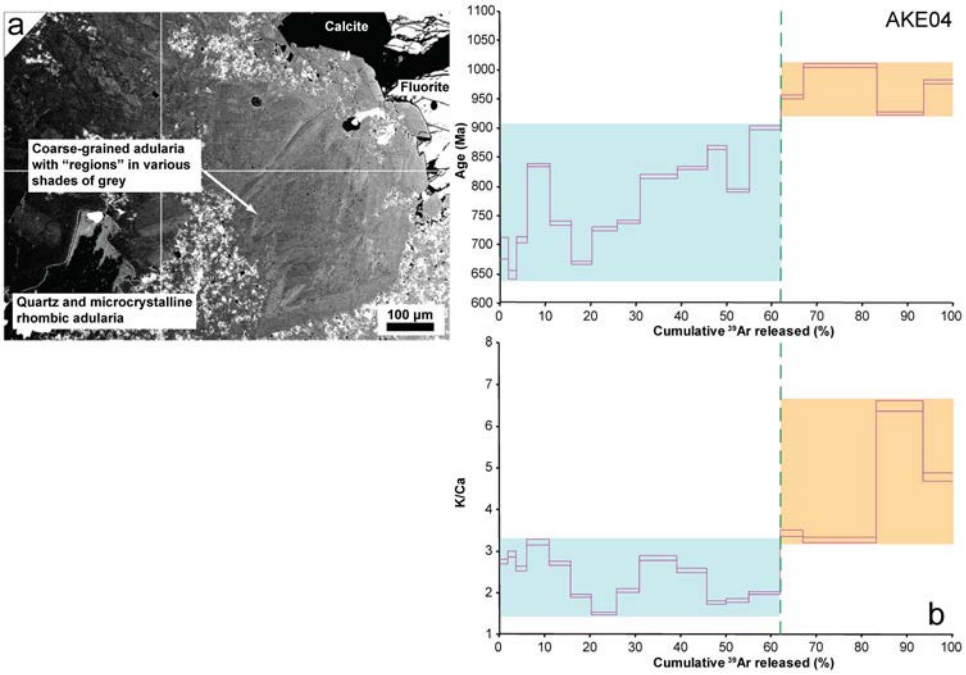

Fig. 9 a. SEM-BSE image of coarse-grained adularia (component 2 in the zoned vein structure) in the basement vein deposit at Åkerlandet (sample AKE04). b. ^{40}Ar-^{39}Ar age spectrum for adularia separates corresponding to coarse-grained adularia presented in Fig. 9a. The K/Ca spectrum is also shown.

Radiogenic isotope geochemistry

Sr isotopes

Calcite from the Åkerlandet vein deposit has a $^{87}Sr/^{86}Sr$ ratio of 0.718878 ± 7 (2σ), while green fluorite shows ratios between 0.717714 ± 5 and 0.718326 ± 16 (Table 4). Calcite and green fluorite aliquots from the Laisvall basement veinlets have similar $^{87}Sr/^{86}Sr$ ratios of 0.720480 ± 10 and 0.720273 ± 8, respectively, whereas purple fluorite has a significantly higher $^{87}Sr/^{86}Sr$ ratio of 0.731944 ± 22. The Rb contents of calcite and fluorite in both deposits are low (below 0.9 ppm Rb), while these mineral phases have high Sr contents ranging between 18 and 70 ppm. The low Rb concentrations in calcite and fluorite indicate that this highly radiogenic Sr composition has been caused by fluid-rock interaction.

Sm-Nd geochemistry and geochronology

The results of Sm and Nd isotope analyses for calcite and fluorite aliquots from Åkerlandet and Laisvall are presented in Table 4. The Sm and Nd elemental concentrations of calcite in the two analyzed deposits display wide ranges (4.22 to 30.91 ppm Sm and 18.13 to 319.33 ppm Nd). The same trend is seen in the elemental concentrations in fluorite (63.70 to 259.20 ppm Sr to 185.42 to 716.60 ppm Nd). Except for the Sm content in calcite from the Laisvall basement veinlets, the Sm and Nd elemental concentrations in calcite and fluorite in the two analyzed deposits are one or two orders of magnitude higher than published data for Sm and Nd contents in calcite and fluorite where isochron age determination using Sm and Nd data was possible and geologically relevant (e.g., Piqué et al., 2008; Barker et al., 2009).

Table 3. ^{40}Ar-^{39}Ar data from adularia aliquot AKE04.

Heating step	$^{40}Ar/^{39}Ar$	±1σ	$^{37}Ar/^{39}Ar$	±1σ	$^{36}Ar/^{39}Ar$	±1σ	$^{40}Ar^*/^{39}Ar_k$	±1σ	^{40}Ar(mol)	$^{40}Ar^*$ (%)	$^{39}Ar_k$ (%)	Age (Ma)	±2σ (Ma)	K/Ca	±2σ
AKE04, J=0.007807±0.0000125															
0.44	169.72808	0.36860	0.15599	0.00174	0.37081	0.00325	60.17188	0.93826	2.282E-14	35.45	1.96	694.82	17.98	2.76	0.06
0.73	100.39599	0.22401	0.14663	0.00169	0.15207	0.00138	55.47536	0.41321	1.194E-14	55.25	1.74	649.24	8.12	2.93	0.07
1.03	85.10707	0.17830	0.16626	0.00176	0.07929	0.00072	61.69514	0.24493	1.354E-14	72.48	2.32	709.36	4.66	2.59	0.05
1.32	88.85626	0.18093	0.13377	0.00139	0.04507	0.00042	75.55505	0.19503	3.053E-14	85.02	5.01	836.54	3.46	3.21	0.07
1.54	78.35567	0.15898	0.15847	0.00163	0.04645	0.00043	64.64879	0.18015	2.528E-14	82.50	4.71	737.23	3.37	2.71	0.06
1.83	69.65056	0.14105	0.22231	0.00226	0.04084	0.00038	57.60747	0.15926	2.211E-14	82.70	4.63	670.08	3.09	1.93	0.04
2.05	74.74442	0.15104	0.28415	0.00287	0.03785	0.00035	63.59305	0.16305	2.822E-14	85.06	5.51	727.32	3.07	1.51	0.03
2.35	72.82941	0.14801	0.20795	0.00214	0.02694	0.00027	64.89166	0.15391	2.526E-14	89.09	5.06	739.50	2.88	2.07	0.04
2.57	80.33182	0.16228	0.15107	0.00155	0.02352	0.00022	73.40084	0.16135	4.560E-14	91.36	8.29	817.35	2.89	2.85	0.06
2.86	81.45658	0.16548	0.16882	0.00173	0.02178	0.00022	75.04039	0.16482	3.689E-14	92.11	6.61	831.97	2.93	2.55	0.05
3.08	87.31944	0.18219	0.24272	0.00249	0.02830	0.00028	78.98842	0.18394	2.544E-14	90.44	4.25	866.70	3.21	1.77	0.04
3.30	79.04698	0.16128	0.23584	0.00240	0.02821	0.00027	70.73869	0.16360	2.705E-14	89.48	4.99	793.35	2.97	1.82	0.04
3.52	89.28668	0.17985	0.21496	0.00219	0.02169	0.00021	82.90574	0.17731	4.181E-14	92.84	6.83	900.51	3.03	2.00	0.04
3.74	91.94884	0.18826	0.12519	0.00130	0.00942	0.00019	89.18051	0.19096	3.197E-14	96.98	5.08	953.39	3.17	3.43	0.07
4.18	99.93001	0.20040	0.13139	0.00134	0.01392	0.00013	95.83310	0.19594	1.105E-13	95.89	16.14	1007.80	3.16	3.27	0.07
4.40	88.93623	0.17854	0.06631	0.00069	0.01055	0.00012	85.82772	0.17587	6.340E-14	96.50	10.41	925.33	2.97	6.48	0.13
4.62	95.50990	0.19457	0.08999	0.00098	0.01084	0.00017	92.31719	0.19465	4.217E-14	96.65	6.45	979.25	3.19	4.78	0.10
Total Fusion Age 861.11±2.37 Ma															

Table 4. Sr-Sm-Nd concentrations and isotopic data for calcite and fluorite in the basement vein deposits and occurrences at Åkerlandet and Laisvall. Sm-Nd data for pink fluorite cement in feldspathic sandstone at Ackerselet in the Laisvall district are reported from Alm et al. (2005). Rb and Sr data of calcite and fluorite are from Saintilan et al. (in press).

	Rb (ppm)[b]	±2σ	Sr (ppm)[b]	±2σ	$^{87}Rb/^{86}Sr$[b]	±2σ 10^{-5}	$^{87}Sr/^{86}Sr$[a]	±2σ 10^{-6}	Sm (ppm)[a]	Nd (ppm)[a]	$^{147}Sm/^{144}Nd$[a]	±2σ 10^{-6}	$^{143}Nd/^{144}Nd$[a]	±2σ 10^{-6}	Reference
Åkerlandet calcite	0.0310	0.0008	68.2873	0.8922	0.00132	4	0.718878	7	30.91	18.13	1.030620	309	0.511475	22	[a]this study, [b]Saintilan, 2015
Åkerlandet fluorite (sample 1)	0.4984	0.0116	18.6341	0.2435	0.07747	226	0.717714	5	n.d	n.d	n.d	n.d.	n.d	n.d.	[a]this study, [b]Saintilan, 2015
Åkerlandet fluorite (sample 2)	n.d.	n.d.	n.d.	n.d.	n.d.	n.d.	0.718326	16	259.20	716.60	0.218750	875	0.511730	8	[a]this study, [b]Saintilan, 2015
Calcite in basement vein at Laisvall	0.1447	0.1200	63.9799	0.1200	0.00050	10	0.720480	10	4.22	319.33	0.007980	32	0.511462	16	[a]this study, [b]Saintilan, 2015
Green fluorite in basement vein at Laisvall	0.5487	0.1400	23.3662	0.1800	n.d	n.d	0.720273	8	95.05	185.42	0.309980	1240	0.511929	10	[a]this study, [b]Saintilan, 2015
Purple fluorite in basement vein at Laisvall	0.8078	0.1400	20.4264	0.1800	n.d	n.d	0.731944	22	63.70	190.71	0.201960	808	0.511824	5	[a]this study, [b]Saintilan, 2015
Ak 2:1 fl (Ackerselet)	n.d.	n.d.	n.d.	n.d.	n.d.	n.d.	n.d.	n.d.	5.18	17.44	0.179500	72	0.511900	10	Alm & Sundblad, 2005
Ak 4:1 fl (Ackerselet)	n.d.	n.d.	n.d.	n.d.	n.d.	n.d.	n.d.	n.d.	5.17	17.89	0.174800	699	0.511917	10	Alm & Sundblad, 2005
Ak 5:1 fl (Ackerselet)	n.d.	n.d.	n.d.	n.d.	n.d.	n.d.	n.d.	n.d.	1.78	8.35	0.129200	517	0.511786	10	Alm & Sundblad, 2005
Ak 5:2 fl (Ackerselet)	n.d.	n.d.	n.d.	n.d.	n.d.	n.d.	n.d.	n.d.	2.96	13.68	0.130700	522	0.511775	10	Alm & Sundblad, 2005
Ak 6:1 fl (Ackerselet)	n.d.	n.d.	n.d.	n.d.	n.d.	n.d.	n.d.	n.d.	3.96	12.92	0.185500	742	0.511941	10	Alm & Sundblad, 2005

The calcite aliquots have $^{143}Nd/^{144}Nd$ ratios between 0.511462 ± 16 and 0.511475 ± 22, while the same ratios in fluorite range from 0.511730 ± 8 to 0.511929 ± 10. The $^{147}Sm/^{144}Nd$ ratios in calcite vary between 0.007980 ± 32 and 1.030620 ± 22, while fluorite shows more homogeneous $^{147}Sm/^{144}Nd$ ratios between 0.201960 ± 808 and 0.309980 ± 1240. On a $^{143}Nd/^{144}Nd$-$^{147}Sm/^{144}Nd$ correlation ("isochron") diagram including the two studied deposits (Fig. 10a), the calcite and fluorite data points scatter and do not define an all-sample Sm-Nd isochron. The fluorite aliquots and the calcite aliquot from the Laisvall basement veinlets and the fluorite aliquot from the Åkerlandet deposit are positively correlated (R = 0.94) and plot along a steep linear trend (MSWD = 315), the slope of which corresponds to an age of 233 ± 180 Ma (initial $^{143}Nd/^{144}Nd$ = 0.51145 ± 25) of poor significance. No age information can be derived from the negative regression for the calcite and fluorite data points from the Åkerlandet deposit alone. Considering the data of the Laisvall basement veinlets alone, the slope of the linear trend defined by the calcite and fluorite data points (MSWD = 148) is also of poor age significance (242 ± 450 Ma, initial $^{143}Nd/^{144}Nd$ ratio of 0.51146 ± 63). Given petrographic evidence indicating that calcite and green fluorite both pre-date purple fluorite deposition, a two-point regression was attempted on the data points of the calcite and green fluorite. The resulting slope yields an age of 236 ± 9 Ma (initial $^{143}Nd/^{144}Nd$ ratio of 0.511450 ± 169) once again of poor significance.

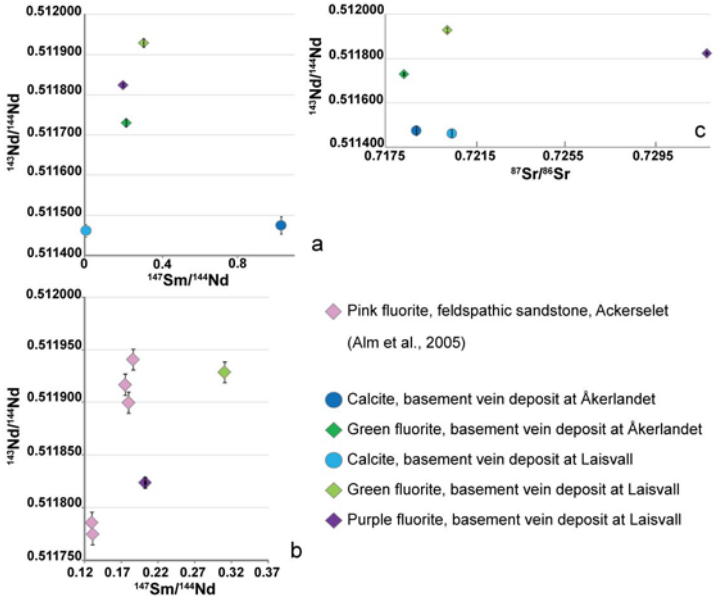

Fig. 10 a. $^{143}Nd/^{144}Nd$-$^{147}Sm/^{144}Nd$ diagram of calcite and fluorite in the basement vein deposits at Åkerlandet and Laisvall. b. $^{143}Nd/^{144}Nd$-$^{147}Sm/^{144}Nd$ diagram of fluorite in the basement veinlets at Laisvall (this study) and fluorite cement in feldspathic sandstone in autochthonous cover rock at Ackerselet in the Laisvall district (data from Alm and Sundblad, 2005). c.$^{143}Nd/^{144}Nd$-$^{87}Sr/^{86}Sr$ diagram of calcite and fluorite in the basement vein deposits at Åkerlandet and Laisvall.

Rare earth element distribution in calcite and fluorite

The full analytical data set for rare earth elements in calcite and fluorite is provided in Appendix 4. Calcite at Åkerlandet has low to moderate rare earth elements and yttrium (REY) concentrations that are rather homogeneous within a single sample for most elements except La, Ce, Nd, and Y (Table 5). Calcite shows systematic REY_{PAAS} patterns with depletion in all REEs except Tm, Yb, Lu, and Y; this

depletion is more significant for LREE and MREE than for HREE (Fig. 11a). The main feature in calcite is the negative Eu_{PAAS} anomaly.

Calcite in basement veinlets at Laisvall has also low to moderate REY concentrations which remain homogeneous except for La, Ce, Nd, and Y (Table 5). The calcite at this deposit shows a similar REY_{PAAS} pattern as the one for calcite at Åkerlandet but the negative Eu_{PAAS} anomaly is less pronounced (Fig. 11a). Calcite in basement veinlets at Laisvall is depleted in the same LREE and MREE as the calcite at Åkerlandet but it is slightly enriched in all HREE and Y.

Green fluorite at Åkerlandet is characterized by moderate to high REY concentrations which are inhomogeneous for all REE and Y except for the HREE (Table 5). It shows a REY_{PAAS} pattern with depletion in La and Ce, net enrichment in Sm, Eu and Gd, and an inverse enrichment in HREE from Tb to Lu (Fig. 11b). The REY_{PAAS} data define a bell-shape pattern. The main features in fluorite at Åkerlandet are the strong positive Eu_{PAAS} anomaly without any negative Ce_{PAAS} anomaly and the depletion and enrichment in La and Y, respectively.

Green and purple fluorite species in basement veinlets at Laisvall have moderate REY concentrations which are inhomogeneous for all REE and Y (Table 5). In general, green fluorite has higher REY concentrations than purple fluorite. Both fluorite types are characterized by depletion in La, Ce and Pr in their REY_{PAAS} patterns but purple fluorite is also slightly depleted in Nd (Fig. 11b). Both fluorite species show a marked enrichment in MREE and HREE from Sm to Ho (Fig. 11b). By contrast to green fluorite at Åkerlandet, both fluorite species at Laisvall are markedly enriched in HREE from Tb to Ho and in particular in Y. The main features in fluorite at Laisvall are the depletion in LREE, the steady enrichment from Sm_{PAAS} to Ho_{PAAS}, and the strong positive Y enrichment.

Fluorite at Åkerlandet has Y/Ho ratios (20 to 59) between the proposed chondritic and seawater ratios (28 and ~57, respectively; Bau and Dulski, 1995 and Bau and Möller, 1992, Table 5). By contrast, the green and purple fluorite species in the basement vein at Laisvall have higher Y/Ho ratios (26 to 76 and 37 to 109, respectively; Appendix 4, Fig. 11c). The La/Ho ratios show an inverse trend, with the lowest La/Ho ratios identified in green and purple fluorite in basement veinlets at Laisvall (1 to 28), while the highest La/Ho ratios (1 to 47) are identified in green fluorite at Åkerlandet (Fig. 11c).

Table 5. Average and standard deviation values of REE and Y for calcite and fluorite in the basement vein deposits and occurrences at Åkerlandet and Laisvall.

Mineral / Deposit	La (ppm)	Ce (ppm)	Pr (ppm)	Nd (ppm)	Sm (ppm)	Eu (ppm)	Gd (ppm)	Tb (ppm)	Dy (ppm)	Ho (ppm)	Er (ppm)	Tm (ppm)	Yb (ppm)	Lu (ppm)	Y (ppm)
Calcite / Åkerlandet vein (n=8)															
Average	10.5	26.5	3.6	17.9	3.5	0.2	3.1	0.4	2.6	0.7	2.4	0.4	4.0	0.8	28.5
Standard deviation	8.4	21.0	2.6	10.7	1.4	0.1	0.9	0.1	0.9	0.2	0.8	0.2	1.5	0.3	8.8
Calcite / vein in basement at Laisvall (n=26)															
Average	14.9	43	5.6	24	4	0.6	4	0.7	4.9	1.1	3.3	0.5	4.0	0.7	37
Standard deviation	13.3	31	3.4	13	2	0.3	3	0.5	4.1	1.1	4.2	0.8	6.8	1.1	51

Mineral / Deposit	La (ppm)	Ce (ppm)	Pr (ppm)	Nd (ppm)	Sm (ppm)	Eu (ppm)	Gd (ppm)	Tb (ppm)	Dy (ppm)	Ho (ppm)	Er (ppm)	Tm (ppm)	Yb (ppm)	Lu (ppm)	Y (ppm)	La/Ho	Y/Ho
Green fluorite / Åkerlandet vein (n=32)																	
Average	24.6	77	20.5	191	72	17.5	58	4.2	16.9	2.6	6.1	0.7	3.9	0.6	106	1.1	20
Standard deviation	7.0	24.8	7.7	72	23.7	5.9	25.8	2.7	9.9	1.5	3.5	0.5	2.6	0.4	75	47	59
Green fluorite / vein in basement at Laisvall (n=32)																	
Average	18.6	54	8.5	50	21.6	4.6	36	6.6	45	9.1	21.8	2.3	10.9	1.3	438	0.9	26
Standard deviation	7.3	25.9	3.2	21.7	12.9	2.8	29.3	5.2	31.9	5.6	13.1	1.5	6.8	0.8	274	28	76
Purple fluorite / vein in basement at Laisvall (n=23)																	
Average	13.6	36	5.3	29.1	11.0	2.2	20.2	4.0	32	7.1	17.9	1.8	9.4	1.1	330	1.0	37
Standard deviation	5.9	15.5	2.3	11.4	5.0	1.1	9.3	2.3	19.2	4.3	11.4	1.2	5.9	0.8	196	14.3	109

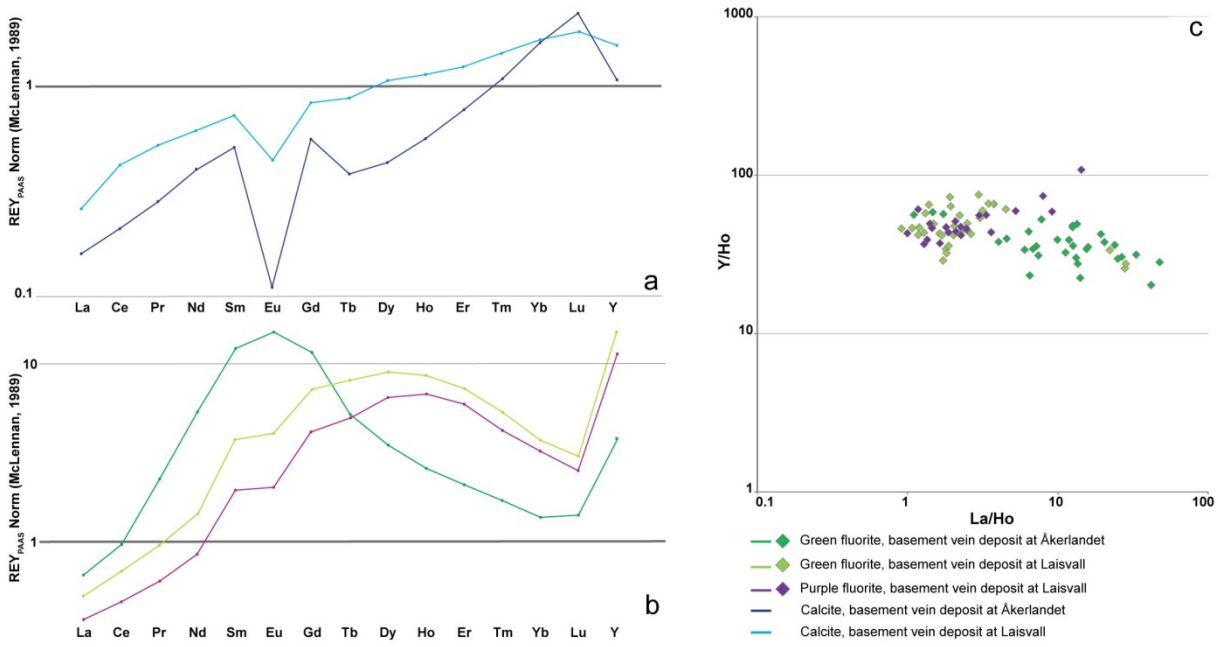

Fig. 11 a. Rare earth elements and yttrium spider diagram normalized to Post-Archean Australian Shale (PAAS; McLennan, 1989) for calcite in the basement vein deposits at Åkerlandet and Laisvall. b. Rare earth elements and yttrium spider diagram normalized to PAAS for fluorite in the basement vein deposits at Åkerlandet and Laisvall. c. Y/Ho-La/Ho diagram for the fluorite species in the basement vein deposits at Åkerlandet and Laisvall.

Stable isotope geochemistry

The analyses of sulfur isotope composition of sulfides (galena and sphalerite) at the Åkerlandet and Järvsand deposits complement a set of seven and one analyses carried out by Johansson (1984) on Åkerlandet and Järvsand samples, respectively. The analyzed galena samples at the Åkerlandet and Järvsand deposits shows δ^{34}S values of –3.1 (± 0.6‰, 2 standard deviations, 2σ) whereas sphalerite at the Åkerlandet deposit has a δ^{34}S value of 0.1‰ (Table 6). The δ^{34}S values of galena at both deposits are similar to those presented by Johansson (1984). Pyrite in the Laisvall basement veinlets has a δ^{34}S value of 6.9‰.

Calcite at Åkerlandet has δ^{13}C values ranging between –14.5 and –14.1‰ (average value and 1 standard deviation at –14.4 ± 0.1‰, n = 6, Table 6), and δ^{18}O values between –18.5 to –18.1‰ (–18.3 ± 0.1‰, n = 6). The δ^{13}C values are slightly higher than (by 0.3 to 0.9‰) or similar to the values presented by Johansson (1984). The δ^{18}O values VPDB obtained in the current study are also slightly higher (by 0.1 to 1.5‰) than the values presented by Johansson (1984) for calcite at Åkerlandet converted to VDPB.

The δ^{13}C values of calcite from the Laisvall basement veinlets (Table 6) vary from –14.3 to –13.7 (–14.0 ± 0.2‰, n = 3) and the δ^{18}O values from –18.9 to –17.3‰ (–18.3 ± 0.1‰, n = 3).

Table 6. Sulfur isotopic composition of Pb-Zn sulfides in the basement vein deposits and occurrences at Åkerlandet, Järvsand and Laisvall. Carbon and oxygen isotopic composition of calcite in the basement vein deposits and occurrences at Åkerlandet and Laisvall.

	Mineral	δ^{34}S (‰) VCDT	±2σ
Basement vein at Åkerlandet	galena	–3.1	0.6
Basement vein at Åkerlandet	sphalerite	0.1	0.6
Basement vein at Järvsand	galena	–3.1	0.6
Basement vein at Laisvall	pyrite	6.9	0.6

	Mineral	δ^{13}C (‰) VPDB	±2σ	δ^{18}O (‰) VPDB	±2σ
Basement vein at Laisvall LAI 1031	calcite	–14.3	0.2	–17.3	0.1
Basement vein at Laisvall LAI 1088–1	calcite	–13.7	0.2	–18.9	0.1
Basement vein at Laisvall LAI 1088–2	calcite	–14.1	0.2	–18.7	0.1
Basement vein at Åkerlandet	calcite	–14.3	0.2	–18.5	0.1
Basement vein at Åkerlandet	calcite	–14.1	0.2	–18.4	0.1
Basement vein at Åkerlandet	calcite	–14.5	0.2	–18.3	0.1
Basement vein at Åkerlandet	calcite	–14.3	0.2	–18.3	0.1
Basement vein at Åkerlandet	calcite	–14.5	0.2	–18.4	0.1
Basement vein at Åkerlandet	calcite	–14.5	0.2	–18.1	0.1

Discussion

Late Sveconorwegian quartz-adularia mineralization at Åkerlandet

An age for precipitation of coarse-grained adularia from component 2 between 950 and 980 Ma would suggest that the fault zone at Åkerlandet was open for fluid circulation during the later part of the Sveconorwegian orogenic event in Sweden (Bingen et al., 2008).

Reactivation of structures in the Paleoproterozoic crystalline basement during the Sveconorwegian orogenic event was shown previously in the central part of Sweden using ^{40}Ar-^{39}Ar (adularia) thermochronology (Sandström et al., 2009). The time span between 950 and 980 Ma corresponds to the emplacement of a major dolerite dyke swarm in the eastern foreland to the Sveconorwegian orogen (Söderlund et al., 2005; Bergman et al., 2012), the orientation of which is compatible with bulk ENE–WSW extension. The structural mapping and data analysis at Åkerlandet with a N–S main shear, NW–SE R-Riedel shears and paleotectonic implications indicating sinistral transtension suggest c. NE–SW bulk extension, i.e., close to the bulk extensional direction for the emplacement of the dolerite dyke swarm (Fig. 12).

The groundmass of microcrystalline quartz and adularia, interpreted as being an alteration of host rocks indicating slightly acidic conditions (pH ~ 4–5), is typical of basement-hosted low-temperature (100°–200° C) hydrothermal systems that often show coarse-grained euhedral to subhedral adularia in open spaces (e.g., metaquartzdioritic Variscan gneiss, Schwarzwald, SW Germany; Glodny and Grauert, 2009; Hercynian basement at Chaillac in the French Massif Central, Sizaret et al, (2004); Baksa Gneiss Complex of the SW Pannonian Basin, Hungary, Fintor et al., 2011).

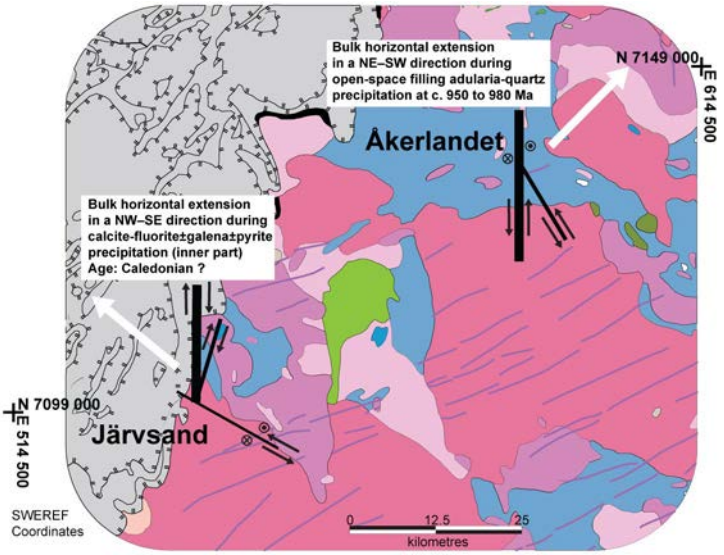

Fig. 12 Interpretation of the paleotectonic setting responsible for hydrothermal fluid flow in basement at different times at the Åkerlandet and Järvsand vein deposits.

Ediacaran or Middle Ordovician (?) sphalerite ± galena mineralization at Åkerlandet

The ^{40}Ar-^{39}Ar data at Åkerlandet suggest that at least one hydrothermal event that was 650 Ma old or younger (see "mixing trend" on Fig. 9b) disturbed coarse-grained adularia after its formation. A candidate for this disturbance is the hydrothermal event causing open-space filling sphalerite precipitation. In addition, the current results cannot exclude the possibility that adularia was also disturbed previously by hydrothermal events between 950 Ma and 650 Ma.

The Rb-Sr sphalerite geochronology data presented by Saintilan et al. (*in press*) yielded two ages for the timing of sphalerite mineralization at Åkerlandet (544 ± 4 Ma and 468 ± 5 Ma), both geologically meaningful. Fluid inclusion microthermometry studies suggested that primary and pseudo-secondary inclusion fluids were trapped in sphalerite at temperatures between 110° and 150°C (Johansson, 1984) during re-opening of fractures. Such temperatures could have caused partial thermal resetting of adularia responsible for the "mixing trend" recorded in the ^{40}Ar-^{39}Ar plateau ages.

The sulfur isotope composition of galena and sphalerite at Åkerlandet and Järvsand (δ^{34}S values from –3.1 to 0.1‰) suggest that reduced sulfur was derived from the leaching of sulfide minerals (mainly pyrrhotite and pyrite) in crystalline basement rocks. This interpretation is compatible with the results of lead isotope geochemical studies on galena and sphalerite (Johansson, 1983a; Johansson and Rickard, 1984; Saintilan, 2015) that identified the leaching of radiogenic lead from local basement rocks as the source of Pb in these basement-hosted vein deposits.

Sphalerite ± galena mineralization at Åkerlandet was likely formed by relatively oxidizing and slightly acidic hydrothermal fluids transporting metals and deriving H_2S as explained above. These slightly acidic conditions are consistent with sericitization in spots observed in the host rock at Åkerlandet.

Similarly, sericitization in granitic host rock around the current calcite-fluorite ± pyrite veins in basement at Laisvall could have been caused when these channelways were used at an earlier stage

as a plumbing system for oxidized, slightly acidic, metal-bearing brines involved in Pb-Zn mineralization in overlying sandstone (Saintilan et al., *submitted to Mineralium Deposita*). The scarcity of reduced sulfur would have prevented precipitation of more sulfides in these veins.

Caledonian calcite-fluorite ± sulfide mineralization at Åkerlandet, Järvsand and Laisvall

Comparison of tectonic regimes at Åkerlandet, Järvsand and in basement veins at Laisvall

The N–S oriented shear zone fault systems at the neighboring Åkerlandet and Järvsand occurrences with different components of movement and directions of horizontal bulk extension (Fig. 12) may reflect formation of brittle structures at these two sites in regionally different tectonic regimes at different times. It is worthwhile noting that, further north along the eastern erosional front of the Caledonian orogen, calcite-fluorite-Zn ± Pb sulfide vein deposits in the Storuman district similar to the one at Åkerlandet (e.g., Ersmarksberget, Gubbträsk) are located in brittle structures with N–S to NE–SW trend and both strike-slip and dip-slip components of movement (Billström et al., 2012), i.e., a geometric pattern similar to that observed at Åkerlandet.

As explained above in the section dealing with adularia-quartz precipitation at Åkerlandet, this stage of open-space filling was linked to NE–SW bulk horizontal extension (Fig. 12). These fractures were re-opened later and space was filled in and cemented by fluorite and calcite.

The calcite-galena veins in the southern part of the mapped area at Järvsand were formed in steep NNE–SSW fractures that are interpreted to be R-shears to a main shear plane corresponding to longer, steep fractures with N–S to NNW–SSE strike. Both these sets display a dextral component of movement suggesting that they formed as a response to NW–SE bulk horizontal extension (Fig. 12).

The sigmoidal features with dextral component of movement are observed in the inner part of the calcite-galena veins formed along R-shear fractures (see inset in Fig. 4) after re-opening and deposition of the outer part. The inner part of the veins is thus interpreted as being related to the above mentioned NW–SE bulk horizontal extension.

Despite the fact that boreholes intersecting the studied basement mineralized veinlets were unoriented, it can be assumed that they belong to the vein systems recognized in the basement to and close to the Laisvall mine by Lilljequist (1965, 1973) and Saintilan et al. (2015). In the basement at Laisvall, Lilljequist (1965, 1973) described steeply dipping to subvertical joints coated with calcite and fluorite and striking NNW–SSE and NNE–SSW to NE–SW. The inferred main feeders in the stratabound Pb-Zn mineralization in Ediacaran to Cambrian sandstone at Laisvall also have these orientations (Saintilan et al., 2015).

In conclusion, fractures in the Baltica basement filled in by calcite, fluorite ± pyrite or galena have strike orientation at NNW–SSE and NNE–SSW to NE–SW in the Storuman and Åkerlandet vein districts, and even further north in the Laisvall district where basement veinlets have there the same

orientation as those of the interpreted feeder faults in Ediacaran to Cambrian sandstone which are inferred to be rooted downwards into the crystalline basement (cf. Saintilan et al., 2015).

Age of calcite-fluorite precipitation

Åkerlandet: The failure of the dating attempt using Sm-Nd isochrons on fluorite-calcite I pairs results probably from the above reported post-deposition dissolution/re-precipitation events. The criteria needed for the calculation of ages from mineral isochrons on coexisting calcite and fluorite species are not met (criteria detailed in Nägler et al., 1995; Barker et al., 2009). The elevated Nd content and low $^{147}Sm/^{144}Nd$ ratio in fluorite (Table 4) can be explained as the result of dissolution. Similarly, the discrepancy between the Nd contents in fluorite parts interpreted to be devoid of fluid inclusions (LA-ICPMS Nd values between 50 and 350 ppm, Table 5) and those including fluid inclusions (ID-TIMS Nd values to 715 ppm) support the hypothesis of disturbance by post-depositional fluid flow (cf. Nägler et al., 1995). Regarding calcite, the Nd content determined by ID-TIMS (~ 18 ppm) is similar to the average Nd value determined by LA-ICPMS, suggesting that the low Nd value might be pristine. However, Sm values in calcite determined by ID-TIMS (~30 ppm) are ten times higher than those determined by LA-ICPMS (~3 ppm); hence some later fluid flow modifying the Sm contents of inclusion fluids in calcite could be envisaged.

Basement veinlets at Laisvall: The attempt to constrain an absolute age using Sm-Nd systematics of green fluorite and coarse-grained calcite pairs at Laisvall, which are two phases that can be considered as coeval owing to their similar $^{87}Sr/^{86}Sr$ ratios (0.7204 and 0.7202, respectively, i.e., less radiogenic than that of purple fluorite; Table 4) and petrographic evidence, failed and this likely for the same reasons as those identified at Åkerlandet. Disturbance of the Nd budget in calcite may be correlated with phases of vein re-opening, calcite brecciation and dissolution, followed by cementation by purple fluorite. However, this brecciation-dissolution event did not apparently affect the Sm budget in calcite, given the similarity of ID-TIMS and LA-ICPMS Sm values (~4 ppm, Tables 4 and 5). The existence of a brecciation event is also supported by the presence of abundant microfractures in green fluorite. The increased permeability may have favored the incorporation of Nd in green fluorite during later fluid flow as suggested by high Nd values in this phase (Tables 4 and 5, Fig. 8).

Two stages of purple fluorite occurs as cement in the Ediacaran to Cambrian sandstone overlying the basement veinlets at Laisvall (Saintilan et al. *submitted to Mineralium Deposita*): (i) minor purple fluorite coeval with strata-bound barite cementation prior to Pb-Zn sulfide mineralization, and (ii) minor purple fluorite in spots deposited after and usually beneath Pb-Zn sulfide mineralized parts of the host sandstones. These authors suggested that the first phase of fluorite precipitation occurred when Ba-bearing, relatively reduced fluids, which had long resided in basement structures and interacted with basement rocks, were expelled upwards in sandstone as a response to early Caledonian orogenic activity. Barite precipitated as the result of mixing with a pool of sulfate

contained in sandstone paleoaquifers. Following the mechanisms for fluorite precipitation presented by Spirakis and Heyl (1988) and Spirakis (2004), fluorite precipitation might have been caused by destabilization of fluoride complexes by bicarbonate ions and/or hydrocarbons that were present in the sandstone paleoaquifers at Laisvall at that time (Saintilan et al., *submitted to Mineralium Deposita*). Similar geometric relationships were reported from the Chaillac deposit in Massif Central, France where sandstone hosting stratiform Ba-F-Fe mineralization overlies Hercynian metamorphic basement that hosts F-Ba-(Pb) vein occurrences (Sizaret et al., 2004). At Chaillac, a clear genetic relationship between sandstone-hosted stratiform and basement-hosted vein-type mineralization styles was shown (Sizaret et al., 2004).

We propose that at Laisvall, after termination of the intense fluid flow that caused Pb-Zn mineralization in Middle Ordovician to be formed by oxidizing, metal-bearing brines using basement structures as plumbing system, the fluids filling structures in basement rocks re-gained equilibrium with basement rocks, i.e., similar conditions to the original Ba-bearing and relatively reduced fluids. The second phase of fluorite precipitation in sandstone, possibly formed by these reduced fluids, might then be younger than the Middle Ordovician sphalerite mineralization at Laisvall (467 ± 5 Ma; Saintilan et al., *in press*), an hypothesis that is explored in the following paragraphs.

Pink fluorite cement occurs also in feldspathic sandstone in outcrops along the Laisan River at Ackerselet, 10 km south of the location of the Laisvall mine (Saintilan, 2010, Boliden AB internal reports, unpub., Fig. 2b). This feldspathic sandstone forms the lowermost part of the Ediacaran to Lower Ordovician sedimentary cover sequence, which unconformably overlies 1.8 Ga granite in the Laisvall district (Fig. 2b). The same feldspathic sandstone has also been identified in the Laisvall mine, where it underlies the Pb-Zn mineralized Lower Sandstone (Willdén, 1980; Saintilan et al., 2015). Mineralization at Ackerselet comprises sub-horizontal mineralized layers recognized for 30 m in N–S and 10 m in W–E directions: (1) A lower fluorite layer ~50 cm thick with grades of 3–7 % CaF_2; and (2) an upper galena layer ~20 cm with grades of 1–2 % Pb separated from the fluorite mineralization by barren interlayers (Saintilan, 2010 in Boliden AB internal reports unpub.). Alm et al. (2005) presented Sm-Nd radiogenic isotope data for five pink fluorite separates sampled at Ackerselet (Table 4). Sm concentrations range from 1.78 to 5.18 ppm, while Nd varies from 8.35 to 17.89 ppm. The $^{143}Nd/^{144}Nd$ ratios range between 0.511775 ± 10 and 0.511941 ± 10, while the $^{147}Sm/^{144}Nd$ ratios vary between 0.017950 ± 72 and 0.185500 ± 742. Fluorite has low Nd contents and low $^{147}Sm/^{144}Nd$ ratios, and may be pristine and undisturbed. Alm et al. (2005) proposed a tentative five-point isochron (MSWD = 8.2) with a slope giving an age of poor significance at 423 ± 130 Ma (initial $^{143}Nd/^{144}Nd$ ratio of 0.511420 ± 130) for fluorite mineralization at Ackerselet. A Sm-Nd age of 401 ± 38 Ma was also reported by Alm et al. (2005) for apparently undisturbed, basement-hosted, fluorite vein mineralization on the western coast of Finland. These poorly constrained ages are compatible with formation post-dating the Middle Ordovician Pb-Zn mineralization (467 ± 5 Ma) at Laisvall (Saintilan

et al., *in press*), i.e., the same relative age as that recognized for the second phase of fluorite mineralization in sandstone beneath the Pb-Zn layers at Laisvall.

As explained above, we suggest that the same channels and plumbing system was used by acidic, metal-bearing fluids and by Ba-bearing and relatively reduced fluids at different times. Taking into account that green fluorite and calcite in basement veinlets are coeval, this green fluorite must post-date Pb-Zn mineralization in sandstone otherwise coarse-grained subhedral calcite crystals in basement veinlets would not have survived the flow of acidic metal-bearing fluids that caused Pb-Zn mineralization in the overlying sandstone.

The green fluorite in basement veinlets at Laisvall analyzed in the present work has similar $^{143}Nd/^{144}Nd$ ratio as the three most radiogenic pink fluorite aliquots from Ackerselet, whereas the purple fluorite has a $^{143}Nd/^{144}Nd$ ratio intermediate between these values and the other two pink fluorite aliquots at Ackerselet (Fig. 10b). At the current state of knowledge, a crude hypothesis may consider that calcite-fluorite veinlets in basement rocks at Laisvall, strata-bound and stratiform pink fluorite mineralization at Ackerselet, and the second phase of fluorite deposition in spots beneath Pb-Zn mineralization in sandstone at Laisvall might be coeval and all post-dating Middle Ordovician Pb-Zn mineralization (467 ± 5 Ma) at Laisvall.

Similar purple fluorite mineralization was encountered in autochthonous and flat-lying sandstone beneath the Caledonian thrust nappes in the Storuman area, directly to the west of the Storuman vein district in Baltica basement studied by Billström et al. (2012). This open mineralization, which is typically 3 to 10 m thick, currently amounts to 28 Mt at 10.2 % CaF_2 and extends over 1.5 km in N–S direction and 800 m in WSW–ENE direction (cf. Tertiary Minerals plc, www.tertiaryminerals.com/projects/fluorspar-projects/storuman). By analogy with the Laisvall area described above, the existence in this area of significant fluorite mineralization may indicate a large plumbing system that may have also produced Pb-Zn mineralization. Therefore, it might be of interest for Pb-Zn exploration to investigate the spatial and chronological relationship between Pb-Zn sulfide and fluorite mineralizations.

Fluid chemistry

REE fluid chemistry and redox conditions in basement veins at Åkerlandet and Laisvall: The weak positive Eu_{PAAS} anomaly in fluorite at Åkerlandet suggests uncoupling of Eu from its trivalent REE neighbors and the presence of significant amounts of Eu as reduced Eu^{2+} (Bau and Möller, 1992; Bau et al., 2003). The negative Eu anomaly in calcite at Åkerlandet and to a lesser extent at Laisvall in Fig. 9a may be explained by the discrimination during calcite precipitation against the incorporation of the large Eu^{2+} ion into the calcite crystal lattice. Like in the F-Ba vein in basement at Chaillac, France (Sizaret et al., 2004) that formed in similar geological and paleohydrological situation as at Laisvall in basement rocks beneath sedimentary cover rocks, the presence of rare pyrite associated with calcite and fluorite, and the presence of reduced Eu^{2+} in mineralizing fluids suggest that fluids were markedly

reduced (log f_{O_2} = around –55) with pH around 5 to 6, i.e., conditions not far from those proposed by Johansson (1984).

The general LREE-depletion and HREE-enrichment trend in fluorite and calcite in the basement veinlets at Laisvall and to a lower extent at Åkerlandet are compatible with the effect of preferential complexation of HREE with F^- and CO_3^{2-}, leading to HREE-enrichment in these fluids. The evolution and migration of these fluids in the basement caused fractionation of REEs with depletion of LREEs and enrichment in HREEs. The strong positive Y_{PAAS} anomalies and the non-chondritic and high Y/Ho ratios in fluorite in basement veins at Åkerlandet and Laisvall are typical of hydrothermal fluorite in medium-temperature hydrothermal systems (e.g., Bau and Dulski, 1995). Positive Y_{PAAS} anomalies in hydrothermal fluorite and a trend showing diminishing La/Ho and increasing Y/Ho ratios (Figs. 11b and 11c) are likely to illustrate migration of aqueous fluids in which REE and Y speciation is dominated by fluoro-complexes.

Åkerlandet: Microthermometry studies of fluid inclusions in sphalerite, calcite, and fluorite of the Åkerlandet vein deposit Johansson (1983b, 1984) reveal that (i) saline fluids were entrapped in sphalerite, at minimum temperatures of around 110° to 160°C; (ii) fluids at about 30 wt.% NaCl eq. were entrapped in fluorite at minimum temperatures of 80° to 120°C; (iii) fluids involved in calcite precipitation contained NaCl and probably other salts (e.g., $CaCl_2$). Last ice melting temperatures in calcite, going down to –40°C, are compatible with the presence of methane and/or $CaCl_2$.

The Sr isotope ratios in calcite and green fluorite at Åkerlandet (0.717–0.719) are much more radiogenic than the reported ratios of seawater from Paleozoic time (less than 0.710; Veizer et al., 1999). These ratios suggest that fluids acquired radiogenic Sr through interaction with crystalline basement rocks over possibly long fluid residence time in fractures. A later fluid flow could have caused the rejuvenation of the Sm-Nd system in green fluorite and calcite leaving unchanged the $^{87}Sr/^{86}Sr$ ratios.

The $\delta^{18}O$ values (–18.5 to –18.1‰, Table 6) of calcite are strongly ^{18}O-depleted compared with the oxygen isotope values of –10 to –7‰ reported for Cambrian to Ordovician carbonate rocks (cf. Veizer et al., 1999; Veizer, 2004; Menotti, 2006). On the other hand, the $\delta^{13}C$ values of calcite between –14.5 and –14.1‰ suggest that oxidation of organic matter supplied isotopically light carbon to the pool of dissolved inorganic carbon. The presence of bitumen lining and coating quartz at the contact with calcite (Figs. 6b and c) suggests that organic compounds could have been present in the fractures prior to and during calcite precipitation. The presence of solid bitumen is compatible with the earlier precipitation of fluorite that may have resulted in part from the alteration of organic compounds (e.g., liquid petroleum) by interaction with hot mineralizing fluids in fractures at the sites of mineralization (cf. Spirakis, 2004).

Interaction of hydrothermal fluids with organic compounds in reducing and neutral conditions may also explain the presence of calcite with the $\delta^{13}C$ and $\delta^{18}O$ values presented above. In addition,

heating of organic matter is one of several processes known to cause pH variation (Spirakis and Heyl, 1988). The petrographic evidence presented in the current study suggests that the sequence of precipitation-dissolution of calcite I before precipitation of calcite II at Åkerlandet could be explained in part by this process (Fig. 6d). These reduced fluids would have the potential to bear H_2S but not the potential to transport metals, hence the absence of sulfides coeval with fluorite and calcite precipitation.

Petrographic observations and the evidence from Sr, O, and C isotope data suggest that the hydrothermal fluids from which fluorite and then calcite precipitated were evolved basement-interacted and organic matter-interacted, neutral and reduced fluids. A mineral generation comprising calcite-quartz-pyrite with asphaltite and similar to that at Åkerlandet has been identified in veins along fractures at Forsmark in the south-western part of the Fennoscandian Shield, southern Sweden (Sandström et al., 2009). This mineral generation and the isotopic composition of calcite were interpreted there to be a result of a Paleozoic event marked by fluids that interacted with organic matter derived from the middle Cambrian to Lower Ordovician Alum Shale Formation (Sandström and Tullborg, 2009; Sandström et al., 2009).

Laisvall: The almost absence of sulfide minerals included in calcite in the basement veinlets at Laisvall suggests that the fluids from which calcite and fluorite precipitated had low H_2S contents or, more likely, were metal deficient because they were reducing. The $\delta^{34}S$ value (6.9‰) for the only pyrite grain found in the basement-hosted veinlets at Laisvall (Table 6) suggests that H_2S was not derived from leaching of sulfide minerals in local basement rocks as this is the case at Åkerlandet and Järvsand. This value is similar to the lower range of $\delta^{34}S$ values in diagenetic pyrite in black shale from the Alum Shale Formation (Wallin, 1982; Rickard et al., 1979; Saintilan et al., *in press*).

The $\delta^{13}C$ values for calcite between –14.3 and –13.7‰ are consistent with oxidation of organic matter supplying isotopically light carbon to the pool of dissolved inorganic carbon, similar to the interpretation presented above for Åkerlandet. These data from stable isotope geochemistry may suggest that oxidation of organic matter and the leaching of pyrite in the Alum Shale Formation in the cover stratigraphic sequence above the crystalline basement supplied isotopically light carbon to the pool of dissolved inorganic carbon and low amounts of H_2S to the mineralizing fluids, which migrated downwards to the basement.

Similarly to the interpretation drawn at Åkerlandet, calcite (range of $\delta^{18}O$ values of –18.7 to –17.3‰) and the two fluorite generations in basement-hosted veinlets at Laisvall precipitated from evolved, basement-interacted (calcite and fluorite with $^{87}Sr/^{86}Sr$ ratios of 0.720–0.732), neutral, metal-poor and relatively reduced fluids. S and C isotope data suggest that these fluids were diluted by organic matter-interacted, H_2S-bearing fluids derived from sedimentary cover rocks including the Alum Shale Formation. The much higher $^{87}Sr/^{86}Sr$ ratio in late purple fluorite (0.732) than in green fluorite and calcite (0.720) implies that it precipitated from fluids more enriched in ^{87}Sr different than

those responsible for green fluorite and calcite, or, these fluids had not been diluted by the above mentioned fluids derived from the cover sedimentary rocks that are assumed to be less radiogenic.

Indeed, hydrothermal fluorite types precipitating simultaneously should have similar Y/Ho and La/Ho ratios (Bau and Dulski, 1995). Furthermore, Bau and Dulski (1995) proposed that the extent of residence time of fluorine-rich aqueous fluids is indicated by increasing Y/Ho ratios, illustrating fractionation within the aqueous fluids. In the Laisvall basement veinlets, purple fluorite, which precipitated after green fluorite, has higher $^{87}Sr/^{86}Sr$ ratios than green fluorite but they have similar ranges of Y/Ho and La/Ho ratios. This might indicate that the scale of diachronity between these phases of fluorite precipitation is relatively small and thereby confirms that these hydrothermal fluids were diluted by fluids derived from sedimentary cover rocks during green fluorite precipitation and it was not the case during purple fluorite precipitation. In addition, the two fluorite generations at Laisvall have higher Y/Ho ratios and lower La/Ho ratios than fluorite at Åkerlandet and Y_{PAAS} anomalies are almost one order of magnitude higher. If fluids at both sites had the same original REE and Y contents, a longer crustal residence time before calcite-fluorite precipitation in the basement veinlets at Laisvall relative to those at Åkerlandet could be suggested.

Conclusions

The current study focused on the Åkerlandet and Järvsand calcite-fluorite-Zn ± Pb sulfide vein deposits and occurrences in Paleoproterozoic crystalline basement rocks (Baltica), and on calcite-fluorite ± pyrite veinlets in Paleoproterozoic granite basement beneath the Pb-Zn Laisvall deposit hosted in Ediacaran to Cambrian sandstone. The results attest of several episodes of hydrothermal fluid flow and mineral precipitation from late Paleoproterozoic to post-Middle Ordovician time in this present-day northern and northwestern part of the Fennoscandian Shield, Sweden. All these deposits have in common a mineral stage of calcite-fluorite ± pyrite and/or galena that was preceded, at the sole Åkerlandet deposit, by two other distinct stages of mineral precipitation.

Activation or reactivation of structures into N–S shear zones with bulk horizontal ENE–WSW extension (e.g., N–S main shear with NW–SE R-Riedel shears and paleotectonic implications indicating sinistral transtension at Åkerlandet) occurred in the Paleoproterozoic crystalline basement during the late Sveconorwegian orogenic event at the same time as a major dolerite dyke swarm was emplaced in the eastern foreland to the Sveconorwegian orogen. At Åkerlandet, coarse-grained euhedral to subhedral adularia dated at 950 to 980 Ma by ^{40}Ar-^{39}Ar thermochronology grew with quartz in open space from slightly acidic (pH ~ 4–5), low-temperature (100°–200° C) fluids.

At Åkerlandet, sphalerite ± galena mineralization grew in open space either at 544 ± 4 Ma (late Ediacaran) or at 468 ± 5 Ma (Middle Ordovician) onto previously deposited adularia and quartz. Zn ± Pb sulfides were formed by saline, relatively oxidizing, low-temperature (110° to 160°C) and slightly acidic hydrothermal fluids transporting metals and deriving H_2S (values of –3.1 to 0.1‰) from

the leaching of minor sulfides in basement rocks. These slightly acidic conditions are consistent with sericitization in spots observed in the host rock.

Fractures filled in by calcite, fluorite ± pyrite or galena with strike orientation at NNW–SSE and NNE–SSW to NE–SW are found in Baltica basement rocks at the Åkerlandet and Järvsand vein occurrences, and even further north in the Laisvall district where veinlets have there the same orientation as the interpreted feeder faults to the strata-bound Laisvall Pb-Zn deposit in Ediacaran to Cambrian sandstone which are inferred to be rooted downwards into the crystalline basement (cf. Saintilan et al., 2015). At Järvsand, structural analysis showed that these veins were formed in steep NNE–SSW fractures that are interpreted to be R-shears to a main shear plane corresponding to longer, steep fractures with N–S to NNW–SSE strike. Both these sets display a dextral component of movement and suggest NW–SE bulk horizontal extension (Fig. 12).

Calcite (range of $\delta^{18}O$ values of –18.7 to –17.3‰) and fluorite generations in basement-hosted veinlets at Laisvall and veins at Åkerlandet precipitated from evolved, basement-interacted (calcite and fluorite with $^{87}Sr/^{86}Sr$ ratios of 0.717–0.732), neutral, metal-poor and relatively reduced fluids (negative Eu anomaly in calcite). S (pyrite with value of 6.9‰, similar to the lower values for pyrite in the Alum Shale Formation) and C (calcite with $\delta^{13}C$ values of –14.3 to –13.7‰) isotope data suggest that these basement fluids were diluted at Laisvall by organic matter-interacted, H_2S-bearing fluids derived from sedimentary cover rocks including the middle Cambrian to Lower Ordovician Alum Shale Formation, whereas at Åkerlandet the presence of bitumen at the contact between quartz and calcite crystals and the C isotope composition of calcite (–14.5 to –14.1‰) suggest that organic compounds (e.g., liquid petroleum) may have been present in basement fractures prior to and during calcite precipitation.

Post-mineralization disturbance of Nd and/or Sm contents in fluorite and calcite at Åkerlandet and in basement veinlets at Laisvall resulted in the failure of attempts to date this mineral stage by using Sm-Nd isotope geochemistry. However, the involvement of organic compounds probably derived from the Alum Shale Formation places a minimum age of fluorite-calcite precipitation post-Lower Ordovician time.

At Laisvall, sericitization in granitic host rock around the current calcite-fluorite ± pyrite veinlets in basement at Laisvall is suggested to have been caused when these channelways were used in Middle Ordovician time (467 ± 5 Ma) as a plumbing system for oxidizing, slightly acidic, metal-bearing brines involved in Pb-Zn mineralization in overlying sandstone (Saintilan et al., *submitted to Mineralium Deposita*). Hence, coarse-grained euhedral to subhedral calcite in basement veinlets would not be likely to survive the flow of such acidic fluids and our working hypothesis considers that fluorite-calcite mineralization in veinlets in basement rocks post-dates the Middle Ordovician (467 ± 5 Ma) Pb-Zn mineralization at Laisvall when the plumbing system in the basement was re-occupied by reduced (negative Eu anomaly recorded in calcite, log f_{O_2} = around –55) and neutral (pH around 5 to 6) that were in equilibrium with basement rocks. A genetic connection between these calcite-fluorite ±

pyrite veinlets in basement at Laisvall and the post-Pb-Zn mineralization stage of purple fluorite mineralization in sandstone stratigraphically below layers of Pb-Zn sulfides in the Laisvall deposit is suggested.

These findings highlight the importance of the recognition of strata-bound bodies of fluorite mineralization in autochthonous sedimentary cover rocks deposited unconformably on basement rocks of the Fennoscandian Shield. These fluorite orebodies may be vector to the identification of channelways in basement rocks that could have been used as plumbing system for metal-bearing fluids at an earlier stage thereby possibly causing Laisvall-type Pb-Zn mineralization in sandstone.

Acknowledgements

This research has been financially supported by Boliden AB (Sweden) and the Swiss National Science Foundation (SNF, Switzerland, FN 146 353). The Geological Survey of Sweden (SGU) provided financial and logistic support for much of the fieldwork in Sweden. The staff members at SGU in Malå are thanked for their help at the national core archive. The authors are grateful to Boliden AB via Hans Årebäck (former exploration manager) for financial and logistic support for the work carried out in Boliden and to the staff working at the core archive in Boliden for their help in supplying drill cores. Dr Kalin Kouzmanov (University of Geneva) is acknowledged for constructive discussion on adularia mineralization. Jarkko Laminen (Boliden AB) is thanked for providing a sample from the Åkerlandet deposit.

References

Alm E, Huhma H, Sundblad K (2005) Preliminary Palaeozoic Sm-Nd ages of fluorite-calcite-galena veins in the southeastern part of the Fennoscandian Shield: Svensk Kärnbränslehantering AB, SKB, Open Access Report R-04-27.

Allmendinger RW, Cardozo NC, Fisher D (2013) Structural Geology Algorithms: Vectors & Tensors: Cambridge, England, Cambridge University Press, 289 pp.

Armstrong JT (1984). Quantitative analysis of silicate and oxide minerals: a re-evaluation of ZAF corrections and proposal for new Bence-Albee coefficients. Microbeam Analysis 19:208-212.

Barker SLL, Bennett VC, Cox SF, Norman MD, Gagan MK (2009) Sm-Nd, Sr, C, O isotope systematics in hydrothermal calcite-fluorite veins: Implications for fluid-rock reaction and geochronology. Chemical Geology 268:58-66

Bau M, Möller P (1992) Rare Earth Element fractionation in metamorphogenic hydrothermal calcite, magnesie and siderite. Mineralogy and Petrology 45:231-246.

Bau M, Dulski P (1995) Comparative study of yttrium and rare-earth element behavior in fluorine-rich hydrothermal fluids. Contributions to Mineralogy and Petrology 119:213-223.

Bau M, Romer RL, Lüders V, Dulski P (2003) Tracing element sources of hydrothermal mineral deposits: REE and Y distribution and Sr-Nd-Pb isotopes in fluorite from MVT deposits in the Pennine Orefield, England. Mineralium Deposita 38:992-1008.

Bergman S, Stephens MB, Andersson J, Kathol B, Bergman T (2012) Geologic map of Sweden: Geologic Survey of Sweden, scale 1:1 000 000, 1 sheet.

Billström K., Broman C, Schneider J, Pratt W, Skogsmo G (2012) Zn-Pb ores of Mississippi Valley-type in the Lycksele-Storuman District, Northern Sweden: A possible rift-related Cambrian mineralising event. Minerals 1:169-207.

Bingen B, Andersson J, Soderlun U, Moller C (2008) The Mesoproterozoic in the Nordic countries. Episodes 31: 29.

Cardozo N, Allmendinger RW (2013) Spherical projections with OSXStereonet: Computers & Geosciences 51:193 - 205.

Dallmeyer RD, Gee DG (1986) $^{40}Ar/^{39}Ar$ mineral dates from retrogressed eclogites within the Baltoscandian miogeocline: Implications for a polyphase Caledonian orogenic evolution: Geologic Society of America Bulletin 97:26-34.

Gee DG (1972) The regional geologic context of the Tåsjö uranium project, Caledonian front, Central Sweden. Geologic Survey of Sweden, Årsbok 66 2, Ser C, 671, 37 p.

Gee DG (1975) A tectonic model for the central part of the Scandinavian Caledonides. American Journal of Science 275A:468-515.

Gee DG, Juhlin C, Pascal C, Robinson P (2010) Collisional orogeny in the Scandinavian Caledonides (COSC). Journal of the Geological Society of Sweden (GFF) 132:29-44.

Glodny J, Grauert B (2009) Evolution of a hydrothermal fluid-rock interaction system as recorded by Sr isotopes: A case study from the Schwarzwald, SW Germany. Mineralogy and Petrology 95:163-178.

Greiling RO, Garfunkel Z (2007) An Early Ordovician (Finnmarkian?) foreland basin and related lithospheric flexure in the Scandinavian Caledonides. American Journal of Science 307:527-553.

Grip E (1967) On the genesis of the lead ores of the eastern border of the Caledonides in Scandinavia. Society of Economic Geologists Monograp 3:208-218.

Grip E (1973) Sulfimalm i fjällkedjan och i det baltiska kambriska flackhavsområdet. In: Grip E, Frietsch R (eds) Malm i Sverige 2, Norra Sverige, Stockholm, Almqvist and Wiksell, p. 10-66 (in Swedish).

Gromet LP, Sjöström H, Bergman S, Claesson S, Essex RM, Andreasson PG, Albrecht L (1996) Contrasts in ages of metamorphism in the Seve Nappes: U-Pb results from the central and northern Swedish Caledonides. Journal of the Geologic Survey of Sweden (GFF) 118:36-38.

Johansson Å (1980) Fluid inclusion thermometry on calcite, sphalerite and fluorite from the Åkerlandet vein, Västerbotten County, Sweden. In: Rickard DT (ed) Annual report of the ore research group, p. 188-200.

Johansson Å (1983a) Composition of sphalerite in some Swedish Pb-Zn bearing veins. In: Lindblom S (ed) Annual report of the ore research group, Stockholm University, pp. 151-166.

Johansson Å (1983b) Lead isotope composition of Caledonian Sulfide-bearing veins in Sweden. Economic Geology 78:1674-1688.

Johansson Å (1984) Fluid inclusion and stable isotope studies on some Caledonian sulfide-bearing veins in Sweden. Economic Geology 79:1736-1748.

Johansson Å, Rickard DT (1984) Isotope composition of Phanerozoic ore leads from the Swedish Segment of the Fennoscandian Shield. Mineralium Deposita 19:249-255.

Koistinen T, Stephens MB, Bogatchev V, Nordgulen Ø, Wennerström M, Korhonen J (2001) Geological map of the Fennoscandian Shield, scale 1:2,000,000, Geological Surveys of Finland, Norway and Sweden and the North-West Department of Natural Resources of Russia.

Kullerud K, Stephens MB, Zachrisson E (1990) Pillow lavas as protoliths for eclogites: evidence from a late Precambrian–Cambrian continental margin, Seve Nappes, Scandinavian Caledonides. Contributions to Mineralogy and Petrology 99:344-351.

Lilljequist R (1973) Caledonian geology of the Laisvall area, Southern Norbotten, Swedish Lappland: Stockholm, Geological Survey of Sweden, C 691, 43p.

Lindahl I, Bjørlykke A (1988) The Geitvann lead-copper (-zinc) mineralization, Porsangerhalvøya, Finnmark, northern Norway. Norsk Geologisk Tidsskrift 68:125-131.

McLennan SM (1989) Rare earth elements in sedimentary rocks: influence of provenance and sedimentary processes. In: Lipin BR, McKay GA (eds) Geochemistry and mineralogy of rare earth elements. Reviews in Mineralogy 21, Mineralogical Society of America, Washington DC, pp. 169-200.

Menotti TA (2006) Lower Paleozoic oxygen isotope values from carbonate rocks: Primary or diagenetic? Senior thesis in Geosciences, Bachelor of Science, Pennsylvania State University, Pennsylvania, USA, pp. 43.

Moorbath S, Vokes FM (1963) Lead isotope abundance studies occurrences in Norway. Norsk Geologisk Tidtskrift 43:283-343.

Nägler TF, Pettke T, Marshall D (1995) Initial isotopic heterogeneity and secondary disturbance of the Sm-Nd system in fluorites and fluid inclusions: A study on mesothermal veins from the central and western Swiss Alps: Chemical Geology, v. 125, p. 241-248.

Nielsen AT, Schovsbo NH (2011) The Lower Cambrian of Scandinavia: Depositional environment, sequence stratigraphy and paleogeography. Earth-Science Reviews 107:207-310

Pease V, Daly JS, Elming S-Å, Kumpulainen R, Moczydłowska M, Puchkov V, Roberts D, Saintot A, Stephenson R (2008) Baltica in the Cryogenian, 850–360 Ma. Precambrian Research 160:46-65.

Pearce NJ, Perkins WT, Westgate JA, Gorton MP, Jackson SE, Neal CR, Chenery SP (1997) A compilation of new and published major and trace element data for NIST SRM 610 and NIST SRM 612 glass reference materials. Geostandards newsletter 21:115-144.

Piqué A, Canals A, Grandia F, Banks DA (2008) Mesozoic fluorite veins in NE Spain record regional base metal-rich brine circulation through basin and basement during extensional tectonics. Chemical Geology 257:139-152.

Rickard DT, Willdén MY, Marinder NE, Donnelly TH (1979) Studies on the genesis of the Laisvall sandstone lead-zinc deposit, Sweden. Economic Geology 74:1255-1285.

Roberts D, Gee DG (1985) An introduction to the structure of the Scandinavian Caledonides. In: Gee DG, Sturt BA (eds) The Caledonide Orogen - Scandinavia and related areas, Chichester, Wiley, pp.55-68.

Roberts D, Siedlecka A (2002) Timanian orogenic deformation along the northeastern margin of Baltica, Northwest Russia and Northeast Norway, and Avalonian–Cadomian connections. Tectonophysics 352:169-184.

Romer RL (1992) Sandstone-hosted lead-zinc mineral deposits and their relation to the tectonic mobilization of the Baltic Shield during the Caledonian orogeny, a reinterpretation. Mineralogy and Petrology 47:67-85.

Romer RL, Wright JE (1993) Lead mobilization during tectonic reactivation of the western Baltic Shield. Geochimica et Cosmochimica Acta 57:2555-2570.

Root D, Corfu F (2012) U-Pb geochronology of two discrete Ordovician high-pressure metamorphic events in the Seve Nappe Complex, Scandinavian Caledonides. Contribution to Mineralogy and Petrology 163:769-788.

Saintilan NJ, Stephens MB, Lundstam E, Fontboté L (2015) Control of reactivated basement structures on sandstone-hosted Pb-Zn deposits along the Caledonian Front, Sweden: Evidence from airborne magnetic field data, structural analysis and ore grade modeling. Economic Geology 110:91-117.

Saintot A, Stephens MB, Viola G and Nordgulen Ø (2011) Brittle tectonic evolution and paleostress field reconstruction in the southwestern part of the Fennoscandian Shield, Forsmark, Sweden. Tectonics 30:TC4002.

Santallier DS (1988) Mineralogy and crystallization of the Seve eclogites in the Vuoggatjålme area, Swedish Caledonides of Norrbotten: Journal of the Geologic Society of Sweden (GFF) 110:89-98.

Sandström B, Tullborg E-L (2009) Episodic fluid migration in the Fennoscandian Shield recorded by stable isotopes, rare earth elements and fluid inclusions in fracture minerals at Forsmark, Sweden. Chemical Geology 266:126-142.

Sandström B, Tullborg E-L, Larson SÅ, Page L (2009) Brittle tectonothermal evolution in the Forsmark area, central Fennoscandian Shield, recorded by paragenesis, orientation and ^{40}Ar-^{39}Ar geochronology of fracture minerals. Tectonophysics 478:158-174.

Sizaret S, Marcoux E, Jébrak M, Touray JC (2004) The Rossignol fluorite vein, Chaillac, France: Multiphase hydrothermal activity and intravein sedimentation. Economic Geology 99:1107-1122.

Skiöld T (1988) Implications of new U-Pb zircon chronology to early Proterozoic crustal accretion in northern Sweden. Precambrian Research 38:147-164.

Söderlund U, Isachsen C, Bylund G, Heaman L, Patchett PJ, Vervoort JD, Andersson UB (2005) U-Pb baddeleyite ages and Hf, Nd isotope chemistry constraining repeated mafic magmatism in the Fennoscandian Shield from 1.6 to 0.9 Ga. Contributions to Mineralogy and Petrology 150:174-194

Spirakis CS (2004) "Fluorite deposits at Encantada-Buenavista, Mexico: products of Mississippi Valley-type processes" [Ore Geol. Rev. 23 (2003), 107-124] - a discussion. Ore Geology Reviews 25:327-328.

Spirakis CS, Heyl AV (1988) Possible effects of thermal degradation of organic matter on the carbonate paragenesis and fluorite precipitation in Mississippi Valley-type deposits. Geology 16:1117-1120

Stephens MB (1986) Stratabound sulfide deposits in the Central Scandinavian Caledonides: 7th IAGOD Symposium and Nordkallot project meeting, Excursion Guide n°2, Ca 60, Geological Survey of Sweden, Uppsala, Sweden, 68 p.

Stephens MB (1988) The Scandinavian Caledonides: a complexity of collisions. Geology Today 4:20-26.

Stephens MB, Follin S, Petersson J, Isaksson H, Juhlin C, Simeonov A (2015) Review of the deterministic modelling of deformation zones and fracture domains at the site proposed for a spent nuclear fuel repository, Sweden, and consequences of structural anisotropy. Tectonophysics 653:68-94.

Sturt BA (1978) The Norwegian Caledonides. Geological Survey of Canada Paper 78:13-16.

Sundblad K (1990) Precambrian metal sources in sulfide deposits in the northernmost part of the Scandes. Journal of the Geologic Society of Sweden (GFF) 111:415-418.

Svenningsen OM (2001) Onset of seafloor spreading in the Iapetus Ocean at 608 Ma: precise age of the Sarek Dyke Swarm, northern Swedish Caledonides. Precambrian Research 110:241-254.

Tanaka T, Togashi S, Kamioka H, Amakawa H, Kagami H, Hamamoto T, Dragusanu C (2000) JNdi-1: a neodymium isotopic reference in consistency with LaJolla neodymium. Chemical Geology 168:279-281.

Veizer J (2004) Isotope data, Phanerozoic database, $\delta^{18}O$ update-2004: http://www.science.uottawa.ca/geology/isotope_data

Veizer J, Ala D, Azmy K, Bruckschen P, Buhl D, Bruhn F, Carden GAF, Diener A, Ebneth S, Godderis Y, Jasper T, Korte C, Pawellek F, Podlaha OG, Strauss H (1999) $^{87}Sr/^{86}Sr$, $\delta^{13}C$ and $\delta^{18}O$ evolution of Phanerozoic seawater. Chemical Geology 161:59-88.

Villagomez D, Spikings R (2013) Thermochronology and tectonics of the Central and Western Cordilleras of Colombia: Early Cretaceous–Tertiary evolution of the Northern Andes. Lithos 160-161:228-249.

Wallin B (1982) Sedimentology of the Lower Cambrian sequence at Vassbo, Sweden. PhD thesis Acta Universitatis Stockholmiensis, Stockholm, Sweden

Wickman FE, Blomqvist NG, Geijer P, Parwel A, Ubisch HV, Welin E (1963) Isotopic constitution of ore lead in Sweden. Arkiv f. Min. Gel. 3:193-257.

Willdén MY (1980) Paleoenvironment of the autochthonous sedimentary rocks sequence at Laisvall, Swedish Caledonides: PhD thesis, Stockholm, Sweden, Stockholms Universitets Geologiska Institutionen, 100 p.

Zachrisson E (1980) Aspects of stratabound base metal mineralisation in the Swedish Caledonides. In: Vokes FM, Zachrisson E (eds) Review of Caledonian-Appalachian stratabound sulfide deposits, Geological Survey of Ireland, Special Paper 5, p.41-61.

CHAPTER 2

Appendices 1, 2, 3, and 4

Appendix 1.

Rb-Sr isotope analysis of sphalerite and whole-rock samples

Details on total procedural blanks and offline reduction of sphalerite Rb-Sr isotope data

Repeated static measurements of the NBS 987 Sr standard during the course of this study yielded 0.71025±4 (2σ mean, n=13). Total procedural blanks (n=8) amounted to 7–20 pg Sr/2 pg Rb for sphalerite residues and 15–25 pg Sr/2–5 pg Rb for the fluid leachates.

For offline reduction of sphalerite Rb-Sr isotope data, lab-internal routines were used that allow for concomitant fractionation correction, spike unmixing, isotope ratio and concentration calculation, and propagation of within-run and external errors (errors on spike/sample ratio and spike and sample weights). Sr isotopic ratios were normalized to $^{86}Sr/^{88}Sr=0.1194$ and measured $^{87}Rb/^{85}Rb$ ratios normalized using a mean fractionation factor δ=0.60226±0.1148 %/[amu] determined from repeated measurements (n=12) of natural Rb extracted from whole-rock samples. Estimated errors of 1.5 and 0.5 % were conservatively assigned to the sample and spike weights, respectively. All data were blank-corrected. Individual uncertainties (2σ) were determined for Rb-Sr elemental concentrations and isotope ratios.

Details of corrections for in-run and external fractionation on whole-rock samples analyses

The $^{87}Sr/^{86}Sr$ ratio was corrected in-run for fractionation using $^{88}Sr/^{86}Sr=8.375209$. The ratio so obtained was subsequently corrected by -0.083‰ for external fractionation based on the measured $^{87}Sr/^{86}Sr$ value of the SRM987 standard compared to a nominal value of this standard of 0.710248. The long-term reproducibility of the SRM987 standard is 10 ppm (N>100 over a period longer than 1 year). The uncertainty on the measurements is determined by the reproducibility of the standard SRM987.

Appendix 2. Microprobe analyses of sphalerite in the Upper Sandstone and Lower Sandstone orebodies at Laisvall, and sphalerite at the Åkerlandet vein deposit in Paleoproterozoic basement.

	S(wt%)	Mn(wt%)	Fe(wt%)	Cu(wt%)	Zn(wt%)	Cd(wt%)	TOTAL (%)	MnS (mol%)	FeS (mol%)	CuS (mol%)	ZnS (mol%)	CdS (mol%)
Sphalerite, Upper Sandstone orebody, Laisvall												
	32.57	0.04	0.47	<0.02	66.50	0.16	99.75	0.07	0.82	-	98.96	0.14
	32.69	0.03	0.48	<0.02	66.74	0.15	100.09	0.06	0.83	-	98.98	0.13
	33.54	0.03	0.46	<0.02	66.90	0.19	101.12	0.05	0.80	-	98.99	0.16
	32.95	0.03	0.51	<0.02	67.08	0.19	100.76	0.06	0.87	-	98.91	0.16
	32.44	0.03	0.51	<0.02	66.39	0.20	99.56	0.04	0.89	-	98.89	0.17
	32.89	<0.01	0.50	<0.02	66.32	0.17	99.89	-	0.88	-	98.97	0.15
	32.58	0.03	0.52	<0.02	65.92	0.19	99.24	0.05	0.92	-	98.87	0.17
	32.82	<0.01	0.49	<0.02	66.31	0.17	99.80	-	0.85	-	99.00	0.15
	32.88	<0.01	0.52	<0.02	66.86	0.18	100.43	-	0.89	-	98.95	0.16
	33.06	0.02	0.52	<0.02	66.81	0.17	100.59	0.04	0.90	-	98.91	0.15
	33.00	<0.01	0.49	<0.02	66.64	0.17	100.31	-	0.86	-	98.99	0.15
	32.82	0.03	0.46	<0.02	66.18	0.17	99.66	0.05	0.81	-	99.00	0.15
	32.81	0.03	0.46	<0.02	66.58	0.19	100.06	0.05	0.80	-	98.99	0.16
	32.90	<0.01	0.46	<0.02	66.73	0.15	100.24	-	0.80	-	99.07	0.13
	32.87	<0.01	0.48	<0.02	66.91	0.17	100.42	-	0.83	-	99.02	0.14
	32.83	<0.01	0.54	<0.02	66.06	0.17	99.60	-	0.95	-	98.90	0.15
	32.81	0.03	0.56	<0.02	66.35	0.16	99.90	0.05	0.98	-	98.83	0.14
	32.84	<0.01	0.54	<0.02	66.31	0.20	99.89	-	0.95	-	98.88	0.17
	33.01	0.03	0.59	<0.02	66.07	0.19	99.89	0.06	1.02	-	98.75	0.16
	32.95	0.03	0.57	<0.02	66.71	0.18	100.43	0.05	0.99	-	98.81	0.15
	32.85	<0.01	0.62	<0.02	66.11	0.17	99.76	-	1.09	-	98.76	0.15
	33.24	<0.01	0.59	<0.02	66.71	0.18	100.73	-	1.03	-	98.82	0.16
	33.65	<0.01	2.22	0.20	64.41	0.19	100.67	-	3.86	0.30	95.68	0.16
	32.90	<0.01	0.60	<0.02	66.53	0.17	100.19	-	1.04	-	98.81	0.15
	33.04	<0.01	0.55	<0.02	66.09	0.16	99.83	-	0.96	-	98.90	0.14
	32.61	0.03	0.56	<0.02	66.38	0.19	99.78	0.05	0.98	-	98.80	0.16
	32.71	0.02	0.57	<0.02	66.48	0.20	99.99	0.04	1.00	-	98.79	0.17
	32.76	0.04	0.55	<0.02	67.14	0.19	100.69	0.07	0.94	-	98.82	0.17
	32.82	0.03	0.63	<0.02	66.68	0.19	100.35	0.05	1.08	-	98.70	0.16
	32.86	0.03	0.64	<0.02	66.41	0.19	100.12	0.05	1.11	-	98.68	0.16
	33.08	0.03	0.61	<0.02	66.47	0.18	100.36	0.05	1.06	-	98.73	0.16
	32.92	0.04	0.59	<0.02	66.36	0.20	100.11	0.06	1.03	-	98.73	0.17
	33.06	0.03	0.60	<0.02	66.30	0.18	100.17	0.06	1.04	-	98.75	0.16
	32.90	0.03	0.56	<0.02	66.55	0.19	100.23	0.06	0.98	-	98.81	0.16
	33.18	<0.01	0.61	<0.02	66.09	0.18	100.07	-	1.07	-	98.77	0.16
Geometric mean	32.91	0.03	0.56	0.20	66.43	0.18	-	0.05	0.98	0.30	98.78	0.15
Standard dev.	0.24	0.00	0.28	0.00	0.46	0.01	-	0.01	0.49	0.00	0.54	0.01
Sphalerite, Lower Sandstone orebody, Laisvall												
	33.27	<0.01	0.21	<0.02	66.81	0.25	100.53	-	0.36	-	99.43	0.21
	33.05	0.02	0.21	<0.02	66.99	0.26	100.54	0.04	0.37	-	99.37	0.23
	33.34	<0.01	0.19	<0.02	67.28	0.25	101.06	-	0.33	-	99.46	0.21
	32.76	<0.01	0.22	<0.02	66.79	0.27	100.04	-	0.37	-	99.39	0.24
	32.76	<0.01	0.20	<0.02	66.55	0.26	99.76	-	0.34	-	99.43	0.23
	31.81	0.01	0.18	<0.02	66.21	0.27	98.48	0.03	0.31	-	99.43	0.24
	32.67	0.03	0.20	<0.02	66.13	0.26	99.29	0.05	0.36	-	99.37	0.23
	32.48	0.03	0.25	<0.02	66.28	0.27	99.31	0.05	0.44	-	99.27	0.24
	32.47	0.03	0.20	<0.02	66.36	0.26	99.31	0.05	0.34	-	99.38	0.22
	32.58	0.03	0.23	<0.02	66.55	0.24	99.63	0.05	0.41	-	99.33	0.21

	S(wt%)	Mn(wt%)	Fe(wt%)	Cu(wt%)	Zn(wt%)	Cd(wt%)	TOTAL (%)	MnS (mol%)	FeS (mol%)	CuS (mol%)	ZnS (mol%)	CdS (mol%)
	32.67	<0.01	0.22	<0.02	66.92	0.26	100.06	-	0.38	-	99.39	0.22
	32.71	<0.01	0.17	<0.02	67.18	0.29	100.34	-	0.29	-	99.46	0.25
	32.93	<0.01	0.25	<0.02	67.18	0.25	100.62	-	0.44	-	99.34	0.21
	32.75	<0.01	0.18	<0.02	67.25	0.27	100.46	-	0.32	-	99.45	0.24
	32.68	0.03	0.21	<0.02	66.46	0.26	99.65	0.06	0.37	-	99.34	0.23
	32.83	0.03	0.20	<0.02	66.44	0.25	99.75	0.05	0.35	-	99.38	0.22
	32.48	<0.01	0.15	<0.02	66.92	0.24	99.79	-	0.25	-	99.54	0.21
	32.20	<0.01	0.21	0.03	66.60	0.26	99.30	-	0.36	0.05	99.37	0.22
	32.69	<0.01	0.18	<0.02	66.48	0.25	99.60	-	0.31	-	99.47	0.22
	32.71	<0.01	0.20	0.03	66.77	0.28	99.99	-	0.34	0.05	99.36	0.24
	32.77	<0.01	0.17	<0.02	67.04	0.26	100.23	-	0.29	-	99.48	0.22
	32.72	<0.01	0.18	<0.02	67.10	0.27	100.27	-	0.32	-	99.45	0.23
	32.74	<0.01	0.17	<0.02	66.50	0.26	99.67	-	0.30	-	99.47	0.22
	32.68	<0.01	0.20	<0.02	67.11	0.26	100.24	-	0.34	-	99.43	0.22
	32.86	<0.01	0.17	<0.02	67.28	0.25	100.56	-	0.29	-	99.50	0.22
	32.80	<0.01	0.17	<0.02	67.01	0.25	100.24	-	0.30	-	99.48	0.22
Geometric mean	32.71	0.03	0.19	0.03	66.78	0.26	-	0.04	0.34	0.05	99.41	0.22
Standard dev.	0.29	0.01	0.03	0.00	0.35	0.01	-	0.01	0.04	0.00	0.06	0.01
Sphalerite, Åkerlandet vein deposit												
	33.15	0.04	3.62	<0.02	63.04	0.48	100.34	0.08	6.28	-	93.23	0.41
	33.09	0.06	3.86	0.05	62.60	0.16	99.81	0.10	6.71	0.08	92.98	0.14
	33.00	0.06	3.78	<0.02	62.32	0.41	99.57	0.10	6.60	-	92.94	0.36
	32.71	0.02	2.08	<0.02	64.52	0.17	99.51	0.04	3.64	-	96.18	0.14
	33.07	0.05	3.37	0.04	62.74	0.17	99.44	0.09	5.90	0.06	93.79	0.15
	32.95	0.03	2.83	0.02	63.28	0.18	99.29	0.05	4.97	0.03	94.79	0.16
	32.77	<0.01	1.50	<0.02	65.30	0.11	99.68	-	2.62	-	97.29	0.09
	32.75	<0.01	2.79	<0.02	63.51	0.18	99.22	-	4.88	-	94.97	0.16
	32.84	0.04	2.99	<0.02	62.98	0.25	99.11	0.08	5.25	-	94.45	0.22
	32.77	0.04	2.46	<0.02	63.79	0.31	99.37	0.07	4.30	-	95.36	0.27
	32.75	0.03	2.38	<0.02	64.10	0.17	99.43	0.05	4.15	-	95.65	0.15
	32.84	0.04	3.63	<0.02	62.07	0.19	98.77	0.08	6.39	-	93.37	0.17
	32.80	0.05	4.12	<0.02	61.96	0.13	99.06	0.09	7.20	-	92.59	0.11
	32.95	<0.01	2.66	<0.02	63.94	0.19	99.74	-	4.63	-	95.20	0.17
	32.76	<0.01	2.69	<0.02	63.63	0.21	99.28	-	4.70	-	95.12	0.18
Geometric mean	32.88	0.04	2.89	0.03	63.31	0.20	-	0.07	5.05	0.05	94.52	0.18
Standard dev.	0.14	0.01	0.71	0.01	0.90	0.10	-	0.02	1.24	0.02	1.31	0.09

Appendix 3. LA-ICPMS analyses of sphalerite in the Upper Sandstone and Lower Sandstone orebodies at Laisvall, and sphalerite at the Åkerlandet vein deposit in Paleoproterozoic basement.

	P ppm	Mn ppm	Fe ppm	Cu ppm	Ga ppm	Rb ppm	Sr ppm	Ag ppm	Cd ppm	In ppm	Sn ppm	Sb ppm	Pb ppm
Sphalerite, Upper Sandstone orebody, Laisvall (n=40)													
	22	222	5510	131	1.20	0.07	0.27	10.86	2496	9.78	0.47	0.77	385
	22	251	5617	127	0.87	0.08	0.17	13.79	2520	3.30	0.58	0.23	530
	21	290	5472	139	1.27	0.11	0.70	13.41	2457	10.06	0.57	0.55	389
	27	262	5080	144	1.07	0.18	1.29	16.42	2498	12.19	0.98	0.56	604
	26	371	5372	137	0.94	0.17	0.83	14.34	2480	16.15	0.66	0.90	569
	24	155	5352	121	0.99	<0.05	0.11	9.03	2504	30	0.62	1.10	359
	30	148	5068	101	0.76	<0.05	0.06	10.05	2382	0.62	0.64	<0.10	358
	27	179	5103	116	0.89	<0.05	0.12	10.86	2466	1.44	0.53	0.28	348
	33	183	4490	149	0.94	0.14	0.48	14.18	2363	2.93	0.53	0.36	659
	34	163	4623	123	0.88	0.11	0.25	9.59	2436	5.67	0.42	0.21	462
	36	184	4328	132	0.88	0.18	0.39	8.43	2161	5.67	0.57	0.20	330
	36	184	4328	132	0.88	0.18	0.39	8.43	2161	5.67	0.57	0.20	330
	38	73	3934	98	1.02	<0.05	0.13	7.39	2088	6.23	0.45	0.55	109
	39	207	4199	134	1.06	0.20	1.61	11.86	2199	6.52	0.49	0.34	519
	163	178	4427	129	1.12	0.21	3.59	11.46	2255	8.22	0.88	2.11	422
	56	118	4114	117	1.21	0.14	0.69	14.13	2107	14.14	0.70	2.12	280
	57	151	4122	124	0.81	0.21	0.69	12.66	2172	7.37	0.38	0.34	342
	72	54	4176	100	0.84	<0.05	0.18	5.01	2134	0.13	0.37	<0.10	190
	77	22	4176	106	0.84	<0.05	<0.02	3.41	2083	0.06	<0.36	<0.10	71
	70	79	4148	100	1.14	<0.05	0.65	10.80	2115	9.71	0.76	0.58	219
	102	228	5457	128	0.91	0.52	2.33	14.59	2157	4.67	0.70	1.34	589
	104	85	5136	97	0.88	<0.05	3.47	6.54	2075	1.24	0.38	0.81	138
	122	140	5285	116	1.32	<0.05	12.08	7.84	2107	12.06	0.80	1.23	207
	127	180	5479	110	1.23	0.80	16.41	16.03	2167	2.40	0.85	1.13	458
	167	146	5549	116	7.46	<0.05	6.25	13.55	2188	13.53	1.78	1.25	303
	162	185	5593	143	12.97	1.61	33	16.36	2129	20.80	2.35	2.45	291
	292	175	5211	115	1.01	1.27	27	22	2132	5.62	0.60	1.75	566
	19	132	3873	134	1.14	0.16	7.86	12.36	2539	3.74	0.41	0.58	423
	20	68	3883	144	1.01	0.12	9.45	8.51	2585	0.34	0.48	<0.10	173
	20	112	3768	165	1.22	0.06	0.25	12.87	2446	0.68	0.64	0.23	383
	31	113	3893	115	2.12	0.36	0.26	11.47	2432	17.30	2.42	2.06	122
	20	158	4192	126	0.93	0.07	0.07	10.35	2695	0.03	0.51	0.19	411
	20	104	4206	107	0.78	<0.05	0.07	5.73	2628	0.42	0.61	0.10	226
	18	110	4153	112	2.76	0.25	10.50	8.71	2508	14.99	0.43	0.80	155
	17	241	4388	136	1.46	0.22	4.09	12.40	2567	10.64	0.39	0.53	364
	16	185	4102	116	0.99	0.06	0.29	10.06	2488	6.28	0.41	0.30	296
	18	74	4093	101	1.08	<0.05	0.17	11.24	2630	13.99	0.41	0.56	94
	17	84	4170	118	0.92	<0.05	0.03	5.12	2494	0.30	<0.36	<0.10	122
	22	203	4064	152	2.05	1.03	0.93	15.57	2280	12.09	0.83	1.58	308
	16	35	3859	84	1.21	<0.05	<0.02	14.89	2145	14.29	1.26	1.84	19
Min	16	22	3768	84	0.76	0.06	0.03	3.41	2075	0.03	0.37	0.10	19
Max	292	371	5617	165	12.97	1.61	33	22	2695	30	2.42	2.45	659
Median	31	157	4328	122	1.02	0.18	0.67	11.35	2372	6.25	0.58	0.58	336
Geometric mean	39	137	4560	121	1.20	0.20	0.80	10.63	2329	3.75	0.63	0.62	275
Standard deviation	58	71	616	17	2.11	0.39	7.28	3.67	190	6.66	0.47	0.66	160
Sphalerite, Lower Sandstone orebody, Laisvall (n=20)													
	16	103	1556	157	16.52	0.06	0.34	7.77	3276	18.78	3.19	1.55	73
	15	135	1612	156	21.48	0.05	0.23	7.28	3241	14.00	5.00	0.78	216
	17	9	1505	112	1.08	<0.05	0.07	7.93	3269	40	4.50	3.79	13
	16	116	1843	180	5.65	0.42	17.06	16.00	3335	14.86	1.18	10.77	486
	18	145	1945	163	8.48	0.24	8.86	11.66	3477	1.61	1.14	6.68	154
	18	87	1893	152	4.80	0.60	30.79	10.99	3412	3.03	0.74	18.57	215
	17	53	2065	158	33	0.15	5.16	9.51	3509	0.68	1.96	0.96	127

	P ppm	Mn ppm	Fe ppm	Cu ppm	Ga ppm	Rb ppm	Sr ppm	Ag ppm	Cd ppm	In ppm	Sn ppm	Sb ppm	Pb ppm
	18	75	2019	185	51	0.32	14.36	14.53	3507	0.61	3.63	13.57	228
	16	114	1782	183	53	0.41	17.87	15.26	3552	3.57	4.32	17.16	299
	16	43	1785	117	5.78	0.20	8.59	5.55	3657	1.45	7.00	2.88	103
	16	30	2139	189	63	0.18	5.48	13.25	3570	0.91	3.83	1.75	263
	15	95	1977	168	37	0.07	1.18	7.89	3637	1.09	4.91	0.35	197
	18	112	1944	186	46	0.12	4.98	9.81	3657	5.25	2.93	1.24	262
	17	92	1756	133	3.53	0.06	4.41	5.69	3789	4.17	0.72	0.80	166
	20	76	1528	298	51	<0.05	0.10	27	3481	36	2.29	20.61	30
	21	12	1746	109	0.93	<0.05	<0.02	2.37	3447	36	8.16	0.21	2
	20	10	1625	116	0.98	<0.05	0.56	3.07	3414	46	4.40	1.03	3
	19	14	1816	106	0.83	<0.05	0.06	1.85	3358	35	6.17	<0.10	2
	18	48	1586	181	21.41	<0.05	<0.02	11.56	3489	36	3.58	6.44	11
	17	14	2768	1274	0.89	<0.05	<0.02	1.55	3396	58	1.08	0.32	2
Min	15	9	1505	106	0.83	0.05	0.06	1.55	3241	0.61	0.72	0.21	2
Max	21	145	2768	1274	63	0.60	30.79	27	3789	58	8.16	20.61	486
Median	17	75	1800	160	12	0.18	4.98	9	3479	10	3.60	1.75	140
Geometric mean	17	50	1826	173	9	0.17	2.01	8	3471	7	2.84	2.44	54
Standard deviation	2	44	279	246	21	0.16	8.30	6	140	18	2.05	6.70	128
Sphalerite, Åkerlandet (n=31)													
	8.05	262	23542	469	410	<0.03	0.03	1.25	1442	0.15	4.37	0.22	0.39
	9.62	329	27892	335	272	<0.03	<0.02	4.30	2836	0.02	0.81	12.67	11.28
	10.31	260	26472	609	558	<0.03	0.10	2.17	1464	<0.02	0.63	1.14	3.14
	11.25	253	23846	358	344	<0.03	<0.02	2.38	1628	0.02	0.66	1.50	2.59
	11.26	306	24795	282	239	<0.03	0.09	2.54	2581	0.03	<0.28	4.23	5.44
	11.44	260	20995	307	266	<0.03	<0.02	2.11	1845	0.03	0.35	1.11	1.91
	12.54	265	20477	265	166	<0.03	<0.02	6.06	1601	0.03	0.69	0.80	8.95
	11.99	389	33514	341	253	<0.03	<0.02	5.19	1131	0.03	5.20	<0.10	1.26
	13.81	428	56366	209	111	<0.03	<0.02	6.35	1516	0.19	4.78	<0.10	0.82
	12.68	103	21404	159	64	<0.03	<0.02	1.04	1358	3.45	0.36	0.12	0.37
	12.62	120	23127	195	101	<0.03	<0.02	1.63	1398	5.50	1.05	0.13	0.54
	11.84	135	23231	176	86	<0.03	<0.02	1.28	1388	1.78	1.07	<0.10	0.22
	12.23	144	24049	155	50	<0.03	<0.02	1.11	1431	0.55	0.87	<0.10	0.52
	13.02	135	23599	154	62	<0.03	0.03	1.77	1399	0.40	0.81	<0.10	0.72
	10.99	206	30830	873	442	1.05	1.02	38.72	1439	0.28	19.79	16.43	298
	11.32	247	34304	883	518	<0.03	0.05	27.83	1923	1.58	40	15.82	466
	11.09	211	30616	697	621	<0.03	0.48	11.16	1560	1.50	26	19.55	6.45
	11.71	309	23445	355	267	<0.03	0.06	4.15	1646	0.03	1.04	1.00	1.44
	10.38	249	22764	326	291	<0.03	0.07	1.92	1285	<0.02	0.93	0.65	0.99
	10.79	285	21878	215	123	0.04	0.30	3.01	2136	<0.02	0.83	2.99	3.57
	10.58	275	23911	459	406	<0.03	<0.02	1.85	1277	<0.02	0.64	0.31	0.41
	10.86	254	21496	396	295	<0.03	0.14	1.37	1209	0.08	2.79	0.30	3.65
	11.64	360	45785	243	65	<0.03	<0.02	8.32	1271	0.18	1.87	0.61	3.54
	10.99	243	32456	146	38	<0.03	0.03	9.32	1031	0.84	1.35	0.10	1.34
	10.63	102	22585	128	20.07	<0.03	<0.02	2.80	1382	8.20	1.45	0.25	1.17
	8.87	340	29587	525	460	<0.03	<0.02	9.69	1165	0.02	2.30	0.67	4.20
	10.74	299	25619	390	309	<0.03	0.05	6.83	1210	0.03	3.37	0.30	1.84
	10.81	308	38245	159	32	<0.03	<0.02	7.26	1150	0.35	2.08	0.47	1.82
	9.71	97	21133	117	9.46	<0.03	0.03	1.37	1358	5.83	1.84	<0.10	0.63
	9.92	97	22242	130	14.98	<0.03	0.02	6.10	1299	10.69	2.34	0.20	5.48
	9.29	267	32866	151	37	<0.03	0.03	6.61	1082	1.18	3.61	0.23	1.54
Min	8.0	97	20477	117	9.46	0.04	0.02	1.04	1031	0.02	0.35	0.10	0.22
Max	13.8	428	56366	883	621	1.05	1.02	38.72	2836	10.69	40	19.55	466
Median	11	260	23911	282	239	0.54	0.06	3.01	1398	0.28	1	0.65	2
Geometric mean	11	224	26660	278	138	0.20	0.07	3.73	1456	0.29	2	0.85	2
Standard deviation	1.2	88	7808	204	177	0.50	0.25	7.82	399	2.72	9	5.76	96

Appendix 4. XRF analyses of oxides and trace elements in stratigraphic units above sandstone hosting mineralization at Laisvall

Sample	11LAI45, dark grey shale	11LAI26, green shale	11LAI03-1, phosphorite, black shale clast polymict conglomerate, poorly galena-mineralized	11LAI03-2, phosphorite, black shale clast polymict conglomerate with sphalerite mineralization
SiO_2 (wt%)	72.32	61.19	-	-
TiO_2	0.45	0.91	-	-
Al_2O_3	7.91	17.63	-	-
Fe_2O_3	6.41	6.23	-	-
MnO	0.18	0.04	-	-
MgO	2.06	2.17	-	-
CaO	2.84	0.72	-	-
Na_2O	0.13	0.60	-	-
K_2O	2.08	5.61	-	-
P_2O_5	0.16	0.26	-	-
LOI	3.16	3.74	-	-
Cr_2O_3	0.01	0.01	-	-
NiO	-	0.01	-	-
T.O.C	1.08	-	-	-
Sum	98.79	99.12	-	-
Sc (ppm)	7.1	14.5	<1	<1
V	54	103	2.9	9.0
Cr	45	81	8.6	13
Mn	1441	311	1433	1156
Co	17	15	3.7	<1
Ni	19.0	34	5.6	3.9
Cu	15.6	12.1	16.6	b.d.
Zn	21	29	1895	24300
Ga	10.8	22	2.2	15.5
Ge	2.1	2.5	<1	<1
As	14	4.3	7.9	0.9
Br	1.5	0.6	1.6	1.4
Rb	111	372	10	30
Sr	40	50	122	77
Y	25	34	21	22
Zr	146	209	50	60
Nb	7.3	15.8	1.7	1.9
Mo	<1	<1	1.7	2.3
Cd	<3	<3	10.1	157
Te	2.7	<2	2.1	2.6
Cs	6.0	18.5	5.2	49
Ba	363	872	67	164
La	30	48	18	15
Ce	54	78	31	35
Nd	28	34	24	23
Sm	5.8	4.2	7.3	7.2
Yb	2.8	2.7	2.0	4.2
Hf	2.1	1.8	7.6	91
Ta	0.4	2.0	2.5	26
W	1.5	2.5	<1	<1
Hg	<1	<1	<1	2.1

Sample	11LAI45, dark grey shale	11LAI26, green shale	11LAI03-1, phosphorite, black shale clast polymict conglomerate, poorly galena-mineralized	11LAI03-2, phosphorite, black shale clast polymict conglomerate with sphalerite mineralization
Tl	<1	2.6	<1	0.9
Pb	13.3	4.5	114	70
Th	6.7	13.7	2.0	3.0
U	1.1	4.2	1.7	1.5

Ag, Sb, I are below the detection limit of 3 ppm

CHAPTER 3

Appendices and data repository

[1]GSA Data Repository item 2015xxx, description of material and methods, and, Tables DR1, DR2, and DR3 (lead isotope compositions of Pb-Zn sulfides and whole rock samples), is available online at www.geosociety.org/pubs/ft20YY.htm, or on request from editing@geosociety.org or Documents Secretary, GSA, P.O. Box 9140, Boulder, CO 80301, USA.

MATERIAL AND METHODS

Mineralized sandstone samples at Laisvall were crushed using a hydraulic press, sieved and the 315–125 μm size fraction was used. A few micrograms of galena were handpicked from the heavy mineral fraction under a binocular microscope. Galena fragments were obtained directly from macroscopic vein samples from the Åkerlandet deposit. Pure galena was dissolved in 14 N HNO_3, dried down and then diluted in 2% HNO_3.

Measurements of Pb isotopic composition was carried out on a Neptune Plus MC-ICPMS at the Department of Earth Sciences, University of Geneva, Switzerland, by adding Tl to the sample solution and using the $^{203}Tl/^{205}Tl$ ratio (0.418922) to correct for internal mass fractionation. ^{204}Hg interference on ^{204}Pb was corrected by monitoring ^{202}Hg. The Pb isotope ratios were also corrected for external fractionation to the values of the SRM981 standard of Todt et al. (1996). The long-term reproducibility of Pb isotope ratios is 0.0048 % for $^{206}Pb/^{204}Pb$, 0.0049 % $^{207}Pb/^{204}Pb$, and 0.0062 % $^{208}Pb/^{204}Pb$.

LEAD ISOTOPE COMPOSITION AND SOURCE MODEL AGES

The slopes with positive and negative uncertainty (2σ) of the respective lines for sulfides from Laisvall and from the combined vein deposits in the Storuman and Åkerlandet districts were determined using a robust, nonparametric regression that makes no assumptions about the cause(s) of the observed scatter of the data from a straight line, and that requires no arbitrary decisions about what data should or should not be included in the regression (Ludwig, 2003).

REFERENCES

Ludwig, K. R., 2003, User's manual for Isoplot 3.00: a geochronological toolkit for Microsoft Excel (No. 4).

Todt, W., Cliff, W.A., Hanser, A., and Hofmann, A.W.,1996, Evaluation of a 202Pb–205Pb double spike for high-precision lead isotope analysis: Earth processes: reading the isotopic code, p. 429-437.

Table DR1. Lead isotope composition of lead-zinc sulfides from the Laisvall deposit.

Stratigraphy	Mineral	$^{206}Pb/^{204}Pb$	$^{207}Pb/^{204}Pb$	$^{208}Pb/^{204}Pb$	Stratigraphy	Mineral	$^{206}Pb/^{204}P$	$^{207}Pb/^{204}Pb$	$^{208}Pb/^{204}Pb$
Upper Sandstone orebody	PbS	21.0531	15.9793	39.7446	Lower Sandstone orebody	PbS	21.0369	15.9777	39.7174
Upper Sandstone orebody	PbS	21.1170	15.9881	39.7405	Lower Sandstone orebody	PbS	21.0769	15.9813	39.7567
Upper Sandstone orebody	PbS	21.1877	15.9951	39.8058	Lower Sandstone orebody	PbS	21.1009	15.9853	39.7748
Upper Sandstone orebody	PbS	21.2444	16.0022	39.8104	Lower Sandstone orebody	PbS	21.1191	15.9871	39.7487
Upper Sandstone orebody	PbS	21.3225	16.0098	39.8655	Lower Sandstone orebody	PbS	21.1506	15.9922	39.7955
Upper Sandstone orebody	PbS	21.3497	16.0134	39.8747	Lower Sandstone orebody	PbS	21.1727	15.9909	39.8224
Upper Sandstone orebody	PbS	21.3761	16.0170	39.9037	Lower Sandstone orebody	PbS	21.1884	15.9927	39.8499
Upper Sandstone orebody	PbS	21.3775	16.0164	39.8966	Lower Sandstone orebody	PbS	21.2028	15.9967	39.8064
Upper Sandstone orebody	PbS	21.4182	16.0191	39.9396	Lower Sandstone orebody	PbS	21.2072	15.9989	39.8087
Upper Sandstone orebody	PbS	21.4380	16.0234	39.9206	Lower Sandstone orebody	PbS	21.2230	15.9974	39.8542
Upper Sandstone orebody	PbS	21.4440	16.0239	39.9228	Lower Sandstone orebody	PbS	21.2255	15.9998	39.8502
Upper Sandstone orebody	PbS	21.4630	16.0280	39.7906	Lower Sandstone orebody	PbS	21.2279	15.9999	39.8584
Upper Sandstone orebody	PbS	21.5629	16.0348	40.0313	Lower Sandstone orebody	PbS	21.2309	15.9995	39.8493
Upper Sandstone orebody	PbS	21.6114	16.0424	40.0019	Lower Sandstone orebody	PbS	21.4806	16.0267	39.9970
Upper Sandstone orebody	PbS	21.6736	16.0522	39.9468	Lower Sandstone orebody	PbS	21.4885	16.0281	40.0043
Upper Sandstone orebody	PbS	21.6999	16.0531	39.9965	Lower Sandstone orebody	PbS	21.7217	16.0520	40.1594
Upper Sandstone orebody	PbS	21.7283	16.0546	40.0942	Lower Sandstone orebody	PbS	21.7272	16.0573	40.0171
Upper Sandstone orebody	PbS	21.7321	16.0587	40.0175	Lower Sandstone orebody	PbS	21.7431	16.0571	40.1420
Upper Sandstone orebody	PbS	21.7847	16.0609	40.0827	Lower Sandstone orebody	PbS	21.6745	16.0281	40.0821
Upper Sandstone orebody	PbS	21.8592	16.0710	40.1496	Lower Sandstone orebody	PbS	21.7112	16.0465	40.2470
Upper Sandstone orebody	PbS	21.2899	16.0116	39.7946	Lower Sandstone orebody	ZnS	21.7257	16.0532	40.1628
Upper Sandstone orebody	PbS	21.5032	16.0226	39.9806	Lower Sandstone orebody	ZnS	21.4785	16.0273	39.9961
Upper Sandstone orebody	ZnS	21.6598	16.0472	40.0159	Lower Sandstone orebody	ZnS	21.7585	16.0662	39.9922
Upper Sandstone orebody	ZnS	21.7526	16.0619	40.0300					

Table DR2. Lead isotope composition of lead-zinc sulfides from basement-hosted vein-type deposits in the Åkerlandet district.

Sample ID	Deposit	Mineral	$^{206}Pb/^{204}Pb$	$^{207}Pb/^{204}Pb$	$^{208}Pb/^{204}Pb$
AKE ZnS	Åkerlandet	ZnS	24.6467	16.3999	42.5560
12AKE01-1	Åkerlandet	PbS	26.0872	16.6000	43.1408
12AKE01-2	Åkerlandet	PbS	24.4282	16.3749	42.3944
12AKE04	Åkerlandet	PbS	24.4785	16.3835	42.4513
12AKE05	Åkerlandet	PbS	24.4635	16.3778	42.4375
12AKE06	Åkerlandet	PbS	24.3837	16.3685	42.3971
JAR-01	Järvsand	PbS	25.5633	16.5296	42.9365

Table DR3. Lead isotope composition of of residues and leachates of upper Cambrian–Lower Ordovician organic-rich shale, Paleoproterozoic crystalline basement rock, and corresponding K-feldspar crystals at Laisvall

Sample	Location	Material	Alteration	$^{206}Pb/^{204}Pb$	2σ	$^{207}Pb/^{204}Pb$	2σ	$^{208}Pb/^{204}Pb$	2σ	Slope	Age (Ma)	2σ error
11LAI45-R	Borehole LAI1613	Grey shale 1.08 wt% TOC		23.2538	0.0022	15.9809	0.0016	43.3809	0.0054	0.0589	563	29
11LAI45-L				19.2289	0.0018	15.7438	0.0015	39.0566	0.0048			
ASF4-R	Borehole LAI1613	Grey shale 0.38 wt% TOC		24.0577	0.0023	16.0591	0.0016	44.5641	0.0055	0.0637	733	16
ASF4-L				19.5524	0.0019	15.7719	0.0015	39.4180	0.0049			
ASF9-R	Borehole LAI177	Grey shale 1.24 wt% TOC		90.1727	0.0087	19.6900	0.0019	46.0311	0.0057	0.0544	388	2
ASF9-L				24.1579	0.0023	16.0982	0.0016	39.9024	0.0049			
ASF10-R	Borehole LAI32	Grey shale 0.66 wt% TOC		25.6900	0.0025	16.2051	0.0016	46.1006	0.0057	0.0607	630	16
ASF10-L				20.8101	0.0020	15.9087	0.0016	40.1985	0.0050			
ASF11-R	Borehole LAI280	Black shale 2.80 wt% TOC		26.7753	0.0026	16.2772	0.0016	40.7723	0.0051	0.0556	438	19
ASF11-L				22.2619	0.0021	16.0260	0.0016	40.1575	0.0050			
11BAS01-R		Granite basement Laisvall	Altered chlorite	18.0322	0.0017	15.4933	0.0015	36.3016	0.0045	0.1287	2079.93	0.94
11BAS01-L	Borehole LAI1576	Granite basement Laisvall		22.2464	0.0021	16.0358	0.0016	41.2127	0.0051			
11BAS02-R		Granite basement Laisvall	Reddened hematite veins	16.9357	0.0016	15.3568	0.0015	35.8509	0.0044	0.0800	1195.6	1.5
11BAS02-L	Borehole LAI1580	Granite basement Laisvall		28.6451	0.0027	16.2934	0.0016	49.9114	0.0062			
11BAS03-R		Granite basement Laisvall	Altered chlorite	17.2239	0.0017	15.4076	0.0015	36.2546	0.0045	0.1223	1989.01	0.79
11BAS03-L	Borehole LAI1577	Granite basement Laisvall		22.2606	0.0021	16.0235	0.0016	40.9480	0.0051			
11BAS04-R		Granite basement Laisvall	Reddish hematite veins	17.5079	0.0017	15.4003	0.0015	36.3184	0.0045	0.0816	1236.09	0.98
11BAS04-L	Borehole LAI1580	Granite basement Laisvall		32.7034	0.0031	16.6409	0.0016	53.7070	0.0067			
11BAS06-R	Outcrop RT90	Granite basement Laisvall	Relatively fresh	17.4479	0.0017	15.3356	0.0015	36.1009	0.0045	0.1287	2079.20	0.98
11BAS06-L	1565939E/7335770	Granite basement Laisvall		23.8849	0.0023	16.1639	0.0016	42.1359	0.0052			
11BAS07-R		Granite basement Laisvall	Fresh - unaltered	17.9293	0.0017	15.3746	0.0015	35.7999	0.0044	0.1136	1856.43	0.57
11BAS07-L	Borehole LAI1580	Granite basement Laisvall		27.1534	0.0026	16.4221	0.0016	42.3981	0.0053			
11BAS01-R		K-feldspar granite		16.4073	0.0016	15.3119	0.0015	35.6046	0.0044	0.1356	2171.5	2.8
11BAS01-L		K-feldspar granite		22.2226	0.0021	16.1007	0.0016	40.4416	0.0050			
11BAS02-R		K-feldspar granite		16.3955	0.0016	15.2843	0.0015	35.6785	0.0044	0.1365	2183.1	2.4
11BAS02-L		K-feldspar granite		21.1174	0.0020	15.9291	0.0016	40.1316	0.0050			
11BAS04-R		K-feldspar granite		17.2127	0.0017	15.3554	0.0015	36.2215	0.0045	0.1440	2275.0	1.6
11BAS04-L		K-feldspar granite		22.5917	0.0022	16.1300	0.0016	41.1700	0.0051			
11BAS06-R		K-feldspar granite		18.5755	0.0018	15.3822	0.0015	36.4082	0.0045	0.1706	2563.0	2.9
11BAS06-L		K-feldspar granite		22.1443	0.0021	15.9911	0.0016	40.3547	0.0050			
11BAS07-R		K-feldspar granite		18.4512	0.0018	15.3053	0.0015	35.5009	0.0044	0.1354	2168.9	3.6
11BAS07-L		K-feldspar granite		25.5507	0.0025	16.2669	0.0016	41.1462	0.0051			
11BAS07-2-R		K-feldspar granite		16.8388	0.0016	15.2734	0.0015	35.5931	0.0044	0.1298	2094.1	2.7
11BAS07-2-L		K-feldspar granite		22.6938	0.0022	16.0332	0.0016	40.5802	0.0050			
11BAS07-3-R		K-feldspar granite		16.2013	0.0016	15.2216	0.0015	35.3196	0.0044	0.1365	2182.16	0.96
11BAS07-3-L		K-feldspar granite		22.3564	0.0021	16.0616	0.0016	40.6393	0.0050			

CHAPTER 4

Appendix 1

Appendix 1. Sulfur isotope data of sulfates and sulfides in the orebodies at Laisvall and Vassbo (Reproducibilty-precision: ±0.3‰).

Mineral	**Stratigraphy or orebody**	**δ^{34}S (‰, VCDT)**
Laisvall deposit (n = 128)		
Pyrite	Grammajukku Formation	–10.1
Barite	Upper Sandstone	17.0
Barite	Upper Sandstone	14.8
Barite	Upper Sandstone	32.7
Barite	Upper Sandstone	28.2
Barite	Upper Sandstone	21.7
Barite	Upper Sandstone	24.8
Barite	Upper Sandstone	18.1
Barite	Upper Sandstone	16.9
Galena	Upper Sandstone	24.2
Galena	Upper Sandstone	23.6
Galena	Upper Sandstone	26.8
Galena	Upper Sandstone	26.7
Galena	Upper Sandstone	28.1
Galena	Upper Sandstone	25.0
Galena	Upper Sandstone	26.9
Galena	Upper Sandstone	26.9
Galena	Upper Sandstone	21.0
Galena	Upper Sandstone	22.4
Galena	Upper Sandstone	24.0
Galena	Upper Sandstone	28.8
Galena	Upper Sandstone	20.6
Galena	Upper Sandstone	24.9
Galena	Upper Sandstone	23.2
Galena	Upper Sandstone	23.8
Galena	Upper Sandstone	23.4
Galena	Upper Sandstone	22.8
Galena	Upper Sandstone	18.7
Galena	Upper Sandstone	20.2

Mineral	Stratigraphy or orebody	$\delta^{34}S$ (‰, VCDT)
Galena	Upper Sandstone	25.8
Galena	Upper Sandstone	26.4
Galena	Aspnäs outcrop	22.6
Galena	Aspnäs outcrop	22.5
Galena in galena-sphalerite-calcite veinlet	Upper Sandstone	28.4
Galena in galena-sphalerite-calcite veinlet	Upper Sandstone	28.7
Galena in galena-sphalerite-calcite veinlet	Upper Sandstone	17.8
Galena in galena-sphalerite-calcite veinlet	Upper Sandstone	18.9
Pyrite	Upper Sandstone	–6.4
Pyrite	Upper Sandstone	26.2
Pyrite	Upper Sandstone	25.3
Pyrite	Upper Sandstone	23.4
Pyrite	Upper Sandstone	21.1
Pyrite	Upper Sandstone	28.2
Pyrite	Upper Sandstone	23.8
Pyrite	Upper Sandstone	25.1
Pyrite	Upper Sandstone	24.6
Pyrite	Upper Sandstone	32.5
Pyrite	Upper Sandstone	31.9
Pyrite	Upper Sandstone	31.9
Pyrite	Upper Sandstone	22.6
Pyrite	Upper Sandstone	21.0
Sphalerite	Upper Sandstone	31.3
Sphalerite	Upper Sandstone	32.3
Sphalerite	Upper Sandstone	28.6
Sphalerite	Upper Sandstone	31.3
Sphalerite	Upper Sandstone	21.4
Sphalerite	Upper Sandstone	29.3
Sphalerite	Upper Sandstone	28.6
Sphalerite	Upper Sandstone	29.0
Sphalerite	Upper Sandstone	28.3
Sphalerite	Upper Sandstone	29.8

Mineral	Stratigraphy or orebody	$\delta^{34}S$ (‰, VCDT)
Sphalerite	Upper Sandstone	29.7
Sphalerite	Upper Sandstone	29.2
Sphalerite	Upper Sandstone	28.3
Sphalerite	Upper Sandstone	29.5
Sphalerite	Upper Sandstone	29.6
Sphalerite	Upper Sandstone	2.3
Sphalerite	Upper Sandstone	28.1
Sphalerite	Upper Sandstone	28.7
Sphalerite	Upper Sandstone	29.8
Sphalerite	Upper Sandstone	33.8
Sphalerite	Upper Sandstone	33.2
Sphalerite	Upper Sandstone	26.1
Sphalerite	Upper Sandstone	27.4
Barite	Lower Sandstone	15.5
Galena	Lower Sandstone	25.0
Galena	Lower Sandstone	27.1
Galena	Lower Sandstone	17.5
Galena	Lower Sandstone	28.9
Galena	Lower Sandstone	27.1
Galena	Lower Sandstone	29.2
Galena	Lower Sandstone	23.7
Galena	Lower Sandstone	24.1
Galena	Lower Sandstone	24.2
Galena	Lower Sandstone	19.8
Galena	Lower Sandstone	21.8
Galena	Lower Sandstone	22.2
Galena	Lower Sandstone	28.7
Galena	Lower Sandstone	23.8
Galena	Lower Sandstone	23.7
Galena	Lower Sandstone	24.1
Galena	Lower Sandstone	24.2
Galena	Lower Sandstone	27.2

Mineral	Stratigraphy or orebody	$\delta^{34}S$ (‰, VCDT)
Galena	Lower Sandstone	21.3
Galena	Lower Sandstone	23.1
Galena	Lower Sandstone	25.0
Galena	Lower Sandstone	12.9
Galena	Lower Sandstone	25.0
Galena	Lower Sandstone	25.4
Galena	Lower Sandstone	17.7
Galena	Lower Sandstone	17.7
Galena in galena-sphalerite-calcite veinlet	Lower Sandstone	26.1
Galena in galena-sphalerite-calcite veinlet	Lower Sandstone	24.3
Pyrite	Lower Sandstone	30.6
Pyrite	Lower Sandstone	27.3
Pyrite	Lower Sandstone	25.6
Pyrite	Lower Sandstone	24.2
Pyrite	Lower Sandstone	24.6
Pyrite	Lower Sandstone	21.7
Pyrite	Lower Sandstone	23.8
Sphalerite	Lower Sandstone	28.2
Sphalerite	Lower Sandstone	27.6
Sphalerite	Lower Sandstone	31.5
Sphalerite	Lower Sandstone	31.2
Sphalerite	Lower Sandstone	29.9
Sphalerite	Lower Sandstone	29.4
Sphalerite	Lower Sandstone	30.8
Sphalerite	Lower Sandstone	31.5
Sphalerite	Lower Sandstone	29.1
Sphalerite	Lower Sandstone	28.3
Sphalerite	Lower Sandstone	25.4
Sphalerite	Lower Sandstone	24.1
Sphalerite	Lower Sandstone	28.9
Sphalerite	Lower Sandstone	29.5
Sphalerite	Lower Sandstone	29.0

Mineral	Stratigraphy or orebody	δ^{34}S (‰, VCDT)
Sphalerite	Lower Sandstone	29.2
Sphalerite	Lower Sandstone	24.9
Sphalerite	Lower Sandstone	26.4

Mineral	Stratigraphy or orebody	δ^{34}S (‰, VCDT)
Vassbo deposit (n= 35)		
Pyrite	Alum Shale Formation	6.8
Pyrite	Alum Shale Formation	7.6
Barite	Quartz sandstone orebody	16.2
Galena	Quartz sandstone orebody	11.5
Galena	Quartz sandstone orebody	14.7
Galena	Quartz sandstone orebody	26.3
Galena	Quartz sandstone orebody	26.3
Galena	Quartz sandstone orebody	16.2
Galena	Quartz sandstone orebody	12.8
Galena	Quartz sandstone orebody	21.9
Galena	Quartz sandstone orebody	22.1
Galena	Quartz sandstone orebody	21.8
Galena	Quartz sandstone orebody	22.0
Galena	Quartz sandstone orebody	16.3
Galena	Quartz sandstone orebody	16.1
Pyrite	Quartz sandstone orebody	–8.0
Pyrite	Quartz sandstone orebody	15.9
Pyrite	Quartz sandstone orebody	13.3
Pyrite	Quartz sandstone orebody	13.1
Pyrite	Quartz sandstone orebody	17.7
Pyrite	Quartz sandstone orebody	16.4
Pyrite	Quartz sandstone orebody	17.1
Pyrite	Quartz sandstone orebody	17.1
Pyrite	Quartz sandstone orebody	16.8
Pyrite	Quartz sandstone orebody	16.3
Pyrite	Quartz sandstone orebody	9.3

Mineral	Stratigraphy or orebody	$\delta^{34}S$ (‰, VCDT)
Pyrite	Quartz sandstone orebody	24.4
Pyrite	Quartz sandstone orebody	28.7
Sphalerite	Quartz sandstone orebody	14.2
Sphalerite	Quartz sandstone orebody	17.8
Sphalerite	Quartz sandstone orebody	21.2
Sphalerite	Quartz sandstone orebody	34.1
Sphalerite	Quartz sandstone orebody	31.6
Sphalerite	Quartz sandstone orebody	20.9
Sphalerite	Quartz sandstone orebody	21.7

CHAPTER 5

Appendices 1, 2, 3, and 4

Appendix 1. Fracture data from the Åkerlandet and Järvsand vein deposits in Paleoproterozoic basement.

Location on map	Fracture strike	Fracture dip	Kinematic indicator	Sense of shear	Comment
Profile 3	170	90			
Profile 3	358	82			
Profile 3	352	86			Calcite vein wall
Profile 3	348	85			Calcite vein wall
Profile 3	330	70			Fracture cleavage in calcite vein. S-surface
Profile 3	320	72			Fracture cleavage in calcite vein. S-surface
Profile 3	328	90			Fracture cleavage in calcite vein. S-surface
Profile 3	270	90			
Profile 3	282	70			
Profile 3	268	62			Displacement across this fracture
Profile 3	126	40			
Profile 3	142	90			
Profile 3	92	78			
Profile 3	66	80			
Profile 3	136	68			
Profile 3	130	82			
Profile 3	138	84			
Profile 3	188	80			
Profile 3	360	88			
Profile 3	360	82			
Profile 3	106	88			
Profile 3	130	80			
Profile 3	130	86			
Profile 3	138	85			Fracture cleavage in calcite vein. S-surface
Profile 3	348	80			
Profile 3	345	90			
Profile 3	354	90			
Profile 3	6	82			
Profile 3	152	90			
Profile 3	156	90			

Location on map	Fracture strike	Fracture dip	Kinematic indicator	Sense of shear	Comment
Profile 3	10	90			Contact leucogranite xenolith and calcite-sulfide vein
Profile 3	330	80			
Profile 3	340	90			
Profile 3	320	90			
Profile 3	326	90			
Profile 3	100	90			
Profile 3	284	84			
Profile 1	6	85			Fracture to east of and outside fracture zone
Profile 1	324	74			Fracture to east of and outside fracture zone
Profile 1	330	76			Eastern boundary of fracture zone
Profile 1	318	80			Calcite breccia with gneiss xenolith
Profile 1	74	90			Calcite-filled
Profile 1	326	85			Calcite-filled
Profile 1	325	82			Calcite-filled
Profile 1	246	82			Locally some green fluorite
Profile 1	178	70			
Profile 1	186	72			
Profile 1	330	80			Calcite-filled
Profile 1	324	70			
Profile 1	260	82			
Profile 1	360	86			Calcite-filled
Profile 1	350	84			Calcite-filled
Profile 1	330	90			Calcite-filled
Profile 1	318	76			
Profile 1	320	72			
Profile 1	308	80			
Profile 1	176	66			Calcite-sulfide vein wall
Profile 1	168	76	Slickenlines with 50^{o} pitch to south	West-side-up (uncertain)	
Profile 1	186	90	Slickenlines with 30^{o} pitch to south	Uncertain	Western boundary of fracture zone
Profile 1	294	70			
Profile 1	292	72			

Location on map	Fracture strike	Fracture dip	Kinematic indicator	Sense of shear	Comment
Profile 1	290	74			
Profile 2	346	78			Eastern boundary of fracture zone
Profile 2	354	82			Eastern boundary of fracture zone
Surface 1	326	78			Calcite-filled
Surface 1	144	82			Calcite-filled
Surface 1	144	80			Calcite-filled
Surface 1	150	78			Calcite-filled
Surface 1	328	80			Calcite-filled
Surface 1	40	86			
Surface 1	166	74	Slickenlines with 60^{o} pitch to south		
Surface 1	218	78			
Surface 1	222	20			
Surface 1	236	50			
Surface 1	148	82			
Surface 1	54	85			
Surface 1	150	90			
Surface 1	168	90			
Surface 1	156	85			
Surface 1	174	82			Calcite-sulfide vein wall (eastern wall). 20-50 cm thick
Surface 1	172	70			Calcite-sulfide vein wall (western wall). 20-50 cm thick
Surface 1	190	85			Fracture cleavage inside calcite-sulfide vein
Surface 1	270	60			Sphalerite along fracture
Surface 1	186	86			Calcite-sulfide vein wall (eastern wall). 20-50 cm thick
Surface 1	148	86			Calcite-filled

Location on map	Fracture strike	Fracture dip	Kinematic indicator	Sense of shear	Comment
North of Järvsjö beach	170	90			
North of Järvsjö beach	184	90			
North of Järvsjö beach	176	86			
North of Järvsjö beach	42	90			

Location on map	Fracture strike	Fracture dip	Kinematic indicator	Sense of shear	Comment
North of Järvsjö beach	46	90			
North of Järvsjö beach	48	90			
North of Järvsjö beach	222	85			
North of Järvsjö beach	30	90			
North of Järvsjö beach	38	90			
North of Järvsjö beach	234	85			
North of Järvsjö beach	120	90			
North of Järvsjö beach	162	80		Dextral	
North of Järvsjö beach	184	80	Inferred R_1 shear to 162/80		
North of Järvsjö beach	186	85	Inferred R_1 shear to 162/80		
North of Järvsjö beach	224	90	Fracture displaced across fracture 162/80		
North of Järvsjö beach	224	86			
North of Järvsjö beach	220	86			
North of Järvsjö beach	220	85			
North of Järvsjö beach	234	85			
North of Järvsjö beach	50	80			
North of Järvsjö beach	40	82			
North of Järvsjö beach	50	90			
North of Järvsjö beach	48	90			
North of Järvsjö beach	40	90			
North of Järvsjö beach	172	80			
North of Järvsjö beach	192	82			
North of Järvsjö beach	188	76			
North of Järvsjö beach	158	64			
North of Järvsjö beach	180	84			
North of Järvsjö beach	96	80			
North of Järvsjö beach	300	85			
North of Järvsjö beach	256	90			
North of Järvsjö beach	302	85			
North of Järvsjö beach	300	82			
North of Järvsjö beach	182	80			

Location on map	Fracture strike	Fracture dip	Kinematic indicator	Sense of shear	Comment
North of Järvsjö beach	176	80			
North of Järvsjö beach	195	80	Inferred R_1 shear to 176/80		
North of Järvsjö beach	186	80			
North of Järvsjö beach	44	90	Fracture displaced across fracture 138/90		
North of Järvsjö beach	40	90			
North of Järvsjö beach	46	82			
North of Järvsjö beach	48	90			
North of Järvsjö beach	138	90		Sinistral	
North of Järvsjö beach	130	85			
North of Järvsjö beach	186	80			
North of Järvsjö beach	184	82			
North of Järvsjö beach	176	82		Sinistral	
North of Järvsjö beach	234	75			
North of Järvsjö beach	76	90			
North of Järvsjö beach	260	80			
North of Järvsjö beach	48	84			
North of Järvsjö beach	40	80			
North of Järvsjö beach	244	80			
North of Järvsjö beach	242	80			
North of Järvsjö beach	228	90			
North of Järvsjö beach	250	90	Fracture displaced across fracture 316/90		
North of Järvsjö beach	46	90	Fracture displaced across fracture 176/82		
North of Järvsjö beach	224	85	Fracture displaced across fracture 292/90		
North of Järvsjö beach	286	90			
North of Järvsjö beach	292	90		Dextral	
North of Järvsjö beach	316	90		Dextral	
North of Järvsjö beach	4	86		Sinistral	
North of Järvsjö beach	2	78			
North of Järvsjö beach	176	82			
North of Järvsjö beach	61	90			
North of Järvsjö beach	40	90	Fracture displaced across fracture 004/86		

Location on map	Fracture strike	Fracture dip	Kinematic indicator	Sense of shear	Comment
North of Järvsjö beach	40	90	Fracture displaced across fracture 004/86		
North of Järvsjö beach	54	78			
North of Järvsjö beach	48	78			
North of Järvsjö beach	39	56			
North of Järvsjö beach	40	90			
North of Järvsjö beach	28	90	Fracture rotated into fracture 004/86		
North of Järvsjö beach	18	78			
North of Järvsjö beach	14	82			
North of Järvsjö beach	40	90			
North of Järvsjö beach	18	88			
North of Järvsjö beach	220	84			
North of Järvsjö beach	224	84			
North of Järvsjö beach	132	90			
North of Järvsjö beach	316	80			
North of Järvsjö beach	308	42			
North of Järvsjö beach	276	82			
North of Järvsjö beach	294	70	Steps (transport direction 360/60)	N-side-up	Major fracture along northern side of small peninsula
North of Järvsjö beach	4	58			
North of Järvsjö beach	4	60			
North of Järvsjö beach	360	54			
North of Järvsjö beach	220	62			
North of Järvsjö beach	220	66			
North of Järvsjö beach	222	64			
North of Järvsjö beach	236	68			
North of Järvsjö beach	286	56			
North of Järvsjö beach	322	70		Dextral	Major fracture along shore
North of Järvsjö beach	12	90	Fracture displaced across fracture 322/70		
North of Järvsjö beach	360	72			
North of Järvsjö beach	216	78			
South of Järvsjö beach	26	90			
South of Järvsjö beach	42	90			

Location on map	Fracture strike	Fracture dip	Kinematic indicator	Sense of shear	Comment
South of Järvsjö beach	164	78			
South of Järvsjö beach	164	78			
South of Järvsjö beach	164	82			
South of Järvsjö beach	168	90			
South of Järvsjö beach	190	88		Dextral	Calcite-sulfide vein wall (6-8 cm vein)
South of Järvsjö beach	190	86			Calcite-sulfide vein wall (6-8 cm vein)
South of Järvsjö beach	196	72	Pegmatite displaced across calcite-sulfide vein		Calcite-sulfide vein wall (20-25 cm vein)
South of Järvsjö beach	190	90			
South of Järvsjö beach	186	82			Bends into fracture 210/85
South of Järvsjö beach	210	85			
South of Järvsjö beach	188	86			
South of Järvsjö beach	190	90			
South of Järvsjö beach	234	72			
South of Järvsjö beach	232	82			
South of Järvsjö beach	240	90			
South of Järvsjö beach	228	82			
South of Järvsjö beach	228	78			
South of Järvsjö beach	224	62			
South of Järvsjö beach	204	60			
South of Järvsjö beach	14	90			
South of Järvsjö beach	8	90			
South of Järvsjö beach	208	78			
South of Järvsjö beach	68	88			
South of Järvsjö beach	58	78			
South of Järvsjö beach	50	76			
South of Järvsjö beach	360	90			
South of Järvsjö beach	358	78			
South of Järvsjö beach	18	90			Calcite-sulfide vein wall (25 cm vein)
South of Järvsjö beach	14	90			Calcite-sulfide vein wall (25 cm vein)
South of Järvsjö beach	16	86			
South of Järvsjö beach	18	90			

Location on map	Fracture strike	Fracture dip	Kinematic indicator	Sense of shear	Comment
South of Järvsjö beach	202	84			
South of Järvsjö beach	30	90			
South of Järvsjö beach	288	74			
South of Järvsjö beach	302	58			
South of Järvsjö beach	304	50			
South of Järvsjö beach	302	50			
South of Järvsjö beach	114	82			
South of Järvsjö beach	320	68			
South of Järvsjö beach	330	72	Steps (possible transport direction 060	NE-side-up	Major fracture along northern side of small peninsula
South of Järvsjö beach	318	70			

Appendix 2. Microprobe analysis of Si, K, Na, Ca, Al, and Ba in adularia at the Åkerlandet vein deposit in Paleoproterozoic basement (n.d.: not determined).

	atomic proportions							wt.% oxides							
No.	**Si**	**K**	**Na**	**Ca**	**Al**	**Ba**	**Total**	**Si**	**K**	**Na**	**Ca**	**Al**	**Ba**	**Total**	**K/Ca**
97	3.00	0.95	0.01	0.02	1.01	0.00	4.98	64.85	16.05	0.08	0.33	18.54	0.18	100.03	49
242	2.99	0.97	0.01	0.01	1.01	0.00	4.99	62.57	15.89	0.12	0.27	18.02	0.23	97.09	60
79	2.99	0.96	0.01	0.01	1.01	0.00	4.99	63.90	16.13	0.06	0.26	18.27	0.24	98.87	61
103	3.00	0.94	0.01	0.01	1.01	0.01	4.97	64.26	15.75	0.10	0.23	18.37	0.34	99.05	68
98	2.99	0.95	0.01	0.01	1.01	0.01	4.98	63.90	15.97	0.09	0.18	18.33	0.34	98.80	91
96	3.00	0.94	0.01	0.01	1.01	0.01	4.97	64.28	15.79	0.10	0.17	18.32	0.34	99.01	91
80	3.00	0.95	0.01	0.01	1.01	0.00	4.98	64.91	16.14	0.06	0.14	18.43	0.16	99.84	115
152	2.99	0.93	0.01	0.01	1.02	0.01	4.97	64.77	15.85	0.13	0.14	18.72	0.56	100.17	116
95	3.00	0.95	0.01	0.01	1.01	0.01	4.98	64.49	15.97	0.10	0.13	18.46	0.30	99.45	121
21	3.00	0.95	0.01	0.01	1.00	0.00	4.97	64.95	16.04	0.09	0.13	18.39	0.24	99.84	121
241	3.00	0.97	0.01	0.01	1.00	0.00	4.98	63.41	15.99	0.08	0.12	17.99	0.10	97.70	131
99	3.00	0.94	0.01	0.01	1.01	0.01	4.97	64.40	15.84	0.09	0.12	18.42	0.44	99.31	136
177	3.00	0.96	0.01	0.01	1.01	0.00	4.98	64.15	16.05	0.11	0.11	18.25	0.25	98.93	140
178	3.00	0.95	0.01	0.01	1.01	0.00	4.98	64.30	16.05	0.10	0.11	18.42	0.13	99.11	149
82	3.00	0.95	0.01	0.01	1.01	0.00	4.97	64.59	15.94	0.10	0.11	18.42	0.26	99.42	150
81	3.00	0.95	0.01	0.00	1.01	0.00	4.98	64.65	16.10	0.08	0.10	18.41	0.19	99.53	166
153	2.99	0.94	0.01	0.00	1.02	0.01	4.98	64.54	15.91	0.12	0.09	18.67	0.53	99.87	169
94	3.00	0.94	0.01	0.00	1.01	0.01	4.97	64.93	15.84	0.13	0.07	18.47	0.33	99.77	216
93	3.01	0.94	0.01	0.00	1.00	0.00	4.96	64.98	15.87	0.08	0.07	18.33	0.26	99.59	223
108	3.00	0.95	0.01	0.00	1.01	0.00	4.97	64.60	15.97	0.10	0.07	18.40	0.26	99.40	226
84	3.00	0.94	0.01	0.00	1.01	0.01	4.97	64.73	15.86	0.10	0.06	18.56	0.37	99.68	246
154	2.98	0.94	0.01	0.00	1.03	0.01	4.98	64.18	15.84	0.12	0.06	18.76	0.60	99.56	253
176	3.00	0.95	0.01	0.00	1.00	0.00	4.98	64.35	15.99	0.11	0.06	18.26	0.23	99.00	257
88	3.00	0.95	0.01	0.00	1.01	0.01	4.97	64.94	16.02	0.07	0.06	18.46	0.34	99.89	261
91	3.00	0.95	0.01	0.00	1.01	0.01	4.97	64.61	15.99	0.10	0.06	18.56	0.40	99.72	264
101	3.00	0.95	0.01	0.00	1.01	0.01	4.98	64.30	15.92	0.12	0.05	18.36	0.31	99.06	303
100	3.00	0.95	0.01	0.00	1.01	0.01	4.97	64.49	15.96	0.08	0.05	18.42	0.36	99.37	306
239	3.00	0.97	0.01	0.00	1.01	0.00	4.99	63.28	16.09	0.12	0.05	18.00	0.10	97.64	309
41	3.00	0.93	0.01	0.00	1.01	0.01	4.96	64.89	15.75	0.08	0.05	18.55	0.55	99.87	311
233	2.99	0.94	0.01	0.00	1.03	0.00	4.98	61.14	15.12	0.10	0.05	17.89	0.24	94.54	318
240	3.00	0.96	0.01	0.00	1.01	0.00	4.98	63.53	15.85	0.10	0.05	18.08	0.16	97.78	319
235	3.00	0.95	0.01	0.00	1.01	0.00	4.97	64.38	15.98	0.09	0.05	18.46	0.20	99.16	324
117	3.01	0.94	0.01	0.00	1.00	0.01	4.97	65.04	15.98	0.07	0.05	18.34	0.35	99.84	332
83	3.00	0.96	0.00	0.00	1.01	0.01	4.98	64.31	16.07	0.05	0.05	18.48	0.33	99.29	336
175	3.00	0.96	0.01	0.00	1.01	0.00	4.99	64.07	16.15	0.11	0.05	18.37	0.17	98.92	339
87	3.01	0.94	0.01	0.00	1.00	0.01	4.97	65.31	16.00	0.07	0.04	18.50	0.32	100.25	358
109	3.00	0.95	0.01	0.00	1.01	0.01	4.97	64.64	15.99	0.10	0.04	18.41	0.30	99.48	386
174	3.00	0.96	0.01	0.00	1.01	0.01	4.98	64.42	16.13	0.12	0.04	18.44	0.28	99.43	394
188	2.98	0.95	0.01	0.00	1.03	0.01	4.99	63.64	15.95	0.13	0.04	18.59	0.47	98.82	408
89	3.00	0.95	0.01	0.00	1.00	0.01	4.97	64.82	16.06	0.08	0.04	18.39	0.42	99.81	411
237	2.99	0.96	0.01	0.00	1.02	0.00	4.98	62.35	15.69	0.10	0.04	17.93	0.07	96.18	412
110	3.00	0.94	0.01	0.00	1.01	0.01	4.97	64.69	15.94	0.10	0.04	18.52	0.30	99.59	419
173	3.00	0.96	0.01	0.00	1.01	0.00	4.98	64.43	16.13	0.09	0.04	18.43	0.19	99.31	420
90	3.00	0.94	0.01	0.00	1.01	0.01	4.97	64.97	16.02	0.11	0.04	18.53	0.38	100.04	432
114	3.00	0.95	0.01	0.00	1.01	0.01	4.97	64.85	16.03	0.13	0.04	18.48	0.34	99.87	444

	atomic proportions							wt.% oxides							
No.	**Si**	**K**	**Na**	**Ca**	**Al**	**Ba**	**Total**	**Si**	**K**	**Na**	**Ca**	**Al**	**Ba**	**Total**	**K/Ca**
157	2.99	0.96	0.01	0.00	1.02	0.01	4.98	64.01	16.07	0.09	0.04	18.57	0.27	99.05	448
86	3.00	0.94	0.01	0.00	1.01	0.01	4.97	64.71	15.94	0.10	0.04	18.44	0.37	99.60	454
92	3.00	0.94	0.01	0.00	1.01	0.01	4.97	64.65	15.93	0.10	0.03	18.41	0.32	99.45	462
268	3.02	0.93	0.01	0.00	0.99	0.00	4.96	64.77	15.69	0.09	0.03	18.07	0.17	98.82	475
158	2.99	0.96	0.01	0.00	1.02	0.01	4.98	63.94	16.07	0.10	0.03	18.47	0.30	98.91	490
124	3.01	0.94	0.01	0.00	1.01	0.01	4.96	65.04	15.86	0.10	0.03	18.50	0.31	99.83	513
155	2.99	0.94	0.01	0.00	1.02	0.01	4.97	64.28	15.89	0.12	0.03	18.56	0.52	99.39	519
122	3.00	0.94	0.01	0.00	1.01	0.01	4.97	65.09	15.99	0.07	0.03	18.63	0.39	100.20	521
172	3.00	0.95	0.01	0.00	1.01	0.00	4.97	64.38	16.02	0.06	0.03	18.37	0.24	99.11	527
112	3.00	0.94	0.01	0.00	1.01	0.01	4.97	64.63	15.93	0.10	0.03	18.49	0.39	99.57	538
246	3.00	0.96	0.01	0.00	1.01	0.00	4.98	63.15	15.80	0.11	0.03	18.08	0.22	97.38	539
156	2.99	0.96	0.01	0.00	1.02	0.01	4.98	63.98	16.01	0.11	0.03	18.43	0.34	98.91	541
104	3.00	0.94	0.01	0.00	1.01	0.01	4.97	64.49	15.85	0.07	0.03	18.42	0.28	99.15	558
257	3.00	0.95	0.01	0.00	1.01	0.00	4.97	63.63	15.78	0.11	0.03	18.09	0.19	97.83	570
102	3.00	0.95	0.01	0.00	1.01	0.01	4.97	64.64	15.99	0.09	0.03	18.39	0.30	99.44	586
258	3.00	0.94	0.01	0.00	1.01	0.01	4.97	63.62	15.70	0.11	0.03	18.21	0.40	98.07	611
49	3.00	0.94	0.01	0.00	1.01	0.01	4.97	65.01	16.02	0.11	0.03	18.45	0.29	99.91	636
232	3.00	0.96	0.01	0.00	1.01	0.00	4.99	62.49	15.72	0.13	0.02	17.89	0.16	96.41	650
159	3.00	0.97	0.01	0.00	1.01	0.00	4.99	63.84	16.14	0.10	0.02	18.23	0.17	98.51	653
167	3.00	0.96	0.01	0.00	1.01	0.00	4.98	64.16	16.06	0.10	0.02	18.43	0.25	99.02	656
137	3.00	0.94	0.01	0.00	1.02	0.01	4.97	64.37	15.90	0.08	0.02	18.50	0.34	99.21	663
27	3.01	0.94	0.01	0.00	1.00	0.00	4.97	65.52	16.07	0.15	0.02	18.47	0.16	100.40	667
107	3.01	0.94	0.01	0.00	1.01	0.00	4.97	64.78	15.93	0.10	0.02	18.38	0.14	99.36	699
161	2.99	0.96	0.01	0.00	1.02	0.00	4.99	63.88	16.13	0.07	0.02	18.43	0.23	98.77	704
207	2.99	0.97	0.00	0.00	1.02	0.01	4.99	63.51	16.07	0.05	0.02	18.33	0.29	98.27	708
74	3.00	0.93	0.01	0.00	1.01	0.01	4.96	64.72	15.74	0.06	0.02	18.50	0.31	99.34	719
116	3.00	0.94	0.01	0.00	1.01	0.01	4.97	64.86	15.91	0.08	0.02	18.52	0.41	99.80	723
127	3.00	0.94	0.01	0.00	1.01	0.01	4.97	64.95	16.00	0.13	0.02	18.54	0.31	99.96	744
31	3.01	0.94	0.01	0.00	1.00	0.01	4.97	65.31	16.00	0.11	0.02	18.36	0.29	100.09	748
123	3.00	0.95	0.01	0.00	1.01	0.01	4.97	64.99	16.09	0.08	0.02	18.56	0.34	100.08	752
121	3.00	0.94	0.01	0.00	1.01	0.01	4.96	65.25	15.92	0.10	0.02	18.60	0.36	100.25	762
170	2.99	0.96	0.01	0.00	1.02	0.00	4.98	64.21	16.07	0.09	0.02	18.51	0.23	99.13	784
244	2.99	0.95	0.01	0.00	1.02	0.01	4.98	63.09	15.74	0.11	0.02	18.15	0.38	97.49	787
248	3.00	0.96	0.01	0.00	1.01	0.01	4.98	63.77	15.93	0.07	0.02	18.23	0.28	98.30	801
238	2.99	0.97	0.01	0.00	1.02	0.00	4.99	62.78	16.02	0.10	0.02	18.28	0.13	97.33	826
48	3.01	0.94	0.01	0.00	1.01	0.00	4.96	64.19	15.69	0.09	0.02	18.30	0.16	98.45	826
106	3.00	0.94	0.01	0.00	1.01	0.01	4.97	64.77	15.86	0.10	0.02	18.46	0.34	99.55	826
85	3.00	0.95	0.01	0.00	1.01	0.01	4.98	64.60	16.04	0.09	0.02	18.45	0.31	99.51	827
285	3.01	0.95	0.01	0.00	1.00	0.00	4.97	64.62	15.98	0.08	0.02	18.32	0.20	99.22	832
165	3.00	0.96	0.01	0.00	1.01	0.00	4.98	64.00	16.13	0.10	0.02	18.36	0.18	98.79	858
225	2.99	0.96	0.01	0.00	1.02	0.00	4.98	63.47	15.94	0.10	0.02	18.33	0.25	98.11	886
236	2.99	0.96	0.01	0.00	1.02	0.01	4.98	62.99	15.77	0.06	0.02	18.12	0.35	97.31	886
271	3.01	0.94	0.01	0.00	1.00	0.00	4.97	63.68	15.64	0.09	0.02	18.00	0.17	97.60	904
255	3.01	0.95	0.01	0.00	1.00	0.00	4.97	64.03	15.80	0.10	0.02	18.15	0.23	98.33	908
68	3.00	0.93	0.01	0.00	1.01	0.01	4.96	64.32	15.65	0.11	0.02	18.37	0.41	98.88	915
291	3.01	0.93	0.01	0.00	1.00	0.00	4.96	65.17	15.84	0.10	0.02	18.29	0.20	99.62	921

	atomic proportions							wt.% oxides							
No.	**Si**	**K**	**Na**	**Ca**	**Al**	**Ba**	**Total**	**Si**	**K**	**Na**	**Ca**	**Al**	**Ba**	**Total**	**K/Ca**
55	3.01	0.93	0.01	0.00	1.01	0.00	4.96	64.82	15.77	0.08	0.02	18.39	0.22	99.29	956
23	3.02	0.93	0.01	0.00	0.99	0.00	4.96	65.79	15.96	0.13	0.02	18.39	0.22	100.50	967
216	3.00	0.94	0.01	0.00	1.01	0.00	4.97	63.89	15.68	0.11	0.02	18.18	0.24	98.12	980
234	3.00	0.88	0.01	0.00	1.03	0.00	4.93	64.81	14.92	0.11	0.02	18.83	0.14	98.82	988
57	3.00	0.95	0.01	0.00	1.01	0.01	4.97	64.67	16.05	0.10	0.02	18.53	0.30	99.66	991
61	3.00	0.95	0.01	0.00	1.01	0.00	4.97	64.65	15.96	0.12	0.02	18.34	0.26	99.35	1004
229	3.00	0.96	0.01	0.00	1.01	0.00	4.98	63.12	15.88	0.10	0.02	18.08	0.14	97.34	1005
144	2.99	0.95	0.01	0.00	1.02	0.01	4.98	64.05	15.91	0.14	0.01	18.50	0.37	98.98	1082
217	3.00	0.95	0.01	0.00	1.01	0.00	4.98	63.84	15.82	0.15	0.01	18.16	0.27	98.25	1084
105	3.00	0.94	0.01	0.00	1.01	0.01	4.97	64.48	15.86	0.09	0.01	18.35	0.32	99.12	1094
22	3.01	0.95	0.01	0.00	1.00	0.00	4.97	65.36	16.17	0.11	0.01	18.36	0.23	100.25	1108
136	3.00	0.95	0.01	0.00	1.02	0.01	4.98	64.64	16.09	0.07	0.01	18.59	0.28	99.68	1149
283	3.00	0.95	0.01	0.00	1.01	0.00	4.97	64.38	15.98	0.08	0.01	18.40	0.26	99.11	1184
187	2.99	0.95	0.01	0.00	1.02	0.01	4.98	63.92	15.87	0.09	0.01	18.52	0.57	98.98	1211
138	3.00	0.95	0.01	0.00	1.01	0.01	4.98	64.41	16.01	0.11	0.01	18.50	0.44	99.48	1251
160	3.00	0.96	0.01	0.00	1.01	0.01	4.98	64.13	16.09	0.10	0.01	18.36	0.28	98.97	1257
265	3.01	0.94	0.01	0.00	1.00	0.00	4.96	64.44	15.72	0.10	0.01	18.20	0.18	98.65	1289
222	2.99	0.94	0.01	0.00	1.02	0.01	4.98	63.18	15.64	0.12	0.01	18.32	0.62	97.89	1293
66	3.01	0.94	0.01	0.00	1.00	0.00	4.96	65.09	15.93	0.12	0.01	18.35	0.13	99.63	1317
210	2.99	0.95	0.01	0.00	1.02	0.01	4.98	63.55	15.80	0.10	0.01	18.40	0.70	98.57	1317
276	3.00	0.95	0.01	0.00	1.01	0.01	4.97	64.06	15.92	0.07	0.01	18.29	0.35	98.70	1349
149	3.00	0.94	0.01	0.00	1.01	0.01	4.97	64.61	15.81	0.12	0.01	18.44	0.33	99.32	1351
128	3.00	0.94	0.01	0.00	1.01	0.01	4.97	64.86	16.00	0.11	0.01	18.60	0.30	99.88	1379
231	2.98	0.97	0.01	0.00	1.03	0.01	5.00	62.46	15.90	0.12	0.01	18.21	0.36	97.05	1420
179	3.00	0.95	0.01	0.00	1.01	0.01	4.97	64.45	15.97	0.10	0.01	18.37	0.34	99.24	1439
256	2.99	0.97	0.01	0.00	1.02	0.00	4.99	63.25	16.06	0.08	0.01	18.26	0.23	97.89	1460
24	3.01	0.93	0.01	n.d.	1.00	0.00	4.96	65.70	15.94	0.09	n.d.	18.52	0.26	100.51	n.d.
25	3.01	0.94	0.01	n.d.	1.00	0.00	4.97	65.65	16.04	0.15	n.d.	18.39	0.17	100.40	n.d.
26	3.01	0.95	0.01	n.d.	1.00	0.00	4.97	65.45	16.16	0.11	n.d.	18.46	0.24	100.43	n.d.
28	3.01	0.95	0.01	n.d.	1.00	0.00	4.97	65.51	16.13	0.11	n.d.	18.54	0.22	100.52	n.d.
29	3.01	0.93	0.01	n.d.	1.00	0.01	4.96	65.42	15.91	0.09	n.d.	18.52	0.33	100.26	n.d.
30	3.01	0.94	0.01	n.d.	1.01	0.01	4.96	65.50	15.96	0.13	n.d.	18.59	0.28	100.46	n.d.
32	3.01	0.94	0.01	n.d.	1.00	0.00	4.96	65.09	15.94	0.09	n.d.	18.44	0.16	99.72	n.d.
33	3.01	0.94	0.01	n.d.	1.00	0.00	4.97	65.33	16.06	0.10	n.d.	18.44	0.20	100.13	n.d.
34	3.00	0.94	0.01	n.d.	1.01	0.01	4.97	64.96	15.90	0.12	n.d.	18.52	0.41	99.92	n.d.
35	3.00	0.94	0.01	n.d.	1.01	0.01	4.97	64.52	15.93	0.09	n.d.	18.52	0.66	99.72	n.d.
36	3.00	0.95	0.01	n.d.	1.01	0.01	4.97	64.82	15.99	0.10	n.d.	18.51	0.31	99.73	n.d.
37	3.01	0.94	0.01	n.d.	1.01	0.01	4.97	65.21	15.96	0.09	n.d.	18.51	0.35	100.12	n.d.
38	3.00	0.95	0.01	n.d.	1.01	0.01	4.97	65.16	16.08	0.09	n.d.	18.54	0.37	100.25	n.d.
39	3.00	0.95	0.01	n.d.	1.01	0.01	4.97	64.86	16.06	0.08	n.d.	18.48	0.28	99.76	n.d.
40	3.01	0.94	0.01	n.d.	1.01	0.00	4.97	65.09	15.97	0.09	n.d.	18.50	0.26	99.91	n.d.
42	3.00	0.93	0.01	n.d.	1.02	0.01	4.97	64.79	15.80	0.11	n.d.	18.62	0.68	100.01	n.d.
43	3.01	0.94	0.01	n.d.	1.00	0.00	4.96	65.64	16.05	0.10	n.d.	18.52	0.13	100.44	n.d.
44	3.01	0.94	0.01	n.d.	1.00	0.00	4.97	65.11	15.99	0.13	n.d.	18.40	0.26	99.90	n.d.
45	3.00	0.95	0.01	n.d.	1.01	0.00	4.97	65.08	16.13	0.11	n.d.	18.54	0.25	100.11	n.d.
46	3.01	0.94	0.01	n.d.	1.00	0.00	4.97	65.02	15.98	0.08	n.d.	18.39	0.10	99.58	n.d.

	atomic proportions							wt.% oxides							
No.	**Si**	**K**	**Na**	**Ca**	**Al**	**Ba**	**Total**	**Si**	**K**	**Na**	**Ca**	**Al**	**Ba**	**Total**	**K/Ca**
47	3.01	0.94	0.01	n.d.	1.00	0.00	4.97	65.34	16.05	0.12	n.d.	18.42	0.13	100.07	n.d.
50	3.01	0.94	0.01	n.d.	1.00	0.00	4.96	65.01	15.94	0.09	n.d.	18.40	0.17	99.61	n.d.
51	3.01	0.95	0.01	n.d.	1.01	0.00	4.97	65.10	16.10	0.08	n.d.	18.49	0.19	99.96	n.d.
52	3.00	0.95	0.01	n.d.	1.01	0.01	4.97	65.01	16.06	0.11	n.d.	18.54	0.36	100.08	n.d.
53	3.00	0.94	0.01	n.d.	1.01	0.01	4.97	65.11	15.94	0.12	n.d.	18.54	0.41	100.12	n.d.
54	3.01	0.93	0.01	n.d.	1.01	0.00	4.96	65.13	15.81	0.07	n.d.	18.45	0.23	99.70	n.d.
56	3.01	0.95	0.01	n.d.	1.01	0.00	4.97	64.96	16.01	0.06	n.d.	18.48	0.11	99.62	n.d.
58	2.99	0.95	0.01	n.d.	1.02	0.01	4.98	64.48	16.06	0.12	n.d.	18.56	0.38	99.59	n.d.
59	3.01	0.95	0.01	n.d.	1.01	0.00	4.97	64.95	16.00	0.12	n.d.	18.42	0.21	99.70	n.d.
60	3.01	0.94	0.01	n.d.	1.01	0.00	4.97	65.02	16.00	0.09	n.d.	18.46	0.20	99.78	n.d.
62	3.00	0.95	0.01	n.d.	1.01	0.00	4.97	64.81	16.02	0.12	n.d.	18.41	0.24	99.60	n.d.
63	3.00	0.95	0.01	n.d.	1.02	0.01	4.97	64.69	16.02	0.07	n.d.	18.59	0.38	99.75	n.d.
64	3.01	0.94	0.01	n.d.	1.01	0.01	4.97	64.82	15.90	0.11	n.d.	18.41	0.28	99.51	n.d.
65	3.01	0.94	0.01	n.d.	1.01	0.00	4.96	65.16	15.94	0.07	n.d.	18.48	0.13	99.78	n.d.
67	3.01	0.94	0.01	n.d.	1.00	0.00	4.96	65.36	15.96	0.10	n.d.	18.44	0.23	100.11	n.d.
69	3.01	0.95	0.01	n.d.	1.01	0.01	4.97	65.01	16.04	0.07	n.d.	18.45	0.34	99.91	n.d.
70	3.01	0.94	0.01	n.d.	1.00	0.01	4.97	65.20	16.03	0.10	n.d.	18.45	0.36	100.14	n.d.
71	3.00	0.95	0.01	n.d.	1.01	0.01	4.98	64.82	16.15	0.09	n.d.	18.55	0.35	99.96	n.d.
72	3.01	0.94	0.01	n.d.	1.00	0.00	4.97	64.87	15.93	0.09	n.d.	18.37	0.16	99.42	n.d.
73	3.00	0.94	0.01	n.d.	1.01	0.01	4.97	64.66	15.83	0.08	n.d.	18.54	0.72	99.83	n.d.
75	3.00	0.94	0.00	n.d.	1.01	0.01	4.97	64.92	15.99	0.05	n.d.	18.53	0.36	99.86	n.d.
76	3.00	0.94	0.01	n.d.	1.01	0.01	4.97	65.14	16.06	0.11	n.d.	18.57	0.37	100.26	n.d.
77	3.01	0.94	0.01	n.d.	1.01	0.01	4.96	65.26	15.91	0.07	n.d.	18.50	0.34	100.08	n.d.
78	3.01	0.95	0.01	n.d.	1.00	0.00	4.97	65.37	16.21	0.11	n.d.	18.46	0.13	100.27	n.d.
111	3.01	0.94	0.01	n.d.	1.00	0.00	4.96	64.69	15.82	0.12	n.d.	18.32	0.24	99.19	n.d.
113	3.00	0.95	0.01	n.d.	1.01	0.01	4.98	64.53	16.03	0.13	n.d.	18.43	0.33	99.45	n.d.
115	3.00	0.94	0.01	n.d.	1.01	0.01	4.97	65.00	15.91	0.12	n.d.	18.52	0.37	99.92	n.d.
118	3.01	0.94	0.01	n.d.	1.01	0.01	4.97	64.68	15.93	0.07	n.d.	18.36	0.39	99.44	n.d.
119	3.00	0.94	0.01	n.d.	1.01	0.01	4.97	65.07	15.95	0.07	n.d.	18.59	0.35	100.04	n.d.
120	3.00	0.95	0.01	n.d.	1.01	0.01	4.97	65.16	16.10	0.08	n.d.	18.59	0.28	100.22	n.d.
125	2.99	0.95	0.01	n.d.	1.02	0.01	4.98	64.41	16.00	0.12	n.d.	18.62	0.38	99.53	n.d.
126	3.00	0.94	0.01	n.d.	1.01	0.00	4.97	64.96	15.91	0.14	n.d.	18.52	0.22	99.75	n.d.
129	3.01	0.94	0.01	n.d.	1.01	0.00	4.97	64.87	15.97	0.10	n.d.	18.40	0.20	99.54	n.d.
130	3.00	0.94	0.01	n.d.	1.01	0.01	4.96	64.97	15.87	0.08	n.d.	18.58	0.38	99.88	n.d.
131	3.01	0.94	0.01	n.d.	1.00	0.00	4.96	65.22	15.90	0.09	n.d.	18.42	0.21	99.84	n.d.
132	3.00	0.94	0.02	n.d.	1.01	0.01	4.98	64.40	15.88	0.17	n.d.	18.46	0.37	99.29	n.d.
133	3.00	0.94	0.01	n.d.	1.02	0.01	4.97	64.50	15.86	0.11	n.d.	18.57	0.41	99.45	n.d.
134	3.00	0.95	0.01	n.d.	1.01	0.01	4.97	64.72	15.96	0.10	n.d.	18.40	0.34	99.52	n.d.
135	3.00	0.95	0.01	n.d.	1.01	0.00	4.98	64.44	15.98	0.14	n.d.	18.49	0.23	99.27	n.d.
139	3.00	0.93	0.01	n.d.	1.01	0.01	4.97	64.79	15.80	0.15	n.d.	18.42	0.45	99.60	n.d.
140	2.99	0.95	0.01	n.d.	1.02	0.01	4.98	64.36	15.95	0.10	n.d.	18.61	0.49	99.52	n.d.
141	2.99	0.95	0.01	n.d.	1.02	0.01	4.98	64.37	16.11	0.11	n.d.	18.64	0.54	99.77	n.d.
142	2.99	0.94	0.01	n.d.	1.02	0.01	4.97	64.22	15.88	0.09	n.d.	18.61	0.46	99.26	n.d.
143	3.00	0.94	0.01	n.d.	1.01	0.01	4.97	64.36	15.87	0.13	n.d.	18.45	0.44	99.25	n.d.
145	3.00	0.95	0.01	n.d.	1.01	0.01	4.98	64.25	15.91	0.14	n.d.	18.41	0.28	98.99	n.d.
146	3.00	0.95	0.01	n.d.	1.01	0.00	4.97	64.44	15.97	0.10	n.d.	18.50	0.22	99.23	n.d.

	atomic proportions							wt.% oxides							
No.	**Si**	**K**	**Na**	**Ca**	**Al**	**Ba**	**Total**	**Si**	**K**	**Na**	**Ca**	**Al**	**Ba**	**Total**	**K/Ca**
147	3.00	0.96	0.01	n.d.	1.00	0.00	4.98	64.50	16.12	0.13	n.d.	18.30	0.21	99.26	n.d.
148	3.01	0.95	0.01	n.d.	1.01	0.00	4.97	64.81	15.98	0.12	n.d.	18.41	0.19	99.51	n.d.
150	3.00	0.95	0.01	n.d.	1.02	0.01	4.98	64.38	16.00	0.10	n.d.	18.50	0.39	99.37	n.d.
151	3.01	0.94	0.01	n.d.	1.00	0.00	4.97	64.79	15.92	0.10	n.d.	18.35	0.22	99.39	n.d.
162	3.00	0.96	0.01	n.d.	1.01	0.00	4.98	63.80	16.07	0.09	n.d.	18.25	0.22	98.43	n.d.
163	3.00	0.96	0.01	n.d.	1.01	0.00	4.98	63.99	16.11	0.11	n.d.	18.39	0.15	98.75	n.d.
164	2.99	0.95	0.01	n.d.	1.02	0.00	4.98	64.03	15.97	0.09	n.d.	18.49	0.19	98.77	n.d.
166	2.99	0.96	0.01	n.d.	1.02	0.00	4.98	64.02	16.15	0.09	n.d.	18.41	0.19	98.86	n.d.
168	2.99	0.96	0.01	n.d.	1.02	0.00	4.98	64.18	16.13	0.07	n.d.	18.47	0.25	99.10	n.d.
169	3.00	0.95	0.01	n.d.	1.01	0.01	4.98	64.57	16.10	0.10	n.d.	18.50	0.31	99.58	n.d.
171	3.00	0.96	0.01	n.d.	1.02	0.00	4.98	64.52	16.14	0.10	n.d.	18.54	0.25	99.57	n.d.
180	3.00	0.95	0.01	n.d.	1.01	0.01	4.97	64.57	15.95	0.10	n.d.	18.53	0.33	99.48	n.d.
181	3.00	0.95	0.01	n.d.	1.02	0.01	4.98	64.61	16.05	0.08	n.d.	18.59	0.41	99.75	n.d.
182	3.01	0.94	0.01	n.d.	1.00	0.01	4.97	64.94	15.98	0.11	n.d.	18.41	0.33	99.77	n.d.
183	3.00	0.94	0.01	n.d.	1.01	0.01	4.97	64.64	15.83	0.11	n.d.	18.51	0.39	99.48	n.d.
184	3.00	0.94	0.01	n.d.	1.01	0.01	4.97	64.57	15.83	0.10	n.d.	18.54	0.51	99.55	n.d.
185	2.99	0.95	0.01	n.d.	1.02	0.01	4.98	64.24	15.94	0.13	n.d.	18.57	0.62	99.50	n.d.
186	3.00	0.95	0.00	n.d.	1.02	0.01	4.97	63.77	15.80	0.05	n.d.	18.34	0.56	98.52	n.d.
189	3.00	0.94	0.01	n.d.	1.01	0.01	4.97	64.41	15.82	0.08	n.d.	18.39	0.44	99.14	n.d.
190	2.99	0.94	0.01	n.d.	1.02	0.01	4.97	64.30	15.80	0.15	n.d.	18.66	0.47	99.38	n.d.
191	2.99	0.95	0.01	n.d.	1.03	0.01	4.98	63.88	15.88	0.10	n.d.	18.64	0.47	98.97	n.d.
192	3.01	0.95	0.01	n.d.	1.00	0.00	4.97	64.64	15.94	0.07	n.d.	18.25	0.16	99.06	n.d.
193	3.00	0.95	0.01	n.d.	1.01	0.01	4.98	64.29	16.00	0.07	n.d.	18.43	0.34	99.13	n.d.
194	3.01	0.95	0.01	n.d.	1.01	0.01	4.97	64.55	15.91	0.07	n.d.	18.33	0.28	99.13	n.d.
195	3.02	0.94	0.01	n.d.	0.99	0.00	4.96	65.12	15.83	0.10	n.d.	18.20	0.13	99.38	n.d.
196	3.01	0.95	0.01	n.d.	1.00	0.00	4.97	64.67	15.93	0.09	n.d.	18.17	0.13	98.99	n.d.
197	3.01	0.94	0.01	n.d.	1.00	0.00	4.96	64.82	15.79	0.11	n.d.	18.19	0.14	99.05	n.d.
198	3.02	0.94	0.01	n.d.	1.00	0.00	4.96	64.83	15.85	0.10	n.d.	18.16	0.14	99.08	n.d.
199	3.00	0.96	0.01	n.d.	1.01	0.00	4.98	63.93	16.02	0.06	n.d.	18.32	0.19	98.52	n.d.
200	3.01	0.95	0.01	n.d.	1.00	0.00	4.97	64.48	16.02	0.09	n.d.	18.16	0.23	98.98	n.d.
201	2.99	0.96	0.01	n.d.	1.02	0.00	4.98	63.69	16.00	0.10	n.d.	18.36	0.27	98.41	n.d.
202	3.00	0.96	0.01	n.d.	1.01	0.00	4.98	63.88	15.95	0.07	n.d.	18.31	0.20	98.41	n.d.
203	3.00	0.96	0.01	n.d.	1.02	0.00	4.98	63.68	15.96	0.06	n.d.	18.32	0.23	98.25	n.d.
204	3.00	0.95	0.01	n.d.	1.01	0.00	4.98	63.90	15.92	0.07	n.d.	18.28	0.20	98.37	n.d.
205	2.99	0.97	0.00	n.d.	1.02	0.01	4.99	63.22	16.09	0.05	n.d.	18.30	0.31	97.97	n.d.
206	3.00	0.95	0.01	n.d.	1.01	0.00	4.98	63.65	15.80	0.12	n.d.	18.21	0.24	98.01	n.d.
208	2.99	0.96	0.01	n.d.	1.02	0.01	4.98	63.69	16.06	0.08	n.d.	18.35	0.29	98.47	n.d.
209	3.00	0.94	0.01	n.d.	1.01	0.00	4.97	64.03	15.74	0.08	n.d.	18.26	0.22	98.33	n.d.
211	3.00	0.95	0.01	n.d.	1.01	0.01	4.98	63.79	15.88	0.08	n.d.	18.21	0.30	98.26	n.d.
212	3.00	0.96	0.01	n.d.	1.01	0.00	4.98	63.41	15.93	0.09	n.d.	18.14	0.24	97.82	n.d.
213	3.00	0.95	0.01	n.d.	1.02	0.01	4.98	63.40	15.82	0.09	n.d.	18.23	0.36	97.90	n.d.
214	3.00	0.94	0.01	n.d.	1.02	0.01	4.97	63.54	15.68	0.11	n.d.	18.24	0.33	97.90	n.d.
215	3.01	0.96	0.01	n.d.	1.00	0.00	4.98	63.98	15.94	0.13	n.d.	18.12	0.17	98.34	n.d.
218	3.00	0.95	0.01	n.d.	1.01	0.01	4.97	63.66	15.76	0.12	n.d.	18.24	0.30	98.08	n.d.
219	2.99	0.95	0.01	n.d.	1.02	0.01	4.99	63.39	15.84	0.16	n.d.	18.34	0.51	98.24	n.d.
220	2.99	0.96	0.01	n.d.	1.02	0.01	4.98	63.38	15.92	0.06	n.d.	18.43	0.47	98.27	n.d.

	atomic proportions							wt.% oxides							
No.	**Si**	**K**	**Na**	**Ca**	**Al**	**Ba**	**Total**	**Si**	**K**	**Na**	**Ca**	**Al**	**Ba**	**Total**	**K/Ca**
221	2.98	0.96	0.01	n.d.	1.03	0.01	4.99	63.20	15.95	0.07	n.d.	18.46	0.54	98.22	n.d.
223	2.98	0.96	0.01	n.d.	1.02	0.01	4.99	63.11	15.94	0.14	n.d.	18.39	0.70	98.28	n.d.
224	2.99	0.96	0.01	n.d.	1.02	0.01	4.99	63.39	16.03	0.13	n.d.	18.34	0.40	98.29	n.d.
226	2.99	0.96	0.01	n.d.	1.02	0.01	4.98	63.10	15.80	0.09	n.d.	18.21	0.28	97.48	n.d.
227	2.99	0.96	0.01	n.d.	1.02	0.00	4.98	63.01	15.88	0.09	n.d.	18.19	0.20	97.37	n.d.
228	2.99	0.96	0.01	n.d.	1.02	0.01	4.99	62.82	15.86	0.11	n.d.	18.24	0.39	97.42	n.d.
230	2.99	0.97	0.00	n.d.	1.02	0.01	4.99	62.50	15.98	0.04	n.d.	18.12	0.31	96.95	n.d.
243	2.99	0.96	0.01	n.d.	1.02	0.01	4.98	62.95	15.80	0.12	n.d.	18.27	0.33	97.46	n.d.
245	2.99	0.96	0.01	n.d.	1.02	0.00	4.98	63.38	15.89	0.10	n.d.	18.24	0.26	97.87	n.d.
247	2.99	0.96	0.01	n.d.	1.02	0.01	4.99	63.01	15.93	0.09	n.d.	18.25	0.38	97.67	n.d.
249	2.99	0.97	0.01	n.d.	1.01	0.01	4.99	63.20	16.02	0.08	n.d.	18.14	0.32	97.76	n.d.
250	3.00	0.96	0.01	n.d.	1.02	0.01	4.98	63.52	15.88	0.09	n.d.	18.26	0.32	98.07	n.d.
251	3.00	0.95	0.01	n.d.	1.01	0.01	4.98	63.81	15.91	0.11	n.d.	18.32	0.29	98.44	n.d.
252	3.01	0.95	0.01	n.d.	1.00	0.00	4.97	63.96	15.77	0.13	n.d.	18.09	0.17	98.12	n.d.
253	3.00	0.95	0.01	n.d.	1.01	0.00	4.98	63.63	15.84	0.11	n.d.	18.20	0.23	98.01	n.d.
254	3.00	0.95	0.01	n.d.	1.01	0.01	4.97	63.79	15.80	0.10	n.d.	18.24	0.34	98.28	n.d.
259	3.00	0.95	0.01	n.d.	1.01	0.00	4.98	63.98	15.95	0.09	n.d.	18.23	0.21	98.47	n.d.
260	3.00	0.96	0.01	n.d.	1.01	0.00	4.98	63.62	15.94	0.12	n.d.	18.14	0.21	98.03	n.d.
261	2.99	0.96	0.01	n.d.	1.02	0.01	4.98	63.68	15.97	0.11	n.d.	18.44	0.35	98.54	n.d.
262	3.00	0.96	0.01	n.d.	1.01	0.00	4.98	63.89	15.98	0.07	n.d.	18.26	0.26	98.46	n.d.
263	3.00	0.95	0.01	n.d.	1.02	0.01	4.98	64.01	15.95	0.09	n.d.	18.43	0.33	98.81	n.d.
264	3.00	0.96	0.01	n.d.	1.01	0.01	4.98	64.12	16.07	0.07	n.d.	18.30	0.33	98.89	n.d.
266	3.02	0.94	0.01	n.d.	0.99	0.00	4.96	64.56	15.76	0.08	n.d.	18.00	0.09	98.51	n.d.
267	3.01	0.94	0.01	n.d.	1.00	0.00	4.96	64.43	15.75	0.08	n.d.	18.22	0.19	98.68	n.d.
269	3.01	0.94	0.01	n.d.	1.00	0.00	4.97	64.60	15.84	0.10	n.d.	18.12	0.23	98.89	n.d.
270	3.01	0.95	0.01	n.d.	1.00	0.00	4.97	64.27	15.98	0.07	n.d.	18.17	0.24	98.72	n.d.
272	3.00	0.95	0.01	n.d.	1.02	0.01	4.98	64.12	16.01	0.07	n.d.	18.43	0.33	98.95	n.d.
273	3.01	0.94	0.01	n.d.	1.00	0.00	4.97	64.50	15.87	0.10	n.d.	18.23	0.17	98.87	n.d.
274	3.00	0.95	0.01	n.d.	1.01	0.01	4.98	64.14	15.92	0.10	n.d.	18.34	0.29	98.80	n.d.
275	3.00	0.96	0.01	n.d.	1.01	0.01	4.98	64.09	16.01	0.06	n.d.	18.28	0.29	98.73	n.d.
277	3.00	0.96	0.01	n.d.	1.01	0.01	4.98	64.36	16.17	0.08	n.d.	18.42	0.31	99.34	n.d.
278	2.99	0.95	0.01	n.d.	1.02	0.01	4.98	64.12	15.91	0.12	n.d.	18.49	0.36	99.00	n.d.
279	3.01	0.94	0.01	n.d.	1.00	0.00	4.97	64.56	15.88	0.15	n.d.	18.25	0.23	99.07	n.d.
280	2.99	0.95	0.01	n.d.	1.02	0.01	4.98	63.78	15.97	0.12	n.d.	18.54	0.52	98.92	n.d.
281	3.00	0.95	0.01	n.d.	1.01	0.00	4.98	64.34	16.02	0.15	n.d.	18.33	0.26	99.10	n.d.
282	2.99	0.95	0.01	n.d.	1.02	0.01	4.98	64.12	15.98	0.12	n.d.	18.51	0.38	99.11	n.d.
284	3.00	0.95	0.01	n.d.	1.01	0.00	4.97	64.42	16.01	0.10	n.d.	18.33	0.24	99.10	n.d.
286	3.01	0.94	0.01	n.d.	1.00	0.00	4.96	64.29	15.73	0.12	n.d.	18.19	0.18	98.52	n.d.
287	3.01	0.94	0.01	n.d.	1.00	0.00	4.97	64.50	15.85	0.08	n.d.	18.21	0.22	98.87	n.d.
288	3.01	0.94	0.01	n.d.	1.01	0.01	4.96	64.72	15.78	0.08	n.d.	18.37	0.30	99.25	n.d.
289	3.01	0.94	0.01	n.d.	1.01	0.01	4.97	64.57	15.77	0.12	n.d.	18.33	0.39	99.18	n.d.
290	3.00	0.94	0.01	n.d.	1.01	0.01	4.97	64.48	15.85	0.07	n.d.	18.50	0.36	99.25	n.d.
292	3.01	0.94	0.01	n.d.	1.00	0.01	4.97	64.98	15.87	0.14	n.d.	18.40	0.29	99.69	n.d.
293	3.01	0.93	0.01	n.d.	1.01	0.00	4.96	64.94	15.78	0.10	n.d.	18.42	0.18	99.42	n.d.
294	3.00	0.94	0.01	n.d.	1.01	0.00	4.97	64.60	15.92	0.13	n.d.	18.49	0.22	99.36	n.d.
295	3.01	0.94	0.01	n.d.	1.01	0.01	4.96	64.87	15.83	0.11	n.d.	18.47	0.29	99.58	n.d.

Appendix 3. ^{40}Ar-^{39}Ar data of adularia samples AKE01 and AKE06.

Heating step	$^{40}Ar/^{39}Ar$	±1σ	$^{37}Ar/^{39}Ar$	±1σ	$^{36}Ar/^{39}Ar$	±1σ	$^{40}Ar^*/^{39}Ar_k$	±1σ	^{40}Ar(mol)	$^{40}Ar^*$ (%)	$^{39}Ar_k$ (%)	Age (Ma)	±2σ (Ma)	K/Ca	±2σ
AKE01, J=0.007807±0.0000125															
0.37	101.02428	0.20281	0.01401	0.00020	0.03763	0.00034	89.90569	0.20506	6.371E-14	88.99	5.53	959.30	3.39	30.69	0.88
0.81	85.52031	0.17143	0.01377	0.00031	0.01869	0.00020	79.99892	0.17031	4.767E-14	93.54	4.88	875.40	2.95	31.22	1.41
1.10	87.30442	0.17502	0.01427	0.00021	0.01403	0.00013	83.15984	0.17122	7.100E-14	95.25	7.13	902.59	2.92	30.14	0.88
1.39	82.97790	0.16634	0.01049	0.00018	0.00864	0.00009	80.42521	0.16352	7.021E-14	96.92	7.41	879.09	2.83	41.00	1.40
1.61	80.98128	0.16260	0.03182	0.00035	0.01034	0.00012	77.92952	0.16004	5.281E-14	96.23	5.71	857.36	2.80	13.51	0.30
1.91	83.00563	0.16642	0.00730	0.00013	0.00687	0.00009	80.97532	0.16428	8.100E-14	97.55	8.55	883.84	2.84	58.89	2.10
2.20	89.29608	0.17893	0.00738	0.00010	0.00568	0.00005	87.61851	0.17628	1.681E-13	98.12	16.50	940.27	2.95	58.28	1.64
2.42	84.69645	0.16989	0.00916	0.00011	0.00520	0.00005	83.15860	0.16740	1.614E-13	98.18	16.70	902.58	2.86	46.97	1.16
2.71	74.08362	0.14856	0.00489	0.00008	0.00700	0.00007	72.01432	0.14567	1.078E-13	97.21	12.75	804.81	2.63	87.84	2.83
2.93	70.98519	0.14279	0.00396	0.00016	0.00563	0.00007	69.32165	0.14115	5.758E-14	97.66	7.11	780.37	2.58	108.67	8.52
3.15	86.80311	0.17418	0.00273	0.00009	0.00570	0.00008	85.11882	0.17238	7.658E-14	98.06	7.73	919.25	2.92	157.71	10.98
Total Fusion Age 885.54±2.43 Ma															
AKE06, J=0.007807±0.0000125															
0.37	73.72335	0.15215	0.11151	0.00130	0.11585	0.00106	39.49897	0.31623	1.373E-14	53.57	3.80	484.96	6.81	3.86	0.09
0.66	51.98616	0.11242	0.11039	0.00146	0.03303	0.00037	42.23690	0.14051	9.018E-15	81.24	3.53	514.19	2.98	3.90	0.10
0.95	47.24851	0.09970	0.12147	0.00137	0.02132	0.00021	40.96113	0.10604	1.121E-14	86.69	4.84	500.63	2.26	3.54	0.08
1.25	55.01982	0.11144	0.13280	0.00140	0.01822	0.00019	49.64833	0.11462	2.327E-14	90.23	8.62	591.04	2.33	3.24	0.07
1.54	56.05655	0.11295	0.09580	0.00101	0.01328	0.00014	52.14069	0.11257	2.952E-14	93.01	10.73	616.17	2.25	4.49	0.10
1.76	48.04379	0.09702	0.08728	0.00093	0.00912	0.00012	45.35695	0.09849	2.685E-14	94.40	11.39	546.95	2.05	4.93	0.11
2.05	52.77611	0.10684	0.14178	0.00153	0.01518	0.00021	48.30365	0.11581	1.951E-14	91.52	7.53	577.34	2.37	3.03	0.07
2.27	56.98747	0.11648	0.23597	0.00246	0.02013	0.00024	51.06586	0.12584	1.765E-14	89.59	6.31	605.37	2.53	1.82	0.04
2.57	57.53488	0.12004	0.22008	0.00231	0.01728	0.00023	52.45229	0.12872	1.716E-14	91.15	6.08	619.28	2.57	1.95	0.04
2.79	59.62453	0.12130	0.20299	0.00212	0.01920	0.00021	53.97175	0.12507	2.194E-14	90.51	7.50	634.40	2.48	2.12	0.04
3.01	59.26985	0.11924	0.21741	0.00227	0.02076	0.00021	53.15838	0.12257	2.506E-14	89.68	8.62	626.33	2.44	1.98	0.04
3.23	64.32725	0.13529	0.29124	0.00303	0.02885	0.00030	55.83505	0.14694	1.482E-14	86.78	4.69	652.78	2.88	1.48	0.03
3.52	46.89815	0.09408	0.12129	0.00125	0.01278	0.00012	43.13413	0.09356	3.766E-14	91.97	16.36	523.67	1.97	3.55	0.07
Total Fusion Age 578.01±1.74 Ma															

Appendix 4. LA-ICPMS analyses of calcite and fluorite at the Åkerlandet and Järvsand vein deposits in Paleoproterozoic basement.

Mineral / Deposit	La (ppm)	Ce (ppm)	Pr (ppm)	Nd (ppm)	Sm (ppm)	Eu (ppm)	Gd (ppm)	Tb (ppm)	Dy (ppm)	Ho (ppm)	Er (ppm)	Tm (ppm)	Yb (ppm)	Lu (ppm)	Y (ppm)
calcite / Åkerlandet	26.50	60	7.07	31	4.47	0.19	3.29	0.41	2.63	0.63	1.99	0.34	2.67	0.47	27
calcite / Åkerlandet	21.52	59	7.87	36	5.67	0.25	4.00	0.56	3.57	0.87	3.10	0.53	4.71	0.82	36
calcite / Åkerlandet	5.92	13.94	2.14	13.18	3.32	0.29	3.48	0.41	2.95	0.80	2.99	0.57	5.51	1.13	33
calcite / Åkerlandet	12.79	38	5.49	24.94	4.63	0.20	3.77	0.50	3.21	0.78	2.64	0.45	3.72	0.66	32
calcite / Åkerlandet	5.97	13.80	2.19	13.19	3.48	0.33	3.59	0.44	2.89	0.76	2.81	0.52	4.92	0.95	34
calcite / Åkerlandet	1.62	3.91	0.52	2.86	0.66	0.07	0.79	0.09	0.51	0.14	0.46	0.07	0.68	0.14	6.54
calcite / Åkerlandet	5.11	12.37	1.92	11.15	2.79	0.26	2.87	0.35	2.37	0.64	2.35	0.45	4.44	0.85	28
calcite / Åkerlandet	4.62	11.87	1.78	10.75	2.75	0.24	3.10	0.39	2.68	0.71	2.79	0.51	5.03	1.07	32
Average	10.51	26.54	3.62	17.87	3.47	0.23	3.11	0.39	2.60	0.66	2.39	0.43	3.96	0.76	29
Standard deviation	8.42	21.02	2.59	10.71	1.42	0.07	0.94	0.13	0.86	0.21	0.80	0.15	1.49	0.31	8.77
calcite / Laisvall	6.56	19.36	2.78	11.75	2.22	0.28	1.86	0.32	2.24	0.48	1.38	0.21	1.56	0.26	14.40
calcite / Laisvall	25.66	72	9.77	40	5.08	0.57	3.13	0.38	2.01	0.40	1.07	0.15	1.00	0.16	11.61
calcite / Laisvall	1.90	6.31	0.96	4.29	0.84	0.11	0.73	0.11	0.68	0.15	0.42	0.06	0.45	0.07	4.27
calcite / Laisvall	11.28	41	6.44	27.79	6.11	0.76	5.62	0.91	5.57	1.11	2.79	0.35	2.09	0.35	33
calcite / Laisvall	13.89	49	6.75	29.60	6.72	1.17	6.69	1.40	9.92	2.21	6.43	1.04	7.93	1.31	63
calcite / Laisvall	9.43	34	4.86	22.73	5.01	0.69	4.79	0.81	5.07	1.03	2.86	0.40	2.76	0.46	29
calcite / Laisvall	16.88	60	8.45	37.17	6.49	0.78	4.98	0.85	5.71	1.22	3.44	0.52	3.92	0.67	33
calcite / Laisvall	5.99	16.06	2.14	9.12	1.60	0.25	1.39	0.27	1.79	0.39	1.18	0.18	1.34	0.22	11.13
calcite / Laisvall	3.58	15.26	2.42	11.11	2.67	0.39	2.36	0.36	2.05	0.34	0.70	0.07	0.30	0.05	9.11
calcite / Laisvall	15.63	60	9.15	40.67	9.51	1.50	9.31	1.78	11.85	2.47	7.00	0.99	7.19	1.19	73
calcite / Laisvall	15.73	41	5.53	23.13	3.83	0.47	3.28	0.50	3.02	0.59	1.47	0.17	0.97	0.16	17.22
calcite / Laisvall	13.26	43	6.40	28.95	5.73	0.77	5.17	0.88	5.57	1.13	2.90	0.38	2.68	0.44	32
calcite / Laisvall	63	132	11.11	38	2.72	0.26	1.65	0.19	1.25	0.23	0.61	0.07	0.50	0.09	6.92
calcite / Laisvall	11.29	41	5.28	25.59	3.92	0.45	3.15	0.44	3.09	0.58	1.56	0.22	1.49	0.27	15.80
calcite / Laisvall	8.68	34	4.75	20.95	5.05	0.65	5.11	0.85	5.78	1.27	3.16	0.51	3.13	0.56	44
calcite / Laisvall	26.75	70	7.12	29.23	4.61	0.56	3.71	0.57	3.69	0.68	1.78	0.23	1.46	0.25	19
calcite / Laisvall	27.81	70	7.78	32	4.39	0.49	3.27	0.49	3.18	0.63	1.93	0.27	2.08	0.33	17.89
calcite / Laisvall	10.06	31	4.11	17.32	2.70	0.35	1.97	0.37	1.90	0.41	1.15	0.18	1.31	0.23	10.83
calcite / Laisvall	3.34	9.93	1.36	5.92	1.08	0.16	1.05	0.18	1.16	0.24	0.66	0.10	0.68	0.11	6.90

Mineral / Deposit	La (ppm)	Ce (ppm)	Pr (ppm)	Nd (ppm)	Sm (ppm)	Eu (ppm)	Gd (ppm)	Tb (ppm)	Dy (ppm)	Ho (ppm)	Er (ppm)	Tm (ppm)	Yb (ppm)	Lu (ppm)	Y (ppm)
calcite / Laisvall	34	78	9.26	36	4.37	0.45	2.93	0.38	2.21	0.43	1.13	0.13	0.83	0.15	12.24
calcite / Laisvall	6.21	23.16	3.81	17.61	4.31	0.67	4.50	0.89	6.00	1.25	3.38	0.45	3.17	0.50	36
calcite / Laisvall	32	101	13.46	57	8.67	1.05	6.03	0.82	5.01	0.96	2.67	0.40	2.71	0.46	24.65
calcite / Laisvall	15.90	56	8.33	36	7.17	0.97	6.54	1.10	7.13	1.44	3.92	0.53	3.57	0.61	44
calcite / Laisvall	2.25	6.12	0.82	3.51	0.59	0.09	0.57	0.10	0.66	0.15	0.39	0.06	0.43	0.08	4.06
calcite / Laisvall	2.44	9.43	1.74	11.72	5.83	1.14	10.63	2.14	18.86	5.32	20.24	3.74	32.23	5.22	244
calcite / Laisvall	3.62	9.20	1.40	8.54	3.83	0.82	6.85	1.34	11.62	3.20	11.91	2.23	19.02	3.00	153
Average	14.87	43	5.62	24.06	4.42	0.61	4.13	0.71	4.89	1.09	3.31	0.52	4.03	0.66	37
Standard deviation	13.41	32	3.54	14.23	2.44	0.37	2.64	0.52	4.18	1.12	4.13	0.76	6.59	1.06	50

Mineral / Deposit	La (ppm)	Ce (ppm)	Pr (ppm)	Nd (ppm)	Sm (ppm)	Eu (ppm)	Gd (ppm)	Tb (ppm)	Dy (ppm)	Ho (ppm)	Er (ppm)	Tm (ppm)	Yb (ppm)	Lu (ppm)	Y (ppm)	La/Ho	Y/Ho
green fluorite / Åkerlandet	23	79	21.0	184	62	13.6	27	1.1	4.8	0.7	2.0	0.2	1.2	0.3	22	33	32
green fluorite / Åkerlandet	24	77	22.8	232	83	20	41	1.4	5.5	0.9	2.2	0.2	1.6	0.2	27	26	31
green fluorite / Åkerlandet	33	67	17.7	142	53	14.7	41	3.2	12.0	2.1	6.0	0.5	3.3	0.4	74	16	35
green fluorite / Åkerlandet	33	89	30	209	99	18.8	77	4.0	11.8	1.6	4.4	0.4	2.2	0.5	62	20	38
green fluorite / Åkerlandet	31	104	34	319	110	28	71	5.4	25	2.5	6.1	0.7	3.7	0.9	119	12	47
green fluorite / Åkerlandet	23.0	65	19.7	201	71	24	48	3.5	12.6	1.9	5.1	0.6	2.9	0.4	77	12	39
green fluorite / Åkerlandet	24.6	111	20.3	220	90	18.6	78	4.2	17.1	2.0	3.9	0.4	3.1	0.3	95	12	48
green fluorite / Åkerlandet	30	70	17.4	150	64	14.4	44	2.5	7.8	1.3	3.6	0.4	2.1	0.3	46	24	36
green fluorite / Åkerlandet	25.3	73	23.4	154	60	17.8	30	1.7	10.2	1.9	3.9	0.5	1.8	0.4	52	14	28
green fluorite / Åkerlandet	29	96	25.5	289	105	19.4	105	10.3	32	3.8	6.1	0.8	3.4	0.6	200	8	53
green fluorite / Åkerlandet	20.4	73	18.3	168	76	17.8	53	6.5	31	5.1	13.5	1.9	10.4	1.4	194	4	38
green fluorite / Åkerlandet	4.1	16	5.0	57	38	9.3	58	4.7	21	3.7	6.1	0.5	2.4	0.5	212	1	57
green fluorite / Åkerlandet	9.0	24	6.2	80	44	12.4	116	9.9	37	5.2	9.0	0.6	2.6	0.6	299	2	57
green fluorite / Åkerlandet	6.7	23	7.9	101	76	18.6	115	12.2	39	4.5	8.8	0.7	4.3	0.7	268	1	59
green fluorite / Åkerlandet	35	119	29	248	56	23.1	24	1.3	4.2	0.7	2.1	0.1	1.0	0.2	21	47	28
green fluorite / Åkerlandet	21.6	74	15.1	159	57	12.8	30	1.9	7.8	1.1	2.7	0.3	2.2	0.3	48	19	43
green fluorite / Åkerlandet	31	122	40	316	49	17.6	27	1.1	3.3	0.8	1.5	0.2	1.5	0.4	15	42	20
green fluorite / Åkerlandet	26.4	62	15.5	110	58	10.1	45	3.7	25.4	3.9	10.9	1.4	9.1	1.4	134	7	34
green fluorite / Åkerlandet	30	98	23.4	275	91	22.0	73	3.2	11.9	1.9	4.6	0.7	4.4	0.6	67	15	34

Mineral / Deposit	La (ppm)	Ce (ppm)	Pr (ppm)	Nd (ppm)	Sm (ppm)	Eu (ppm)	Gd (ppm)	Tb (ppm)	Dy (ppm)	Ho (ppm)	Er (ppm)	Tm (ppm)	Yb (ppm)	Lu (ppm)	Y (ppm)		La/Ho	Y/Ho
green fluorite / Åkerlandet	28.1	85	26.4	276	98	19.9	90	6.5	31.4	6.2	12.5	1.8	9.8	1.7	247		5	40
green fluorite / Åkerlandet	25.7	104	25.4	216	94	27.2	72	3.4	14.4	2.0	4.9	0.6	3.4	0.4	74		13	36
green fluorite / Åkerlandet	26.0	83	21.8	180	71	18.8	45	1.7	6.3	1.0	3.1	0.3	2.5	0.3	31		25	30
green fluorite / Åkerlandet	28.9	86	28.6	281	126	25.8	101	8.6	29	4.5	5.9	0.6	3.6	0.5	201		6	44
green fluorite / Åkerlandet	24.8	57	12.1	96	55	10.3	52	4.0	21	3.5	10.0	1.4	8.1	1.3	124		7	36
green fluorite / Åkerlandet	20.5	57	11.4	100	46	8.5	49	4.0	18.9	3.4	7.6	1.2	6.4	0.8	117		6	34
green fluorite / Åkerlandet	30	93	27.8	260	98	30	70	4.5	18.5	3.0	6.9	0.7	4.9	0.6	120		10	39
green fluorite / Åkerlandet	25.7	76	18.2	221	78	20.5	58	3.8	19.5	3.5	13.5	1.2	6.7	0.9	109		7	31
green fluorite / Åkerlandet	28.1	69	17.0	125	51	13.8	47	4.3	20.1	4.3	12.3	1.4	7.6	1.4	102		6	23
green fluorite / Åkerlandet	23.5	90	25.2	240	73	13.3	59	3.9	14.0	1.8	3.8	0.5	1.9	0.6	87		13	49
green fluorite / Åkerlandet	19.0	80	17.7	129	43	8.8	25	1.7	8.2	1.4	2.5	0.4	2.0	0.2	31		14	23
green fluorite / Åkerlandet	21.5	51	11.7	113	33	8.3	26	2.6	10.4	1.9	3.6	0.6	2.3	0.4	63		11	33
green fluorite / Åkerlandet	24.7	79	21.4	260	111	22.5	54	2.6	9.3	1.9	5.3	0.5	2.5	0.4	57		13	30
Average	24.6	77	20.5	191	72	17.5	58	4	17	2.6	6.1	0.7	3.9	0.6	106	Minimum	1	20
Standard deviation	9	30	9	83	29	7	29	3	10	2	4	0	3	0	77	Maximum	47	59
green fluorite / Laisvall	11.2	31	4.2	20.4	7.9	1.4	8.6	1.8	11.5	2.5	5.1	0.6	2.6	0.3	153		4	61
green fluorite / Laisvall	22.9	68	8.4	40	14.6	2.9	32.3	9.0	74.2	17.5	54.6	7.3	33.3	4.3	1011		1	58
green fluorite / Laisvall	8.2	19.4	5.3	35	21.4	4.0	18.4	2.8	14.9	2.6	5.3	0.5	2.2	0.3	157		3	60
green fluorite / Laisvall	18.0	45.4	7.5	56	28.4	6.1	51.5	12.6	95	19.9	45.2	4.4	16.0	2.2	921		1	46
green fluorite / Laisvall	12.5	45.6	5.6	25.4	8.8	3.0	16.0	5.0	30	7.7	18.4	2.3	8.7	1.5	330		2	43
green fluorite / Laisvall	6.2	22.5	3.8	25.3	12.6	2.6	24.4	4.3	33	5.8	10.7	1.1	3.9	0.5	272		1	47
green fluorite / Laisvall	14.8	41	8.7	33	18.0	3.6	23.3	4.7	40	10.7	29.9	3.4	18.1	2.1	701		1	66
green fluorite / Laisvall	25.1	59	8.1	55	17.5	4.5	25.0	5.3	47	10.1	29.3	3.2	15.0	2.4	505		2	50
green fluorite / Laisvall	28.9	69	12.4	103	48	11.3	120	24.3	147	24.6	46	4.1	19.0	1.9	1041		1	42
green fluorite / Laisvall	27.5	78	14.9	76	32.4	10.1	65	9.0	45	7.3	19.5	1.6	7.7	1.0	486		4	66
green fluorite / Laisvall	6.1	32	5.5	42	17.4	2.5	24.2	3.3	11.8	2.0	5.5	0.3	1.4	0.2	155		3	76
green fluorite / Laisvall	12.8	38	7.4	32	15.0	2.2	27.9	7.0	44	10.8	21.0	2.2	11.4	0.9	507		1	47
green fluorite / Laisvall	13.7	37	5.9	33	11.2	1.7	17.7	4.1	30.9	6.2	28.1	1.9	8.8	1.2	347		2	56
green fluorite / Laisvall	12.9	41	6.7	37	14.5	3.9	21.6	4.2	32.9	6.4	15.5	1.9	10.7	1.2	269		2	42
green fluorite / Laisvall	20.8	65	12.2	93	52	8.3	106	14.9	90	12.3	26.0	1.9	8.0	1.0	517		2	42

Mineral / Deposit	La (ppm)	Ce (ppm)	Pr (ppm)	Nd (ppm)	Sm (ppm)	Eu (ppm)	Gd (ppm)	Tb (ppm)	Dy (ppm)	Ho (ppm)	Er (ppm)	Tm (ppm)	Yb (ppm)	Lu (ppm)	Y (ppm)		La/Ho	Y/Ho
green fluorite / Laisvall	22.8	76	12.7	84	48	8.4	61	9.7	63	11.2	24.6	2.8	12.8	1.8	537		2	48
green fluorite / Laisvall	14.6	33	5.0	29	10.9	2.2	13.8	2.3	18.6	4.2	11.5	1.4	10.6	1.1	282		3	67
green fluorite / Laisvall	25.1	147	14.2	44	40	9.1	17.4	3.7	28.9	14.0	22.3	2.7	18.4	1.1	481		2	34
green fluorite / Laisvall	20.2	70	9.3	46	6.0	0.9	5.3	0.7	4.7	0.9	3.0	0.4	3.0	0.5	31		22	34
green fluorite / Laisvall	35.0	112	16.1	71	11.2	1.1	7.0	0.9	5.9	1.3	3.5	0.5	4.2	0.7	33		28	26
green fluorite / Laisvall	14.1	41	5.9	25.8	3.6	0.5	2.7	0.4	2.4	0.5	1.3	0.2	1.4	0.3	14		28	28
green fluorite / Laisvall	22.0	60	9.1	65	21.7	6.0	37	5.9	43	9.9	26.3	3.1	10.0	1.4	439		2	44
green fluorite / Laisvall	15.5	37	7.5	40	15.2	2.9	22.1	3.0	30	5.9	19.2	1.8	9.4	0.9	252		3	43
green fluorite / Laisvall	17.5	45	7.5	53	19.1	5.7	33	6.8	55.4	10.2	19.7	1.7	7.2	1.0	297		2	29
green fluorite / Laisvall	11.1	29.7	5.1	31	13.7	3.5	19.8	2.6	16.1	3.0	6.6	0.7	2.9	0.4	199		4	66
green fluorite / Laisvall	12.3	35	5.7	31	14.6	2.7	18.5	5.1	40	9.6	23.3	2.2	12.4	1.1	420		1	44
green fluorite / Laisvall	22.3	70	9.2	74	32	6.6	56	9.6	58	11.9	36	2.7	14.2	1.7	430		2	36
green fluorite / Laisvall	27.3	57	11.1	82	45	7.9	110	17.0	101	14.3	23.3	3.0	10.5	2.0	1049		2	73
green fluorite / Laisvall	29.2	79	11.4	62	26.7	7.1	43	8.7	53	9.7	23.3	2.5	12.6	1.8	524		3	54
green fluorite / Laisvall	17.4	39	6.9	38	14.5	2.6	21.6	4.4	39	9.0	23.8	2.9	16.3	2.3	579		2	64
green fluorite / Laisvall	31.1	69	11.6	68	31	7.2	57	14.4	91	17.1	38.3	4.4	19.1	2.2	556		2	32
green fluorite / Laisvall	15.9	45	6.0	43	17.9	3.6	29.5	5.1	41	10.7	33.0	3.3	18.4	2.0	530		1	50
Average	18.6	54	8.5	50	21.6	4.6	36	6.6	45	9.1	21.8	2.3	10.9	1.3	438	Minimum	0.9	26
Standard deviation	8.4	28.2	3.7	24.1	13.5	3.0	29.6	5.3	32.7	5.9	13.7	1.5	7.1	0.9	286	Maximum	28	76
purple fluorite / Laisvall	20.8	52	8.5	45	14.5	3.3	28.3	5.5	48	11.1	31.3	2.5	13.6	2.1	489		2	44
purple fluorite / Laisvall	19.8	56	8.4	45	20.8	3.8	25.6	7.5	65	13.7	30.0	3.9	16.8	1.9	647		1	47
purple fluorite / Laisvall	19.4	52	7.8	33	12.7	2.5	21.6	4.6	40	9.3	25.6	2.8	13.3	1.9	412		2	44
purple fluorite / Laisvall	6.3	17.1	2.6	18.3	6.8	1.1	8.6	1.4	9.6	1.9	5.0	0.5	2.8	0.3	106		3	56
purple fluorite / Laisvall	20.8	56	6.3	38	14.8	3.0	27.5	5.9	58	12.7	36.5	2.9	17.2	2.0	476		2	37
purple fluorite / Laisvall	25.9	56	7.7	33	14.0	3.4	23.8	5.7	46	11.5	28.9	3.7	17.6	1.9	483		2	42
purple fluorite / Laisvall	10.0	24.9	4.4	22.1	9.8	2.0	14.9	2.9	23.9	4.1	8.9	1.3	8.0	0.6	186		2	46
purple fluorite / Laisvall	15.2	41	6.1	36	12.8	2.7	23.7	4.9	26.0	6.2	14.7	1.7	6.8	0.8	287		2	46
purple fluorite / Laisvall	15.9	42	4.9	34	7.2	0.7	8.1	2.0	13.2	4.4	9.8	1.3	10.6	1.1	195		4	44
purple fluorite / Laisvall	8.0	18.0	3.4	19.0	7.9	1.5	12.6	1.3	7.0	1.0	2.3	0.2	0.9	0.1	75		8	74
purple fluorite / Laisvall	20.1	50	6.4	30	9.4	1.9	19.8	3.8	39	9.7	32.2	2.9	16.2	2.2	499		2	52

Mineral / Deposit	La (ppm)	Ce (ppm)	Pr (ppm)	Nd (ppm)	Sm (ppm)	Eu (ppm)	Gd (ppm)	Tb (ppm)	Dy (ppm)	Ho (ppm)	Er (ppm)	Tm (ppm)	Yb (ppm)	Lu (ppm)	Y (ppm)		La/Ho	Y/Ho
purple fluorite / Laisvall	6.1	11.9	2.1	10.6	3.2	0.5	4.9	0.8	5.7	1.2	3.1	0.3	1.5	0.2	70		5	60
purple fluorite / Laisvall	12.3	39	4.7	27.4	10.1	2.6	21.0	3.5	25.6	5.5	11.9	1.1	5.6	0.7	260		2	48
purple fluorite / Laisvall	18.9	59	9.6	51.1	20.5	3.9	34.6	8.2	65	13.4	30.9	3.3	14.8	2.1	669		1	50
purple fluorite / Laisvall	11.9	37	5.3	27.3	11.3	2.3	24.5	5.4	45	12.0	28.4	2.7	15.3	1.6	518		1	43
purple fluorite / Laisvall	15.3	39	6.8	36	16.5	3.4	29.5	7.1	42	8.5	20.8	1.7	8.5	1.2	400		2	47
purple fluorite / Laisvall	2.3	4.6	0.5	3.1	0.9	0.2	b.d.	0.1	0.6	0.2	0.5	0.0	0.2	0.1	17		14	109
purple fluorite / Laisvall	11.0	29.7	3.7	25.3	10.5	1.9	19.9	5.0	37	9.3	26.0	2.7	16.8	1.9	573		1	61
purple fluorite / Laisvall	8.9	24.4	3.9	28.6	11.7	2.8	26.9	4.8	34	6.6	13.3	1.0	4.0	0.3	261		1	39
purple fluorite / Laisvall	10.3	31.1	3.7	25.6	9.7	2.3	19.7	3.8	25.9	8.0	18.1	1.3	9.0	0.9	297		1	37
purple fluorite / Laisvall	15.0	41	6.9	43	17.0	3.8	32.9	6.2	55	10.3	25.3	2.6	12.4	1.4	481		1	47
purple fluorite / Laisvall	5.6	14.9	3.0	15.9	5.4	0.9	8.3	1.3	11.9	1.9	4.4	0.4	3.9	0.3	106		3	56
purple fluorite / Laisvall	14.1	33	4.2	20.7	5.0	0.9	8.0	1.3	9.8	1.5	3.5	0.3	1.2	0.1	92		9	59
Average	13.6	36	5.3	29.1	11.0	2.2	20.2	4.0	31.9	7.1	17.9	1.8	9.4	1.1	330	Minimum	1	37
Standard deviation	6.8	17.8	2.6	13.5	5.7	1.2	10.3	2.4	20.4	4.6	12.0	1.2	6.2	0.8	208	Maximum	14	109